frontiers | Research Topics

Quality control for efficacy and safety of herbal medicinal products

Edited by
Jian-bo Yang, Zhichao Xu, Wei Cai, Yong Li and Wing Lam

Published in
Frontiers in Pharmacology

ISSN 1664-8714
ISBN 978-2-8325-2655-2
DOI 10.3389/978-2-8325-2655-2

About Frontiers

Frontiers is more than just an open access publisher of scholarly articles: it is a pioneering approach to the world of academia, radically improving the way scholarly research is managed. The grand vision of Frontiers is a world where all people have an equal opportunity to seek, share and generate knowledge. Frontiers provides immediate and permanent online open access to all its publications, but this alone is not enough to realize our grand goals.

Frontiers journal series

The Frontiers journal series is a multi-tier and interdisciplinary set of open-access, online journals, promising a paradigm shift from the current review, selection and dissemination processes in academic publishing. All Frontiers journals are driven by researchers for researchers; therefore, they constitute a service to the scholarly community. At the same time, the *Frontiers journal series* operates on a revolutionary invention, the tiered publishing system, initially addressing specific communities of scholars, and gradually climbing up to broader public understanding, thus serving the interests of the lay society, too.

Dedication to quality

Each Frontiers article is a landmark of the highest quality, thanks to genuinely collaborative interactions between authors and review editors, who include some of the world's best academicians. Research must be certified by peers before entering a stream of knowledge that may eventually reach the public - and shape society; therefore, Frontiers only applies the most rigorous and unbiased reviews. Frontiers revolutionizes research publishing by freely delivering the most outstanding research, evaluated with no bias from both the academic and social point of view. By applying the most advanced information technologies, Frontiers is catapulting scholarly publishing into a new generation.

What are Frontiers Research Topics?

Frontiers Research Topics are very popular trademarks of the *Frontiers journals series*: they are collections of at least ten articles, all centered on a particular subject. With their unique mix of varied contributions from Original Research to Review Articles, Frontiers Research Topics unify the most influential researchers, the latest key findings and historical advances in a hot research area.

Find out more on how to host your own Frontiers Research Topic or contribute to one as an author by contacting the Frontiers editorial office: frontiersin.org/about/contact

Quality control for efficacy and safety of herbal medicinal products

Topic editors

Jian-bo Yang — National Institutes for Food and Drug Control, China
Zhichao Xu — Northeast Forestry University, China
Wei Cai — Hunan University of Medicine, China
Yong Li — Institute of Materia Medica, Chinese Academy of Medical Sciences and Peking Union Medical College, China
Wing Lam — Yale University, United States

Citation

Yang, J.-b., Xu, Z., Cai, W., Li, Y., Lam, W., eds. (2023). *Quality control for efficacy and safety of herbal medicinal products*. Lausanne: Frontiers Media SA. doi: 10.3389/978-2-8325-2655-2

Table of contents

frontiers | Frontiers in Pharmacology

TYPE Editorial
PUBLISHED 25 May 2023
DOI 10.3389/fphar.2023.1162698

OPEN ACCESS

EDITED BY
Filippo Drago,
University of Catania, Italy

REVIEWED BY
Massimiliano Berretta,
University of Messina, Italy

*CORRESPONDENCE
Wing Lam,
lamwingyale@hotmail.com

RECEIVED 09 February 2023
ACCEPTED 11 May 2023
PUBLISHED 25 May 2023

CITATION
Lam W, Cai W, Li Y, Xu Z and Yang J (2023), Editorial: Quality control for efficacy and safety of herbal medicinal products.
Front. Pharmacol. 14:1162698.
doi: 10.3389/fphar.2023.1162698

Editorial: Quality control for efficacy and safety of herbal medicinal products

Wing Lam[1]*, Wei Cai[2], Yong Li[3], Zhichao Xu[4] and JianBo Yang[5]

[1]Department of Pharmacology, Yale University, New Haven, CT, United States, [2]School of Pharmaceutical Sciences, Hunan University of Medicine, Huaihua, China, [3]Institute of Materia Medica, Chinese Academy of Medical Sciences and Peking Union Medical College, Beijing, China, [4]College of Life Science, Northeast Forestry University, Harbin, China, [5]National Institutes for Food and Drug Control, Beijing, China

KEYWORDS

quality control, efficacy, safety, herbal medicinal products, DNA barcode, UPLC-HRMS, data mining

Editorial on the Research Topic
Quality control for efficacy and safety of herbal medicinal products

Introduction

Herbal medicines have a long-standing history in human culture, serving as the foundation for various traditional medical systems, including Traditional Chinese Medicine, Ayurveda, Unani, and Siddha. In Asia and some other countries, plant-based medicines are often regarded as mainstream treatments for a range of complex diseases and symptoms. However, in many developed Western nations, such as the United States, herbal products are predominantly marketed as dietary supplements, which are not permitted to make claims about diagnosing, curing, mitigating, treating, or preventing diseases.

Although botanical medicines are often perceived as safer due to their natural, plant-derived origins, there have been numerous reports of toxicity among cancer patients using herbal medicines (Olaku and White, 2011). To gain acceptance as legitimate medicine within the Western medical framework, researchers and developers must address quality control Research Topic and enhance our understanding of the safety profile of herbal medicines through rigorous scientific approaches. This will help ensure that these products meet the guidance and regulatory standards of different countries. Adhering to the Botanical Drug Development Guidance for Industry, the United States FDA approved a select few herbal products for sale as prescription drugs. Notable examples include sinecatechins (Veregen®) and crofelemer (Mytesi™).

Over the past 20 years, significant progress has been made in developing and adapting numerous cutting-edge techniques to address the efficacy and safety of herbal medicinal products. In this Research Topic Research Topic, we have included nine original research articles that cover various aspects of quality control for the efficacy and safety of herbal medicinal products. We hope that these articles will enhance our understanding of the importance of quality control in the realm of botanical medicinal products.

To develop herbal medicine, the correct herb species must be identified as the first step. Therefore, developing methods for accurate herbal authentication is foundational. In

the past, experienced herbalists were relied on for selection based on morphology, color, smell, and taste. In addition to these traditional methods, which can be too subjective, technological advances that provide much more precise data have been invented and applied to herbal authentication. Mahima et al. provide very detailed information about using DNA barcoding techniques for herbal authentication. The Mahima et al. article introduces the history and the trend of DNA barcoding for the herbal industry (Mahima et al.). Mahima et al. collected many examples in which DNA barcoding techniques were applied to the authentication and detection of contaminants. In addition, Mahima et al. cover the view of different countries' Pharmacopoeia or regulatory agencies on DNA barcoding for herbal products. Furthermore, Mahima et al. also discuss the most updated DNA barcoding methodologies (Mahima et al.). Universal DNA barcoding based on nuclear DNA has limitations in differentiating species of some plant families, for example, *Bidens* species. Wu et al. analyze DNA sequences from 12 chloroplast and eight mitochondrial genomes of five species and one variety of Bidens using bioinformatics (Wu et al.). They reveal that complete chloroplast genomes could be used as a super barcode to authenticate Bidens species accurately (Wu et al.). In addition, highly variable regions of trnS-GGA-rps4 could potentially be used as a specific barcode to identify Bidens species (Wu et al.).

Besides plant species authentication, herbal products must also meet contamination standards set by their respective country government agencies. Pesticide residues with known harmful linkages to health found in herbal products are a serious safety concern. Some farmers are even using new pesticides to avoid detection. Wang et al. describe using high-performance liquid (HPLC-MS/MS) and gas (GC-MS/MS) chromatography to effectively detect 168 pesticides in 1,017 samples of 10 herbs that are commonly sold in markets (Wang et al.). They report that the pesticide levels in Chinese Herbal Medicines of the same type had varied distribution. In addition, Wang et al. use bioinformatics to assess short-term and long-term intake risk and cumulative dietary risk (Wang et al.).

Differences in seasonal and environmental factors have demonstrated that separate batches of the same herb may have different efficacy. Furthermore, herbal medicines contain multiple active chemicals, and their metabolism by the human body could be very different depending on their interactions Innovative methods that could effectively identify and quantify multiple active metabolites and/or contaminants, such as pesticides, should be very useful in assessing efficacy and toxicity. One such tool, UHPLC-HRMS (ultra-high-performance liquid chromatography-high resolution mass spectrometry), is a very powerful instrument that has very high sensitivity and precision for molecular identification and quantification. By introducing the advantages of UPLC-HRMS and its specific applications, such as chemical characterization, determination of TCM components, chemical fingerprint analysis, identification of the authenticity of TCMs, and identification of illegal additives, Ma et al. discuss how to apply this technology to study metabolites. They also collected some examples in which researchers used UHPLC-HRMS technology with PCA and OPLS-DA statistical methods to study mechanisms of action of various Traditional Chinese Medicines (TCM) (Ma et al.).

For the past two decades, steady progress has been made in generating and accumulating data on herbal medicine. This information is collected in publicly available online databases. Applying computational methods to take advantage of this big data could facilitate the quality control of herbal medicines. Using network pharmacology and molecular docking methods, An et al. identify toxic components of Fuzi and its potential targets that are associated with neurotoxicity. They also validate that Aconitine in Fuzi could affect mitochondrial function, induce apoptosis, and inhibit MARK and AKT phosphorylation in neuron cells. An et al. also confirm that Aconitine could reduce the number of normal hippocampal neurons by inducing apoptosis. In another study, Chen et al. use data processing techniques to identify active compounds from herbal medicine (Chen et al.). In their report, they rank 20 potential Quality-markers (Q-marker) of Jiuzhi Dahuang Wan (JZDHW: processed Rhubarb) using non-targeted/targeted data mining technologies and the time-concentration curve (AUC) pooled methods (Chen et al.). Ultimately, the compound rhein was selected as a Q-marker, and it was validated in mice that it could reduce LPS-induced pneumonia by inhibiting IL1β and IL6 production and pathological changes in lung tissue (Chen et al.). Chen et al. also find that rhein could be used to predict the overall anthraquinone metabolism of JZDHW *in vivo*.

In this Research Topic, we also selected three articles focusing on Polygonum multiflorum Thunb (PM) (the dried root of PM, or Polygoni Multiflori Radix) because it has been reported in the past few decades to occasionally cause hepatoxicity. PM has a long usage history in treating different diseases, but its preparation can have very different properties; raw PM is better suited for detoxifying and anti-swelling, while processed PM has immunomodulating, tonifying properties. According to the TCM application, processed (stewed with black bean juice, steamed with black bean juice, and steamed with water) PM preparations are less toxic to humans. To investigate this, Gu et al. compare polysaccharide changes in raw PM and processed PM. They find that processed PM could reduce polysaccharides Mw, indicating that polysaccharides degradation occurred somewhere during the processing (Gu et al.). They also find that processing increases the molar ratio of Glc/GalA in processed PM polysaccharides. Therefore, the Mw and Glc/Gal A ratios could serve as quality control markers for processed PM. They reveal that both processed PM and raw PM could promote the cell viability of RAW264. 7 macrophages, but processed PM polysaccharides exhibited stronger induction on IL6, TNFa, and iNOS mRNA expression than raw PM (Gu et al.). Their result indicates that the changes in polysaccharides during the processing could affect its immunomodulatory activity.

Articles by Song et al. and Kang et al. both aim to address PM's reported hepatotoxicity. Song et al. integrate metabolomics and the pseudo-targeted spectrum–effect relationship to capture potential hepatotoxic components in PM. Song et al. compare compounds between raw PM and processed PM based on tentative UPLC-Q-TOF-MS identification and toxicity and attenuation methods. Using three mathematical models (gray relational analysis, orthogonal partial least squares analysis, and back propagation artificial neural network methods), they correlate the quantity of proposed pseudo-targeted MS of 16 differential components from 50 PM batches and the hepatocytotoxicity of 50 batches of PM. Their

analysis pinpoints three distinct components (emodin dianthrones, emodin-8-O-β-D-glucopyranoside, PM 14–17) that could serve as PM toxicity markers (Song et al.).

To identify toxic components in PM, Kang et al. study the hepatotoxicity impact of PM's anthraquinones on bile acid (BA) homeostasis in mice. By comparing the impact of PM extract to individual anthraquinones on liver function, they reveal that physcion and PM extract could alter BA metabolism and the expression of Bsep and Mrp2 during treatment (Kang et al.). By examining the metabolism of bile acids and protein/mRNA expression of bile salt export pump (Bsep) and multidrug resistance-associated protein 2 (Mrp2), Kang et al. provide a new mechanism of action to elucidate how liver function can be affected by PM.

Due to space constraints in this Research Topic Research Topic, we are only able to feature nine exceptional articles that focus on herbal authentication, metabolite/chemical identification, big data mining, and analysis. These articles present innovative approaches for improving the quality control, efficacy, and safety of herbal medicinal products. Many other Research Topic related to the efficacy and safety of herbal medicinal products, such as interactions between standard treatments and herbal/natural products, will be included in "*Quality control for efficacy and safety of herbal medicinal products: volume II*." We look forward to presenting more compelling articles in our upcoming Research Topic Research Topic.

Author contributions

All authors listed have made a substantial, direct, and intellectual contribution to the work and approved it for publication.

Conflict of interest

The authors declare that the research was conducted in the absence of any commercial or financial relationships that could be construed as a potential conflict of interest.

Publisher's note

References

Olaku, O., and White, J. D. (2011). Herbal therapy use by cancer patients: A literature review on case reports. *Eur. J. Cancer* 47, 508–514. doi:10.1016/j.ejca.2010.11.018

frontiers in Pharmacology

ORIGINAL RESEARCH
published: 01 February 2022
doi: 10.3389/fphar.2021.818268

Levels and Health Risk of Pesticide Residues in Chinese Herbal Medicines

Ying Wang[1], Yan Gou[2†], Lei Zhang[3], Chun Li[4], Zhao Wang[1], Yuanxi Liu[1], Zhao Geng[2], Mingrui Shen[5], Lei Sun[1], Feng Wei[1], Juan Zhou[2], Lihong Gu[4], Hongyu Jin[1] and Shuangcheng Ma[1]**

[1]Institute for Control of Chinese Traditional Medicine and Ethnic Medicine, National Institutes for Food and Drug Control, Beijing, China, [2]Sichuan Institute for Drug Control, Sichuan Testing Center of Medical Devices/NMPA Key Laboratory of Quality Evaluation of Chinese Patent Medicines, Chengdu, China, [3]China National Center for Food Safety Risk Assessment, Beijing, China, [4]Guangzhou Institute for Drug Control, NMPA Key Laboratory for Quality Evaluation of Traditional Medicine, Guangzhou, China, [5]Chinese Pharmacopoeia Commission, Beijing, China

OPEN ACCESS

Edited by:
Wei Cai,
Hunan University of Medicine, China

Reviewed by:
Jian Xue,
Chinese Academy of Medical Sciences and Peking Union Medical College, China
Canping Pan,
China Agricultural University, China
Rolf Teschke,
Hospital Hanau, Germany

***Correspondence:**
Shuangcheng Ma
masc@nifdc.org.cn
Hongyu Jin
jhyu@nifdc.org.cn

†These authors have contributed equally to this work and share first authorship

Specialty section:
This article was submitted to Experimental Pharmacology and Drug Discovery, a section of the journal Frontiers in Pharmacology

Received: 19 November 2021
Accepted: 16 December 2021
Published: 01 February 2022

Citation:
Wang Y, Gou Y, Zhang L, Li C, Wang Z, Liu Y, Geng Z, Shen M, Sun L, Wei F, Zhou J, Gu L, Jin H and Ma S (2022) Levels and Health Risk of Pesticide Residues in Chinese Herbal Medicines. Front. Pharmacol. 12:818268. doi: 10.3389/fphar.2021.818268

In the present study, 168 pesticides in 1,017 samples of 10 Chinese herbal medicines (CHMs) were simultaneously determined by high-performance liquid (HPLC-MS/MS) and gas (GC-MS/MS) chromatography–tandem mass spectrometry. A total of 89.2% of the samples encompassed one or multiple pesticide residues, and the residue concentrations in 60.5% of samples were less than 0.02 mg kg^{-1}, revealing the relatively low residue levels. The hazard quotient and hazard index methods were used to estimate the health risk for consumers. For a more accurate risk assessment, the exposure frequency and exposure duration of CHMs were involved into the exposure assessment, which was obtained from a questionnaire data of 20,917 volunteers. The results of chronic, acute, and cumulative risk assessment indicated that consumption of CHMs is unlikely to pose a health risk to consumers. Ranking the risk of detected pesticides revealed that phorate, BHC, triazophos, methidathion, terbufos, and omethoate posed the highest risk. Our results also showed that pollution of the aboveground medicinal part was more serious. Although exposure to pesticides in tested CHMs was below dangerous levels, more strict controlled management should be carried out for banned pesticides due to the high detection rate and illegal use in the actual planting practice.

Keywords: chinese herbal medicines, pesticide residues, exposure frequency, risk scoring, cumulative evaluation

INTRODUCTION

Recently, the efficacy of Chinese herbal medicines (CHMs) has been generally recognized by domestic and foreign markets. The World Health Organization (WHO) indicates that 75% of the worldwide population use CHMs for their fundamental medical and health care needs (Pan et al., 2014). At the same time, with the increasing global acceptance of CHMs, their use has also expanded to other sectors such as health products, food supplements (Piemontese, 2017), cosmetics (Xie et al., 2015), and food-flavoring agents (Nabavi et al., 2015).

With the rapid increase of demand for CHMs in the global market, concerns for the efficacy and safety of CHMs were raised. The efficiency of CHMs is controversial due to the lack of literature reports. Teschke *et al.* studied the literature of traditional Chinese medicines (TCMs) used in the treatment of gastrointestinal disorders. When analyzing published clinical trials, it was found that all indications lacked placebo-controlled, randomized, double-blind trials (Teschke et al., 2015). Finally, it is considered that although the use of TCM in the treatment of various diseases has a long history,

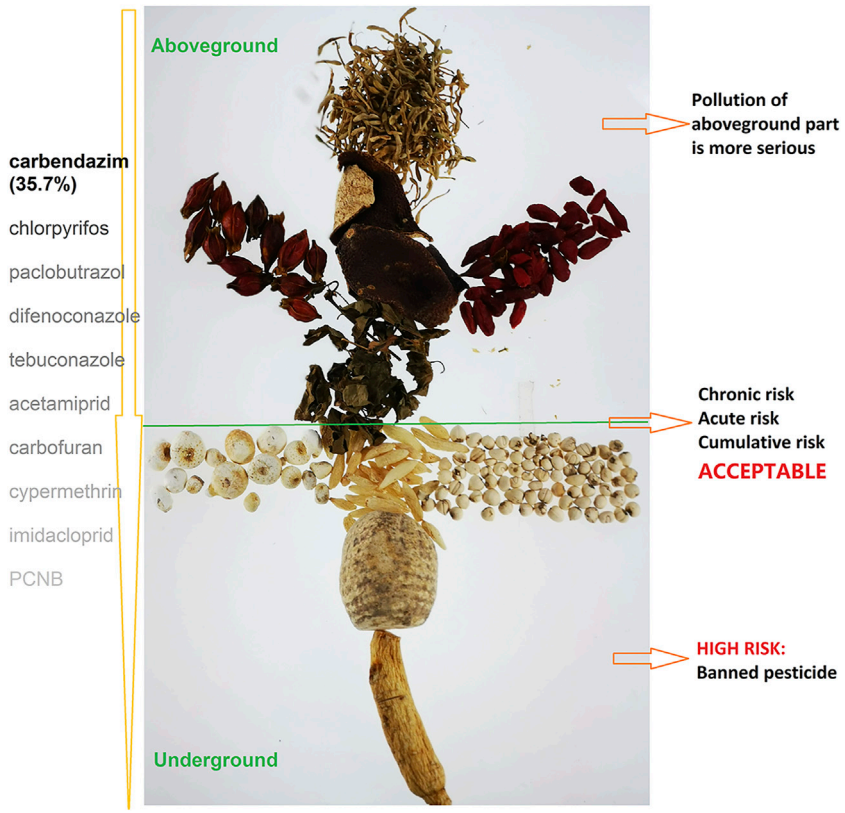

GRAPHICAL ABSTRACT |

high-quality test verification is lacking. Totally, 13 journals related to TCM published in China were randomly selected by Wang et al., and the reporting quality of randomized controlled trials (RCTs) in TCM journals was evaluated. The findings of this study suggested that the reporting of some important methodological components of RCTs is incomplete, and the reporting quality of these trials still needs to be improved (Wang et al., 2007). Investigations assessing the adverse effects of TCM mainly focus on liver damage, which is rarely found in a German TCM hospital that carefully analyzed TCM preparations for product quality before treatment of patients (Melchart et al., 2017). Many phytochemicals have been confirmed to be beneficial to human health, for example, exerting hepatoprotective effects (Domitrovi'c and Potocnjak, 2016), but more cases of liver injury caused by phytocompounds have been reported with increasing frequency. The risk assessment of herb-induced liver injury (HILI) for individual cases was achieved using the Roussel Uclaf Causality Assessment Method (RUCAM) (Danan Teschke, 2016) under the recommendations of the Chinese Society of Hepatology (GSH) (Yu et al., 2017). With the data provided for worldwide published 12,068 HILI cases (Teschke et al., 2020), the risk of liver injury associated with the use of CHMs was evidenced by using RUCAM to verify a causal relationship. The investigation of the causes of HILI is the focus of attention at present.

It has been reported that potential hepatotoxins in herbal medicinal products may be related to the presence of plant-originated components (phyto-hepatotoxins) as well as exogenous pollutants (non-phyto-hepatotoxins) (Quan et al., 2020). The term "phyto-hepatotoxins" refers to any potential hepatotoxic compound synthesized by medicinal plants, most of which are secondary metabolites produced to protect medicinal plants from external attacks. Recently, a total of 296 phytochemicals have been reported to have potential hepatotoxicity, of which alkaloids and terpenoids are the two major categories (He et al., 2019). For example, there have been many reports of liver injury induced by pyrrolizidine alkaloids (PAs) (Wiesner, 2021; Steinhoff, 2021b). The toxicity of plants containing certain PAs has long been recognized in grazing animals and humans. In 2013, PAs in 221 herbal teas and herbal tea samples were analyzed by the German Federal Institute for risk assessment (BfR) [BfR (German Federal Institute for Risk Assessment), 2013], and the potential contamination of weeds containing PAs (such as *Senecio* species) to medicinal plant materials is being discussed. The herbal Medicinal Products Committee (HMPC) issued a public statement on the possible contamination of herbal products with PAs in 2016. In 2020, the HMPC recommended in its new draft public statement a daily intake of 1.0 μg of pyrrolizidine alkaloids per day for adults, including contamination of herbal products in 2020. Generally, exogenous contaminants are divided into three main groups, including metals, mycotoxins, and pesticide residues (Steinhoff, 2021a). Especially,

pesticides in CHMs can directly influence their safety and efficacy, while long-term exposure to pesticide residues may cause toxic chemicals to accumulate in the body. Chronic pesticide poisoning may lead to endocrine disorders, infertility, immunosuppression, carcinogenic, and teratogenic effects (Singh et al., 2018).

Due to the increasing scarcity of wild CHM resources, artificial planting has become the primary source of CHMs. Nearly half of the 600 common CHMs were artificially planted (Wei et al., 2015). The utilization of pesticides is inevitable in large-scale planting of CHMs due to the occurrence of diseases and insect pests. Pesticide residues seriously affect the quality and safety of CHMs and export trade, which is a matter of great concern for the international market (Zhang L. et al., 2012). In 2013, Greenpeace stated that pesticide residues were identified in 74% of CHM samples, and the amounts of residues in particular samples were several times the respective maximum residue limits (MRLs) established by the European Union (Greenpeace, 2013). They reached the conclusion that pesticide residues in CHMs pose health safety problems. The MRL is usually used to judge whether pesticide residues in the product meet the quality requirements. In the current (ChP Chinese Pharmacopoeia, 2020) edition (ChP Chinese Pharmacopoeia, 2020), the 33 banned pesticides were limited in plant medicinal materials; in the European pharmacopoeia 9th edition [EP (European Pharmacopiea), 2018] and the US pharmacopoeia 41st edition (USP The United States Pharmacopeia, 2018), the MRLs of 77 pesticides in herbal medicines were established. At present, the screening of pesticide residues in CHMs often involves hundreds of pesticide indicators, most of which have no MRL, making it difficult to determine whether they exceed the standard values. Moreover, the MRL is a product limit and not a safety limit (Wanwimolruk et al., 2015). Foods that contain pesticide residues beyond the recommended MRLs are not necessarily unsafe. In several instances, there is a margin between counted intake and health-based guidance values. Consumers intake level and consumption frequency are important factors affecting the conclusions of risk assessment.

As a main risk assessment method, exposure assessment is commonly used for evaluating the risk of chemicals in food and the environment. State agencies use the obtained data for making regulation policies. Short- and long-term risk assessments are commonly used in exposure assessments for acute and chronic risk analyses of CHM ingestion, respectively. Cumulative risk assessment is necessary to evaluate the accumulation of pesticides in CHMs because many herbs may be polluted by more than one pesticide, which may cause combined effects. In conjunction with dietary risk evaluation, an adequate scoring method would be beneficial for highlighting the chemical risk in food monitoring. The risk ranking scheme method, which was proposed by the British Veterinary Drug Residues Committee [VRC (The Veterinary Residues Committeee Matrix Ranking Subgroup), 2013], has been described in many studies (Nie et al., 2014; Fang et al., 2015; Li et al., 2015).

Previous risk assessment analyses have mainly been focusing on vegetables and fruits. Recently, researchers have paid more attention to systematic evaluation and risk analysis of several pesticides in Chinese herbs (Luo et al., 2021; Xiao J. J. et al., 2018; Xiao J. J. et al., 2018). The hazard quotient (HQ) and hazard index (HI) methods have been applied to evaluate the potential health risk of CHMs in recent research (Wu et al., 2020). However, most of these studies refer to the food model without considering the consumption characteristics of CHMs. China is the biggest producer and exporter of CHMs. Therefore, the risk assessment and pollution situation of pesticides in CHMs are a great matter of concern in China as well as worldwide. At present, Chinese state agencies have realized the importance and urgency of enhancing pesticide regulation in CHMs. The goal of this research was to explore the contamination status and perform the risk assessment of pesticide residues in CHMs in China to provide monitoring suggestions for the CHM industry. The risk of exposure to pesticides in CHMs has been ranked by utilizing a matrix ranking process. Moreover, a risk assessment model applied for the characteristics of CHMs has been explored and proposed.

MATERIALS AND METHODS

Materials and Reagents

Pesticide standards were provided by the Ministry of Agriculture (Beijing, China), the National Institute for Food and Drug Control, and Dr. Ehrenstorfer GmbH, and all had >96% purity. The Carb/NH_2 SPE cartridge (500 mg, 6 ml), HLB SPE cartridge (500 mg, 6 ml), and PSA (40–63 μm, 60 Å) were acquired from Agela Technologies (Tianjin, China). QuEChERS (Quick, easy, cheap, effective, rugged, and safe) silica gel dispersive purge tubes (containing 300 mg C_{18}, 300 mg PSA, 90 mg GC-e, 300 mg Silica gel, and 900 mg anhydrous $MgSO_4$) used for dispersive solid-phase extraction analysis were from Shimadzu (Japan). Analytical sodium chloride, glacial acetic acid, and solvents were provided by Sinopharm Chemical Reagent Co., Ltd. (Shanghai, China). HPLC grade acetonitrile and acetone were from Fisher Scientific (United States).

Individual 100 μg/ml pesticide stock solutions were prepared in toluene or acetone and stored at −20°C until analysis. Mixtures of working standard solutions at a series of concentrations were made by diluting aliquots of the stock mixture in acetonitrile.

Sample Collection

A Total of 1,017 samples, including 127 Ginseng radix rhizome (GR), 47 Lycii fructus (LF), 98 Houttuyniae herba (HH), 125 Ophiopogonis radix (OR), 105 Alismatis rhizome (AR), 35 Citri reticulatae pericarpium (CR), 155 Chuan Bei Mu (including *Fritillaria cirrhosa,* Fritillaria unibracteata, Fritillaria przewalskii, Fritillaria delavayi, Fritillaria taipaiensis, Fritillaria unibracteata) (FC), 175 Pinelliae rhizome (PR), 105 Gardeniae fructus (GF), and 45 Lonicerae japonicae flos (LJ) specimens, were collected in major production regions in China. The samples were purchased from cultivation regions, herbal markets, decoction companies, and pharmacies, representing almost all available channels for purchasing CHMs in China. Samples were 3 kg or more and categorized by quartering. Samples were kept at −20°C until analysis.

Sample Preparation

Method 1 (pretreatment of GR, LF, CR, and LJ samples): 5 g of the sample (powder) was accurately weighed into a 50 ml tube after homogenization; then, 3.0 g sodium chloride and 50 ml acetonitrile were added into the centrifuge tube. After shaking for 2 min, the mixture was centrifuged at 4,000 rpm for 5 min. The upper layer was moved to another 50 ml centrifuge tube. Next, 50 ml acetonitrile was added into the residue of the crude extract and vortexed for 2.0 min, after which the supernatant was combined and transferred into a round-bottom flask and evaporated at 40°C till near dryness. The resulting residue was dissolved in 10.0 ml acetonitrile. Totally, 2.0 ml extract was then loaded into a Carb/NH_2 column, which was prepared using 5 ml of acetonitrile: toluene 3:1 (v/v). The extract solution was passed through the column at a flow rate of 1 ml min^{-1}. The retained analytes were eluted with 20 ml of acetonitrile: toluene 3:1 (v/v). The collected eluate was evaporated at 40°C to near dryness. Finally, the residue was redissolved in 5.0 ml acetonitrile for analysis.

Method 2 (pretreatment of HH, OR, AR, FC, PR, and GF samples): 3 g of the homogenized sample was accurately weighed into a 50 ml centrifuge tube, and 15 ml of deionized water (containing 1% acetic acid) was added and evenly vortexed. After incubation at room temperature for 30 min, 15 ml acetonitrile was added and vortexed for 5 min and immediately cooled in an ice-water bath for 30 min. A WondaPak QuEChERS extraction package containing anhydrous magnesium sulfate ($MgSO_4$, 6 g) and anhydrous CH_3COONa (1.5 g) was added; then, the tube was vigorously vortexed for 5 min and immediately cooled in an ice-water bath for 10 min. The tube was centrifuged at 8,000 rpm for 5 min to separate the two layers. For further cleanup, 8 ml of the supernatant was transferred to a 15 ml WondaPak QuEChERS Silica gel dispersive purge tube. The mixture was vigorously vortexed for 5 min and centrifuged at 8,000 rpm for 5 min. Then, the supernatant was filtered through a 0.22 μm nylon organic filtration for analysis.

Sample Analysis

UPLC-MS/MS

A Waters Acquity UPLC instrument interfaced with a XEVO Triple Quad mass spectrometry system (Waters Co., United States) was used for sample analysis. Separation was carried out on a 2.10 × 100 mm column (ACQUITY UPLC BEH C_{18} column; Waters). The mobile phase included solutions A (5 mM ammonium formate and 0.1% formic acid in water) and B (5 mM ammonium formate and 0.1% formic acid in 95% methanol); the following gradient was applied at a flow rate of 0.4 ml min^{-1}: 0–0.8 min, 20% B; 0.8–11.0 min, 20–100% B; 11.0–13.0 min, 100% B; 13.0–14.0 min, 100–20% B; 14.0–18.0 min, 20% B. The injection volume was 1 μl. The drying gas flow was at 8 L/min, and the oven temperature was 30°C. Detection was performed in the multiple reaction monitoring (MRM) modes, operated in the electrospray positive/negative ionization mode (ESI^+/ESI^-). Instrument parameters were optimized to improve sensitivity, and the source temperature, cone voltage, desolvation gas flow, cone gas flow, and desolvation temperature were set at 150°C, 30 V, 900 L/Hr, 50 L/Hr, and 500°C, respectively.

GC-MS/MS

A Shimadzu gas chromatograph equipped with a tandem mass spectrometer quadrupole QP2010 (EI source) was used to perform analysis with a DB-17MS capillary column (30 m length × 0.25 mm id × 0.25 mm film thickness). The oven temperature was programmed at 60°C for 2 min, after which it was gradually increased to 150°C at a rate of 15°C/min and to 280°C at 6°C/min, held for 8 min. The inlet temperature was 250°C. The injection volume was at 1 μl in the splitless mode. The carrier gas was helium, used at a flow rate of 1.0 ml/min. The mass spectrometer was operated in the MRM mode with nitrogen as the collision gas at a flow rate of 1.5 ml/min. The temperatures of the ion source and transfer lines were 230°C and 280°C, respectively. The solvent delay was set at 6.0 min.

Health Risk Assessment

Chronic and Acute Intake Risk Assessments

Oral exposures to pesticide residues in CHMs were estimated by combining the concentration data with consumption data for CHMs. Body weight data were obtained from WHO statistics [WHO (World Health Organization), 2016]. The acceptable daily intake (ADI) and acute reference dose (ARfD) were obtained from the JMPR database [WHO (World Health Organization), 2017]. The resulting dietary exposure estimate was then compared with relevant toxicological reference values (such as ADI or ARfD) for the pesticides of concern. Assessments were undertaken for chronic (long-term) or acute (short-term) exposures. The chronic hazard quotient (HQc) and the acute hazard quotient (HQa) were used to evaluate the chronic and acute dietary exposure risks, respectively. HQc and HQa were calculated according to **Eq. 1**, **2**, respectively:

$$HQc = \frac{R \times CR \times EF \times Ed}{bw \times AT \times ADI} \quad (1)$$

where R is the average residue level of the pesticide in the sample (mg/kg); *CR* is the average CHM consumption (kg/day); EF is the exposure frequency, which was 90 days per year based on the previous investigation; Ed represents the exposure time, which was 20 years according to the questionnaire results; and AT is the average time, which was always equal to life expectancy, 365 days/year × 70 years; bw is the average body weight of Chinese adults (63 kg). When HQc <1, the risk was considered acceptable; at HQc >1, an unacceptable risk was considered; the higher the value, the higher the risk

$$HQa = \frac{HR \times LP}{bw \times ARfD} \quad (2)$$

where HR is the highest residue and LP is the large portion (kg). At HQa <1, the risk does not constitute a health threat in the short term. Conversely, when HQa is higher than 1, an unacceptable risk is considered; the higher the HQa value, the greater the acute risk exposure.

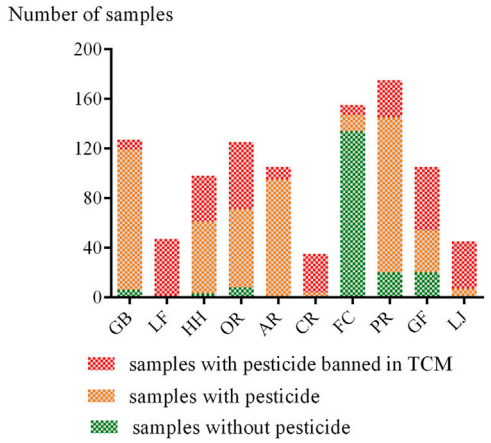

FIGURE 1 | Pesticide residues in various CHMs.

When carrying out exposure assessments, the percentage of left-detected numbers in the data set of residue concentration is vital. Treatment and calculation of these values may affect the assessment results (Ooijen et al., 2009). In this study, residue concentrations lower than LOQs were treated as 0.5 × LOQ according to WHO recommendations and seemed acceptable (GEMS/food Global Environment Monitoring System, 2016).

Cumulative Risk Assessment

The hazard index (HI) is a parameter used for cumulative risk assessment (Asante Duah, 1998; Li et al., 2018), which is expressed as the sum of HQc values for each pesticide in the sample according to **Eq. 3**. The HI measurement is clear, understandable, and directly related to the reference dose value. As a quick and simple method, the HI measurement has been used in primary cumulative risk assessment of various sample types such as air (Xiao et al., 2015), soil (Chang et al., 2014), and food (Lyulyukin et al., 2018). In this study, the HI approach was applied to evaluate the cumulative risk of pesticides in CHMs

$$HI = \sum_{i=1}^{n} HQc \tag{3}$$

where n is the total number of pesticides. At HI > 1, the CHMs involved should be considered a risk to the consumers; meanwhile, HI < 1 indicates that the CHMs involved are considered acceptable in the long term.

Risk Scoring System

Pesticide residue risk score (TS) is a mixture of toxicity and exposure scores. The toxicity score is composed of distinct values for A and B, while the exposure score encompasses four distinct scores for C, D, E, and F. TS is calculated by **Eq. 4**:

$$TS = (A + B)' (C + D + E)' F \tag{4}$$

where A represents toxicity, as acquired through the Ministry of Agriculture website at the People's Republic of China (ICAMA Institute for the Control of Agrochemicals, MOA of China, 2017); B represents potency pesticide score; C is a score for the percentage of CHMs in a diet; D represents a score for the incidence of pesticide use through planting; E represents a score for the amount of highly exposed population; F is a score for pesticide levels. The higher the mean amount of pesticide residual risk score, the higher the risk.

RESULTS

Method Validation

The in-house validation data fulfilled the requirements of the European SANTE/12830/2021 Guideline (European Commission, 2020). This was carried out by the investigation of the following parameters: limit of quantitation (LOQ), precision, linearity, accuracy, and matrix effect (ME). The LOQ for each pesticide was calculated as the lowest concentration of the target compound producing a signal-to-noise ratio (S/N) of 10. The accuracy and precision of the method were assessed by recovery experiments with three replicates spiked at three levels (LOQ, 5 × LOQ and 10 × LOQ). Linearity was studied by using matrix-matched calibration. The ME was obtained by comparing the signal intensity of the standard with and without the matrix at the same concentration.

The linearity of the matrix-matched calibration curve was good for all the pesticides in related concentration ranges, with correlation coefficients (r^2) greater than 0.99. The values of LOQ were well below the MRLs in vegetables and teas established by the Ministry of Agriculture of China (GB 2763-2019, 2019). The recoveries for all detected pesticides were in the range of 65.4–118.7% (RSD≦20%), indicating that the method may meet the detection requirements. The results showed that most pesticides exhibited different ME levels in 10 kinds of herbs. Thus, a matrix-matched calibration standard solution was used for quantification to avoid the inaccuracy of quantitative caused by ME.

Pesticide Residues Identified in CHM Samples

Among the 168 detected pesticides, 84 were detected in the 1,017 samples, including 17 banned pesticides, which suggests that some farmers were still using these pesticides; alternatively, the residues of pesticides used in previous years were still high in amounts and effective in the soil. Although banned pesticides have been detected in CHMs, according to the ChP Chinese Pharmacopiea (2020) version, only 25 batches of samples exceeded the MRLs, with an unqualified rate of 2.5%. Among them, carbendazim was the most frequently detected compound (35.7%). Carbendazim is a fungicide widely used in CHMs as well as in fruits and vegetables in China, which can effectively control many diseases caused by fungi. The frequencies of detection (%) in total samples were as follows: carbendazim (35.7%) > chlorpyrifos (34.1%) > paclobutrazol (26.7%) > difenoconazole (20.5%) > tebuconazole (18.5%) > acetamiprid (17.7%) > carbofuran (17.0%) > cypermethrin (16.0%) > imidacloprid

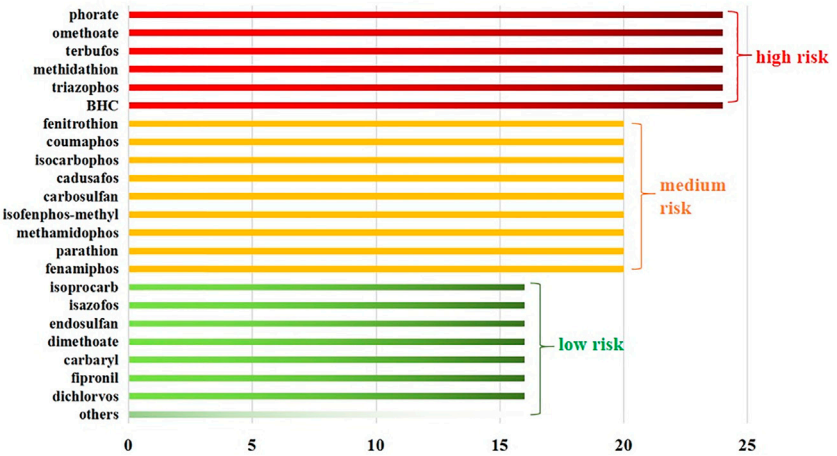

FIGURE 2 | Risk scoring of 84 detected pesticides in CHMs.

(15.0%) > pentachloronitrobenzene (PCNB, 14.6%). The residue levels ranged from 0.001 mg kg^{-1} to 38.316 mg kg^{-1}. Among them, compounds with concentrations <0.020 mg kg^{-1} were 60.5%; those with a concentration range of 0.020–0.500 mg kg^{-1} were 32.3%, and pesticides with levels >0.500 mg kg^{-1} were 7.2%, indicating that most of the pesticide residues were detected in low amounts. The detection rates and detailed concentration ranges of pesticides are provided in Supporting Information (**Supplementary Material S1**).

Of the 1,017 analyzed samples, 110 (10.8%) were residue-free, 134 (13.2%) contained one pesticide, and 773 (76.0%) contained multiple residues. The overall rate of samples containing multi-pesticide residues was higher than the rate of samples with no or single residue. We also found that samples contaminated with more than four detectable pesticides amounted to 49.1%, indicating that many CHMs were exposed to multi-pesticide conditions. Besides, multi-pesticide residues in samples are usually a combination of one or two fungicides and one or two insecticides. The detection rate of pesticides in each Chinese herb, including the detection rate of banned pesticides is shown in **Figure 1**. The results showed that the detection rates of pesticides in CR, LF, LJ, and AR were the highest (up to 100%). We also found that the detection rates of banned pesticides in LF, CR, LJ, and GF were relatively high, above 50%.

Intake Risk Assessment

Long-Term Consumer Exposure

The HQc values for pesticides detected in 10 CHMs are shown in **Supplementary Material S2**. The HQc values were 2.0 × 10^{-6}–7.86 × 10^{-2} for GR, 1.0 × 10^{-6}–4.61 × 10^{-3} for LF, 1.0 × 10^{-6}–2.93 × 10^{-2} for HH, 4.0 × 10^{-6}–1.08 × 10^{-3} for OR, 7.0 × 10^{-6}–0.124 for AR, 7.0 × 10^{-6}–3.02 × 10^{-2} for CR, 7.0 × 10^{-6}–3.12 × 10^{-3} for FC, 4.0 × 10^{-6}–3.75 × 10^{-3} for PR, 4.0 × 10^{-6}–3.47 × 10^{-3} for GF, and 4.0 × 10^{-6}–1.63 × 10^{-2} for LJ. Overall, for chronic exposure risk assessment, the HQc values were notably lower than 1, which indicated that long-term exposure of consumers to pesticide residues through the consumption of each of the 10 kinds of CHMs may not raise health concerns. Among the detected pesticides, the highest average value of HQc was obtained for triazophos, that is, 0.024 (mainly due to the high level of triazophos residues detected in AR). It was followed by PCNB at 0.016 and chlorpyrifos at 0.012.

Short-Term Consumer Exposure

Acute exposure risk assessment of 37 kinds of pesticides (including 2,4-D butylate, diflubenzuron, pyridaben, DDT, paclobutrazol, trifluralin, hexaflumuron, thiophanate-methyl, isofenphos-methyl, metalaxyl, BHC, chlorantraniliprole, permethrin, isazofos, cyprodinil, azoxystrobin, pyrimethanil, propargite, bitertanol, propamocarb hydrochloride, isocarbophos, quintozene, phoxim, omethoate, etoxazole, diethofencarb, iprodione, butralin, fludioxonil, tolclofos-methyl, metsulfuron-methyl, propoxur, prometryn, piperonyl butoxide, uniconazole, coumaphos, and fenobucarb) could not be performed since ARfD values were non-detected for these compounds or because there were no related records in the JMPR database. HQa values for the pesticides detected are provided in **Supplementary Material S2**. The maximum residue concentrations and consumption of CHMs were used for the determination of the worst-case scenario. The results showed that the HQa values were 3.0 × 10^{-6}–1.35 × 10^{-3} for GR, 2.9 × 10^{-5}–1.70 × 10^{-2} for LF, 6.0 × 10^{-6}–0.179 for HH, 3.0 × 10^{-6}–3.33 × 10^{-3} for OR, 3.0 × 10^{-6}–1.125 for AR, 3.3 × 10^{-5}–0.239 for CR, 8.0 × 10^{-6}–8.33 × 10^{-3} for FC, 1.6 × 10^{-5}–7.18 × 10^{-5} for PR, 2.0 × 10^{-6}–6.29 × 10^{-2} for GF, and 3.0 × 10^{-6}–3.83 × 10^{-2} for LJ. Except for triazophos with a HQa in AR of 1.12, the remaining pesticides had HQa values far below 1 and within the acceptable levels.

Risk Scoring for the Detected Pesticides in CHMs

A comprehensive analysis revealed that the 84 detected pesticides could be classified into three categories according to the total score determined by the matrix ranking scheme (**Figure 2**). Six pesticides (7.1%) had a total score of or above 24 and were

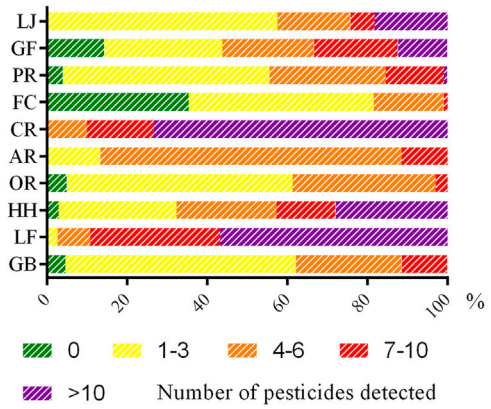

FIGURE 3 | Distribution of pesticides in various CHMs.

considered to potentially pose a high risk in this study. Their shared feature was high toxicity, while some could induce carcinogenicity as well as reproductive and developmental toxicity. Based on the total score, 10.7 and 82.1% of the pesticides were classified into the medium-risk and low-risk groups, respectively. The calculation process of the score has been provided in the Supporting Information (**Supplementary Material S3**).

Cumulative Dietary Risk Assessment

As described in 3.2, there were 773 samples (76.0%) with multiple pesticide residues. The human body acts as a final accumulator of chemical pollutants, which can lead to health problems (Graillot et al., 2012). When two or more chemicals or other substances cause common toxicity through the same or similar main biochemical event sequence, a common toxicity mechanism can be determined. Therefore, it is necessary to analyze the cumulative risk of pesticide residues in CHMs.

We calculated the HI values for 10 CHMs and found 0.093 for GR, 0.022 for LF, 0.069 for HH, 0.004 for OR, 0.228 for AR, 0.165 for CR, 0.005 for FC, 0.006 for PR, 0.012 for GF, and 0.044 for LJ. These results indicated that the cumulative intake of multiple pesticides through the consumption of CHMs was not likely to pose a health risk to consumers.

DISCUSSION

Selection of CHMs and Pesticide Indexes

A total of 10 herbs that are widely used and sold on the market were selected in this study. These 10 herbs not only have therapeutic effects but also can be used as health products in daily life. They are very representative of CHMs: GR and OR are root medicinal materials; AR, FC, and PR are stem medicinal materials; LF and GF are fruit medicinal materials; LJ is a flower medicinal material; HH is a whole plant; and CR is a fruit peel. In addition, the genuine areas of the 10 selected herbs are distributed all over the country; the medicinal parts of the selected herbs are from the underground part to the aboveground part, and the growing environments vary from a low altitude to a high altitude. The representativeness of samples has a great influence on the accuracy of risk assessment results. The varieties of CHMs selected in this study have a good reference value for reflecting the pesticide residues of CHMs in China.

In the early stages of this study, a large number of field investigations were conducted on these 10 medicinal herbs, the pests, and common diseases, and the used pesticides are well studied and understood. At the same time, referring to the relevant guidance of the Ministry of Agriculture on high-toxicity and high-residue pesticides, 168 pesticides were finally selected as detection indexes. The 168 tested pesticide indicators are very representative and mainly include most pesticides that are banned in China as well as the pesticide varieties commonly used in the cultivation of CHMs.

Risk Assessment of Pesticides in Different Medicinal Positions

In this study, the pesticide pollution of different medicinal parts substantially varied. Pesticide residues were more frequently detected in the whole grass or some aboveground herbs (such as flowers and fruits) compared with other medicinal parts. CHMs are summarized in **Figure 3**. The results revealed the presence of four or more pesticides in samples: CR accounted for 100%, and LF accounted for 97%; meanwhile, GR and OR accounted for only 38 and 36%, respectively. A total of 10 or more pesticides were detected in samples, with CR accounting for 73%, LF accounting for 57%, and GR and OR accounting for 0%. In particular, 22 pesticides were detected in one batch of CR samples. This may be due to the large contact area of this medicinal material when spraying pesticides in the planting process. It also suggests that certain CHM samples, including flowers and fruits, tend to be susceptible to a variety of diseases and insect pests in the planting process, which is why growers need to apply different pesticide varieties.

There were also differences in the types of pesticides detected in various medicinal parts. We divided 10 medicinal materials into two categories: the rhizome and aerial part. Then, the distribution of pesticides with a detection rate of more than 5% in both herb categories was analyzed. The results indicated that the detection rate of insecticides in the aboveground parts of herbs was relatively high, for example, carbofuran, fenpropathrin, cypermethrin, fenvalerate, etc., while root and rhizome herbs were more likely to be polluted by organochlorine and plant growth regulators, which might be due to the long-term contact with soil in the cultivation process. The pesticides in the soil absorbed by plants mainly originate from the pesticides sprayed on this soil before, rather than the horizontal transfer process, which is defined as the component release by donor plants and intake by the roots of acceptor plants (Selmar et al., 2019). Recent studies have outlined that alkaloids, including PAs, are transferred from living donor plants to the nearby plants.

Uncertainty Analysis

In most instances, the median residue value of pesticides is lower than the mean value in CHMs. In most international institutions, the average value is preferred in the assessment of chronic exposure of most pollutants [EFSA (European Food Safety

Authority), 2009; FAO (Food and Agriculture Organization)/WHO (World Health Organization), 2011]. If the median is selected as average consumption, the possibility of individuals in the population contacting high-pollution food in their lifetime might be negligible due to median values not being affected by high-pollution samples. Moreover, the human body should have the opportunity to take in food at each pollution level during the lifetime, so the average value is closer to the average levels in relation to the human body's lifetime intake of pollutants. In this study, the average concentration was used because it is suitable and conservative for estimating the worst-case scenario.

How to accurately evaluate the acute intake risk of pesticide residues remains an unresolved issue. Studies have used the P99.5 for acute risk evaluation (Zhang Z. H. et al., 2012), while others used a P97.5 instead (Zhao et al., 2013). In this study, the maximum residue concentration was used for HQa assessment. Different results would be obtained in two case scenarios based on the HR value at the maximum point or at the P97.5 in the short-term risk assessment. The acute exposure risk of triazophos in AR was 1.12, which indicated that the acute risk from pesticide exposure via AR consumption was unacceptable in the short term. However, the acute exposure risk of triazophos in AR was notably decreased to an acceptable value of 0.87 when a P97.5 value was used for the calculation.

The daily consumption ranges of these 10 herbs were described by the Pharmacopoeia of the People's Republic of China. When enough accurate consumption data are available, risk assessment results are more accurate. The daily consumption ranges of these 10 herbs were 5–25 g. Thus, 0.015 kg/d (median value) and 0.025 kg/d (max value) were used as the average and maximum consumption levels, respectively. In risk assessment of pesticides in CHMs, consumers are considered to take CHMs during the lifetime in the calculation of chronic exposure assessment (Luo et al., 2021; Xiao J. et al., 2018). It is more conservative because it is not taking the frequency of CHM consumption into consideration. To obtain more accurate risk assessment results, realistic consumption of CHMs should be considered in exposure assessment. From 2017 to 2018, a questionnaire survey about the consumption of CHMs was conducted in two cities (Beijing and Chongqing) and nine provinces in China. A total of 20,917 volunteers (11,497 women and 9,420 men) participated in the survey. Among these volunteers, the age range was 18–70 years. Among these volunteers, 72.63% were 18–44 years old, 19.51% were 45–59 years old, 7% were 7 years old, and 7.86% were over 60 years old. There are 11,358 urban residents and 9,559 rural residents who participated in the survey. According to the questionnaire data, the duration of P95 CHM intake was 90 days per year, and the exposure time was 20 years (Zuo et al., 2019). In the present study, the frequency of CHM consumption and exposure duration were used in chronic exposure assessment to make the results closer to the real situation.

It is important to note that the dietary risk in this study came from the consumption of raw products; thus, the processing factor (PF) was defaulted to 1. It would led to higher or lower estimations of the risk of pesticides in CHMs without consideration of PF. There are many studies on PF in food health risk assessment (Yigit and Velioglu, 2020). However, the processing of CHMs is different from that of food, for example, Chinese patent medicines containing ginseng are mostly processed by water decoction or 75% ethanol extraction. The transfer rate of pesticides may vary greatly under different processing conditions. According to our previous study (Wang et al., 2019), the transfer rate of PCNB in ginseng after water decoction is less than 1%, while the transfer rate of PCNB is as high as 95% with 75% ethanol extraction. The PFs of pesticides in CHMs will be further studied and included into the exposure assessment model to improve the accuracy of the assessment.

Guidelines and Pesticide Use Advice

In this study, the HI method was used in the chronic, acute, and cumulative risk assessment of pesticides in CHMs. Risk assessment studies examining pesticides in CHMs refer to the food model. However, in view of the significant differences between CHMs and food, it is very important to explore crucial parameters for pesticide risk assessment in CHMs. The National Medical Products Administration (NMPA) has been committed to such research. Through a large number of questionnaires associated with CHM consumption characteristics, the risk assessment model for pesticides in CHMs was proposed. In China, we established a health risk assessment model for pesticides in CHMs for the first time, which is a realistic and refined model applicable to CHMs. To better monitor the safety of CHMs, the "Guidelines for risk assessment of exogenous harmful residues in Chinese herbal medicine" were proposed by our study and published in the 2020 edition of the Chinese Pharmacopoeia. Meanwhile, the guidelines have been submitted to the International Regulatory Cooperation for Herbal Medicines (IRCH) of the WHO. The guidelines we proposed have been applied to assess the risk of heavy metals in CHMs (Zuo et al., 2020). These guidelines are of great significance in assessing the risk of pesticide residues in CHMs and provide data support for the formulation of pesticide regulatory policies in CHMs.

The risk ranking scheme method considers toxicity as a risk of greater importance; that is, pesticide toxicity has a leading role in the score. In addition, another advantage is that the risk score can also be calculated for pesticides that lack ADI values or have carcinogenic effects. Of the high-risk and medium-risk pesticides examined in this study, 80% were banned by the Ministry of agriculture of China. Although exposure to pesticide residues in most tested CHMs was below dangerous levels, the present results showed that banned pesticides with relatively high detection rates may pose the highest risk, indicating that more strict control management should be carried out for banned pesticides. In addition, while planting traditional Chinese medicine herbs, the usage history and residual background of soil should be investigated in advance to prevent the CHMs from being polluted.

CONCLUSION

We investigated pesticide residues in 1,017 samples of 10 CHMs and assessed potential health risk to inhabitants. The results of health risk assessment, including chronic, acute, and cumulative risk assessment, indicated that the consumption of CHMs is unlikely to pose a health risk to consumers. The risk ranking score obtained in this study showed that phorate, BHC, triazophos,

methidathion, terbufos, and omethoate, three of which are prohibited in CHM planting in China, pose a relatively high risk. Consequently, more strict supervision of banned pesticides is essential to ensure the safety of CHMs. We also found that the pesticide pollution of different medicinal parts substantially varied. Pesticide residues were more frequently detected in the whole grass or some aboveground herbs (such as flowers and fruits) compared with other medicinal parts. Moreover, the detection rate of insecticides in the aboveground parts of herbs was relatively high, while root and rhizome herbs were more likely to be polluted by organochlorine and plant growth regulators. Furthermore, a health risk assessment model for pesticide residues in CHMs was established in this study. The proposed model involved the realistic exposure frequency and exposure duration of CHMs, which makes the health risk of pesticides in CHMs more scientific and accurate.

DATA AVAILABILITY STATEMENT

The original contributions presented in the study are included in the article/**Supplementary Material**, further inquiries can be directed to the corresponding authors.

AUTHOR CONTRIBUTIONS

The contributions of various authors were as follows: YW, SM, and HJ: study conception and design. YG, YW, ZG, CL, YL, and MS: data acquisition and analysis. YW, LZ, and LS: manuscript drafting. ZW, FW, JZ, and LG: manuscript revision.

FUNDING

This study was supported by the "13th Five-Year Plan" and "Creation of Major New Drugs" as well as "The study on EU registration of compound Chinese medicine" (NO. 2018ZX09303-024) from the Important Program of Ministry of Science and Technology of the People's Republic of China.

ACKNOWLEDGMENTS

Many people have made invaluable contributions both directly and indirectly to this research. The authors thank the Chinese Pharmacopoeia Commission for organizing this research project and providing research ideas. The authors are grateful to the data provided by the Sichuan Institute for Food and Drug Control and Guangzhou Institute for Drug Control.

SUPPLEMENTARY MATERIAL

The Supplementary Material for this article can be found online at https://www.frontiersin.org/articles/10.3389/fphar.2021.818268/full#supplementary-material

REFERENCES

Asante-Duah, D. K. (1998). *Risk Assessment in Environmental Management*. United States: John Wiley & Sons.

BfR (German Federal Institute for Risk Assessment) (2013). Pyrrolizidine Alkaloids in Herb Teas and Teas. Statement 018/2013 of the BfR of 05. Available at: www.bfr.bund.de. https://mobil.bfr.bund.de/cm/343/pyrrolizidinalkaloide-in-kraeutertees-und-tees.pdf (Accessed July 5, 2013).

Chang, J. W., Chen, C. Y., Yan, B. R., Chang, M. H., Tseng, S. H., Kao, Y. M., et al. (2014). Cumulative Risk Assessment for Plasticizer-Contaminated Food Using the hazard index Approach. *Environ. Pollut.* 189, 77–84. doi:10.1016/j.envpol.2014.02.005

ChP (Chinese Pharmacopiea) (2020). *No.0212 General Rules for Medicinal Materials and Decoction Pieces*. 2020 Edition. China Medical Science Press: Beijing, China, 29–31.

Danan, G., and Teschke, R. (2016). RUCAM in Drug and Herb Induced Liver Injury: The Update. *Int. J. Mol. Sci.* 17, 14. doi:10.3390/ijms17010014

Domitrović, R., and Potočnjak, I. (2016). A Comprehensive Overview of Hepatoprotective Natural Compounds: Mechanism of Action and Clinical Perspectives. *Arch. Toxicol.* 90, 39–79. doi:10.1007/s00204-015-1580-z

EFSA (European Food Safety Authority) (2009). Scientific Opinion of the Panel on Contaminants in the Food Chain on a Request from the European Commission on Cadmium in Food. *EFSA J.* 980, 43–44. doi:10.2903/j.efsa.2008.689

EP (European Pharmacopiea) (2018). *Pesticide Residue*. 0th Edition. Strasbourg, France, 286–288.

European Commission, (2020) Guidance Document on Pesticide Analytical Methods for Risk Assessment and Post-approval Control and Monitoring Purposes SANTE/2020/12830[S]. Available at: https://ec.europa.eu/food/system/files/202102/pesticides_mrl_guidelines_2020-12830.pdf (Accessed February 24, 2021).

Fang, L., Zhang, S., Chen, Z., Du, H., Zhu, Q., Dong, Z., et al. (2015). Risk Assessment of Pesticide Residues in Dietary Intake of Celery in China. *Regul. Toxicol. Pharmacol.* 73, 578–586. doi:10.1016/j.yrtph.2015.08.009

FAO (Food and Agriculture Organization/WHO (World Health Organization) (2011). Seventy-third Report of the Joint FAO/WHO Expert Committee on Food Additives[R]//Evaluation of Certain Food Additives and Contaminants. Available at: https://apps.who.int/iris/handle/10665/44515 (Accessed January 16, 2011).

GB 2763-2019 (2019).National Food Safety Standard-Maximum Residue Limits for Pesticides in Food. Ministry of Agriculture of the People's Republic of China [S]. Beijing, China. Available at: http://www.nhc.gov.cn/sps/s7891/201908/63e76359a0144efb90d469071b608bf0.shtml (Accessed July 22, 2020).

GEMS/food Global Environment Monitoring System (2016). Food Contamination Monitoring and Assessment Programme. Available at: http://www.who.int/foodsafety/areas_work/chemical-risks/gems-food/en/(Accessed December 20, 2015).

Graillot, V., Takakura, N., Hegarat, L. L., Fessard, V., Audebert, M., and Cravedi, J. P. (2012). Genotoxicity of Pesticide Mixtures Present in the Diet of the French Population. *Environ. Mol. Mutagen* 53, 173–184. doi:10.1002/em.21676

Greenpeace (2013). Chinese Herbs: Elixir of Health or Pesticides Cocktail? Available at: http://www.greenpeace.org/international/Global/eastasia/publications/reports/foodagriculture/2013/chinese-herbs-pesticides-report.pdf (Accessed March 4, 2014).

He, S., Zhang, C., Zhou, P., Zhang, X., Ye, T., Wang, R., et al. (2019). Herb-Induced Liver Injury: Phylogenetic Relationship, Structure-Toxicity Relationship, and Herb-Ingredient Network Analysis. *Int. J. Mol. Sci.* 20, 3633. doi:10.3390/ijms20153633

ICAMA (Institute for the Control of Agrochemicals, MOA of China) (2017). China Pesticide Information Network. Available at: http://www.chinapesticide.gov.cn/hysj/index. jhtml (Accessed January 12, 2017).

Li, Z., Nie, J., Yan, Z., Cheng, Y., Lan, F., Huang, Y., et al. (2018). A Monitoring Survey and Dietary Risk Assessment for Pesticide Residues on Peaches in China. *Regul. Toxicol. Pharmacol.* 97, 152–162. doi:10.1016/j.yrtph.2018.06.007

Li, Z. X., Nie, J. Y., Yan, Z., Xu, G. F., Li, H. F., Kuang, L. X., et al. (2015). Risk Assessment and Ranking of Pesticide Residues in Chinese Pears. *J. Integr. Agric.* 14, 2328–2339. doi:10.1016/S2095-3119(15)61124-8

Luo, L., Dong, L., Huang, Q., Ma, S., Fantke, P., Li, J., et al. (2021). Detection and Risk Assessments of Multi-Pesticides in 1771 Cultivated Herbal Medicines by LC/MS-MS and GC/MS-MS. *Chemosphere* 262, 127477. doi:10.1016/j.chemosphere.2020.127477

Lyulyukin, M. N., Kolinko, P. A., Selishchev, D. S., and Kozlov, D. V. (2018). Hygienic Aspects of TiO2-Mediated Photocatalytic Oxidation of Volatile Organic Compounds: Air Purification Analysis Using a Total hazard index. *Appl. Catal. B: Environ.* 220, 386–396. doi:10.1016/j.apcatb.2017.08.020

Melchart, D., Hager, S., Albrecht, S., Dai, J., Weidenhammer, W., and Teschke, R. (2017). Herbal Traditional Chinese Medicine and Suspected Liver Injury: A Prospective Study. *World J. Hepatol.* 9 (9), 1141–1157. doi:10.4254/wjh.v9.i29.1141

Nabavi, S. F., Di Lorenzo, A., Izadi, M., Sobarzo-Sánchez, E., Daglia, M., and Nabavi, S. M. (2015). Antibacterial Effects of Cinnamon: From Farm to Food, Cosmetic and Pharmaceutical Industries. *Nutrients* 7, 7729–7748. doi:10.3390/nu7095359

Nie, J. Y., Li, Z. X., Liu, C. D., Fang, J. B., Wang, C., Guo, Y. Z., et al. (2014). Risk Assessment of Pesticide Residues in Apples. *Sci. Agric. Sin.* 47, 3655–3667. (in Chinese). doi:10.3864/j.issn.0578-1752.2014.18.013

Ooijen, H. J., Bakker, M., and van der Voet, H. (2009). Identification and Handling of Uncertainties in Dietary Exposure Assessment. Report 320103004/2009. Available at: https://www.researchgate.net/publication/37789070_Identification_and_handling_of_uncertainties_in_dietary_exposure_assessment National Institute for Public Health and the Environment (RIVM).

Pan, S.-Y., Litscher, G., Gao, S.-H., Zhou, S.-F., Yu, Z.-L., Chen, H.-Q., et al. (2014). Historical Perspective of Traditional Indigenous Medical Practices: The Current Renaissance and Conservation of Herbal Resources. *Evidence-Based Complement. Altern. Med.* 2014, 1–20. doi:10.1155/2014/525340

Piemontese, L. (2017). Plant Food Supplements with Antioxidant Properties for the Treatment of Chronic and Neurodegenerative Diseases: Benefits or Risks? *J. Diet. Suppl.* 14, 478–484. doi:10.1080/19390211.2016.1247936

Qing, X., Yutong, Z., and Shenggao, L. (2015). Assessment of Heavy Metal Pollution and Human Health Risk in Urban Soils of Steel Industrial City (Anshan), Liaoning, Northeast China. *Ecotoxicology Environ. Saf.* 120, 377–385. doi:10.1016/j.ecoenv.2015.06.019

Quan, N. V., Dang Xuan, T., and Teschke, R. (2020). Potential Hepatotoxins Found in Herbal Medicinal Products: A Systematic Review. *Int. J. Mol. Sci.* 21 (14), 1–18. doi:10.3390/ijms21145011

Selmar, D., Radwan, A., Hijazin, T., Abouzeid, S., Yahyazadeh, M., Lewerenz, L., et al. (2019). Horizontal Natural Product Transfer: Intriguing Insights into a Newly Discovered Phenomenon. *J. Agric. Food Chem.* 67 (32), 8740–8745. doi:10.1021/acs.jafc.9b03619

Singh, N. S., Sharma, R., Parween, T., and Patanjali, P. K. (2018). Pesticide Contamination and Human Health Risk Factor. *Mod. Age Environ. Probl. their Remediation*, 49–68. doi:10.1007/978-3-319-64501-8_3

Steinhoff, B. (2021a). Challenges in the Quality of Herbal Medicinal Products with a Specific Focus on Contaminants. *Phytochem. Anal.* 32 (2), 117–123. doi:10.1002/pca.2879

Steinhoff, B. (2021b). Pyrrolizidine Alkaloid Contamination in Medicinal Plants: Regulatory Requirements and Their Impact on Production and Quality Control of Herbal Medicinal Products. *Planta Med.* doi:10.1055/a-1494-3623

Teschke, R., Wolff, A., Frenzel, C., Eickhoff, A., and Schulze, J. (2015). Herbal Traditional Chinese Medicine and its Evidence Base in Gastrointestinal Disorders. *World J. Gastroenterol.* 21, 4466–4490. doi:10.3748/wjg.v21.i15.4466

Teschke, R., Eickhoff, A., Schulze, J., and Danan, G. (2020). Herb-induced Liver Injury (HILI) with 12,068 Worldwide Cases Published with Causality Assessments by Roussel Uclaf Causality Assessment Method (RUCAM): An Overview. *Transl. Gastroenterol. Hepatol.* 6, 51. doi:10.21037/tgh-20-149

USP The United States Pharmacopeia (2018). *Pesticide Residue Analysis*. 41th Edition. Washington, DC: US Pharmacopeia Origination Press, 6290–6292.

VRC (The Veterinary Residues Committeee Matrix Ranking Subgroup) (2013). Matrix Ranking for Prioritising Substances from the Non-Statutory Surveillance Scheme. Available at: http://www.vmd.defra.gov.uk/VRC/pdf/papers/2013/vrc1334.pdf (Accessed September 4, 2013).

Wang, G., Mao, B., Xiong, Z. Y., Fan, T., Chen, X. D., Wang, L., et al. (2007). The Quality of Reporting of Randomized Controlled Trials of Traditional Chinese Medicine: a Survey of 13 Randomly Selected Journals from mainland China. *Clin. Ther.* 29 (7), 1456–1467. doi:10.1016/j.clinthera.2007.07.023

Wang, Y., Li, Y. L., Yu, X. L., Wang, Z., Jin, H. Y., and Ma, S. C. (2019). Determination of Processing Factors of Quintozene in *Panax Ginseng* and Their Application in Dietary Exposure Assessment. *Chin. Trad. Patent. Med.* 41 (2), 368–373. (in Chinese). doi:10.19540/j.cnki.cjcmm.20190319.102

Wanwimolruk, S., Kanchanamayoon, O., Phopin, K., and Prachayasittikul, V. (2015). Food Safety in Thailand 2: Pesticide Residues Found in Chinese Kale (*Brassica oleracea*), a Commonly Consumed Vegetable in Asian Countries. *Sci. Total. Environ.* 532, 447–455. doi:10.1016/j.scitotenv.2015.04.114

Wei, J. H., Tu, P. F., Li, G., Wang, W. Q., Yang, C. M., and Sui, C. (2015). Situation and Trends in Development of Chinese Medicinal Agriculture in China. *Mod. Chin Med* 17, 94–100. (in Chinese). doi:10.13313/j.issn.1673-4890.2015.2.002

WHO (World Health Organization) (2016). Consultations and Workshops: Dietary Exposure Assessment of Chemicals in Food: Report of a Joint FAO/WHO Consultation. Available at: http://apps.who.int/iris/bitstream/10665/44027/1/9789241597470_eng.pdf(Accessed June 26, 2016).

WHO (World Health Organization) (2017). Inventory of Evaluations Performed by the Joint Meeting on Pesticide Residues (JMPR). Available at: http://apps.who.int/pesticide- residues-jmpr-database/Home/Range/All (Accessed September 15, 2017).

Wiesner, J. (2021). Regulatory Perspectives of Pyrrolizidine Alkaloid Contamination in Herbal Medicinal Products. *Planta Med.* doi:10.1055/a-1494-1363

Wu, P. L., Wang, P. S., Gu, M. Y., Xue, J., and Wu, X. L. (2020). Human Health Risk Assessment of Pesticide Residues in Honeysuckle Samples from Different Planting Bases in China. *Sci. Total. Environ.* 759, 142747. doi:10.1016/j.scitotenv.2020.142747

Xiao, J., Xu, X., Wang, F., Ma, J., Liao, M., Shi, Y., et al. (2018). Analysis of Exposure to Pesticide Residues from Traditional Chinese Medicine. *J. Hazard. Mater.* 365, 857–867. doi:10.1016/j.jhazmat.2018.11.075

Xiao, J.-J., Duan, J. S., Xu, X., Li, S. N., Wang, F., Fang, Q. K., et al. (2018). Behavior of Pesticides and Their Metabolites in Traditional Chinese Medicine Paeoniae Radix Alba during Processing and Associated Health Risk. *J. Pharm. Biomed. Anal.* 161, 20–27. doi:10.1016/j.jpba.2018.08.029

Xie, Y. J., Kong, W. J., Yang, M. H., and Yang, S. H. (2015). Research Progress of Chinese Herbal Medicine Raw Materials in Cosmetics. *Zhongguo Zhong Yao Za Zhi* 40 (20), 3925–3931. (in Chinese). doi:10.4268/cjcmm20152006

Yigit, N., and Velioglu, Y. S. (2020). Effects of Processing and Storage on Pesticide Residues in Foods. *Crit. Rev. Food Sci. Nutr.* 60 (21), 3622–3641. doi:10.1080/10408398.2019.1702501

Yu, Y. C., Mao, Y. M., Chen, C. W., Chen, J. J., Chen, J., Cong, W. M., et al. (2017). CSH Guidelines for the Diagnosis and Treatment of Drug-Induced Liver Injury. *Hepatol. Int.* 11, 221–241. doi:10.1007/s12072-017-9793-2

Zhang, L., Yan, J., Liu, X., Ye, Z., Yang, X., Meyboom, R., et al. (2012). Pharmacovigilance Practice and Risk Control of Traditional Chinese Medicine Drugs in China: Current Status and Future Perspective. *J. Ethnopharmacol.* 140, 519–525. doi:10.1016/j.jep.2012.01.058

Zhang, Z. H., Tang, T., Xu, H., Li, Z., Yang, G. L., and Wang, Q. (2012). Dietary Intake Risk Assessment of for Chlorfenuron Residue in Fruits and Vegetables. *Sci. Agric. Sin.* 45, 1982–1991. (in Chinese). doi:10.3864/j.issn.0578-1752.2012.10.011

Zhao, M., Wang, C., Li, T., Yi, N., He, X., Wu, H., et al. (2013). Acute Risk Assessment of Cumulative Dietary Exposure to Organophosphorus Pesticide

Among People in Jiangsu Province. *Wei Sheng Yan Jiu* 42, 844–848. (in Chinese). doi:10.19813/j.cnki.weishengyanjiu.2013.05.028

Zuo, T. T., Jin, H. Y., Zhang, L., Liu, Y. L., Nie, J., Chen, B. L., et al. (2020). Innovative Health Risk Assessment of Heavy Metals in Chinese Herbal Medicines Based on Extensive Data. *Pharmacol. Res.* 159, 104987. doi:10.1016/j.phrs.2020.104987

Zuo, T. T., Wang, Y., Zhang, L., Shi, S. M., Shen, M. R., Liu, L. N., et al. (2019). Guideline of Risk Assessment of Exogenous Harmful Residues in Traditional Chinese Medicines. *Chin. J. Pharm. Anal.* 39, 1902–1907. (in Chinese). doi:10.16155/j.0254-1793.2019.10.20

Conflict of Interest: The authors declare that the research was conducted in the absence of any commercial or financial relationships that could be construed as a potential conflict of interest.

Publisher's Note: All claims expressed in this article are solely those of the authors and do not necessarily represent those of their affiliated organizations or those of the publisher, the editors, and the reviewers. Any product that may be evaluated in this article or claim that may be made by its manufacturer is not guaranteed or endorsed by the publisher.

frontiers in Pharmacology

ORIGINAL RESEARCH
published: 14 February 2022
doi: 10.3389/fphar.2022.842131

Identification of Medicinal *Bidens* Plants for Quality Control Based on Organelle Genomes

*Liwei Wu[1†], Liping Nie[1†], Shiying Guo[2†], Qing Wang[1], Zhengjun Wu[2], Yulin Lin[1], Yu Wang[1], Baoli Li[1], Ting Gao[3] and Hui Yao[1,4]**

[1]National Engineering Laboratory for Breeding of Endangered Medicinal Materials, Institute of Medicinal Plant Development, Chinese Academy of Medical Sciences and Peking Union Medical College, Beijing, China, [2]China Resources Sanjiu Medical & Pharmaceutical Co., Ltd, Shenzhen, China, [3]Key Laboratory of Plant Biotechnology in Universities of Shandong Province, College of Life Sciences, Qingdao Agricultural University, Qingdao, China, [4]Engineering Research Center of Chinese Medicine Resources, Ministry of Education, Beijing, China

OPEN ACCESS

Edited by:
Jian-Bo Yang,
National Institutes for Food and Drug Control (China), China

Reviewed by:
Komwit Surachat,
Prince of Songkla University, Thailand
Bo Wang,
Hubei Provincial Institute of Drug Control, China
Xu-Mei Wang,
Xi'an Jiaotong University, China

***Correspondence:**
Hui Yao
scauyaoh@sina.com

†These authors have contributed equally to this work and share first authorship

Specialty section:
This article was submitted to Experimental Pharmacology and Drug Discovery, a section of the journal Frontiers in Pharmacology

Received: 23 December 2021
Accepted: 18 January 2022
Published: 14 February 2022

Citation:
Wu L, Nie L, Guo S, Wang Q, Wu Z, Lin Y, Wang Y, Li B, Gao T and Yao H (2022) Identification of Medicinal Bidens Plants for Quality Control Based on Organelle Genomes. Front. Pharmacol. 13:842131. doi: 10.3389/fphar.2022.842131

Bidens plants are annuals or perennials of Asteraceae and usually used as medicinal materials in China. They are difficult to identify by using traditional identification methods because they have similar morphologies and chemical components. Universal DNA barcodes also cannot identify *Bidens* species effectively. This situation seriously hinders the development of medicinal *Bidens* plants. Therefore, developing an accurate and effective method for identifying medicinal *Bidens* plants is urgently needed. The present study aims to use phylogenomic approaches based on organelle genomes to address the confusing relationships of medicinal *Bidens* plants. Illumina sequencing was used to sequence 12 chloroplast and eight mitochondrial genomes of five species and one variety of *Bidens*. The complete organelle genomes were assembled, annotated and analysed. Phylogenetic trees were constructed on the basis of the organelle genomes and highly variable regions. The organelle genomes of these *Bidens* species had a conserved gene content and codon usage. The 12 chloroplast genomes of the *Bidens* species were 150,489 bp to 151,635 bp in length. The lengths of the eight mitochondrial genomes varied from each other. Bioinformatics analysis revealed the presence of 50–71 simple sequence repeats and 46–181 long repeats in the organelle genomes. By combining the results of mVISTA and nucleotide diversity analyses, seven candidate highly variable regions in the chloroplast genomes were screened for species identification and relationship studies. Comparison with the complete mitochondrial genomes and common protein-coding genes shared by each organelle genome revealed that the complete chloroplast genomes had the highest discriminatory power for *Bidens* species and thus could be used as a super barcode to authenticate *Bidens* species accurately. In addition, the screened highly variable region *trnS-GGA-rps4* could be also used as a potential specific barcode to identify *Bidens* species.

Keywords: *bidens*, species identification, super barcode, organelle genomes, quality control

1 INTRODUCTION

Bidens plants are annuals or perennials of Asteraceae. In China, this genus includes 10 species (Shi et al., 2011), five of which are medicinal plants recorded in different local standards for Chinese medicinal materials. *Bidens* plants have a long history of medicinal use in China (Chen et al., 2009). There are many kinds of compounds in the *Bidens* plants, including flavonoids, phenylpropanoids, triterpenoids, alkaloids and organic acids, of which flavonoids are the main effective components in the medicinal *Bidens* plants (Wang et al., 2010). Modern pharmacological studies show that these compounds in *Bidens* plants have antiinflammatory, analgesic, antibacterial, antitumor, hypolipidemic, and liver protection functions (Lin et al., 2013; Shandukani et al., 2018). However, some problems exist in the records of these medicinal plants in local standards. For example, their scientific names are inconsistent with their Chinese names and records in the Flora of China. *Bidens* plants commonly have homonyms and synonyms. Furthermore, they are difficult to identify by using traditional identification methods because they have similar morphologies and chemical components (Bartolome et al., 2013; Chen et al., 2013; Wang et al., 2014; Yang et al., 2020). Reports on the molecular identification of *Bidens* species are limited. Tsai et al. (2008) (Tsai et al., 2008) used the noncoding regions of the chloroplast genome (*trnL* intorn and *trnL-trnF*) and nuclear ribosomal DNA (ITS1, 5.8S and ITS2) to identify *Bidens* species and found that ITS1, 5.8S, ITS2 and the *trnL* intron could separate only *Bidens biternata* and *B. pilosa* var. *pilosa* from each other. Our preliminary experiments showed that the universal DNA barcodes ITS, ITS2 and *psbA-trnH* were all ineffective in identifying *Bidens* species. The difficulties encountered in the identification of *Bidens* species seriously hinder the development of medicinal *Bidens* plants and reduce their medicinal quality. An accurate and effective method for identifying medicinal *Bidens* plants is urgently needed.

The main content of phylogenomic studies includes the use of large-scale molecular data to investigate the phylogenetic relationships between organisms at the genomic level and the application of evolutionary relationships to study the evolutionary mechanisms of genomes, such as the process of DNA repair and the functional annotation of unknown genes (Delsuc et al., 2005). In general, plant cells contain three kinds of genomes, namely, the chloroplast, mitochondrial and nuclear genomes. The chloroplast and mitochondrial genomes are also called organelle genomes. The relative abundances of the three genomic DNA in cells show significant differences. For example, a leaf cell of the model plant *Arabidopsis thaliana* contains approximately 1,000 copies of chloroplast DNA, 100 copies of mitochondrial DNA and two copies of nuclear genomic DNA (Logan 2006). Given the important role of the chloroplast and mitochondrial genomes in phylogenetic and nucleo-cytoplasmic interactions, their sequence analysis is becoming increasingly important. The chloroplast is an organelle that plays an important role in plant photosynthesis (Clegg et al., 1994). The chloroplast genome is more conserved than the nuclear genome in terms of gene content and order and contains more variations than DNA barcodes. Therefore, the chloroplast genome is widely used in species identification and plant evolution studies. Zhang et al. (Zhang et al., 2019) found that the whole chloroplast genome could be used as a super barcode to identify *Dracaena* species. Chen et al. (Chen et al., 2018; Chen et al., 2019) successfully identified six *Ligularia* and three *Ephedra* herbs by using the chloroplast genome as a super barcode. A growing number of works have provided support showing that identifying related species by using the molecular markers of the chloroplast genome or the complete chloroplast genome as super barcodes is practicable. The mitochondrial genome, another important organelle genome, is usually similar to the chloroplast genome, which has a circular molecular structure. The mitochondrial genome is used in species identification because it is complex and highly variable with abundant noncoding regions and introns and a relatively fixed sequence (An et al., 2017; Park and Lee, 2020; Jeong and Lee, 2021). The mitochondrial genome of angiosperms could reveal the phylogenetic relationship between species and be used to investigate intraspecific differentiation (Fujii et al., 2010). However, the number of reported mitochondrial genomes is not as large as that of chloroplast genomes.

Studying organelle genomes is an essential way to analyse the genetic information of a species. The excavation of organelle genomes is helpful for analysing the inherent properties and changes of organelle genomes and thus contributes to the genetic evolution, identification and breeding research of various species. In addition, organelle genomes are important data sources for comparative genomics, phylogenetics and population genetics (Qian 2014). Organelle genomes are smaller and easier to sequence than nuclear genomes. In this work, we sequenced and analysed the 12 chloroplast and eight mitochondrial genomes of five species and one variety of *Bidens* to solve the difficulties encountered in the identification of *Bidens* species. Finally, we constructed phylogenetic trees by using different datasets and analysed the feasibility of identifying *Bidens* species on the basis of organelle genomes. This research could provide a foundation for the species identification, phylogeny, medication safety and plant resource protection of *Bidens*.

2 MATERIALS AND METHODS

2.1 DNA Sources

The DNA sources were the fresh leaves of *B. biternata*, *B. bipinnata*, *B. pilosa* var. *pilosa*, *B. pilosa* var. *radiata*, *B. parviflora* and *B. tripartita*. These species were identified by Prof. Yulin Lin from the Institute of Medicinal Plant Development (IMPLAD), Chinese Academy of Medical Sciences and Peking Union Medical College. Voucher specimens were deposited in the herbarium at IMPLAD. The ID numbers and collecting locations are shown in **Supplementary Table S1**. The total DNA of the species was extracted by using the DNeasy Plant Mini Kit (Qiagen Co., Germany), and DNA concentration and quality were assessed by using Nanodrop 2000C spectrophotometry and electrophoresis in 1% (w/v) agarose gel, respectively.

2.2 DNA Sequencing, Assembly and Annotation

The DNA was used to generate libraries with an average insert size of 350 bp and sequenced by using Illumina NovaSeq6000 in accordance with standard protocols, and the sequencing information was shown in **Supplementary Tables S2, S3**. Paired-end sequencing was performed to obtain 150 bp sequences at both ends of each molecule. Adapters and low-quality regions in the original data were trimmed by applying Trimmomatic software (Bolger et al., 2014). Reference organelle sequences from the family of Asteraceae were downloaded from NCBI genome resources (https://www.ncbi.nlm.nih.gov/genome). The gene sequences of each reference were extracted to build a custom database, and clean reads were mapped by using BWA 0.7.17 (Li and Durbin 2009). NOVOPlasty 4.2 (Dierckxsens et al., 2017) was used to assemble organelle genomes, which needed a sequence as the initial seed. For the chloroplasts, a read from the *psbA* gene was selected as the seed input, and the output chloroplast sequences were manually adjusted for the start position. For the mitochondria, seed reads from the conserved *cox* and *nad* genes were separately tested, and the output contigs were combined and manually linked to obtain the mitochondrial sequences. Then, clean reads were mapped back to the chloroplast and mitochondrial genomes and inspected in IGV (Robinson et al., 2017) to exclude any assembly error. Finally, a custom-made script that took the assembly and the bam files as input was utilised to correct ambiguous bases and generate the complete organelle genome sequences. The sequences were initially annotated by using the CPGAVAS2 software (Shi et al., 2019) and the GeSeq (Tillich et al., 2017) and corrected manually. tRNAs were annotated by using tRNAscan-SE software (Schattner et al., 2005). Genes, introns and coding region boundaries were compared with reference sequences. Then the borders of LSC, SSC and IR regions in the chloroplast genomes were validated by designing primers and polymerase chain reaction (**Supplementary Table S4**).

2.3 Structural Analyses

Chloroplast and mitochondrial genome maps were generated by using the Organellar Genome DRAW v1.2 (Lohse et al., 2007) and manually corrected. The CodonW software (Sharp and Li 1987) was adopted to analyse codon usage. Simple sequence repeats (SSRs) were detected by using the MISA (Beier et al., 2017) with the definition of ≥ 10 repeat units for mononucleotide SSRs, ≥ 5 repeat units for dinucleotide SSRs, ≥ 4 repeat units for trinucleotide SSRs, and ≥ 3 repeat units for tetranucleotide, pentanucleotide and hexanucleotide SSRs. Long repeated sequences were detected by using REPuter (Kurtz et al., 2001). Sequence homology analysis was carried out by using EMBOSS (Rice et al., 2000). The boundaries of the four regions of the chloroplast genomes were compared by applying IRscope (Amiryousefi et al., 2018).

2.4 Comparative and Phylogenetic Analyses

The chloroplast genomes of *Bidens* species were compared by using mVISTA software (Frazer et al., 2004). The nucleotide diversity (Pi) values of shared genes and intergenic spacers were calculated with DnaSP software (Librado and Rozas 2009). By combining the mVISTA results and Pi values, seven highly variable regions were screened out. The complete organelle genome sequences of Asteraceae species and common protein-coding genes shared by these genomes were used to construct maximum likelihood (ML) phylogenetic trees by utilising IQ-TREE (Nguyen et al., 2015) with a bootstrap of 1,000 repetitions. ML analysis was conducted based on the TVM + F + R4 (complete chloroplast genomes), TVM + F + I + G4 (complete mitochondrial genomes), TVM + F + R3 (common protein-coding genes shared by chloroplast genomes), and GTR + F + G4 (common protein-coding genes shared by mitochondrial genomes) models. MEGA software (Tamura et al., 2013) was used to construct Neighbor-joining (NJ) phylogenetic trees based on seven highly variable regions. NJ analysis was conducted based on the K2P model.

3 RESULTS

3.1 Organelle Genome Structure of *Bidens* Species

The 12 chloroplast genomes of these *Bidens* species showed a typical circular tetramerous structure and included two inverted repeats (IRs), a large single copy (LSC) and a small single copy (SSC) (**Figure 1A**). The lengths of the chloroplast genomes of the same species were the same or similar. The total lengths of the chloroplast genomes were 150,489 bp (*B. tripartita*) to 151,635 bp (*B. pilosa* var. *radiata*). The sizes of the LSC regions ranged from 83,499 bp (*B. tripartita*) to 83,899 bp (*B. biternata*). The sizes of the SSC regions varied between 17,628 bp (*B. tripartita*) and 18,439 bp (*B. pilosa* var. *radiata*). The sizes of the IR regions varied from 24,652 bp (*B. bipinnata*) to 24,701 bp (*B. pilosa* var. *radiata*). The total GC contents of the 12 chloroplast genomes were all 37.5%, indicating that the base composition of the *Bidens* species was relatively conserved (**Supplementary Table S5**).

The 12 chloroplast genomes were all annotated with 130 genes, including 85 protein-coding genes, 37 tRNA genes and eight rRNA genes (**Supplementary Table S6**). Amongst these genes, 17 were located in IR regions. They included six protein-coding genes (*ndhB*, *rpl2*, *rpl23*, *rps7*, *rps12* and *ycf2*), four rRNA genes (*rrn4*, *rrn4.5*, *rrn5* and *rrn16*) and seven tRNA genes (*trnA-UGC*, *trnI-CAU*, *trnI-GAU*, *trnL-CAA*, *trnN-GUU*, *trnR-ACG* and *trnV-GAC*). In addition, *ycf1* and *rps19* were annotated as pseudogenes. At the junctions, the gene positions in the boundary regions of the chloroplast genomes of the *Bidens* species were conserved. The difference was that the *ndhF* gene of *B. tripartita* was located at the boundary of the SSC and IRb regions, and the *ndhF* genes of the other five species were located in the SSC regions (**Figure 2**). Coding regions (protein-coding regions, tRNA genes and rRNA genes) accounted for 56.0–59.4% of the regions, and the rest were noncoding regions (pseudogenes, introns and gene spacers).

The eight mitochondrial genomes of these *Bidens* species all had a circular molecular structure (**Figure 1B**; **Supplementary Figure S1**) that ranged in length from 183 kb (*B. pilosa* var.

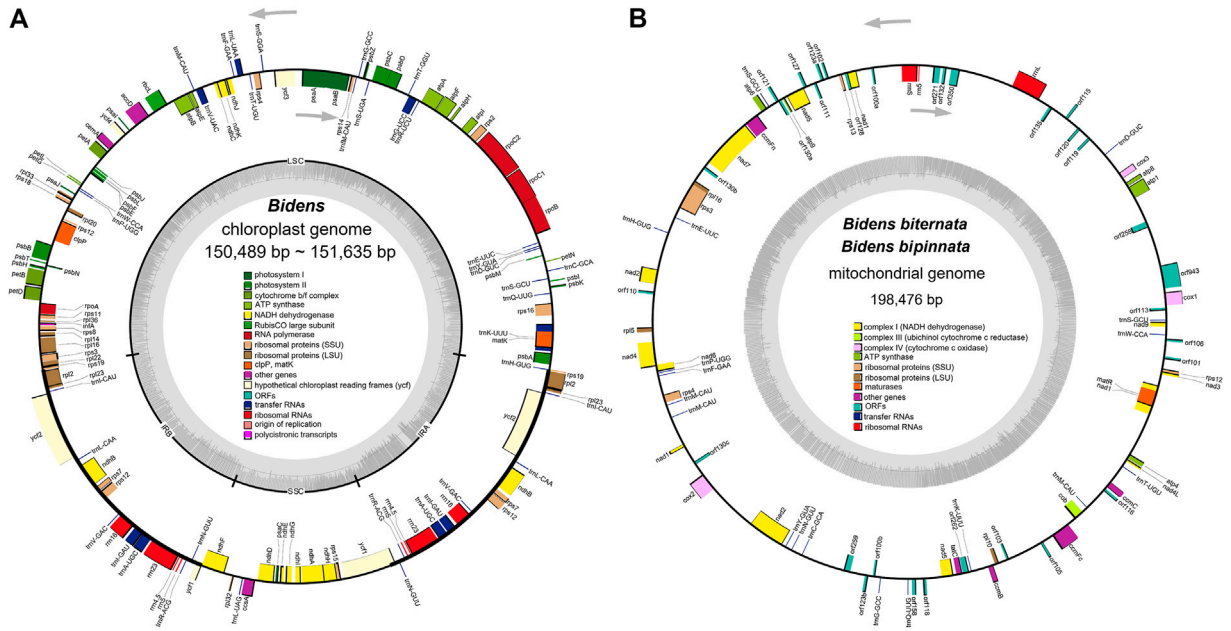

FIGURE 1 | Chloroplast **(A)** and mitochondrial **(B)** genome maps of *Bidens* species. The transcription directions of the inner and outer genes are listed clockwise and anticlockwise, respectively, and are represented by arrows. The dark grey colour in the inner circle corresponds to the GC content, whereas the light grey colour corresponds to the AT content.

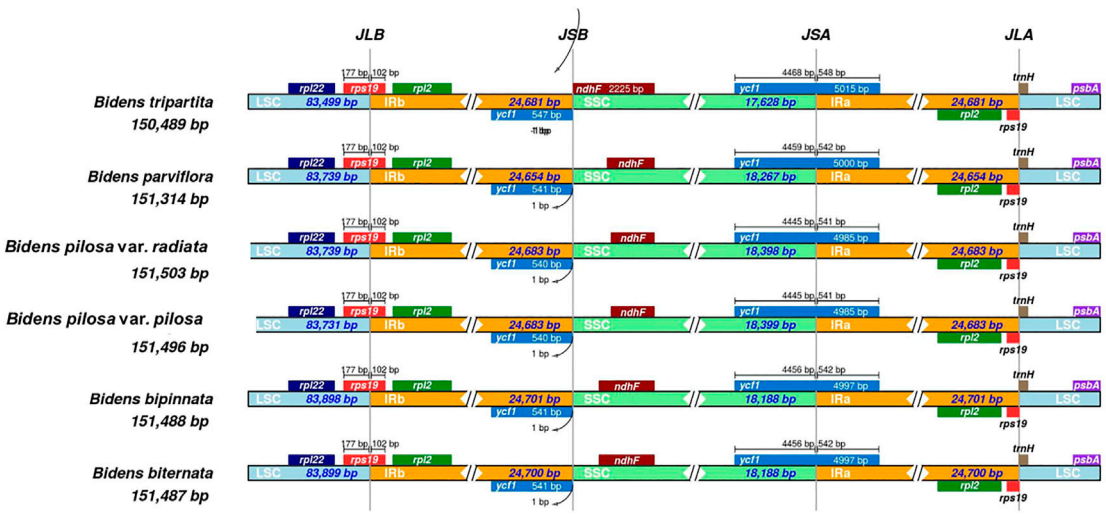

FIGURE 2 | Comparison amongst the borders of LSC, SSC and IR regions in the chloroplast genomes of *Bidens* species. The number above the gene features indicates the distance between the ends of genes and the border sites. These features are not to scale. JLB: junction of LSC/IRb; JSB: junction of IRb/SSC; JSA: junction of SSC/IRa; JLA: junction of IRa/LSC.

pilosa) to 216 kb (*B. tripartita*). The GC contents were between 45.4 and 45.8%. The mitochondrial genomes of *B. biternata* and *B. bipinnata* were annotated with 83 genes, including 30 protein-coding genes, 18 tRNA genes, three rRNA genes and 32 open reading frames (ORFs). A total of 81, 87, 90 and 82 genes were annotated in the mitochondrial genomes of *B. pilosa* var. *pilosa*, *B. pilosa* var. *radiata*, *B. parviflora* and *B. tripartita*, respectively. The total proportion of all genes in the mitochondrial genomes of the *Bidens* species was between 24.4 and 28.6% (**Supplementary Table S7**).

The genes annotated in the mitochondrial genomes of the *Bidens* species could be divided into 11 categories (**Supplementary Table S8**). The similar gene types and numbers of complex I, complex III, complex IV, complex V,

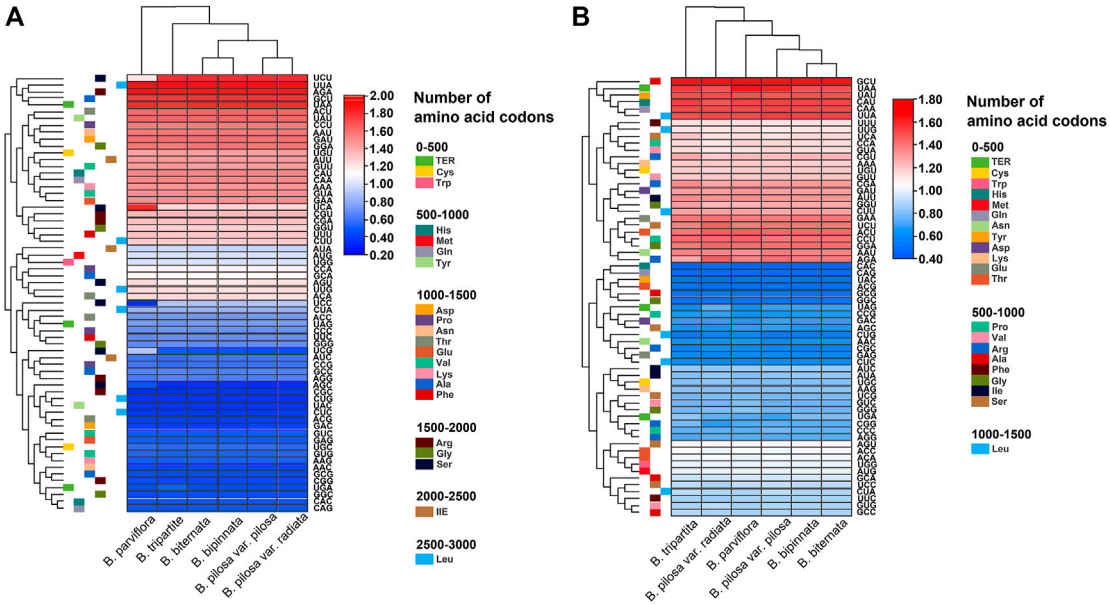

FIGURE 3 | Heat map of the RSCU values of the chloroplast **(A)** and mitochondrial **(B)** genomes of *Bidens* species.

rRNA genes and maturation enzyme genes indicated that these genes were highly conserved in the mitochondrial genomes. The number of tRNA genes ranged from 18 to 20, and the number of ORFs was quite different.

3.2 Relative Synonymous Codon Usage

The relative synonymous codon usage (RSCU) of the chloroplast and mitochondrial genomes of the *Bidens* species was calculated on the basis of all protein-coding genes (**Figure 3**). The results showed that the chloroplast and mitochondrial genomes of the *Bidens* species contained 64 types of codons encoding 20 amino acids. Leucine, serine and arginine all had six types of codons. Amongst all amino acids, leucine had the highest number of codons, whereas cysteine had the lowest.

Given that methionine and tryptophan possess only one codon each, no codon usage bias was found, and the RSCU value was 1. Codon usage bias was found for the rest of the amino acid codons. In the chloroplast genomes, 30 codons were found with RSCU > 1, of which 29 were A/U-ending codons, and 34 codons were found with RSCU ≤ 1, of which 31 were G/C-ending codons. The highest and lowest RSCU values were recorded for UUA and CGC, which encoded leucine and arginine, respectively. In the mitochondrial genomes, 30 codons were found with RSCU > 1, of which 28 were A/U-ending codons, and 34 codons were found with RSCU ≤ 1, of which 30 were G/C-ending codons. The highest and lowest RSCU values were recorded for GCU and CAC, which encoded alanine and histidine, respectively. These results indicated that the chloroplast and mitochondrial genomes exhibited a higher bias towards A/U-ending codons than towards G/C-ending codons.

3.3 Simple Sequence Repeats and Long Repetitive Sequences in the Organelle Genomes of *Bidens* Species

In this study, a total of 56 (*B. parviflora*) to 71 (*B. tripartita*) SSRs were detected in the chloroplast genomes of these *Bidens* species. The distribution of SSRs in the three samples of *B. biternata* was the same. It was also the same in the four samples of *B. bipinnata*. *Bidens bipinnata* had one more mononucleotide repeat than *B. biternata*, and the remaining SSR types and numbers were the same. SSR distribution differed between the two *B. pilosa* var. *radiata* samples. The MW551955 sample had two more mononucleotide repeats, one more dinucleotide repeat and one more trinucleotide repeat than the MW551952 sample, indicating obvious SSR polymorphism in the chloroplast genome of *B. pilosa* var. *radiata*. Mononucleotide to hexanucleotide repeats were present in the *Bidens* species, most of which were mononucleotide repeats, followed by dinucleotide and tetranucleotide repeats (**Supplementary Table S9**). The SSRs of the mitochondrial genomes of the *Bidens* species were also analysed. A total of 50 (*B. pilosa* var. *pilosa*) to 62 (*B. pilosa* var. *radiata*) SSRs were detected in the mitochondrial genomes of the *Bidens* species. Six types of SSR were detected in the mitochondrial genomes of *B. biternata*, *B. bipinnata*, *B. pilosa* var. *radiata* and *B. parviflora*, whereas only five types were detected in *B. pilosa* var. *pilosa* and *B. tripartita* (**Supplementary Table S10**).

Some repetitive sequences with length ≥ 30 bp and sequence similarity ≥ 90% were found. These sequences were called long repetitive sequences, namely, forward (F), palindrome (P), reverse (R) and complement (C). In the chloroplast genomes

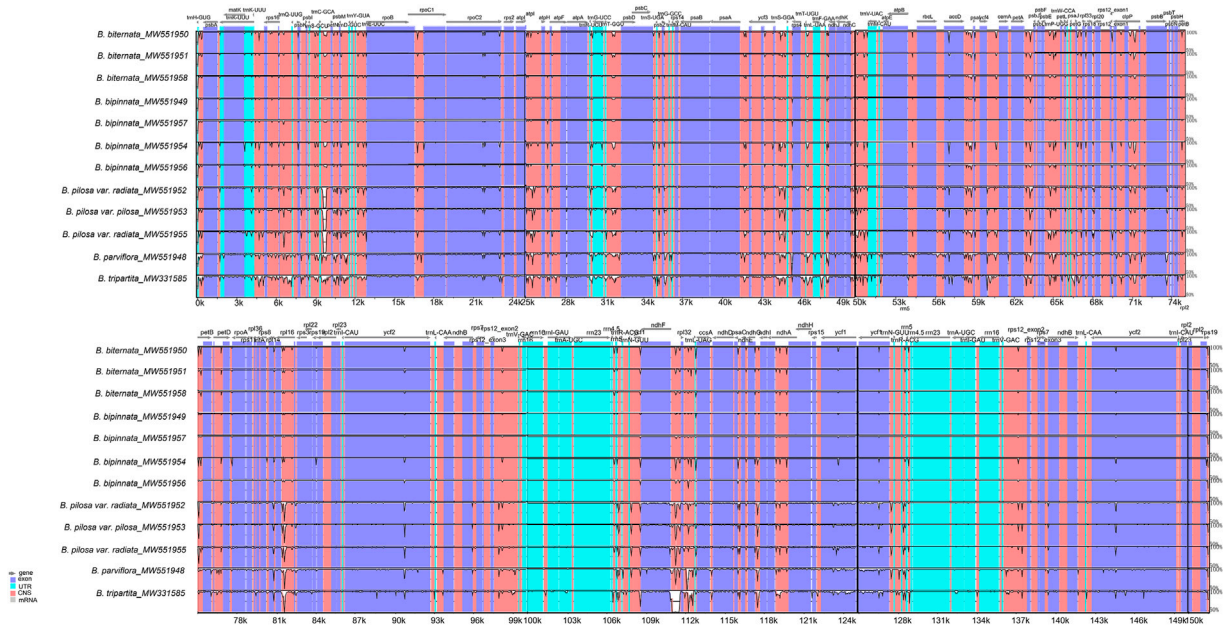

FIGURE 4 | Global alignment of the chloroplast genomes of *Bidens* species. The *x*-axis represents the coordinates in the chloroplast genome. The *y*-axis indicates the average percent identity of sequence similarity, which ranged between 50 and 100%, in the aligned regions.

of *Bidens* species, our analysis revealed 46 (*B. biternata* and *B. bipinnata*) to 114 (*B. pilosa* var. *radiata*) long repeats, most of which were F and P repeats. The long repeats mainly had lengths of 30–39 bp and included four types. Repeats that were larger than 40 bp were mainly F and P repeats. No repeats with lengths of 50–59 and 60–69 bp were found in *B. biternata*, *B. bipinnata* and *B. parviflora*, and no repeat with lengths of 60–69 bp was found in *B. tripartita* (**Supplementary Table S11**). The mitochondrial genomes of *Bidens* species all contained F and P repeats. The mitochondrial genomes of *B. biternata*, *B. bipinnata*, *B. pilosa* var. *pilosa*, *B. pilosa* var. *radiata* and *B. parviflora* contained R repeats. Only the mitochondrial genomes of *B. biternata*, *B. bipinnata* and *B. pilosa* var. *pilosa* contained C repeats. The mitochondrial genome of *B. tripartita* did not contain R and C repeats. The F and P repeats accounted for more than 90% of the long repeats in the mitochondrial genomes of the *Bidens* species. The number of long repeats was the highest in *B. pilosa* var. *radiata* and *B. tripartita*, with 106 and 108 F repeats, respectively. In these species, the number of repeats with lengths of 30–39 bp was the largest, followed by that of repeats with lengths of 40–99 bp; repeats with length ≥ 1 kb were rare (**Supplementary Table S12**).

3.4 Variation in the Organelle Genomes of *Bidens* Species

Consistent with the chloroplast genome analysis above, the global comparison of the chloroplast genomes of the *Bidens* species showed that the seven chloroplast genomes of *B. biternata* and *B. bipinnata* were highly similar. A high degree of similarity was found between the samples of *B. pilosa* var. *pilosa* and *B. pilosa* var. *radiata*. The difference between *B. tripartita* and the other five species was the largest, and a mutation locus was found in the intergene region of *ndhF-rpl32*. In addition, the results revealed that the variation in the noncoding region was considerably greater than that in the coding region. Most of the variation was located in the LSC and SSC regions, and slight variation occurred in the IR regions. The rRNA genes of these species were highly conserved with little variation (**Figure 4**).

The Pi values of the shared genes and intergenic spacers of the chloroplast genomes of the *Bidens* species were calculated. **Figure 5** shows the intergenic spacers and genes with Pi > 0. Intergenic spacers had more polymorphisms than gene regions, and these results were consistent with the mVISTA analysis results. By combining the mVISTA and Pi results, seven candidate highly variable regions (Pi > 0.018; length > 200 bp) were screened out for species identification and relationship studies.

Consistent with the result based on chloroplast genomes, the results of collinearity and homology analysis showed that the mitochondrial genomes of *B. biternata* and *B. bipinnata* had high homology. The mitochondrial genomes of *B. pilosa* var. *pilosa*, *B. pilosa* var. *radiata*, *B. parviflora* and *B. tripartita* were quite different from those of *B. biternata* and *B. bipinnata* (**Figure 6**). The dot plot of the mitochondrial genome sequences between *B. biternata* and *B. bipinnata* showed an evident line on the diagonal, indicating that the chloroplast genome sequences of *B. biternata* and *B. bipinnata* had high homology (**Supplementary Figure S2**). In the dot plot of mitochondrial genome sequences between *B. pilosa* var. *pilosa* and *B. pilosa* var. *radiata*, only several diagonal lines made up of marker points were parallel to the diagonal lines, which represent

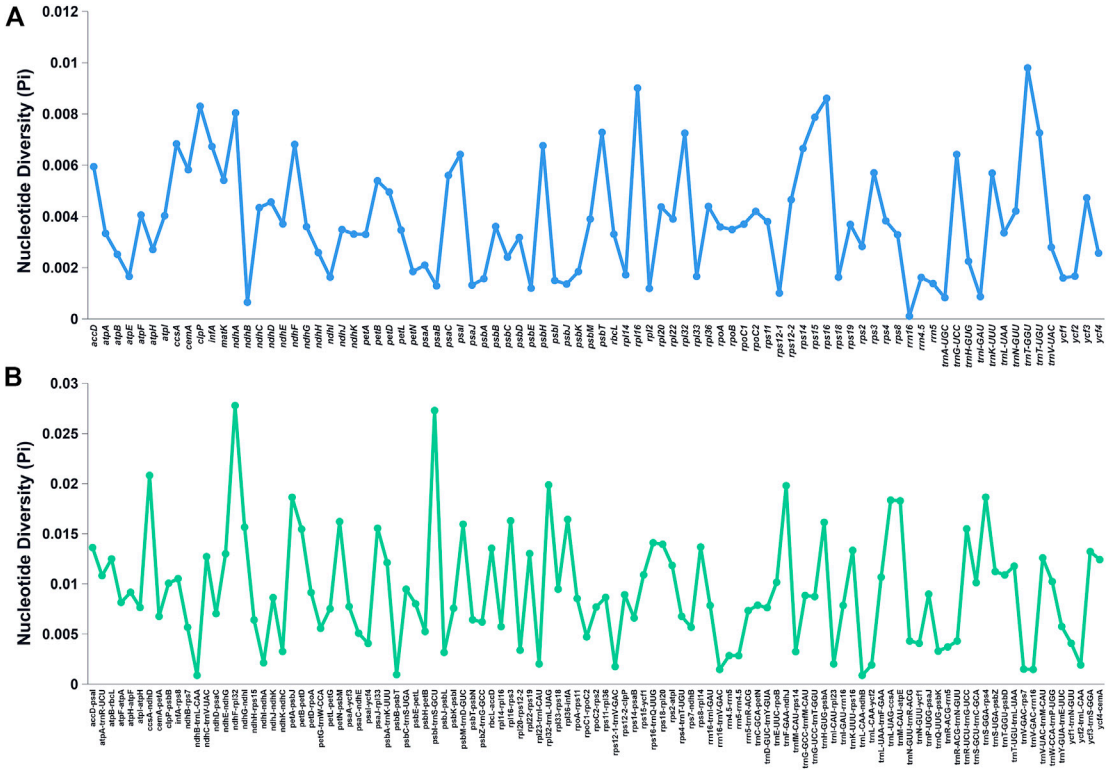

FIGURE 5 | Nucleotide diversity of various shared regions in the chloroplast genomes of *Bidens* species. **(A)** Pi values in the gene regions. **(B)** Pi values in the intergenic spacer regions.

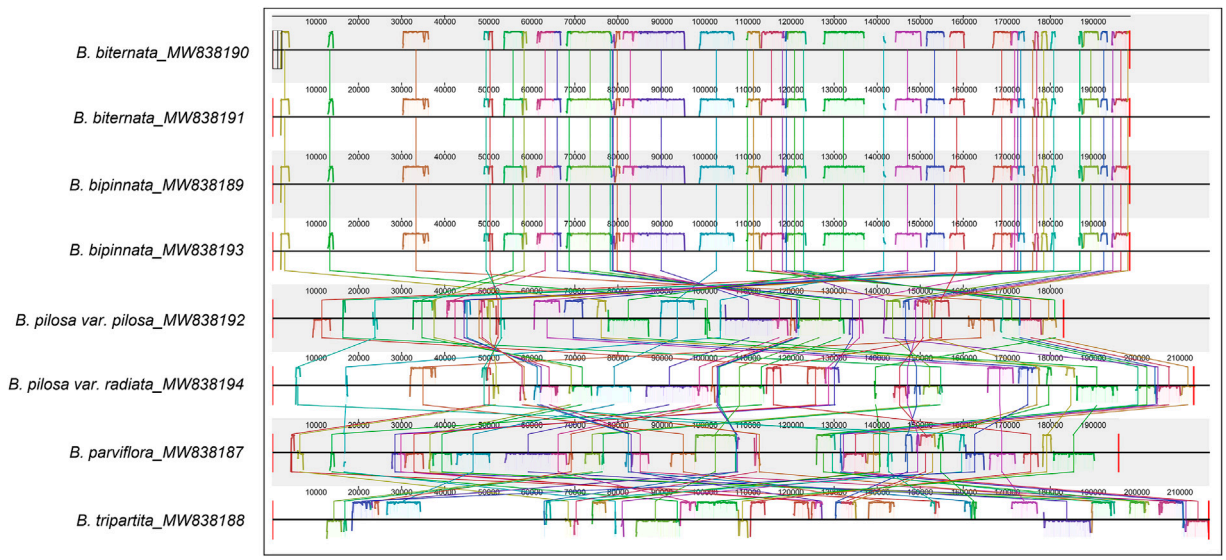

FIGURE 6 | Collinearity analysis of the chloroplast genomes of *Bidens* species. Local collinear blocks are represented by blocks of the same colour connected by lines.

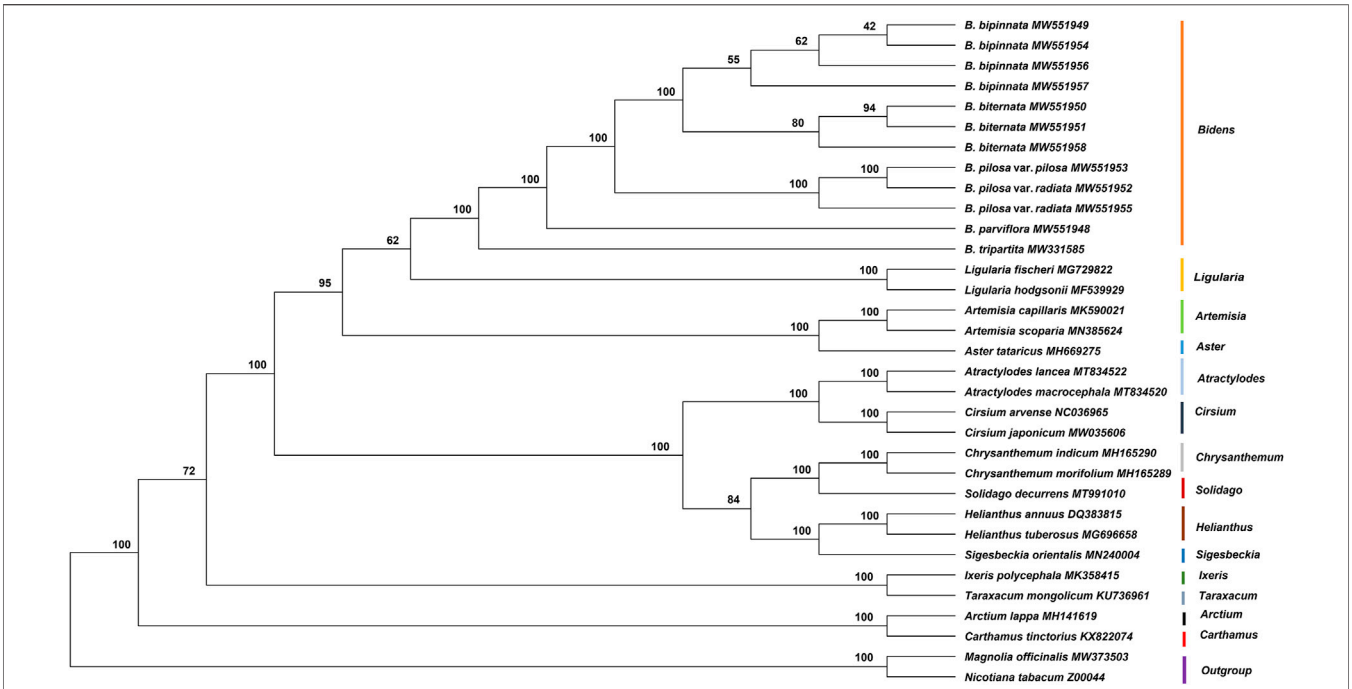

FIGURE 7 | Phylogenetic tree constructed by using the ML method based on the complete chloroplast genome sequences of Asteraceae species. The numbers at the nodes are the values for bootstrap support.

the same substring of two sequences. This result indicated that the mitochondrial genome sequences of *B. pilosa* var. *pilosa* and *B. pilosa* var. *radiata* have low homology (**Supplementary Figure S3**).

3.5 Identification and Phylogenetic Analysis of *Bidens* Species

In the current study, the complete chloroplast genome sequences of five species and one variety of *Bidens* and 21 other Asteraceae species were used to construct a phylogenetic tree with *Magnolia officinalis* and *Nicotiana tabacum* as the outgroups (**Figure 7**). The results showed that the *Bidens* species clustered in a big branch and that different samples of the same species clustered together. The three samples of *B. biternata* clustered in one branch, which was sister to the cluster comprising the four samples of *B. bipinnata*. *Bidens pilosa* var. *radiata* and *B. pilosa* var. *pilosa* clustered together. *Bidens tripartita* and *B. parviflora* clustered in a single branch, respectively. In addition, the species in *Ligularia* were close to those in *Bidens*.

Then, the common protein-coding genes shared in these chloroplast genomes were applied to construct the ML phylogenetic tree (**Supplementary Figure S4**). The result was slightly different from the finding based on the complete chloroplast genome sequences. The four samples of *B. bipinnata* did not cluster together. For the seven candidate highly variable regions, only *trnS-GGA-rps4* showed the capability to identify *Bidens* species (**Supplementary Figure S5**). The species of *B. bipinnata*, *B. biternata* and *B. pilosa* clustered in different branches, respectively. In contrast to the tree based on the complete chloroplast genome, *B. parviflora* was sister to the *B. pilosa* species but with a low bootstrap value.

The ML phylogenetic tree was constructed by using the complete mitochondrial genomes and common protein-coding genes shared by the mitochondrial genomes of Asteraceae species, including the *Bidens* species (**Supplementary Figures S6, S7**). The *Bidens* species did not cluster together in the tree based on the complete mitochondrial genomes, whereas the *Bidens* species clustered together in the tree based on the common protein-coding genes shared by these mitochondrial genomes. However, species within the genus *Bidens* were indistinguishable from each other. The results showed that in contrast to the chloroplast genome, the mitochondrial genome was unsuitable for the identification and phylogenetic analysis of *Bidens* species.

4 DISCUSSION

The lengths of the chloroplast genomes of these *Bidens* species were similar to those of other reported Asteraceae species, such as *Ligularia* species (151,118–151,253 bp) (Chen et al., 2018), *Artemisia frigida* (151,076 bp) (Liu et al., 2013) and *Stilpnolepis centiflora* (151,017 bp) (Shi and Xie 2020). The GC contents of the chloroplast genomes of the *Bidens* species were all 37.5%, which was similar to those of *Carthamus tinctorius* (Lu et al., 2016), *Saussurea involucrata* (Xie et al., 2017) and *Arctium lappa* (Xing et al., 2019). The majority of the chloroplast genomes of Asteraceae species, such as *Soroseris umbrella* (Lv et al., 2020), *Saussurea inversa* and *Saussurea medusa* (Wang et al., 2021), as well as *Pertya phylicoides* (Wang et al., 2020), contained

approximately 130 genes, which included approximately 113 unique genes. The global comparison of the chloroplast genomes showed that the variation of the noncoding region was considerably larger than that of the coding region, most of the variation was located in the LSC and SSC regions, and very little variation occurred in the IR regions. The same findings were also found for *Arctium lappa* (Nie et al., 2020), *Ligularia* species (Chen et al., 2018) and *Artemisia* species (Liu et al., 2013). Moreover, we compared the CDS of the chloroplast genomes of 11 Asteraceae medicinal plants, including the *Bidens* species in this study, *Bidens frondose* (Knope et al., 2020), *Arctium lappa* (Nie et al., 2020), *Atractylodes lancea* (Shi et al., 2021), *Aster tataricus* (Shen et al., 2018) and *Artemisia annua* (Shen et al., 2017). The results showed that although the gene composition of the chloroplast genome of Asteraceae medicinal plants was highly conserved, slight variations were still present. The chloroplast genome of *A. annua*, but not the chloroplast genomes of other 10 medicinal plants, contained the photosystem II gene *psbG*. Only the chloroplast genome of *B. frondose* did not contain the *ycf1* gene. The chloroplast genomes of 11 medicinal plants contained the *ycf2* gene, whereas in the chloroplast genome of *A. tataricus*, *ycf2* gene did not repeat in the IR regions. The *ycf15* gene existed only in the chloroplast genome of *B. frondose* and *A. annua* and not in other medicinal plants (**Supplementary Figure S8**). Bioinformatics analysis revealed the presence of SSRs and long repeats in the chloroplast genome of *Bidens* species. Given that long repeats are abundant in the chloroplast genomes of some highly recombinant algae and angiosperms, especially at the end of the recombinant site, they are considered to be one of the main reasons for promoting the recombination of chloroplast genomes. However, in the chloroplast genome without recombination, the role of these repeats remains unclear (Qian 2014). The SSRs and long repeats contained in the chloroplast genome can be used as important sources of molecular markers for the development of research on *Bidens* species.

The lengths of the mitochondrial genomes of these *Bidens* species were similar to those of most land plants reported in the organelle database of NCBI (**Supplementary Figure S9**) and was similar to that of *Tanacetum vulgare* (Won et al., 2018). The total GC content of the mitochondrial genomes of the *Bidens* species was between 45.4 and 45.8% and were similar to that of *Helianthus annuus* (Grassa et al., 2016). The number of CDS in the mitochondrial genomes of the *Bidens* species was approximately 30 genes and was similar to that of most of reported plants in the NCBI organelle genome databases (30–45). In contrast to those of the conserved chloroplast genome, the sizes and structures of the mitochondrial genomes of angiosperms vary greatly (Levings and Brown 1989; Adams et al., 2002). Studies have shown that the plant mitochondrial genome is a mixture of DNA molecules with different shapes (Kubo and Newton 2008). The mitochondrial genomes of chrysanthemum and sunflower are circular (Makarenko et al., 2019; Wynn and Christensen 2019), whereas those of wheat, rape and cucumber comprise multiple rings (Handa 2003; Ogihara et al., 2005; Alverson et al., 2011). The mitochondrial genomes of plants are considerably larger than those of animals and range from 200 to 2,500 kb with a variation of more than 10 times (Levings and Brown 1989). In most angiosperms, the size of the mitochondrial genome is concentrated within the range of 300–600 kb (Levings and Brown 1989). The secondary structure of the mitochondrial genome is complex and changeable, and gene recombination frequently occurs in the mitochondrial genomes of angiosperms (Kubo and Newton 2008; Gualberto and Newton 2017). Mitochondrial genomes are generally used for high-level classification, such as intergenus and interfamily classification (Qiu et al., 2010).

In this study, phylogenetic trees were constructed on the basis of the complete chloroplast genomes, complete mitochondrial genomes, common protein-coding genes shared by each organelle genome, and seven selected highly variable regions. The complete chloroplast genomes showed the best capability for the identification and phylogenetic analysis of *Bidens* species. The chloroplast genome is an ideal material for species authentication and phylogenetic studies because it can be maternally inherited, usually does not undergo genetic recombination and has highly conserved gene content and order (Verma and Daniell 2007; Jansen and Ruhlman 2012). In fact, chloroplast genomes have been successfully used as a super barcode to identify numerous species and individuals (Doorduin et al., 2011; Kane et al., 2012; Chen et al., 2019; Wu et al., 2020). The phylogenetic trees constructed in this study demonstrated that complete chloroplast genome sequences can also be used as a super barcode for the identification of *Bidens* species. *Bidens pilosa* var. *pilosa* and *B. pilosa* var. *radiata* had similar morphological characteristics. In the Flora of China database, *B. pilosa* var. *radiata* and *B. pilosa* var. *pilosa* have been merged into one species named *B. pilosa*, and the Latin name *B. pilosa* var. *radiata* has been listed as a synonym of *B. pilosa*. In this study, the chloroplast genomes of *B. pilosa* var. *pilosa* and *B. pilosa* var. *radiata* were similar to each other. The ML phylogenetic tree showed that *B. pilosa* var. *radiata* and *B. pilosa* var. *pilosa* clustered together with a bootstrap value of 100%. Therefore, the analysis results of this study provided support for the merging of *B. pilosa* var. *pilosa* and *B. pilosa* var. *radiata* into the same species.

CONCLUSION

In this study, 12 chloroplast and eight mitochondrial genomes of five species and one variety of *Bidens* were analysed. Then, identification and phylogenetic analysis were performed by constructing phylogenetic trees on the basis of the complete chloroplast genomes, complete mitochondrial genomes, common protein-coding genes shared by the chloroplast genomes, common protein-coding genes shared by the mitochondrial genomes, and seven selected highly variable regions. The results of phylogenetic trees based on the complete chloroplast genomes and *trnS-GGA-rps4* showed that different samples of the same species clustered together. This work indicated that complete chloroplast genomes could be used as a super barcode to authenticate *Bidens* species accurately, and

the screened highly variable region *trnS-GGA-rps4* could be used as a potential specific barcode to identify *Bidens* species.

DATA AVAILABILITY STATEMENT

The original contributions presented in the study are publicly available. This data can be found here: The 12 chloroplast genomes and eight mitochondrial genomes of the six *Bidens* species assembled in this study were deposited in GenBank with the accession numbers MW551948-MW551958, MW331585 (chloroplast genomes), and MW838187-MW838194 (mitochondrial genomes).

AUTHOR CONTRIBUTIONS

LW, LN, and QW performed the experiments. SG and TG assembled and annotated the organelle genomes. LW, LN, and SG analysed the data. LW and LN wrote the manuscript. ZW, YL, YW, and BL collected plant material. HY, BL, and TG acquired the funding. HY conceived the research and revised the manuscript. All authors read and approved the final manuscript. All authors have read and agreed to the published version of the manuscript.

FUNDING

This research was funded by National Science & Technology Fundamental Resources Investigation Program of China (No. 2018FY100700), National Natural Science Foundation of China (No. 81903748), and Chinese Academy of Medical Sciences (CAMS) Innovation Fund for Medical Sciences (CIFMS) (No. 2021-I2M-1-071).

SUPPLEMENTARY MATERIAL

The Supplementary Material for this article can be found online at: https://www.frontiersin.org/articles/10.3389/fphar.2022.842131/full#supplementary-material

REFERENCES

Adams, K. L., Qiu, Y. L., Stoutemyer, M., and Palmer, J. D. (2002). Punctuated Evolution of Mitochondrial Gene Content: High and Variable Rates of Mitochondrial Gene Loss and Transfer to the Nucleus during Angiosperm Evolution. *Proc. Natl. Acad. Sci. U S A.* 99 (15), 9905–9912. doi:10.1073/pnas.042694899

Alverson, A. J., Rice, D. W., Dickinson, S., Barry, K., and Palmer, J. D. (2011). Origins and Recombination of the Bacterial-Sized Multichromosomal Mitochondrial Genome of Cucumber. *Plant Cell* 23 (7), 2499–2513. doi:10.1105/tpc.111.087189

Amiryousefi, A., Hyvönen, J., and Poczai, P. (2018). IRscope: an Online Program to Visualize the junction Sites of Chloroplast Genomes. *Bioinformatics* 34 (17), 3030–3031. doi:10.1093/bioinformatics/bty220

An, S. M., Kim, S. Y., Noh, J. H., and Yang, E. C. (2017). Complete Mitochondrial Genome of *Skeletonema marinoi* (Mediophyceae, Bacillariophyta), a Clonal Chain Forming Diatom in the West Coast of Korea. *Mitochondrial DNA A. DNA Mapp. Seq. Anal.* 28 (1), 19–20. doi:10.3109/19401736.2015.1106523

Bartolome, A. P., Villaseñor, I. M., and Yang, W. C. (2013). *Bidens pilosa* L. (Asteraceae): Botanical Properties, Traditional Uses, Phytochemistry, and Pharmacology. *Evid. Based Complement. Alternat Med.* 2013, 340215. doi:10.1155/2013/340215

Beier, S., Thiel, T., Münch, T., Scholz, U., and Mascher, M. (2017). MISA-web: a Web Server for Microsatellite Prediction. *Bioinformatics* 33 (16), 2583–2585. doi:10.1093/bioinformatics/btx198

Bolger, A. M., Lohse, M., and Usadel, B. (2014). Trimmomatic: a Flexible Trimmer for Illumina Sequence Data. *Bioinformatics* 30 (15), 2114–2120. doi:10.1093/bioinformatics/btu170

Chen, F., Wu, F., Wang, D., and He, X. (2009). Pharmacognosy Identification of *Bidens bipinnata* L. *Lishizhen Med. Materia Med. Res.* 20 (2), 329–330. 10.1155/2013/340215.

Chen, J., Wei, J. H., Cai, S. F., Zhang, H. J., Zhang, X. H., Liang, W. J., et al. (2013). Chemical Constituents in Whole Herb of *Bidens pilosa* var. *radiata*. *Zhong Yao Cai* 36 (3), 410–413. doi:10.13863/j.issn1001-4454.2013.03.022

Chen, X., Cui, Y., Nie, L., Hu, H., Xu, Z., Sun, W., et al. (2019). Identification and Phylogenetic Analysis of the Complete Chloroplast Genomes of Three *Ephedra* Herbs Containing Ephedrine. *Biomed. Res. Int.* 2019, 5921725. doi:10.1155/2019/5921725

Chen, X., Zhou, J., Cui, Y., Wang, Y., Duan, B., and Yao, H. (2018). Identification of *Ligularia* Herbs Using the Complete Chloroplast Genome as a Super-barcode. *Front. Pharmacol.* 9, 695. doi:10.3389/fphar.2018.00695

Clegg, M. T., Gaut, B. S., Learn, G. H., Jr., and Morton, B. R. (1994). Rates and Patterns of Chloroplast DNA Evolution. *Proc. Natl. Acad. Sci. U S A.* 91 (15), 6795–6801. doi:10.1073/pnas.91.15.6795

Delsuc, F., Brinkmann, H., and Philippe, H. (2005). Phylogenomics and the Reconstruction of the Tree of Life. *Nat. Rev. Genet.* 6 (5), 361–375. doi:10.1038/nrg1603

Dierckxsens, N., Mardulyn, P., and Smits, G. (2017). NOVOPlasty: De Novo Assembly of Organelle Genomes from Whole Genome Data. *Nucleic Acids Res.* 45 (4), e18. doi:10.1093/nar/gkw955

Doorduin, L., Gravendeel, B., Lammers, Y., Ariyurek, Y., Chin-A-Woeng, T., and Vrieling, K. (2011). The Complete Chloroplast Genome of 17 Individuals of Pest Species Jacobaea Vulgaris: SNPs, Microsatellites and Barcoding Markers for Population and Phylogenetic Studies. *DNA Res.* 18 (2), 93–105. doi:10.1093/dnares/dsr002

Frazer, K. A., Pachter, L., Poliakov, A., Rubin, E. M., and Dubchak, I. (2004). VISTA: Computational Tools for Comparative Genomics. *Nucleic Acids Res.* 32, W273–W279. doi:10.1093/nar/gkh458

Fujii, S., Kazama, T., Yamada, M., and Toriyama, K. (2010). Discovery of Global Genomic Re-organization Based on Comparison of Two Newly Sequenced rice Mitochondrial Genomes with Cytoplasmic Male Sterility-Related Genes. *BMC Genomics* 11, 209. doi:10.1186/1471-2164-11-209

Grassa, C. J., Ebert, D. P., Kane, N. C., and Rieseberg, L. H. (2016). Complete Mitochondrial Genome Sequence of Sunflower (*Helianthus annuus* L.). *Genome Announc* 4 (5), e00981–00916. doi:10.1128/genomeA.00981-16

Gualberto, J. M., and Newton, K. J. (2017). Plant Mitochondrial Genomes: Dynamics and Mechanisms of Mutation. *Annu. Rev. Plant Biol.* 68, 225–252. doi:10.1146/annurev-arplant-043015-112232

Handa, H. (2003). The Complete Nucleotide Sequence and RNA Editing Content of the Mitochondrial Genome of Rapeseed (*Brassica napus* L.): Comparative Analysis of the Mitochondrial Genomes of Rapeseed and *Arabidopsis thaliana*. *Nucleic Acids Res.* 31 (20), 5907–5916. doi:10.1093/nar/gkg795

Jansen, R. K., and Ruhlman, T. A. (2012). *Plastid Genomes of Seed Plants*. New York: Springer.

Jeong, Y., and Lee, J. (2021). The Complete Mitochondrial Genome of the Benthic Diatom *Pleurosigma inscriptura*. *Mitochondrial DNA B Resour.* 6 (9), 2584–2586. doi:10.1080/23802359.2021.1945970

Kane, N., Sveinsson, S., Dempewolf, H., Yang, J. Y., Zhang, D., Engels, J. M., et al. (2012). Ultra-barcoding in Cacao (*Theobroma* spp.; Malvaceae) Using Whole

Chloroplast Genomes and Nuclear Ribosomal DNA. *Am. J. Bot.* 99 (2), 320–329. doi:10.3732/ajb.1100570

Knope, M. L., Bellinger, M. R., Datlof, E. M., Gallaher, T. J., and Johnson, M. A. (2020). Insights into the Evolutionary History of the Hawaiian *Bidens* (Asteraceae) Adaptive Radiation Revealed through Phylogenomics. *J. Hered.* 111 (1), 119–137. doi:10.1093/jhered/esz066

Kubo, T., and Newton, K. J. (2008). Angiosperm Mitochondrial Genomes and Mutations. *Mitochondrion* 8 (1), 5–14. doi:10.1016/j.mito.2007.10.006

Kurtz, S., Choudhuri, J. V., Ohlebusch, E., Schleiermacher, C., Stoye, J., and Giegerich, R. (2001). REPuter: the Manifold Applications of Repeat Analysis on a Genomic Scale. *Nucleic Acids Res.* 29 (22), 4633–4642. doi:10.1093/nar/29.22.4633

Levings, C. S., 3rd, and Brown, G. G. (1989). Molecular Biology of Plant Mitochondria. *Cell* 56 (2), 171–179. doi:10.1016/0092-8674(89)90890-8

Li, H., and Durbin, R. (2009). Fast and Accurate Short Read Alignment with Burrows-Wheeler Transform. *Bioinformatics* 25 (14), 1754–1760. doi:10.1093/bioinformatics/btp324

Librado, P., and Rozas, J. (2009). DnaSP V5: a Software for Comprehensive Analysis of DNA Polymorphism Data. *Bioinformatics* 25 (11), 1451–1452. doi:10.1093/bioinformatics/btp187

Lin, M., Chen, F., Ge, J., Tang, J., and Ni, W. (2013). Protective Effects of Total Flavonoids of *Bidens bipinnata* Lon Acute Inflammation and Possible Mechanism. *Chin. J. Clin. Pharmacol. Ther.* 18 (6), 614–620. doi:10.1211/jpp/60.10.0016

Liu, Y., Huo, N., Dong, L., Wang, Y., Zhang, S., Young, H. A., et al. (2013). Complete Chloroplast Genome Sequences of Mongolia Medicine *Artemisia frigida* and Phylogenetic Relationships with Other Plants. *PLoS One* 8 (2), e57533. doi:10.1371/journal.pone.0057533

Logan, D. C. (2006). The Mitochondrial Compartment. *J. Exp. Bot.* 57 (6), 1225–1243. doi:10.1093/jxb/erj151

Lohse, M., Drechsel, O., and Bock, R. (2007). OrganellarGenomeDRAW (OGDRAW): a Tool for the Easy Generation of High-Quality Custom Graphical Maps of Plastid and Mitochondrial Genomes. *Curr. Genet.* 52 (5-6), 267–274. doi:10.1007/s00294-007-0161-y

Lu, C., Shen, Q., Yang, J., Wang, B., and Song, C. (2016). The Complete Chloroplast Genome Sequence of Safflower (*Carthamus tinctorius* L.). *Mitochondrial DNA A. DNA Mapp. Seq. Anal.* 27 (5), 3351–3353. doi:10.3109/19401736.2015.1018217

Lv, Z. Y., Zhang, J. W., Chen, J. T., Li, Z. M., and Sun, H. (2020). The Complete Chloroplast Genome of *Soroseris umbrella* (Asteraceae). *Mitochondrial DNA B Resour.* 5 (1), 637–638. doi:10.1080/23802359.2019.1711223

Makarenko, M. S., Usatov, A. V., Tatarinova, T. V., Azarin, K. V., Logacheva, M. D., Gavrilova, V. A., et al. (2019). Characterization of the Mitochondrial Genome of the MAX1 Type of Cytoplasmic Male-Sterile sunflower. *BMC Plant Biol.* 19, 51. doi:10.1186/s12870-019-1637-x

Nguyen, L. T., Schmidt, H. A., von Haeseler, A., and Minh, B. Q. (2015). IQ-TREE: a Fast and Effective Stochastic Algorithm for Estimating Maximum-Likelihood Phylogenies. *Mol. Biol. Evol.* 32 (1), 268–274. doi:10.1093/molbev/msu300

Nie, L., Cui, Y., Chen, X., Xu, Z., Sun, W., Wang, Y., et al. (2020). Complete Chloroplast Genome Sequence of the Medicinal Plant *Arctium lappa*. *Genome* 63 (1), 53–60. doi:10.1139/gen-2019-0070

Ogihara, Y., Yamazaki, Y., Murai, K., Kanno, A., Terachi, T., Shiina, T., et al. (2005). Structural Dynamics of Cereal Mitochondrial Genomes as Revealed by Complete Nucleotide Sequencing of the Wheat Mitochondrial Genome. *Nucleic Acids Res.* 33 (19), 6235–6250. doi:10.1093/nar/gki925

Park, S. I., and Lee, J. (2020). The Complete Mitochondrial Genome of *Pyropia pulchra* (Bangiophyceae, Rhodophyta). *Mitochondrial DNA B Resour.* 5 (3), 3157–3158. doi:10.1080/23802359.2020.1806132

Qiu, Y. L., Li, L., Wang, B., Xue, J. Y., Hendry, T. A., Li, R. Q., et al. (2010). Angiosperm Phylogeny Inferred from Sequences of Four Mitochondrial Genes. *J. Syst. Evol.* 48 (6), 391–425. doi:10.1111/j.1759-6831.2010.00097.×

Qian, J. (2014). *Study on Chloroplast and Mitochondrial Genomes of Salvia Miltiorrhiza*. Beijing: Chinese Academy of Medical Sciences & Peking Union Medical College.

Rice, P., Longden, I., and Bleasby, A. (2000). EMBOSS: the European Molecular Biology Open Software Suite. *Trends Genet.* 16 (6), 276–277. doi:10.1016/s0168-9525(00)02024-2

Robinson, J. T., Thorvaldsdóttir, H., Wenger, A. M., Zehir, A., and Mesirov, J. P. (2017). Variant Review with the Integrative Genomics Viewer. *Cancer Res.* 77 (21), e31–e34. doi:10.1158/0008-5472.Can-17-0337

Schattner, P., Brooks, A. N., and Lowe, T. M. (2005). The tRNAscan-SE, Snoscan and snoGPS Web Servers for the Detection of tRNAs and snoRNAs. *Nucleic Acids Res.* 33, W686–W689. doi:10.1093/nar/gki366

Shandukani, P. D., Tshidino, S. C., Masoko, P., and Moganedi, K. M. (2018). Antibacterial activity and *In Situ* efficacy of *Bidens pilosa* Linn and Dichrostachys cinerea Wight et Arn extracts against common diarrhoea-causing waterborne bacteria. *BMC Complement. Altern. Med.* 18 (1), 171. doi:10.1186/s12906-018-2230-9

Sharp, P. M., and Li, W. H. (1987). The Codon Adaptation Index--a Measure of Directional Synonymous Codon Usage Bias, and its Potential Applications. *Nucleic Acids Res.* 15 (3), 1281–1295. doi:10.1093/nar/15.3.1281

Shen, X., Guo, S., Yin, Y., Zhang, J., Yin, X., Liang, C., et al. (2018). Complete Chloroplast Genome Sequence and Phylogenetic Analysis of *Aster tataricus*. *Molecules* 23 (10), 2426. doi:10.3390/molecules23102426

Shen, X., Wu, M., Liao, B., Liu, Z., Bai, R., Xiao, S., et al. (2017). Complete Chloroplast Genome Sequence and Phylogenetic Analysis of the Medicinal Plant *Artemisia annua*. *Molecules* 22 (8), 1330. doi:10.3390/molecules22081330

Shi, L., Chen, H., Jiang, M., Wang, L., Wu, X., Huang, L., et al. (2019). CPGAVAS2, an Integrated Plastome Sequence Annotator and Analyzer. *Nucleic Acids Res.* 47 (W1), W65–W73. doi:10.1093/nar/gkz345

Shi, M., Xie, H., Zhao, C., Shi, L., Liu, J., and Li, Z. (2021). The Complete Chloroplast Genome of *Atractylodes japonica* Koidz. Ex Kitam. And its Phylogenetic Inference. *Mitochondrial DNA B Resour.* 6 (7), 2038–2040. doi:10.1080/23802359.2021.1927217

Shi, X., and Xie, K. (2020). The Complete Chloroplast Genome Sequence of *Stilpnolepis centiflora* (Asteraceae), an Endemic Desert Species in Northern China. *Mitochondrial DNA B Resour.* 5 (3), 3545–3546. doi:10.1080/23802359.2020.1829127

Shi, Z., Chen, Y. L., Chen, Y. S., Lin, Y. R., Liu, S. W., Ge, X. J., et al. (2011). *Flora of China*. Beijing: Science Press. Vols. 20–21.

Tamura, K., Stecher, G., Peterson, D., Filipski, A., and Kumar, S. (2013). MEGA6: Molecular Evolutionary Genetics Analysis Version 6.0. *Mol. Biol. Evol.* 30 (12), 2725–2729. doi:10.1093/molbev/mst197

Tillich, M., Lehwark, P., Pellizzer, T., Ulbricht-Jones, E. S., Fischer, A., Bock, R., et al. (2017). GeSeq - Versatile and Accurate Annotation of Organelle Genomes. *Nucleic Acids Res.* 45 (W1), W6–W11. doi:10.1093/nar/gkx391

Tsai, L. C., Wang, J. C., Hsieh, H. M., Liu, K. L., Linacre, A., and Lee, J. C. (2008). *Bidens* Identification Using the Noncoding Regions of Chloroplast Genome and Nuclear Ribosomal DNA. *Forensic Sci. Int. Genet.* 2 (1), 35–40. doi:10.1016/j.fsigen.2007.07.005

Verma, D., and Daniell, H. (2007). Chloroplast Vector Systems for Biotechnology Applications. *Plant Physiol.* 145 (4), 1129–1143. doi:10.1104/pp.107.106690

Wang, B., Zhao, Q., Wang, X. H., and Fu, Z. X. (2020). The Complete Chloroplast Genome of *Pertya phylicoides* (Asteraceae, Pertyeae): a Shurby Endemic Species from China. *Mitochondrial DNA B Resour.* 5 (1), 963–964. doi:10.1080/23802359.2020.1722763

Wang, J., He, R., Zhang, H., Hu, Y., Wang, J., Wang, L., et al. (2021). Complete Chloroplast Genome of *Saussurea inversa* (Asteraceae) and Phylogenetic Analysis. *Mitochondrial DNA B* 6 (1), 8–9. doi:10.1080/23802359.2020.1845108

Wang, R., Wu, Q. X., and Shi, Y. P. (2010). Polyacetylenes and Flavonoids from the Aerial Parts of *Bidens pilosa*. *Planta Med.* 76 (9), 893–896. doi:10.1055/s-0029-1240814

Wang, X. Y., Chen, G. R., Deng, Z. Y., Zhao, J., Ge, J. F., Li, N., et al. (2014). Chemical Constituents from *Bidens bipinnata*. *Zhongguo Zhong Yao Za Zhi* 39 (10), 1838–1844. doi:10.4268/cjcmm20141017

Won, S. Y., Jung, J. A., and Kim, J. S. (2018). The Complete Mitochondrial Genome Sequence of *Chrysanthemum boreale* (Asteraceae). *Mitochondrial DNA B Resour.* 3 (2), 529–530. doi:10.1080/23802359.2018.1468226

Wu, L., Nie, L., Xu, Z., Li, P., Wang, Y., He, C., et al. (2020). Comparative and Phylogenetic Analysis of the Complete Chloroplast Genomes of Three *Paeonia* Section *Moutan* Species (Paeoniaceae). *Front. Genet.* 11, 980. doi:10.3389/fgene.2020.00980

Wynn, E. L., and Christensen, A. C. (2019). Repeats of Unusual Size in Plant Mitochondrial Genomes: Identification, Incidence and Evolution. *G3 (Bethesda)* 9 (2), 549–559. doi:10.1534/g3.118.200948

Xie, Q., Shen, K. N., Hao, X., Nam, P. N., Ngoc Hieu, B. T., Chen, C. H., et al. (2017). The Complete Chloroplast Genome of Tianshan Snow Lotus (*Saussurea involucrata*), a Famous Traditional Chinese Medicinal Plant of the Family Asteraceae. *Mitochondrial DNA A. DNA Mapp. Seq. Anal.* 28 (2), 294–295. doi:10.3109/19401736.2015.1118086

Xing, Y.-P., Xu, L., Chen, S.-Y., Liang, Y.-M., Wang, J.-H., Liu, C.-S., et al. (2019). Comparative Analysis of Complete Chloroplast Genomes Sequences of *Arctium lappa* and *A. tomentosum*. *Biol. Plant.* 63, 565–574. doi:10.32615/bp.2019.101

Yang, X., Bai, Z. F., Zhang, D. W., Zhang, Y., Cui, H., and Zhou, H. L. (2020). Enrichment of Flavonoid-Rich Extract from *Bidens bipinnata* L. By Macroporous Resin Using Response Surface Methodology, UHPLC-Q-TOF MS/MS-assisted Characterization and Comprehensive Evaluation of its Bioactivities by Analytical Hierarchy Process. *Biomed. Chromatogr.* 34 (11), e4933. doi:10.1002/bmc.4933

Zhang, Z., Zhang, Y., Song, M., Guan, Y., and Ma, X. (2019). Species Identification of *Dracaena* Using the Complete Chloroplast Genome as a Super-barcode. *Front. Pharmacol.* 10, 1441. doi:10.3389/fphar.2019.01441

Conflict of Interest: Author SG and ZW are employed by China Resources Sanjiu Medical & Pharmaceutical Co., Ltd. The remaining authors declare that the research was conducted in the absence of any commercial or financial relationships that could be construed as a potential conflict of interest.

frontiers in Pharmacology

ORIGINAL RESEARCH
published: 21 March 2022
doi: 10.3389/fphar.2022.865066

Exploration of Q-Marker of Rhubarb Based on Intelligent Data Processing Techniques and the AUC Pooled Method

Jiayun Chen[1†], *Xiaojuan Jiang*[1†], *Chunyan Zhu*[1], *Lu Yang*[2], *Minting Liu*[1], *Mingshe Zhu*[1,3] *and Caisheng Wu*[1*]

[1]*Fujian Provincial Key Laboratory of Innovative Drug Target Research and State Key Laboratory of Cellular Stress Biology, School of Pharmaceutical Sciences, Xiamen University, Xiamen, China,* [2]*College of Pharmacy, Jiamusi University, Jiamusi, China,* [3]*MassDefect Technologies, Princeton, NJ, United States*

OPEN ACCESS

Edited by:
Jian-Bo Yang,
National Institutes for Food and Drug Control, China

Reviewed by:
Jian-Bo Wan,
University of Macau, China
Jiangeng Huang,
Huazhong University of Science and Technology, China
Jianye Dai,
Lanzhou University, China

***Correspondence:**
Caisheng Wu
wucsh@xmu.edu.cn

[†]*These authors have contributed equally to this work*

Specialty section:
This article was submitted to Experimental Pharmacology and Drug Discovery, a section of the journal Frontiers in Pharmacology

Received: *29 January 2022*
Accepted: *21 February 2022*
Published: *21 March 2022*

Citation:
Chen J, Jiang X, Zhu C, Yang L, Liu M, Zhu M and Wu C (2022) Exploration of Q-Marker of Rhubarb Based on Intelligent Data Processing Techniques and the AUC Pooled Method. Front. Pharmacol. 13:865066. doi: 10.3389/fphar.2022.865066

Rhubarb, as a traditional Chinese medicine, has several positive therapeutic effects, such as purging and attacking accumulation, clearing heat and purging fire, cooling blood, and detoxification. Recently, Rhubarb has been used in prescriptions for the prevention and treatment of COVID-19, with good efficacy. However, the exploration of effective quantitative approach to ensure the consistency of rhubarb's therapeutic efficacy remains a challenge. In this case, this study aims to use non-targeted and targeted data mining technologies for its exploration and has comprehensively identified 72 rhubarb-related components in human plasma for the first time. In details, the area under the time-concentration curve (AUC)-pooled method was used to quickly screen the components with high exposure, and the main components were analyzed using Pearson correlation and other statistical analyses. Interestingly, the prototype component (rhein) with high exposure could be selected out as a Q-marker, which could also reflect the metabolic status changes of rhubarb anthraquinone in human. Furthermore, after comparing the metabolism of different species, mice were selected as model animals to verify the pharmacodynamics of rhein. The *in vivo* experimental results showed that rhein has a positive therapeutic effect on pneumonia, significantly reducing the concentration of pro-inflammatory factors [interleukin (IL)-6 and IL-1β] and improving lung disease. In short, based on the perspective of human exposure, this study comprehensively used intelligent data post-processing technologies and the AUC-pooled method to establish that rhein can be chosen as a Q-marker for rhubarb, whose content needs to be monitored individually.

Keywords: rhubarb, Q-marker, AUC-pooled method, intelligent data processing techniques, rhein

Abbreviations: AUC, Area Under the Time-concentration Curve; CMC, Carboxymethyl Cellulose; HREIC, High Resolution Extraction Ion Chromatography; IL, Interleukin; JZDHW, Jiuzhi Dahuang Wan; LPS, Lipopolysaccharide; Q-marker, Quality-markers; SD, Sprague Dawley; TCM, Traditional Chinese Medicine; tm, Time; TNFα, Tumour Necrosis Factor Alpha; UPLC-HRMS, Ultra performance Liquid Chromatography-High Resolution Mass Spectrometry.

INTRODUCTION

Traditional Chinese medicine (TCM) is a traditional treasure of China, with thousands of years of clinical experience. It plays an important role in disease prevention and treatment, escorting human health. However, due to the origin of varieties, growth conditions, processing process, storage conditions and other reasons, the types and contents of TCM ingredients might be easily changed, which has a significant impact on safety and effectiveness (Bai et al., 2018; Zhang et al., 2018; Ren et al., 2020). Therefore, it is necessary to establish the perfect quality standard for TCM to ensure the consistency of efficacy. For this purpose, Liu *et al.* proposed the concept of Quality-marker (Q-marker) to provide a novel research direction for the quality evaluation of TCM (Liu et al., 2016). Specifically, Q-marker is a component inherent in TCM or generated in the preparation process, which can be qualitatively and quantitatively analyzed. More importantly, it should also have good biological activity, with clear therapeutic effects *in vivo*. However, the exploration to screen out a suitable Q-marker from hundreds or thousands of components of TCM remains a challenge.

As a typical case, Rhubarb is a traditional Chinese medicine (TCM) commonly used clinically, which is mainly from the dried roots and rhizomes of *Rheum palmatum* L., *Rheum tangicum* Maxim. ex Balf., or *Rheum officinale* Baill. Rhubarb has the following effects when used clinically: purging and attacking accumulation, clearing away heat and fire, cooling blood and detoxification, removing blood stasis and clearing menstruation, removing dampness, and reducing yellowness (Chinese Pharmacopoeia Commission, 2020). At the same time, as a part of the "three-medicines and three-decoctions" Huashi Baidu decoction and Lianhua Qingwen capsules, rhubarb has also played an irreplaceable role in the treatment of new coronary pneumonia (COVID-19), showing potential anti-inflammatory effect (Huang et al., 2020; Zhuang et al., 2020). In order to guarantee the efficacy of rhubarb, it is necessary to conduct quality control on it. Based on different preparation methods, the 2020 Chinese Pharmacopoeia calculates the content of total anthraquinone and free anthraquinone (above 1.5 and 0.02%, respectively) as to control the quality of rhubarb, in terms of the total amount of aloe-emodin, rhein, emodin, chrysophanol, and physcion. It is generally believed that substances that produce curative effects are TCM prototype components or their metabolites, which enter systemic circulation to reach the target organs (Li et al., 2018; Zhou et al., 2020; Zhu et al., 2020; Yang et al., 2021). Although anthraquinones show good pharmacological activities *in vitro*, including laxative, anticancer, hepatoprotective, anti-inflammatory, antibacterial, analgesic, and other effects (Xiang et al., 2020). However, they might not be absorbed into the body and exhibit disappointing effects *in vivo*, which might lead to an undesired failure in quality control (He et al., 2018). Therefore, it is necessary to pay attention to the pharmacokinetics of TCM *in vivo*. Carrying out research from the *in vivo* perspective will be more conducive to discover the pharmacodynamic material basis of rhubarb and determine the most suitable Q-marker.

The components of rhubarb are complex. It is very difficult to carry out pharmacokinetic studies on multiple components simultaneously. The area under the time-concentration curve (AUC) pooled method can simplify the traditional pharmacokinetic experiment model by using the same principle (Hop et al., 1998). The plasma volume ratio at each time point can be obtained using the following formula $v_1 : v_2 : \cdots : v_i = (t_1 - t_0) : (t_2 - t_0) : (t_3 - t_1) : \cdots : (t_i - t_{i-1})$. The plasma is then mixed. In a single plasma sample after mixing, the measured concentration multiplied by the time (tm) of the last blood collection is theoretically equal to $AUC_{0\text{-tm}}$. Compared with the traditional method, the AUC pooled method greatly reduces the number of samples and the analysis time, allowing experimental results to be obtained more quickly and easily. This method is especially suitable for the study of metabolism *in vivo*. It is worth mentioning that there are metabolic differences in the effects of TCM among different species due to differences in the subtypes and activities of metabolic enzymes (Martignoni et al., 2006; Li et al., 2020; Hammer et al., 2021). Therefore, using the AUC pooled method can also quickly obtain the exposure proportions of the prototype and metabolite components in different species. Thus, species that are similar to humans are used as models for drug efficacy verification.

Based on ultra-performance liquid chromatography-high resolution mass spectrometry (UPLC-HRMS) technology and various intelligent mass spectrometry data processing technologies that were developed previously (Zhu et al., 2020), this study aims to conduct the pioneer comprehensive exploration of rhubarb-related components in humans. Due to the safety consideration in human trials, only marketed drug, which contains rhubarb as main part of formulation and has been approved by National Medical Products Administration, can be suitable for this study. In this case, Jiuzhi Dahuang Wan (JZDHW) has met the above requirement and been chosen as the typical medicine formulae in this exploration. The formulae instructions show that the ingredients are rhubarb, while the auxiliary material is rice wine. Due to the simple compositions of JZDHW, impacts of other components on this metabolic study can be effectively avoided, which further facilitates the discovery of the actual substances in rhubarb exposed to humans. More importantly, combined with the AUC pooled method, this study could visually display the prototype and metabolite components with high exposure. Furthermore, the relationship of exposure between different prototype and metabolite components could be obtained through correlation statistical analysis. After that, the Q-markers of rhubarb were rapidly screened from the perspective of human exposure, and the Q-markers were pharmacodynamically verified.

MATERIALS AND METHODS

Chemicals and Reagents

JZDHW (batch number: 0470049) was purchased from Tianjin lerentang pharmaceutical factory (Tianjin, China). Chrysazin, *p*-coumaric acid, gallic acid (*E*)-piceatannol, aloe-emodin, emodin, chrysophanol, physcion, rhein, kaempferol, catechin,

quercetin, rutin, lindleyin, isoquercitrin, sennoside C, emodin 8-*O*-*β*-*d*-glucoside, rhapontin, rhein 8-*O*-*β*-*d*-glucoside, quercitrin, and sennoside A were supplied by Baoji Chenguang Biotechnology Co., Ltd. (Baoji, China). Sprague Dawley (SD) rat blank plasma and human blank plasma were provided by Shanghai Yuanye Bio-Technology Co., Ltd. (Shanghai, China). Oasis® HLB 6 cc (500 mg) extraction cartridges were purchased from Waters Corporation (Milford, MA, United States). Methanol and acetonitrile were purchased from TEDIA (Fairfield, OH, United States). Formic acid was purchased from Anaqua Chemical Supply (Wilmington, DE, United States). Ultra-pure water was prepared using a Milli-Q water purification system (Bedford, MA, United States). Heparin sodium was purchased from Shanghai Aladdin Bio-Chem Technology Co., LTD. (Shanghai, China). LPS was purchased from Beijing Solarbio Technology Co., LTD. (Beijing, China). Mouse interleukin (IL)-6 uncoated ELISA, mouse tumour necrosis factor alpha (TNFα) uncoated ELISA, and mouse IL-1β uncoated ELISA kits were obtained from Thermo Fisher Scientific Co. (Waltham, MA, United States). Carboxymethyl cellulose (CMC) was purchased Shanghai Macklin Biochemical Co., Ltd. (Shanghai, China).

JZDHW Composition Analysis

JZDHW powder (20 mg) was dissolved in 1 ml 70% methanol, sonicated, vortexed, and filtered using a 0.22 μm filter membrane to obtain a final test solution.

Plasma Sample Collection

Human Plasma Sample Collection

After 12 h of fasting, three healthy female subjects (authors of this study) were orally administered one bag of JZDHW (6 g). Intravenous blood sampling (1% heparin sodium anticoagulant) was conducted at a total of 12 time points (before administration and 0.25, 0.5, 1, 2, 3, 4, 6, 8, 10, 12, and 24 h after administration). The blood samples were then centrifuged for 10 min at 4,000 rpm/min, and the supernatants were stored in aliquots at −80°C. Subject's informed consent were obtained and the work described was carried out in accordance with The Code of Ethics of the World Medical Association (Declaration of Helsinki).

Animal Plasma Sample Collection

A total of 12 female SD rats (180–220 g) and 56 female C57BL/6 mice (18–22 g, except for eight mice at 12 and 24 h, four mice at other time points, respectively) were purchased from Shanghai SLAC Laboratory Animal Co., Ltd. (Shanghai, China). After 1 week of adaptive feeding, followed by fasting for 12 h, rhubarb solution (JZDHW were ground to a powder and dissolved in ultra-pure water) was administered by oral gavage at a dose of 8 g/kg. Blood samples (1% heparin sodium anticoagulant) were collected before administration and 0.25, 0.5, 1, 2, 3, 4, 6, 8, 10, 12, and 24 h after administration, after which all samples were centrifuged at 4,000 rpm/min for 10 min. The supernatant was then aliquoted and stored at −80°C. All animal care and experimental procedures in this experiment conform to the Guide for the Care and Use of Laboratory Animals of Xiamen University (the ethic approval number: XMULAC20210101).

Sample Preparation

Pre-Treatment for the Mixed Plasma-AUC Pooled Method

A total of 2.5, 5, 7.5, 15, 20, 20, 30, 40, 40, 40, 140, and 120 μL of human plasma was collected at 0, 0.25, 0.5, 1, 2, 3, 4, 6, 8, 10, 12, and 24 h after administration, respectively. The human plasma was then mixed uniformly to obtain 480 μL plasma, followed by addition of 20 μL of internal standard (50 μg/ml chrysazin, Protein was then precipitated with three times the volume of methanol. The supernatant after centrifugation was blown dry with nitrogen, and the residue was reconstituted with 100 μL of 70% methanol for testing. Each set of samples was evaluated in triplicate. The rat/mouse plasma samples were evaluated using the same procedure as that for human plasma.

Protocols for the solid-phase extraction processing method, AUC pooled method development, and verification of quality control sample preparation and pre-processing methods are provided in the Supplementary Materials. Additionally, the reasons for using chrysazin as the internal standard are as follows. Firstly, chrysazin is an anthraquinone compound, whose physicochemical properties are similar to those of the main components of rhubarb. Secondly, chrysazin and its isomers are neither contained in rhubarb itself nor in plasma samples. Last but not least, chrysazin does not chemically react with the tested sample, and its chromatographic peak can be completely separated.

Pre-Treatment Method for Human Plasma Samples at a Single Time Point

480 μL human plasma was collected at each of 12 time points, followed by addition of 20 μL of internal standard (50 μg/ml chrysazin). Protein was precipitated with three times the volume of methanol. The supernatant after centrifugation was blown dry with nitrogen, and the residue was reconstituted with 100 μL of 70% methanol for testing. Each set of samples was evaluated in triplicate.

UPLC-HRMS Analysis

The samples were analysed using a Thermo Fisher Q Exactive Orbitrap liquid chromatography with tandem mass spectrometry system equipped with electrospray ionization (Thermo Fisher Scientific) in negative ion mode, which was controlled by Thermo Xcalibur 3.0.63 (Thermo Fisher Scientific). An ACQUITY UPLC CSH C18 column (50 mm × 2.1 mm, 1.7 μm; Waters Corporation) was used to separate the sample at a temperature of 35°C. Mobile phase A was H_2O with 0.1% formic acid, and mobile phase B was 100% acetonitrile with a flow rate of 0.3 ml/min. The injection volume was set at 3 μL. The mobile phase gradient was set as follows: 0–7 min, 95%–60% (A); 7–15.5 min, 60%–40% (A); 15.5–18 min, 40%–20% (A); 18–20 min, 20%–5% (A); 20–23 min, 5%–5% (A); 23–23.1 min, 5%–95% (A); and 23.1–27 min, 95%–95% (A).

The MS parameters were set as follows: full MS resolution 35,000, scanning range *m/z* 100–1,000, dd-MS2 resolution

17,500, collision energy 35%, spray voltage 3.5 kV, capillary temperature 320°C, sheath gas (N2) flow rate 35 arb, auxiliary gas (N2) flow rate 10 arb, and sweep gas (N2) flow rate five arb.

Pharmacodynamic Verification of the Pneumonia Model

A total of 40 female C57BL/6 mice, 18–22 g, were purchased from Shanghai SLAC Laboratory Animal Co., Ltd. The mice were randomly divided into five groups: the control group (A), model group (B), rhein group (C), and JZDHW group (D). The mice were reared adaptively for 1 week. Before modelling experiments, groups A and B were administered with 0.4% CMC, group C was administered with 85 mg/kg rhein, and group D was administered with 1.6 g/kg JZDHW at a volume of 20 ml/kg. All treatments were administered by oral gavage. Immediately following pre-treatment, a pneumonia model was established using the LPS nasal drip method. Mice were anesthetized by intraperitoneal injection of chloral hydrate. Treatments were orally administered every 12 h, followed by six consecutive administrations. The mice were sacrificed 12 h after the last administration, followed by collection of the serum and lung tissue. ELISA kits were used to detect the changes in serum inflammatory factors (TNFα, IL-6, and IL-1β). GraphPad Prism 8.0.2 software (GraphPad Software, San Diego, CA, United States) was used for statistical analysis. The significance of the data was evaluated using a two-tailed Student's t-test and one-way analysis of variance. Significant differences between groups are represented by * for $p < 0.05$, ** for $p < 0.01$, and *** for $p < 0.001$. Haematoxylin and eosin staining was used to analyse the pathological condition of lung tissue. In addition, we established a pancreatitis model to supplement the anti-inflammatory activity of JZDHW components. For detailed experimental methods regarding the pancreatitis model, please see the Supplementary Materials.

RESULTS

Analysis of JZDHW Components

The compositions of rhubarb anthraquinones are relatively similar in structure. To achieve the most effective separation of the compounds, we utilized an ACQUITY UPLC CSH C18 (50 mm × 2.1 mm, 1.7 μm) column and optimized the elution conditions. We selected three typical rhubarb anthraquinone reference substances (rhein, emodin, and chrysophanol; 10 μg/ml) to optimize the MS parameters, including the appropriate ionization mode (positive ion mode/negative ion mode), spray voltage, capillary temperature, capillary voltage, RF lens, flow rate of auxiliary gas, and other parameters. According to the final optimized conditions, JZDHW test solution was analysed by UPLC-HRMS. The total ion chromatogram is shown in **Figure 1**, with the corresponding data shown in **Supplementary Table S1**. A total of 223 compounds were detected from JZDHW. Compound identification was completed using Compound Discoverer 3.1 software (Thermo Fisher Scientific) combined with data reported in the literature (Lin et al., 2006; Cao et al., 2017; Niziol et al., 2017; Xian et al., 2017; Qin et al., 2020). The main parameters of the software were set as follows: Align Retention Times: Maximum Shift: 2 min; Mass tolerance: 5 ppm; Detect Compound: Mass Tolerance: 5 ppm; Intensity Tolerance: 30%; Min. Peak Intensity: 500,000; Data Sources: mzCloud, mzVault, MassList, and ChemSpider Search; and S/N Threshold: 3. Finally, according to the software search report, combined with fragment information, the structures of 165 components were speculated, of which 20 were further confirmed with reference substances. The components in JZDHW included anthraquinones, anthrones, tannins, phenbutyl ketones, and corresponding glycosides. Among them, free and bound anthraquinones were the main components, including emodin, rhein, aloe-emodin, and their glycosides.

Analysis of Metabolites in Human Plasma

A variety of targeted and non-targeted intelligent MS data post-processing technologies (Wu et al., 2016; Zhu et al., 2020; Chen T et al., 2021; Chen X et al., 2021), such as high resolution extraction ion chromatography (HREIC), precise-and-thorough background-subtraction, mass defect filter, and data-independent acquisition-product-ion filter, have been used in recent years to establish a research strategy for the comprehensive identification of TCM-related compounds *in vivo*. The present study directly searched the prototype and metabolite components of JZDHW from the perspective of the human body based on the technical strategy developed in the early stage. For the first time, 72 JZDHW-related compounds were identified in human plasma samples, including 11 prototype components, such as rhein, emodin, and gallic acid, and 61 related metabolites, including primarily glucuronidated and sulphated metabolites (**Supplementary Table S2**) (Song et al., 2010; Zhu et al., 2015; Huang et al., 2019; Xu et al., 2019). **Figure 2** shows an extracted ion chromatogram of human plasma samples after completion of the methanol precipitation method. In addition, **Supplementary Figure S1** shows an extracted ion chromatogram of human plasma samples pre-treated with solid phase extraction.

Semi-Quantitative Determination of Exposure of JZDHW-Related Compounds in Human Plasma as Determined Using the AUC Pooled Method

Traditionally, the exposure of compounds *in vivo* is obtained by measuring the drug concentration at multiple time points to draw a drug-time curve, and then obtaining exposure parameters such as AUC. For TCM, this method has some improvements: the components of TCM are complex, and it is difficult to quantify multiple components; more importantly, many components cannot be obtained as reference materials, thus exposure data cannot be quantitatively obtained. In this study, we applied the AUC pooled method to study the exposure of TCM for the first time. Using the formula $v_1 : v_2 : \cdots : v_i = (t_1 - t_0) : (t_2 - t_0) : (t_3 - t_1) : \cdots : (t_i - t_{i-1})$, we calculated the volume ratio of plasma at different time points, and then mixed the plasma samples. The measured concentration

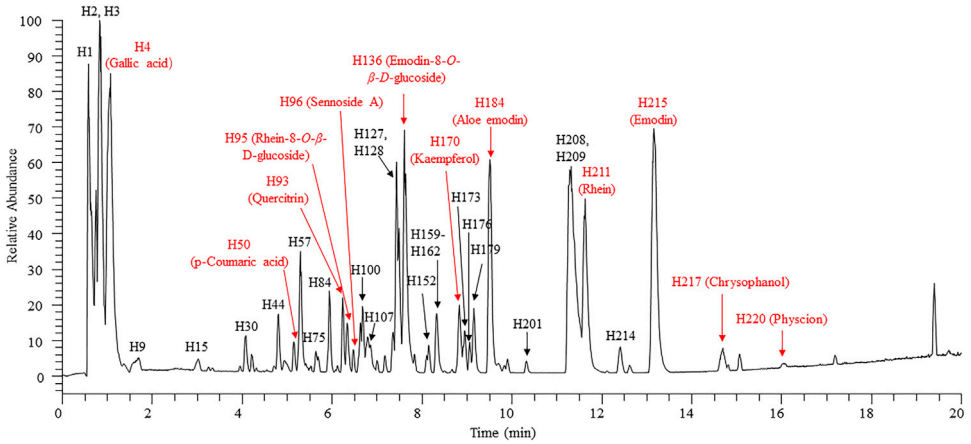

FIGURE 1 | High-resolution total ion chromatogram of rhubarb. Red: compounds verified by reference substances.

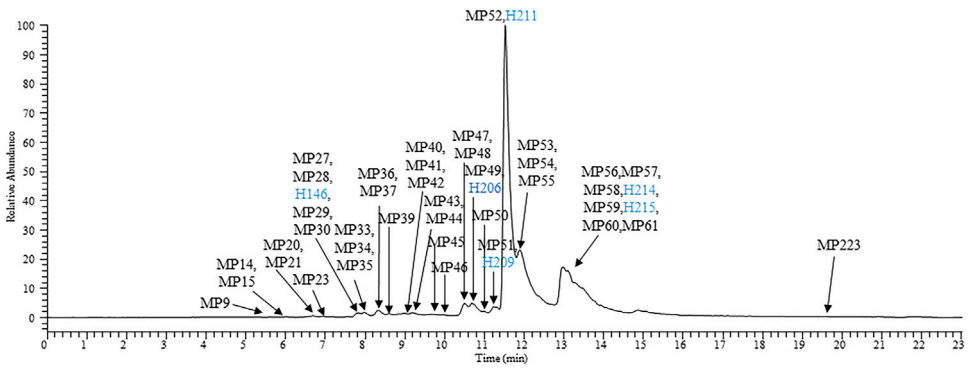

FIGURE 2 | High-resolution extracted ion chromatogram of the main exposed components of human plasma samples processed using the methanol protein precipitation method. Blue: prototype components of rhubarb.

(indicated by the peak area without reference substance) multiplied by the last collection time value directly represents the exposure of prototype and metabolite components *in vivo* (as shown in **Figure 3A**). Taking rhein as an example, a combination of the traditional and AUC pooled methods was used to determine the AUC values of the human and rat plasma samples. As shown in **Table 1**, the difference between the two methods was 12.78% in rat samples and 0.58% in human samples, both of which are within 15%, indicating that the AUC pooled method can effectively replace the traditional method to obtain more accurate AUC values.

In this study, the human plasma collected at each time point was mixed and measured according to the AUC pooled method. The exposure difference in human plasma was visually shown using peak area data from HREIC. Among the 20 compounds with high exposure, H211 (rhein), M52 (oxidized aloe emodin), MP54 (sulphated emodin isomer), and H214 (laccaic acid D) were the main substances *in vivo*, followed by the sulphated metabolites of anthraquinone compounds such as emodin, chrysophanol, aloe-emodin, and rhein (**Figure 3B**). It is worth mentioning that the exposure of the top ten components accounted for 90% of the exposure of all compounds *in vivo*. Among the top ten exposed components, only H211 (rhein) could be obtained as a reference substance, and therefore could be considered as a potential Q-marker of JZDHW.

To further determine whether rhein can reflect or predict the overall metabolic trend of JZDHW anthraquinone and its metabolites in the human body, we compared the percentage concentrations of the nine other top components at different collection time points with those of rhein using Pearson correlation coefficient analysis (**Figure 4**). We found that all nine components had a strong correlation with rhein ($0.8 < R < 1$, $p < 0.001$). Therefore, rhein could be selected as a Q-marker to reflect the pharmacokinetic trend of anthraquinone components of JZDHW in humans.

Selection of Pharmacodynamic Model Animals

Animals such as rats and mice are commonly used in the study of TCM pharmacodynamics. However, metabolism varies in

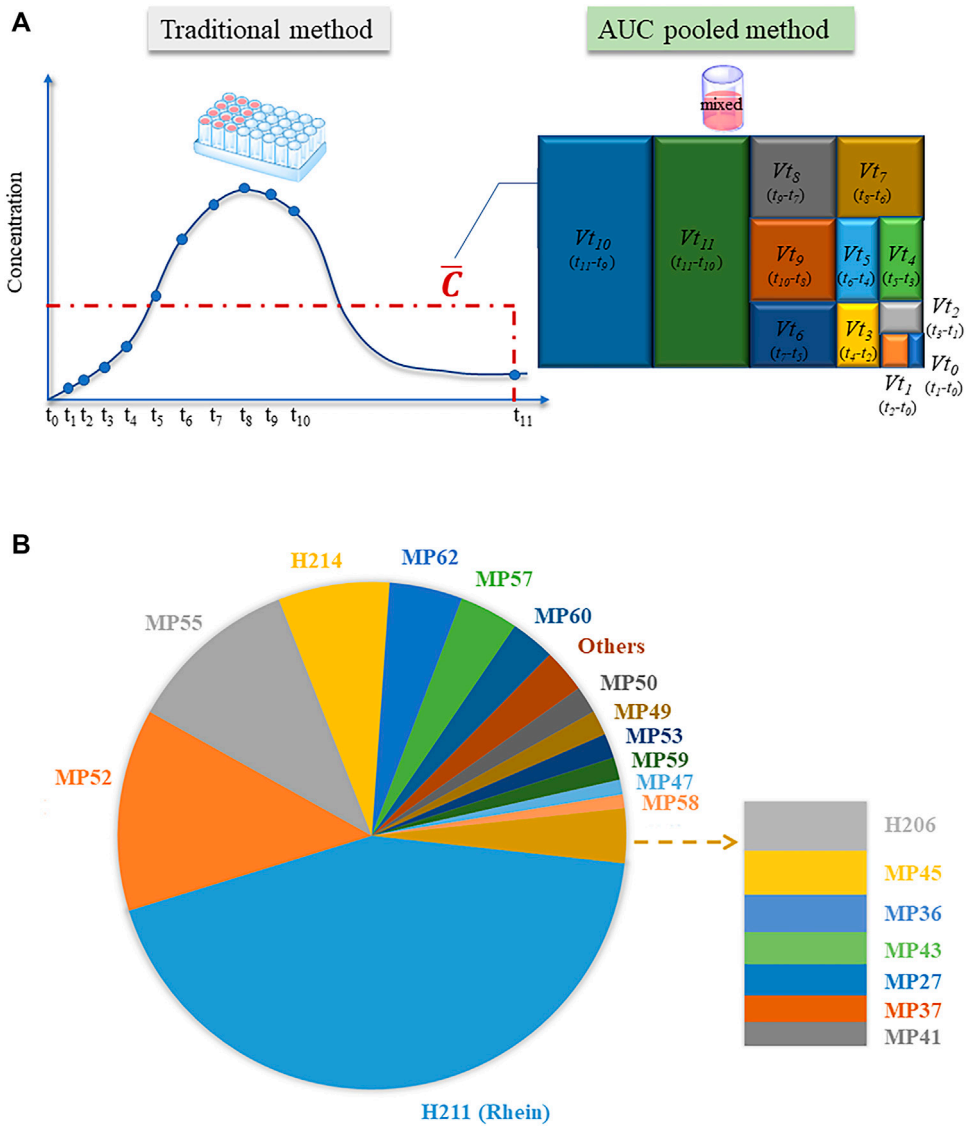

FIGURE 3 | Research on the area under the time-concentration curve (AUC) of relevant components *in vivo*. **(A)** Operational differences between the traditional and AUC pooled methods; **(B)** Top 20 rhubarb-related components *in vivo*.

TABLE 1 | Determination of the area under the time-concentration curve (AUC) using the AUC pooled and traditional methods.

	Rat-rhein	Human-rhein
No pooled-AUC(mg/L*h)	72517.5 ± 42.2	57651 ± 47.8
AUC-pooled (mg/L*h)	81786.81 ± 24.7	57984.4 ± 19.3
Difference	12.78%	0.58%

different species. Only on the basis of verifying the metabolism consistency of animals and humans, the obtained pharmacodynamic data had more reference significance for clinical research. We analysed the plasma samples of SD rats and C57BL/6 mice after oral administration of JZDHW solution and searched for 192 JZDHW-related compounds (**Supplementary Table S2**). The top 10 compounds in human exposure were also well exposed in rats and mice (**Figure 5A**), accounting for 51 and 62% of all exposed compounds in their bodies, respectively (**Figure 5B**). Mice were slightly better than rats. It is worth mentioning that the exposure of rhein was the highest in all three species. Moreover, the main metabolites of rhein-glucuronidated and sulphated metabolites could be found in rodents (**Figure 5C**). In **Figure 5C**, rats, mice, and human had different metabolic binding sites. No matter that it was sulfation or glucuronidation, both humans and rodents had their own preferred metabolic sites, which might be caused by difference types of metabolic enzymes. In addition, comparing the total peak areas of rhein sulfated metabolites with those of glucuronidated metabolites in three species, it was found that sulfation was more preferred in humans while glucuronidation was more preferred in

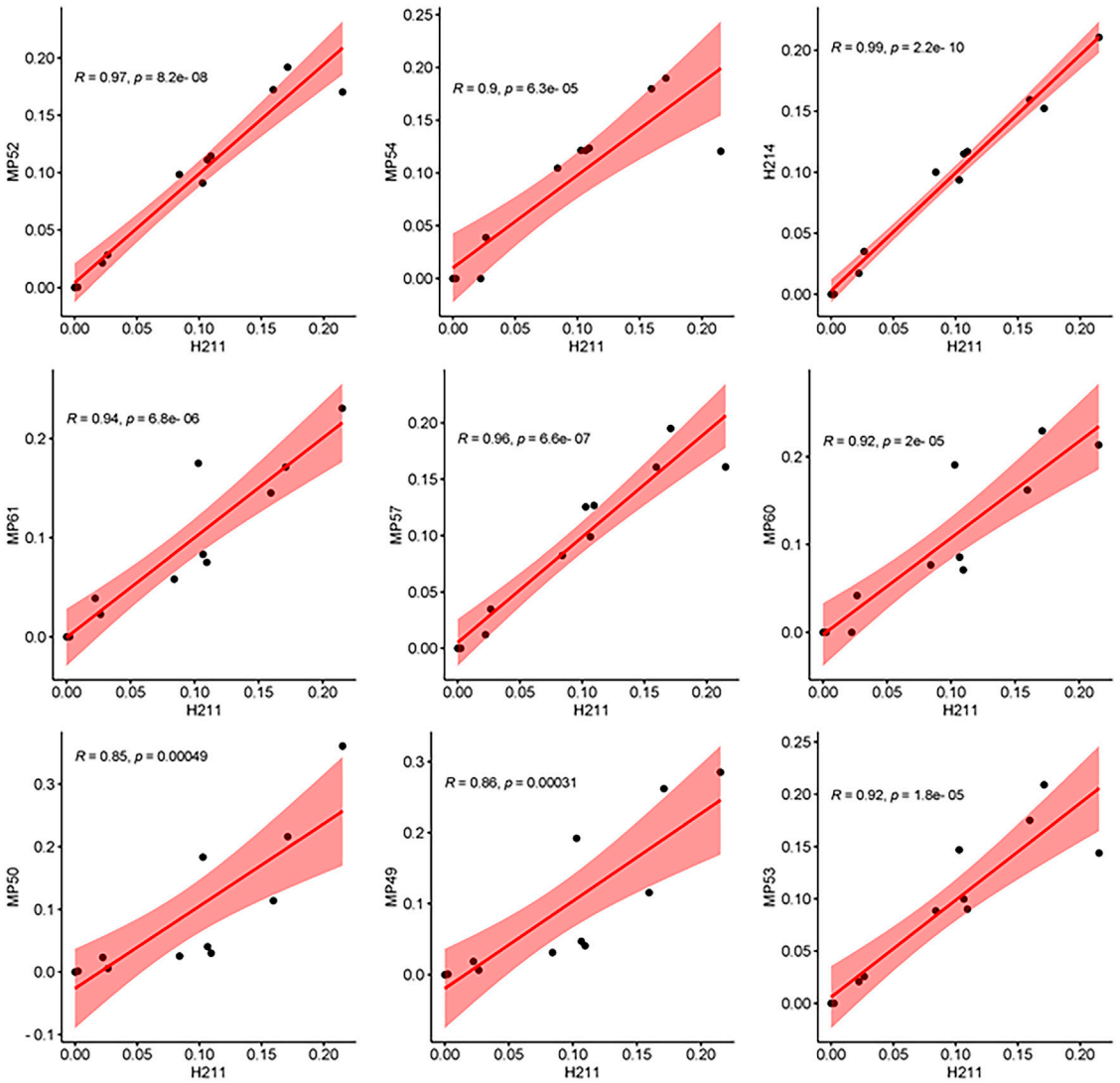

FIGURE 4 | Pearson correlation analysis between the main exposed compounds and rhein.

mice and rats. This finding may be caused by differences in the activity of metabolic enzymes. In general, in terms of metabolic pathways and binding sites, there were no significant differences between rats and mice. However, the main exposed compounds of JZDHW in humans can be well exposed in rats and mice. In short, rodents can also be used as a suitable model animal to study the efficacy of rhubarb.

Pharmacodynamic Verification

Pneumonia is associated with inflammatory stimulation from microorganisms, such as endotoxin, which causes severe pneumonia. As a potent endotoxin, lipopolysaccharide is used by many scholars to induce the establishment of an animal model of pneumonia to evaluate the efficacy of the drug in recent years. This is a relatively simple, efficient, safe, low-cost, and mature method. Based on LPS-induced pulmonary inflammation in C57BL/6 mice, four groups were established to compare the effects of pneumonia treatment: the control, model, rhein, and JZDHW groups. In clinical treatment, the human dosage of JZDHW is 6 g/d. By considering the conversion based on body surface area of human (70 kg) and mice (0.02 kg), the dose for mice was about 0.0156 g/d. In order to ensure the pharmaceutical efficacy, a double dosage was applied. Therefore, the dose of JZDHW was determined as 1.6 g/kg. The dose of rhein was consistent with that of total anthraquinone in JZDHW, which was calculated according to the 2020 edition of Pharmacopoeia of the People's Republic of China. In details, the dose of rhein was 85 mg/kg. After the animal experiments (**Figure 6A**), we analysed the pathological changes in the lung tissue and changes in the serum pro-inflammatory factors. Inflammatory cell infiltration, alveolar haemorrhage, interstitial oedema, thickening of the alveolar septum, and fibrin exudation in the alveoli are the main features of LPS-induced pneumonia. According to the histopathological

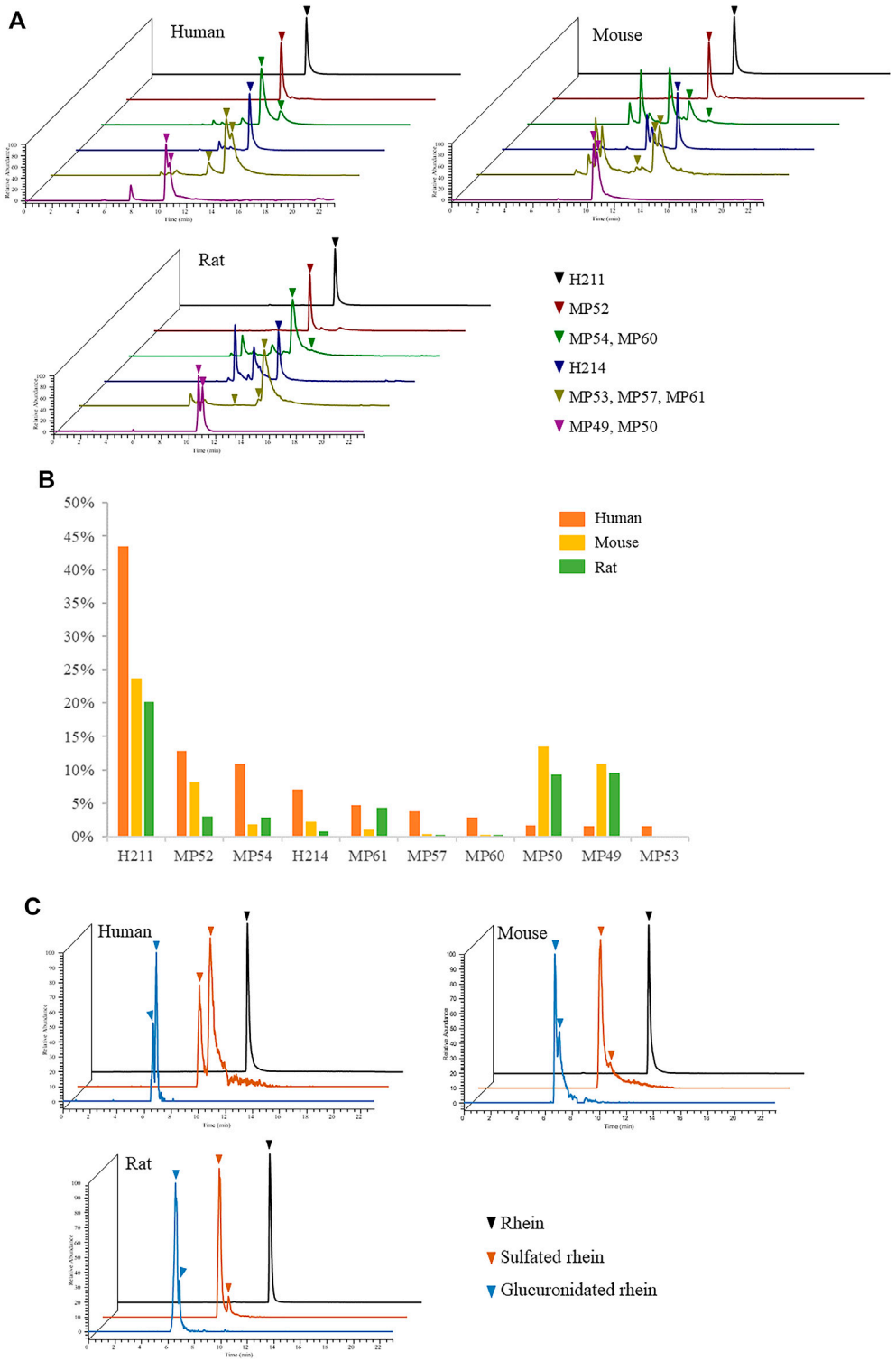

FIGURE 5 | Metabolism of rhubarb in humans, rats, and mice. **(A)** Exposure of the top 10 compounds in human exposure in different species; **(B)** Proportion of the top 10 compounds in human exposure in different species; **(C)** Metabolism of rhein in different species.

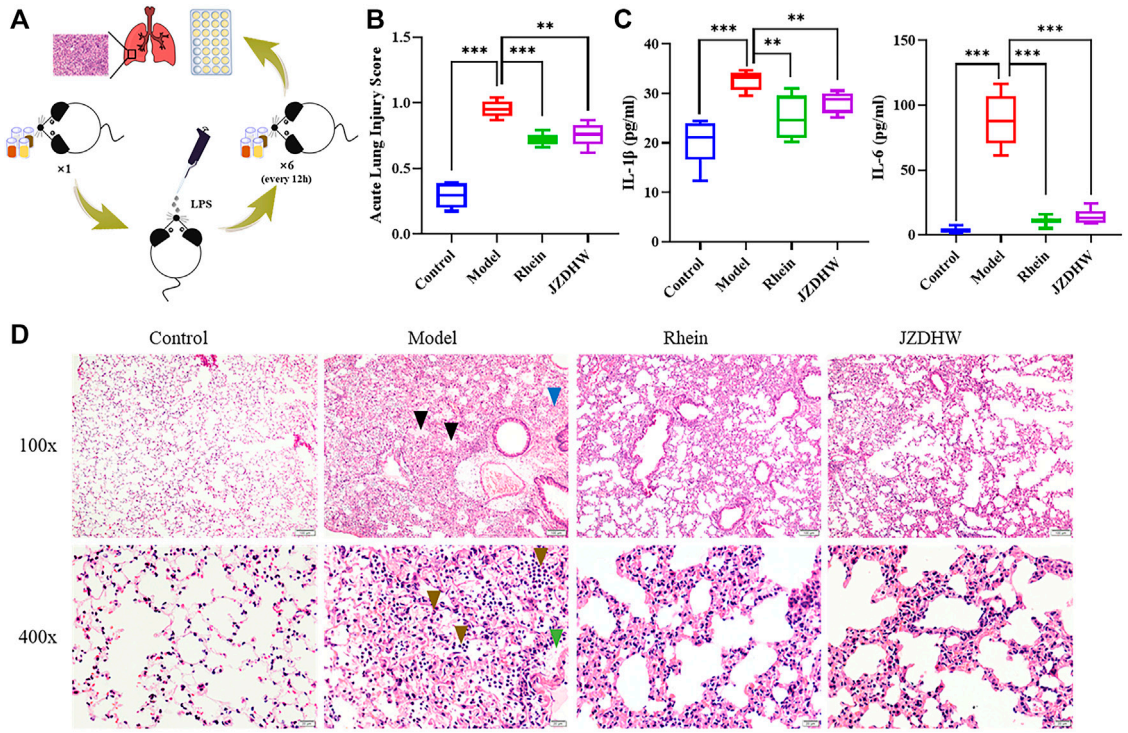

FIGURE 6 | Therapeutic effect of rhubarb and its monomers on pneumonia. **(A)** Schematic diagram of the experiment; **(B)** Acute lung injury score; **(C)** Pro-inflammatory factor ELISA test; **(D)** Tissue section (100 × magnification and ×400). ▼indicates oedema, ▼indicates bleeding, ▼indicates inflammatory cells, and ▼indicates fibrin oozing out of the alveoli. The results are given as mean ± standard error of the mean (n = 6).

characteristics of the acute lung injury scoring system (Li et al., 2019) (**Figure 6B**), the scores of the therapy groups were significantly reduced compared with those in the model group. Furthermore, the oedema of the therapy groups was significantly relieved, and the infiltration of inflammatory cells was significantly reduced ($p < 0.01$) (**Figure 6D**). In addition, the concentrations of serum pro-inflammatory factors IL-1β and IL-6 in the therapy groups were significantly lower than those in the model group (**Figure 6C**). Combined with the current epidemic COVID-19, the clinical studies have shown that cytokine storms were prone to occur in infected patients, leading to inflammation, infiltration of macrophages, neutrophils, and multiple organ damage. More importantly, IL-6 was one of the key inflammatory factors. Therefore, cytokine storm can be induced by LPS stimulation to simulate that of COVID-19. In summary, JZDHW and its monomer (rhein) can effectively alleviate the symptoms of acute pneumonia and can be used as candidate drugs for COVID-19.

DISCUSSION

From the perspective of the human body, this study used the laboratory's self-built data post-processing system to search and identify prototype and metabolite compounds of JZDHW by UPLC-HRMS. We used the simple and practical AUC pooled method to quickly obtain the exposure of each component and screened out the main exposed substances. We then performed correlation analysis on the pharmacokinetic curve to find a representative Q-marker, rhein (**Figure 7**). The results showed that the AUC pooled method can effectively aid in the quick determination of potential Q-markers of TCM.

Before establishing an animal model to evaluate pharmacodynamics, it should be verified that the main prototype and metabolite compounds in the chosen animal are consistent with those in humans. The exposure difference between humans and animals is often ignored by studies on the efficacy of TCM. This study considered the possibility of the existence of this difference, and experimentally proved that the Q-marker rhein is retained in the plasma of SD rats and C57BL/6 mice, and generated glucuronidated and sulphated metabolites, which were similar to those in humans. This guaranteed the reliability of our animal model selection. In addition to the acute pneumonia model, we also conducted an efficacy verification in an acute pancreatitis model (the dosages for both models were determined by the same principle). The results showed that rhein could significantly reduce the concentration of serum amylase and lipase, which are diagnostic indicators of acute pancreatitis, and reduce pathological symptoms such as bleeding, oedema, necrosis, and inflammatory cell infiltration. The concentration of pro-inflammatory factors IL-6 and IL-1β were also reduced, indicating a positive anti-inflammatory effect (**Figure 8**). In this study, based on human exposure and the AUC pooled method, the anthraquinone monomer rhein with high

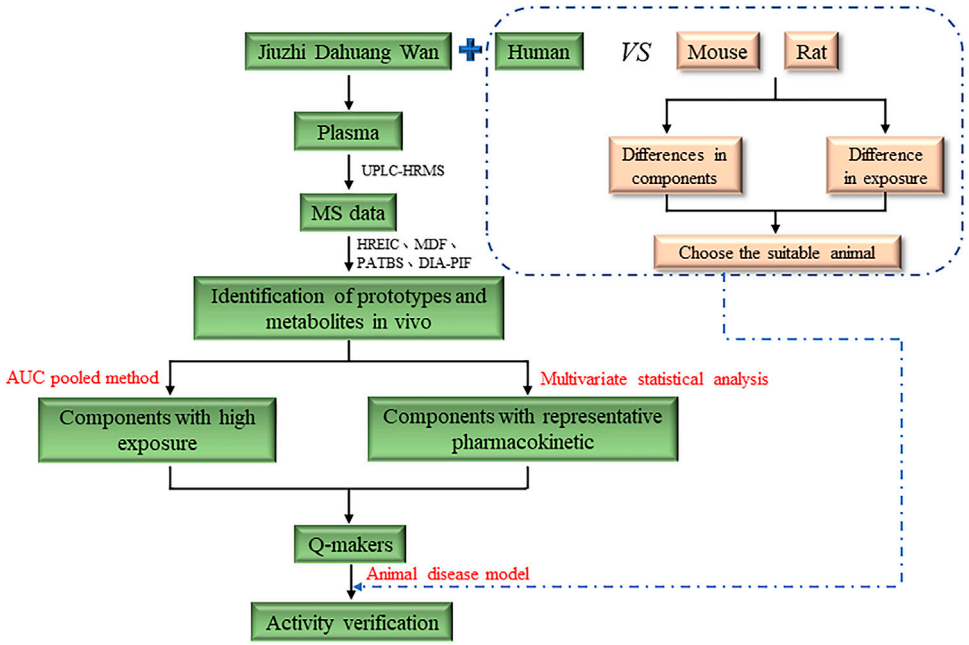

FIGURE 7 | Workflow of the research strategy.

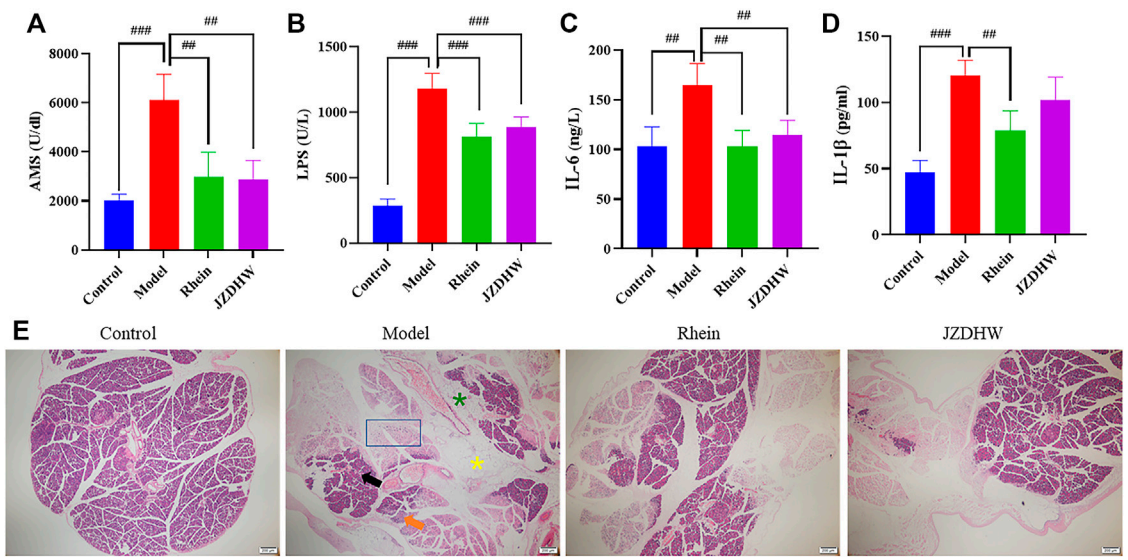

FIGURE 8 | Therapeutic effect of rhubarb and its monomers on pancreatitis. **(A)** Serum amylase; **(B)** Lipase; **(C)** IL-6; **(D)** IL-1β; **(E)** Tissue section (40 × magnification), ⬆ indicates haemorrhage, ⬆ indicates oedema, * indicates fatty acid, * indicates inflammatory cells, and ▭ indicates necrosis. The results are given as mean ± standard error of the mean (n = 6). Significant differences between groups are represented by # for $p < 0.05$, ## for $p < 0.01$ and ### for $p < 0.001$.

exposure *in vivo* and a significant anti-inflammatory effect was recorded. More importantly, rhein can represent the overall metabolic changes of JZDHW anthraquinone in humans and rodents.

Therefore, based on the Chinese Pharmacopoeia and our research data, we believed that, besides to the monitoring of the total content of total anthraquinones and free anthraquinones, it was also necessary to control the content of rhein individually, because of its high content in rhubarb, good pharmacokinetic properties, and good pharmacological effects *in vivo*. However, there are many anthraquinone compounds in rhubarb, which may be mutual conversion *in vivo*, leading interference to formulation of the quality standard range of Q-marker. Our previous studies had shown that chrysophanol

and aloe-emodin could be converted into rhein in rats. However, the amount of rhein converted from other anthraquinone compounds *in vivo* was little, because chrysophanol and aloe-emodin also underwent glucuronidation, sulfation and other reactions. And the application of this phenomenon to humans was uncertain. In addition, from the perspective of drug interactions, other anthraquinone compounds, which had an effect on the absorption and metabolism of rhein, still needed to be further elucidated. Therefore, it was necessary to combine the influence of other anthraquinones, when determining the quality control range of rhein.

CONCLUSION

Through the pharmacokinetics exploration of rhubarb in humans for the first time based on the AUC pooled semi-quantitative method and the pharmacodynamic verification of different animal models, rhein can be experimentally proved to be Q-marker of rhubarb, whose content needs to be strictly controlled. Furthermore, the research strategy established in this study might also be beneficial in the identification of Q-markers in other TCM, and provide a reference for the improvement of quality standards, so as to carry out stricter quality control of TCM.

DATA AVAILABILITY STATEMENT

The original contributions presented in the study are included in the article/**Supplementary Material**, further inquiries can be directed to the corresponding author.

ETHICS STATEMENT

Ethical review and approval was not required for the study on human participants in accordance with the local legislation and institutional requirements. The patients/participants provided their written informed consent to participate in this study. The animal study was reviewed and approved by the Xiamen University Laboratory Animal Center.

AUTHOR CONTRIBUTIONS

JC: Resources, Investigation, Formal analysis, Writing-Original Draft; XJ: Investigation, Writing-Original Draft; CZ: Writing-Review and Editing; LY: Resources; ML: Resources; MZ: Writing-Review and Editing, Software; CW: Conceptualization, Writing-Review and Editing, Supervision, Project administration, Funding acquisition. All authors have read and agreed to the published version of the manuscript.

FUNDING

This work was supported by the National Natural Science Foundation of China (Grant Numbers 82141215, 82173779, U1903119).

SUPPLEMENTARY MATERIAL

The Supplementary Material for this article can be found online at: https://www.frontiersin.org/articles/10.3389/fphar.2022.865066/full#supplementary-material

REFERENCES

Bai, G., Zhang, T., Hou, Y., Ding, G., Jiang, M., and Luo, G. (2018). From Quality Markers to Data Mining and Intelligence Assessment: A Smart Quality-Evaluation Strategy for Traditional Chinese Medicine Based on Quality Markers. *Phytomedicine* 44, 109–116. doi:10.1016/j.phymed.2018.01.017

Cao, Y. J., Pu, Z. J., Tang, Y. P., Shen, J., Chen, Y. Y., Kang, A., et al. (2017). Advances in Bio-Active Constituents, Pharmacology and Clinical Applications of Rhubarb. *Chin. Med.* 12, 36. doi:10.1186/s13020-017-0158-5

Chen, T., Liang, W., Zhang, X., Lu, X., Zhao, C., and Xu, G. (2021). Nontargeted Screening of Veterinary Drugs and Their Metabolites in Milk Based on Mass Defect Filtering Using Liquid Chromatography-High-resolution Mass Spectrometry. *Electrophoresis*. [Preprint]. Available at https://analyticalsciencejournals.onlinelibrary.wiley.com/doi/10.1002/elps.202100296 [Accessed March 4, 2022]

Chen, X., Wu, Y., Chen, C., Gu, Y., Zhu, C., Wang, S., et al. (2021). Identifying Potential Anti-COVID-19 Pharmacological Components of Traditional Chinese Medicine Lianhuaqingwen Capsule Based on Human Exposure and ACE2 Biochromatography Screening. *Acta Pharm. Sin. B* 11, 222–236. doi:10.1016/j.apsb.2020.10.002

Chinese Pharmacopoeia Commission (2020). *Pharmacopoeia of the People's republic of China. Part I*. Beijing: Chemical Industry Press.

Hammer, H., Schmidt, F., Marx-Stoelting, P., Pötz, O., and Braeuning, A. (2021). Cross-species Analysis of Hepatic Cytochrome P450 and Transport Protein Expression. *Arch. Toxicol.* 95, 117–133. doi:10.1007/s00204-020-02939-4

He, J., Feng, X., Wang, K., Liu, C., and Qiu, F. (2018). Discovery and Identification of Quality Markers of Chinese Medicine Based on Pharmacokinetic Analysis. *Phytomedicine* 44, 182–186. doi:10.1016/j.phymed.2018.02.008

Hop, C. E., Wang, Z., Chen, Q., and Kwei, G. (1998). Plasma-pooling Methods to Increase Throughput for *In Vivo* Pharmacokinetic Screening. *J. Pharm. Sci.* 87, 901–903. doi:10.1021/js970486q

Huang, Y. F., Bai, C., He, F., Xie, Y., and Zhou, H. (2020). Review on the Potential Action Mechanisms of Chinese Medicines in Treating Coronavirus Disease 2019 (COVID-19). *Pharmacol. Res.* 158, 104939. doi:10.1016/j.phrs.2020.104939

Huang, Z., Xu, Y., Wang, Q., and Gao, X. (2019). Metabolism and Mutual Biotransformations of Anthraquinones and Anthrones in Rhubarb by Human Intestinal flora Using UPLC-Q-TOF/MS. *J. Chromatogr. B Analyt. Technol. Biomed. Life Sci.* 1104, 59–66. doi:10.1016/j.jchromb.2018.10.008

Li, D., Zhang, R., Cui, L., Chu, C., Zhang, H., Sun, H., et al. (2019). Multiple Organ Injury in Male C57BL/6J Mice Exposed to Ambient Particulate Matter in a Real-Ambient PM Exposure System in Shijiazhuang, China. *Environ. Pollut.* 248, 874–887. doi:10.1016/j.envpol.2019.02.097

Li, H. J., Wei, W. L., Li, Z. W., Yao, C. L., Wang, M. Y., Zhang, J. Q., et al. (2020). Systematic Comparison of Metabolic Differences of Uncaria Rhynchophylla in Rat, Mouse, Dog, Pig, Monkey and Human Liver Microsomes. *Anal. Bioanal. Chem.* 412, 7891–7897. doi:10.1007/s00216-020-02922-z

Li, Z., Liu, J., Li, Y., Du, X., Li, Y., Wang, R., et al. (2018). Identify Super Quality Markers from Prototype-Based Pharmacokinetic Markers of Tangzhiqing Tablet (TZQ) Based on *In Vitro* Dissolution/Permeation and *In Vivo* Absorption Correlations. *Phytomedicine* 45, 59–67. doi:10.1016/j.phymed.2018.04.001

Lin, C. C., Wu, C. I., Lin, T. C., and Sheu, S. J. (2006). Determination of 19 Rhubarb Constituents by High-Performance Liquid Chromatography-Ultraviolet-Mass Spectrometry. *J. Sep. Sci.* 29, 2584–2593. doi:10.1002/jssc.200500307

Liu, C. X., Chen, S. L., Xiao, X. H., Zhang, T. J., Hou, W. B., and Liao, M. L. (2016). A New Concept on Quality Marker of Chinese Materia Medica: Quality Control for Chinese Medicinal Products. *Chin. Tradit. Herb. Drugs* 47, 1443–1457. doi:10.7501/j.issn.0253-2670.2016.09.001

Martignoni, M., Groothuis, G. M., and de Kanter, R. (2006). Species Differences between Mouse, Rat, Dog, Monkey and Human CYP-Mediated Drug Metabolism, Inhibition and Induction. *Expert Opin. Drug Metab. Toxicol.* 2, 875–894. doi:10.1517/17425255.2.6.875

Nizioł, J., Sekuła, J., and Ruman, T. (2017). Visualizing Spatial Distribution of Small Molecules in the Rhubarb Stalk (Rheum Rhabarbarum) by Surface-Transfer Mass Spectrometry Imaging. *Phytochemistry* 139, 72–80. doi:10.1016/j.phytochem.2017.04.006

Qin, T., Wu, L., Hua, Q., Song, Z., Pan, Y., and Liu, T. (2020). Prediction of the Mechanisms of Action of Shenkang in Chronic Kidney Disease: A Network Pharmacology Study and Experimental Validation. *J. Ethnopharmacol.* 246, 112128. doi:10.1016/j.jep.2019.112128

Ren, J. L., Zhang, A. H., Kong, L., Han, Y., Yan, G. L., Sun, H., et al. (2020). Analytical Strategies for the Discovery and Validation of Quality-Markers of Traditional Chinese Medicine. *Phytomedicine* 67, 153165. doi:10.1016/j.phymed.2019.153165

Song, R., Xu, L., Xu, F., Li, Z., Dong, H., Tian, Y., et al. (2010). *In Vivo* metabolism Study of Rhubarb Decoction in Rat Using High-Performance Liquid Chromatography with UV Photodiode-Array and Mass-Spectrometric Detection: a Strategy for Systematic Analysis of Metabolites from Traditional Chinese Medicines in Biological Samples. *J. Chromatogr. A.* 1217, 7144–7152. doi:10.1016/j.chroma.2010.09.028

Wu, C., Zhang, H., Wang, C., Qin, H., Zhu, M., and Zhang, J. (2016). An Integrated Approach for Studying Exposure, Metabolism, and Disposition of Multiple Component Herbal Medicines Using High-Resolution Mass Spectrometry and Multiple Data Processing Tools. *Drug Metab. Dispos.* 44, 800–808. doi:10.1124/dmd.115.068189

Xian, J., Fu, J., Cheng, J. T., Zhang, J., Jiao, M. J., Wang, S. H., et al. (2017). Isolation and Identification of Chemical Consituents from Aerial Parts of Rheum Officinale. *J. Exp. Tradit. Med. Formulae* 23, 45–51. doi:10.13422/j.cnki.syfjx.2017140045

Xiang, H., Zuo, J., Guo, F., and Dong, D. (2020). What We Already Know about Rhubarb: a Comprehensive Review. *Chin. Med.* 15, 88. doi:10.1186/s13020-020-00370-6

Xu, Y., Zhang, L., Wang, Q., Luo, G., and Gao, X. (2019). An Integrated Strategy Based on Characteristic Fragment Filter Supplemented by Multivariate Statistical Analysis in Multi-Stage Mass Spectrometry Chromatograms for the Large-Scale Detection and Identification of Natural Plant-Derived Components in Rat: The Rhubarb Case. *J. Pharm. Biomed. Anal.* 174, 89–103. doi:10.1016/j.jpba.2019.05.049

Yang, W., Jiang, X., Liu, J., Qi, D., Luo, Z., Yu, G., et al. (2021). Integrated Strategy from *In Vitro*, *In Situ*, *In Vivo* to In Silico for Predicting Active Constituents and Exploring Molecular Mechanisms of Tongfengding Capsule for Treating Gout by Inhibiting Inflammatory Responses. *Front. Pharmacol.* 12, 759157. doi:10.3389/fphar.2021.759157

Zhang, T., Bai, G., Han, Y., Xu, J., Gong, S., Li, Y., et al. (2018). The Method of Quality Marker Research and Quality Evaluation of Traditional Chinese Medicine Based on Drug Properties and Effect Characteristics. *Phytomedicine* 44, 204–211. doi:10.1016/j.phymed.2018.02.009

Zhou, S., Ai, Z., Li, W., You, P., Wu, C., Li, L., et al. (2020). Deciphering the Pharmacological Mechanisms of Taohe-Chengqi Decoction Extract against Renal Fibrosis through Integrating Network Pharmacology and Experimental Validation *In Vitro* and *In Vivo*. *Front. Pharmacol.* 11, 425. doi:10.3389/fphar.2020.00425

Zhu, C., Cai, T., Jin, Y., Chen, J., Liu, G., Xu, N., et al. (2020). Artificial Intelligence and Network Pharmacology Based Investigation of Pharmacological Mechanism and Substance Basis of Xiaokewan in Treating Diabetes. *Pharmacol. Res.* 159, 104935. doi:10.1016/j.phrs.2020.104935

Zhu, H., Bi, K., Han, F., Guan, J., Zhang, X., Mao, X., et al. (2015). Identification of the Absorbed Components and Metabolites of Zhi-Zi-Da-Huang Decoction in Rat Plasma by Ultra-high Performance Liquid Chromatography Coupled with Quadrupole-Time-Of-Flight Mass Spectrometry. *J. Pharm. Biomed. Anal.* 111, 277–287. doi:10.1016/j.jpba.2015.03.043

Zhuang, W., Fan, Z., Chu, Y., Wang, H., Yang, Y., Wu, L., et al. (2020). Chinese Patent Medicines in the Treatment of Coronavirus Disease 2019 (COVID-19) in China. *Front. Pharmacol.* 11, 1066. doi:10.3389/fphar.2020.01066

Conflict of Interest: Author MZ is employed by company MassDefect Technologies.

The remaining authors declare that the research was conducted in the absence of any commercial or financial relationships that could be construed as a potential conflict of interest.

Publisher's Note: All claims expressed in this article are solely those of the authors and do not necessarily represent those of their affiliated organizations, or those of the publisher, the editors and the reviewers. Any product that may be evaluated in this article, or claim that may be made by its manufacturer, is not guaranteed or endorsed by the publisher.

frontiers | Frontiers in Pharmacology

ORIGINAL RESEARCH
published: 18 May 2022
doi: 10.3389/fphar.2022.878817

Hepatotoxicity of the Major Anthraquinones Derived From Polygoni Multiflori Radix Based on Bile Acid Homeostasis

Li Kang[1,2,3†], Dan Li[2,4†], Xin Jiang[2†], Yao Zhang[5], Minhong Pan[4], Yixin Hu[2], Luqin Si[2], Yongjun Zhang[6] and Jiangeng Huang[2*]*

[1]School of Pharmaceutical Science, South-Central MinZu University, Wuhan, China, [2]School of Pharmacy, Tongji Medical College, Huazhong University of Science and Technology, Wuhan, China, [3]National Demonstration Center for Experimental Ethnopharmacology Education, South-Central MinZu University, Wuhan, China, [4]Department of Pharmacy, Shenzhen University General Hospital, Shenzhen, China, [5]College of Pharmacy, Key Laboratory of Xinjiang Phytomedicine Resource and Utilization, Ministry of Education, Shihezi University, Shihezi, China, [6]The Third Affiliated Hospital of School of Medicine, Shihezi University, Shihezi, China

OPEN ACCESS

Edited by:
Jian-bo Yang,
National Institutes for Food and Drug Control, China

Reviewed by:
Ke Lan,
Sichuan University, China
Kyunghee Yang,
Simulations Plus, United States

***Correspondence:**
Yongjun Zhang
zhangyongjun@shzu.edu.cn
Jiangeng Huang
jiangenghuang@hust.edu.cn

†These authors have contributed equally to this work

Specialty section:
This article was submitted to Experimental Pharmacology and Drug Discovery, a section of the journal Frontiers in Pharmacology

Received: 18 February 2022
Accepted: 15 April 2022
Published: 18 May 2022

Citation:
Kang L, Li D, Jiang X, Zhang Y, Pan M, Hu Y, Si L, Zhang Y and Huang J (2022) Hepatotoxicity of the Major Anthraquinones Derived From Polygoni Multiflori Radix Based on Bile Acid Homeostasis. Front. Pharmacol. 13:878817. doi: 10.3389/fphar.2022.878817

Polygoni Multiflori Radix (PMR), the dried root of *Polygonum Multiflorum* Thunb., has been widely used as traditional Chinese medicines in clinical practice for centuries. However, the frequently reported hepatotoxic adverse effects hindered its safe use in clinical practice. This study aims to explore the hepatotoxic effect of PMR extract and the major PMR derived anthraquinones including emodin, chrysophanol, and physcion in mice and the underlying mechanisms based on bile acid homeostasis. After consecutively treating the ICR mice with PMR extract or individual anthraquinones for 14 or 28 days, the liver function was evaluated by measuring serum enzymes levels and liver histological examination. The compositions of bile acids (BAs) in the bile, liver, and plasma were measured by LC-MS/MS, followed by Principal Component Analysis (PCA) and Partial Least Squares Discriminate Analysis (PLS-DA). Additionally, gene and protein expressions of BA efflux transporters, bile salt export pump (Bsep) and multidrug resistance-associated protein 2 (Mrp2), were examined to investigate the underlying mechanisms. After 14-day administration, mild inflammatory cell infiltration in the liver was observed in the physcion- and PMR-treated groups, while it was found in all the treated groups after 28-day treatment. Physcion and PMR extract induced hepatic BA accumulation after 14-day treatment, but such accumulation was attenuated after 28-day treatment. Based on the PLS-DA results, physcion- and PMR-treated groups were partially overlapping and both groups showed a clear separation with the control group in the mouse liver. The expression of Bsep and Mrp2 in the physcion- and PMR-treated mouse liver was decreased after 14-day treatment, while the downregulation was abrogated after 28-day treatment. Our study, for the first time, demonstrated that both PMR extract and tested anthraquinones could alter the disposition of either the total or individual BAs in the mouse bile, liver, and plasma *via* regulating the BA efflux transporters and induce liver injury, which provide a theoretical basis for the quality control and safe use of PMR in practice.

Keywords: Polygoni Multiflori Radix, anthraquinones, bile acids, homeostasis, transporter

1 INTRODUCTION

Polygoni Multiflori Radix (PMR), originated from the tuberous root of *Polygonum multiflorum* Thunb., is a well-known traditional Chinese medicine and has been commonly used in clinical practice in either raw or processed forms for different indications such as detoxification, carbuncle elimination, malaria prevention, bowel relaxation, hair-darkening, nourishment of the liver and kidney, and so on (Chinese Pharmacopoeia Commission, 2015). Although PMR was widely used in clinical practice or as a tonic, a series of cases of hepatic adverse effects associated with PMR or the herbal medicine products containing PMR were constantly reported (But et al., 1996; Park et al., 2001; Cárdenas et al., 2006; Laird et al., 2008; Cho et al., 2009; Jung et al., 2011; Dong et al., 2014). Accordingly, the supervisions of clinical usage of PMR have been conducted by the drug regulatory agencies in Canada, Australia, the United Kingdom, and China (Canadian Adverse Reaction Newsletter, 2003; Medicines and Healthcare products Regulatory Agency, 2006; Complementary Medicines Evaluation Committee, 2008; China Food and Drug Administration, 2014). Therefore, the safe and effective use of PMR in clinical practice has become an important and urgent problem which needed to be resolved.

According to previous reports, more than 100 components from PMR had been isolated and identified including stilbenes, anthraquinones, dianthrones, flavonoids, and phenolic acids (Yang et al., 2016; Wang et al., 2017; Yang et al., 2017; Yang et al., 2018b; Yang et al., 2019). After oral administration in rats with PMR extract, 41 compounds were detected in the rat plasma with stilbenes and quinones as the major components (Wang et al., 2017). The stilbenes were reported to possess anti-oxidative, anti-aging, anti-tumor, and hepatoprotective activities (Lin et al., 2015; Wu et al., 2017; Zhang and Chen, 2018), while the anthraquinones were mainly used for anti-bacterial, anti-fungal, and anti-cancer activities (Lin et al., 2015; Dong et al., 2016; Xun et al., 2019). As for the aspect of toxicity, several anthraquinones including emodin and emodin-8-*O*-*β*-D-glucoside, dianthrones such as (*C*is)-emodin-emodin dianthrones and (*T*rans)-emodin-emodin dianthrones as well as stilbenes such as (Trans)-2, 3, 5, 4′-tetrahydroxy stilbene-2-*O*-*β*-D-glucopyranoside and (*C*is)-2, 3, 5, 4′-tetrahy droxystilbene-2-*O*-*β*-D-glucopyranoside have been identified as the potential components for the hepatotoxicity of PMR (Yang et al., 2021). Moreover, among the known anthraquinones, emodin, physcion, and chrysophanol were the most detectable components in the plasma after oral consumption of PMR extract (Li et al., 2020a). These anthraquinones were also reported to induce liver toxicity *via* multiple mechanisms including reactive oxygen species induced endoplasmic reticulum stress and mitochondrial dysfunction as well as cytochrome c release mediated apoptosis (Lai et al., 2009; Qu et al., 2013). In addition, Zhang et al. (2020a) have also suggested that the stilbene in PMR could synergize the idiosyncratic hepatotoxicity of anthraquinones from PMR.

Bile acids (BAs), the major components of bile, are formed from cholesterol through various enzymatic reactions in the hepatocytes (García-Cañaveras et al., 2012). The homeostasis of BAs plays a crucial role in the metabolism of lipid, glucose, and energy (Verkade et al., 1995; Houten et al., 2006; Kuipers et al., 2014), and the disorder of BAs would cause hepatobiliary diseases (Stanimirov et al., 2015), gallstones (Berr et al., 1992), or gastrointestinal cancers (Bernstein et al., 2005). In recent years, several metabolomic (Dong et al., 2015; Zhang et al., 2015; Xia et al., 2017; Yan et al., 2020; Zhang et al., 2020b) and transcriptome (Jiang et al., 2018) analyses demonstrated that the toxicity mechanisms of PMR-induced liver injury may relate to the disruption of BA homeostasis and the metabolism of energy, amino acids, fatty acids, and lipids. Moreover, cholestasis was also observed after treating the rats with PMR extract for 28 days (Wang et al., 2015). In addition, our group has demonstrated that emodin and physcion, the major components of PMR, could alter BA disposition and induce BA accumulation in the sandwich-cultured rat hepatocytes (Kang et al., 2017). However, whether these anthraquinones have any influence on the BA homeostasis contributing to the PMR-induced liver injury after its long-term exposure *in-vivo* remains unknown. In this study, to investigate the hepatotoxicity of PMR extract and three individual anthraquinone from PMR, namely, emodin, chrysophanol, and physcion, the ICR mice were consecutively administered with PMR extract or the pure anthraquinones for 14 or 28 days.

2 MATERIALS AND METHODS

2.1 Chemicals and Reagents

Emodin, chrysophanol, physcion, and 2,3,4',5-tetrahydroxystilbene-2-*O*-*β*-D-glucoside (TSG) (purities >98%) were obtained from Nanjing Jingzhu Co. Ltd. (Jiangsu, China). The aspartate aminotransferase (AST), serum alanine aminotransferase (ALT), triglyceride (TG), and γ-glutamine transferase (γ-GGT) assay kits were supplied by Nanjing Jiancheng Bioengineering Institute (Jiangsu, China). The bicinchoninic acid (BCA) protein assay kit was purchased from Beyotime (Jiangsu, China). Individual BA together with deuterium-labelled glycol-chenodeoxycholic acid (d4-GCDCA) were obtained as previously described (Huang et al., 2011). All other chemicals and reagents were of analytical grade and readily available from commercial sources.

2.2 Preparation of the Ethanol Extract of PMR

The raw PMR from Dabashan, Sichuan Province, identified by Prof. Jianping Wang, Huazhong University of Science and Technology, was used in our study. The PMR extract was prepared by crushing the raw materials into powder, followed by refluxing for 48 h with 75% (v/v) ethanol at a solid–liquid ratio of 1:6 and filtration. The extraction was repeated five times and the combined filtrates were concentrated to remove the ethanol and then lyophilized for further use.

2.3 Identification and Determination of Major Anthraquinones From PMR Ethanol Extract

The major components from PMR extract were identified based on the previous study (Li et al., 2021). Briefly, 0.2 g PMR extract

was sonicated with 25 ml acetone for 1 h and centrifuged at 1800 g for 10 min. The supernatant was evaporated to dryness, reconstituted with 2 ml methanol (MeOH), and filtered for HPLC analyses. Additionally, the contents of major PMR derived anthraquinones including emodin, chrysophanol, and physcion in the solution were determined *via* HPLC and the contents of all the analytes were calculated as percentage (%, g/100 g crude material).

2.4 Animals and Treatment

Male ICR mice, weighing 30 ± 5 g, were obtained from the Laboratory Animal Center of Tongji Medical College, Huazhong University of Science and Technology (HUST, Wuhan, China). The mice were acclimatized to the environmentally controlled condition (temperature of 22–27°C, relative humidity of 40%–70%, and 12 h light/dark cycle) for 7 days with free access to food and water before and during the treatment interval. The anthraquinones and PMR extract powder was dissolved in 0.5% (w/v) CMC-Na each day before treatment, and the guideline for the volume of oral administration is 1 ml/100 g body weight in mice. Eighty ICR mice were randomly divided into 10 groups (n = 8): five of the groups were consecutively orally administered with 0.5% (w/v) carboxymethylcellulose sodium (CMC-Na) solution, 100 mg/kg emodin, 100 mg/kg chrysophanol, 100 mg/kg physcion, or 1.5 g/kg PMR extract (equivalent to 30 g crude material/kg) for 14 days; the other five groups received the same doses for 28 days. Twenty-four hours after the last dose, the animals were sacrificed and the blood, bile, and liver tissues were collected for further analyses. All animal experiment procedures were approved by the Institutional Animal Care and Use Committee of Tongji Medical College, HUST.

2.5 Biochemical Analysis and Histopathological Examination

The blood samples were collected and centrifuged at 1,000 g for 10 min, and the supernatant sera were obtained. Biomarkers, including AST, ALT, TG, and γ-GGT in the serum, were determined using the commercially available kits according to the manufacturer's instructions. Moreover, the livers fixed in 4% formalin were embedded in paraffin and sliced to a thickness of 5 μM. After staining with hematoxylin and eosin (H&E), the slices were examined under a light microscope for structural changes.

2.6 Sample Preparation

The sample preparation procedure was based on our previous method for the analysis of BAs with slight modification (Huang et al., 2011). For the plasma samples, the d4-GCDCA (internal standard, IS) solution (10 μl, 1 μg/ml) was spiked into 100 μl plasma, followed by the addition of 1 ml ice-cold alkaline acetonitrile (ACN) containing 5% (v/v) NH_4OH, vortexed for 10 min and centrifuged at 16,000 × g for 10 min. The supernatant was aspirated, evaporated, and reconstituted in 100 μl of 50% MeOH in water. For the liver samples, after homogenizing approximately 100 mg of liver with 2 volumes of H_2O, 10 μl IS solution was spiked into 300 μl liver homogenate and 2 ml of ice-cold 5% NH_4OH in ACN was added. After vortexing for 10 min, the samples were centrifuged at 16,000 × g for 10 min. The supernatant was aspirated, and the pellet was extracted with another 1 ml of ice-cold 5% NH_4OH in ACN. The supernatants were pooled, evaporated to dryness, and reconstituted with 100 μl 50% MeOH in water. As for the bile samples, the Supelclean™ LC-18 SPE cartridges (Sigma–Aldrich, St. Louis, MO) were used for sample extraction. First, the bile samples were diluted 20- and 2000-fold with deionized water. Then, 100 μl of diluted bile samples spiked with 10 μl IS was loaded onto SPE cartridges which were preconditioned with 2 ml MeOH, followed by 2 ml H_2O. Thereafter, the loaded cartridges were washed with 2 ml H_2O and eluted with 4 ml MeOH. Finally, the eluted solution was evaporated to dryness and reconstituted with 100 μl 50% MeOH in water.

2.7 LC-MS/MS Analysis

Simultaneous determination of individual endogenous BAs in the bile, liver homogenate, and plasma was performed according to our previously published liquid chromatography with the tandem mass spectrometry (LC-MS/MS) method with slight modifications (Huang et al., 2011). Chromatographic separation was achieved on a Waters ACQUITY HSS T3 column (2.1 × 100 mm, 1.8 μm; Waters, United States). The mobile phase consisted of 7.5 mM ammonium acetate, adjusted to pH 7.0 using 10 M ammonium hydroxide (mobile phase A) and MeOH (mobile phase B) and the flow rate was 0.3 ml/min. The elution gradient profile started from 50% mobile phase B, linearly increased to 90% mobile phase B in 20 min, held at 90% for 2 min, and brought back to 50% in 0.01 min followed by 4 min re-equilibration. The BA analysis was performed on a Shimadzu Prominence UFLC system (Shimadzu Corporation, Japan) and an API 4000 QTrap® triple quadrupole mass spectrometer (AB SCIEX, United States) with an electrospray ionization (ESI) source. All the BAs were measured in negative ionization mode using mass transitions listed in our previous report. The main working parameters for the MS were set as: capillary voltage, −4000 V; source temperature, 600°C; curtain gas flow, 20 psi; nebulizer gas flow, 35 psi; and collision energy, high.

2.8 Quantitative Real-Time PCR

Total RNA was extracted from liver using TRIzol reagent according to the manufacture's instruction (Invitrogen, United States). The RNA samples were reversed-transcribed into complementary DNA (cDNA) *via* Fermentas RevertAid First Strand cDNA Synthesis Kit (ThermoFisher, United States) according to the manufacturer's protocol. The cDNA was amplified using an ABI Step-One Sequence Detection System (Applied Biosystems, United States) with SYBR Green PCR Master Mix (Bio-Rad, United States). The gene expression was determined by normalization with control gene Gapdh using the ΔΔCt method and the primer sequences are set as: Bsep (Gene ID: 27413, forward: 5′-GCTGCCAAGGATGCTAATGC-3′ and reverse: 5′-TTGGGTTTCCGTATGAGGGC-3′), Mrp2 (Gene ID: 12780, forward: 5′- CCTTGGGCTTTCTTTGGCTC-3′ and reverse: 5′-ACACAACGAACACCTGCTTG-3′), and Gapdh (Gene ID: 14433, forward: 5′-GTCGGTGTGAACGGATTTGG-3′ and reverse: 5′-TCAGATGCCTGCTTCCCATTC-3′).

2.9 Western Blotting

Total protein in the liver was extracted with RIPA Lysis Buffer (Beyotime) containing 1 mM PMSF, and the total protein concentration was determined using the BCA protein assay kit. An equal amount of proteins (50 μg) was separated by electrophoresis on sodium dodecyl sulfate/8.75% polyacrylamide gel electrophoresis and transferred to nitrocellulose blotting membranes (Millipore, United States) for 2 h through wet transfer method using Mini Trans-Blot (Bio-Rad, United States). Subsequently, the membranes were blocked with 5% nonfat milk dissolving in 0.5% TBST buffer for 1.5 h and then incubated overnight at 4°C with specific primary antibodies including Bsep (goat, Santa Cruz Biotech), Mrp2 (rabbit, Abcam), and β-actin (mouse, Proteintech). After washing the membrane with 0.5% TBST buffer for three times, the membranes were further incubated with corresponding secondary antibodies at room temperature for 1 h. The protein bands were visualized using an enhanced chemiluminescence detection system (Millipore, United States).

2.10 Data Processing and Statistical Analysis

All values were indicated as mean ± standard deviation (mean ± SD). Statistical analyses were carried out using GraphPad Prism 7.0 (GraphPad Software Inc., United States). Differences between the two groups were analyzed by Student's t-test, while multiple comparisons were carried out by one-way ANOVA followed by Dunnett's post hoc test. Differences with a probability value (P) < 0.05 were statistically significant. MetaboAnalyst 5.0 was used to perform the Principal Component Analysis (PCA) and Partial Least Squares Discriminant Analysis (PLS-DA) for the evaluation of the differences of the BAs in the liver, bile, and plasma between the control and treatment groups.

3 RESULTS

3.1 HPLC Chromatogram of PMR Extract and the Contents of Major Anthraquinones

The HPLC chromatogram of the PMR extract is shown in **Supplementary Figure S1**. The retention time of TSG, one of the major quality control marker components of PMR, was 4.131 min and that of emodin, chrysophanol, and physcion was 9.154, 10.157, and 11.886 min, respectively. The contents of emodin, chrysophanol, and physcion were 0.047 ± 0.00026, 0.0063 ± 0.00046, and 0.014 ± 0.00025 (%, g/100 g crude material), respectively.

3.2 Biochemical and Histopathological Analysis

To assess the hepatotoxicity of the PMR extract and its major components, several biochemical biomarkers indicating liver injury in serum were investigated. As shown in **Figure 1A**, after administration for 14 days, ALT, AST, TG, and γ-GGT levels showed no significant change in all the groups. After treating the animals for 28 days, it was noted that the AST levels were significantly increased in all the treated groups. Additionally, the levels of TG and γ-GGT were also increased in the PMR-treated group. The histopathological analysis of the liver (**Figure 1B**) indicated mild inflammatory cell infiltration after treating the mice with physcion or PMR extract for 14 days. However, there was no lesion observed in emodin- or chrysophanol-treated groups after 14-day treatment. With the treatment time prolonging to 28 days, inflammatory cell infiltration was observed in all the treated groups as shown in **Figure 1B**.

3.3 Quantitative Analysis of BAs

3.3.1 Alteration of Individual BA in the Mouse Liver, Bile, and Plasma

To investigate the changes of BA profiles after treating the mice with PMR extract or its major anthraquinones, the abundance of 36 BAs in the plasma, liver homogenate, and bile were determined. After treating the mice for 14 or 28 days, 19 different BAs were detected in the liver homogenate. As shown in **Figure 2**, compared with the control group, the concentrations of cholic acid (CA), chenodeoxycholic acid (CDCA), deoxycholicacid (DCA), ursodeoxycholic acid (UDCA), tauro-cholic acid (TCA), tauro-β-muricholic acid (TMCA), tauro-chenodeoxycholic acid (TCDCA), tauro-deoxycholic acid (TDCA), and glyco-cholic acid (GCA) in the liver were significantly increased after treating the mice with physcion and PMR for 14 days. In addition, it was found that the concentrations of sulfated BAs including β-muricholic acid-sulfate (MCA-S), tauro-cholic acid-sulfate (TCA-S), and tauro-chenodeoxycholic acid-sulfate (TCDCA-S) were significantly decreased after treating the mice with PMR for 14 days. In the emodin-treated group, the significant accumulation of CA, β-muricholic acid (MCA), CDCA, UDCA, TMCA, and cholic acid-sulfate (CA-S) were observed after treating the mice for 14 days. As for chrysophanol, only the concentrations of CA, CDCA, lithocholic acid (LCA), and CA-S were increased. After consecutively treating the mice for 28 days, the content of CA, MCA, and tauro-lithocholic acid-sulfate (TLCA-S) were significantly increased in all the treated groups. In the meantime, the quantities of TMCA and TCDCA in the liver were significantly decreased in all the treated groups. After treating the mice with these anthraquinones for 28 days, hepatic accumulation of CDCA and DCA was increased, while tauro-lithocholic acid (TLCA) in the liver were significantly decreased. In addition, the quantities of TCA were increased, whereas tauro-ursodeoxycholic acid (TUDCA) was decreased in the emodin- or PMR-treated groups. Chrysophanol and physcion were found to increase the UDCA levels in the mouse liver.

After treating the mice for 14 days, it was noted that almost all the detected BAs in the bile in our current study were significantly decreased after treating the mice with anthraquinones or PMR extract (**Figure 3**). However, after treating the mice for 28 days, the inhibition of active BA excretion was significantly attenuated and the bile level of a fewer number of BAs was found to be decreased compared to the 14-day treatment groups. Only the decrease of TUDCA, TDCA, and TCA-S in the emodin-treated group; TCDCA, TUDCA, and ursodeoxycholic acid-sulfate (UDCA-S) in the chrysophanol-treated group; TDCA and MCA-S in the physcion-treated group; as well as MCA, TDCA, GCA, and CA-S caused by PMR were observed. Moreover, the content of TCA, TMCA, and CA-S in the

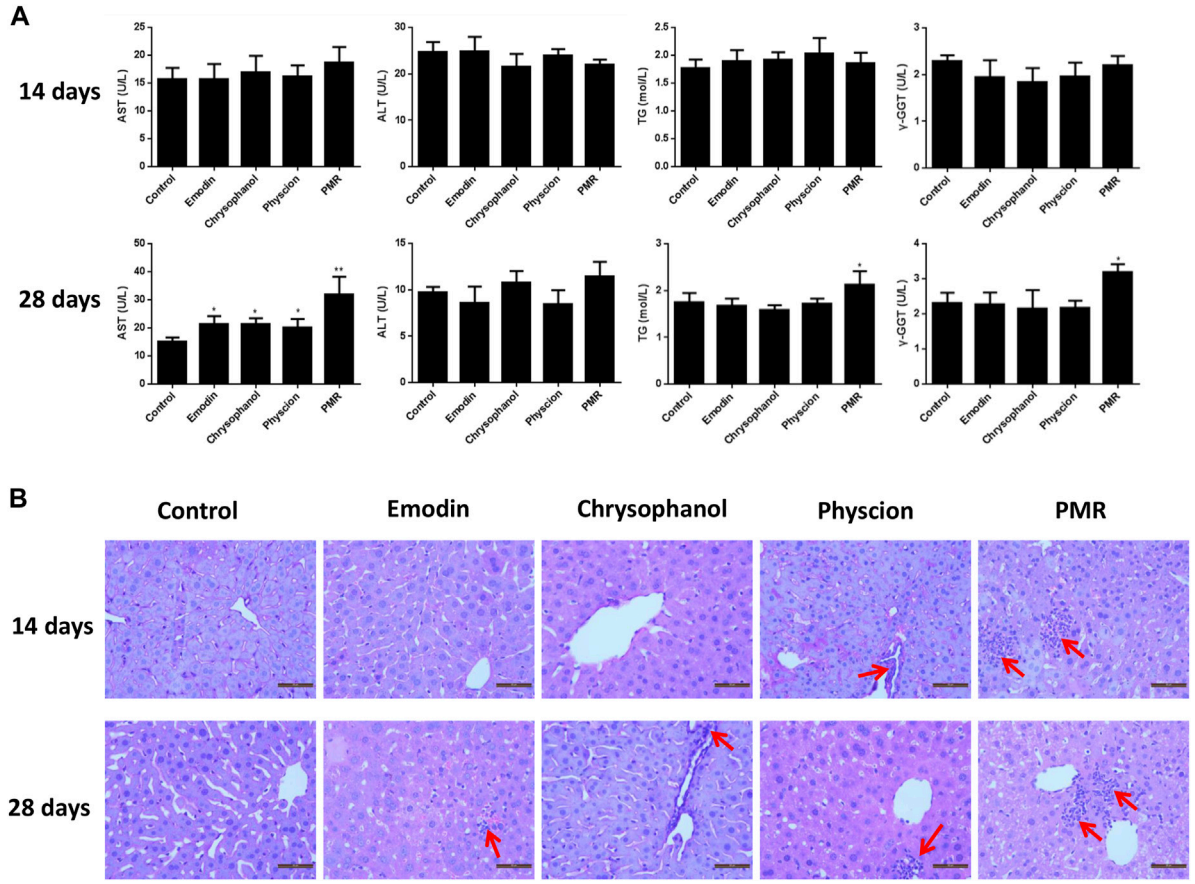

FIGURE 1 | Serum levels of AST, ALT, TG, and γ-GGT **(A)** and typical liver histopathological section photos (**(B)** Hematoxylin and eosin stained, original magnification ×400) in different groups of mice following 14- or 28-day treatment with anthraquinones or PMR extract. Inflammatory cell infiltration was indicated by the solid arrow. Data were presented as mean ± SD (n = 8). $^{*}p < 0.05$, $^{**}p < 0.01$ compared with control group.

chrysophanol group; TCA and TMCA in the physcion group; and CA in the PMR group were significantly increased.

As for the plasma (**Supplementary Figure S2**), only seven BAs were detected and it was found that except for β-muricholic acid (MCA), emodin had no significant influence on the detectable BAs after treating for 14 days. However, another two anthraquinones, chrysophanol and physcion, were found to decrease the content of CDCA, TMCA, and TLCA-S. In the PMR-treated group, the quantity of TCA was increased and the concentrations of MCA, TMCA, TDCA, and TLCA-S were decreased after treating for 14 days. After treating the mice for 28 days, the concentrations of CA were decreased in the chrysophanol and physcion treatment groups. Moreover, physcion was found to significantly elevate the concentrations of TDCA in the plasma after 28-day administration.

3.3.2 Disruption of the Total BAs in Mouse Liver, Bile, and Plasma

As shown in **Figure 4A**, compared with the control group, it was noted that the total BAs in the liver was significantly increased after treating with physcion or PMR extract for 14 days. In the meantime, the total BAs in the bile were significantly decreased in these two groups (**Figure 4B**). Moreover, the content of the total BAs in the plasma was also significantly decreased after treating with chrysophanol or physcion for 14 days (**Supplementary Figure S3**). However, the accumulation of total BAs in the liver after treating with physcion for 28 days was attenuated in the absence of significant difference with the control group (**Figure 4**), while the total BAs in the liver after treatment with PMR extract for 28 days were significantly increased in comparison with the control group (**Figure 4**). In addition, the total BAs in the bile after treating with anthraquinones or PMR extract for 28 days showed no difference with the control group. Similar to the total BAs, the total CA, total CDCA, total UDCA, and total DCA in the liver were significantly increased in the physcion- and PMR-treated groups after 14-day dosing (**Figure 4A**), while the concentrations of these total BAs in the bile were decreased in these two groups (**Figure 4B**). Moreover, in the liver, the total CDCA in the emodin- and chrysophanol-treated groups, total MCA and total UDCA in the emodin-treated groups were also significantly increased after 14-day treatment (**Figure 4A**). The concentration of total LCA was found significantly decreased in the bile and plasma but not changed in the liver after treating for 14 days (**Figure 4B**, **Supplementary**

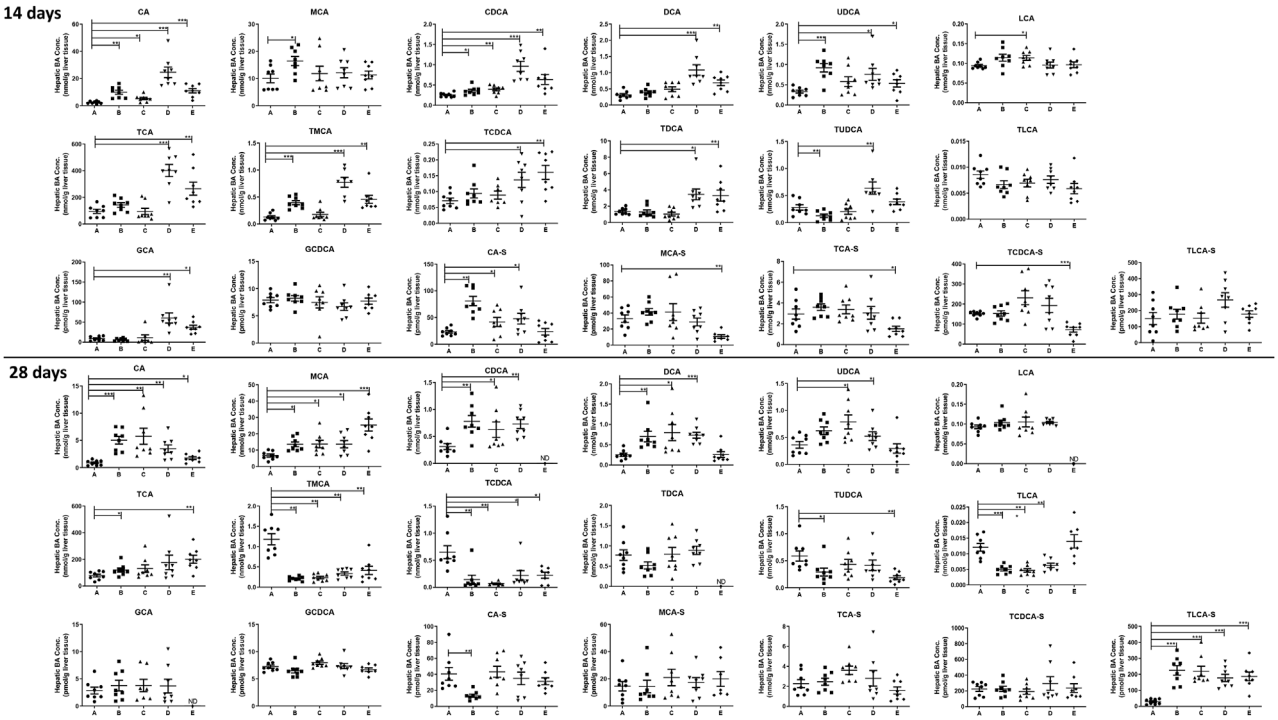

FIGURE 2 | Concentration of the individual BAs in the mouse liver after the anthraquinones or PMR consumption for 14 or 28 days (A: control, B: emodin, C: chrysophanol, D: physcion, E: PMR). The data are expressed as the mean ± SD (n = 6–8). $^{*}p < 0.05$, $^{**}p < 0.01$, $^{***}p < 0.001$ compared with control group, ND: not detected.

Figure S3). After treating for 28 days, accumulation of the total LCA in the liver was significantly increased in all the PMR- or anthraquinones-treated groups (**Figure 4A**), but not altered in the mouse bile and plasma (**Figure 4B**, **Supplementary Figure S3**). Furthermore, after treating for 14 days, the tested anthraquinones and PMR could not obviously affect the composition of amidated BAs in the mouse liver and bile. Unexpectedly, the percentage of amidated BAs in the mouse plasma was reduced by emodin treatment for 14 days, while chrysophanol significantly increased the percentage of amidated BAs in the mouse plasma. Moreover, the composition of amidated BAs in the mouse plasma was not obviously altered by either physcion or PMR extract (**Supplementary Table S1**). After 28-day treatment, except for the physcion, other two anthraquinones and PMR decreased the percentage of amidated BAs in the liver, while the percentage of amidated BAs in the bile and plasma was not changed after PMR or anthraquinones treatment (**Supplementary Table S1**).

3.4 PCA and PLS-DA Analysis

The datasets of the BA concentrations in different matrices from different treatment groups were used for PCA and PLS-DA analyses. The parameters used to assess the modelling quality included R2X, R2Y, and Q2Y and the values of R2 and Q2 were more than 0.5, indicating the successful establishment of the model. PCA was employed to reveal the BA disposition changes in different matrices. As shown in **Figure 5**, after treating the mice for 14 days, the PMR-treated groups showed a clear separation with the control group in the mouse bile and liver (**Figure 5**) on the score plot. In the meantime, all the treated groups showed a clear separation with the control group and PMR separated well with all the other anthraquinones groups after the 14-day administration in the bile (**Figure 5**). In the plasma, no separation was showed between the treated and control groups. With the administration duration prolonging to 28 days, the physcion treated groups showed a clear separation with the control group in the liver (**Figure 5**). The PLS-DA was adopted to evaluate and maximize the discrimination between the control and treated groups. As shown in **Figure 6** and **Supplementary Figure S4**, a clear separation between the control and physcion/PMR treated groups was observed in the mouse liver, bile, and plasma after treating for 14 days. However, emodin and chrysophanol could not be separated with the control group on the PLS-DA score plot of bile in the liver, bile, and plasma after 14-day administration. With the administration duration prolonging to 28 days, the PMR group separated well with the control and the other three anthraquinones-treated groups in the liver. However, in the bile and plasma, no clear separation was observed among the control group and the treated groups after 28-day administration on the PCA or PLS-DA score plots (**Figure 5**, **6**, **Supplementary Figure S4**).

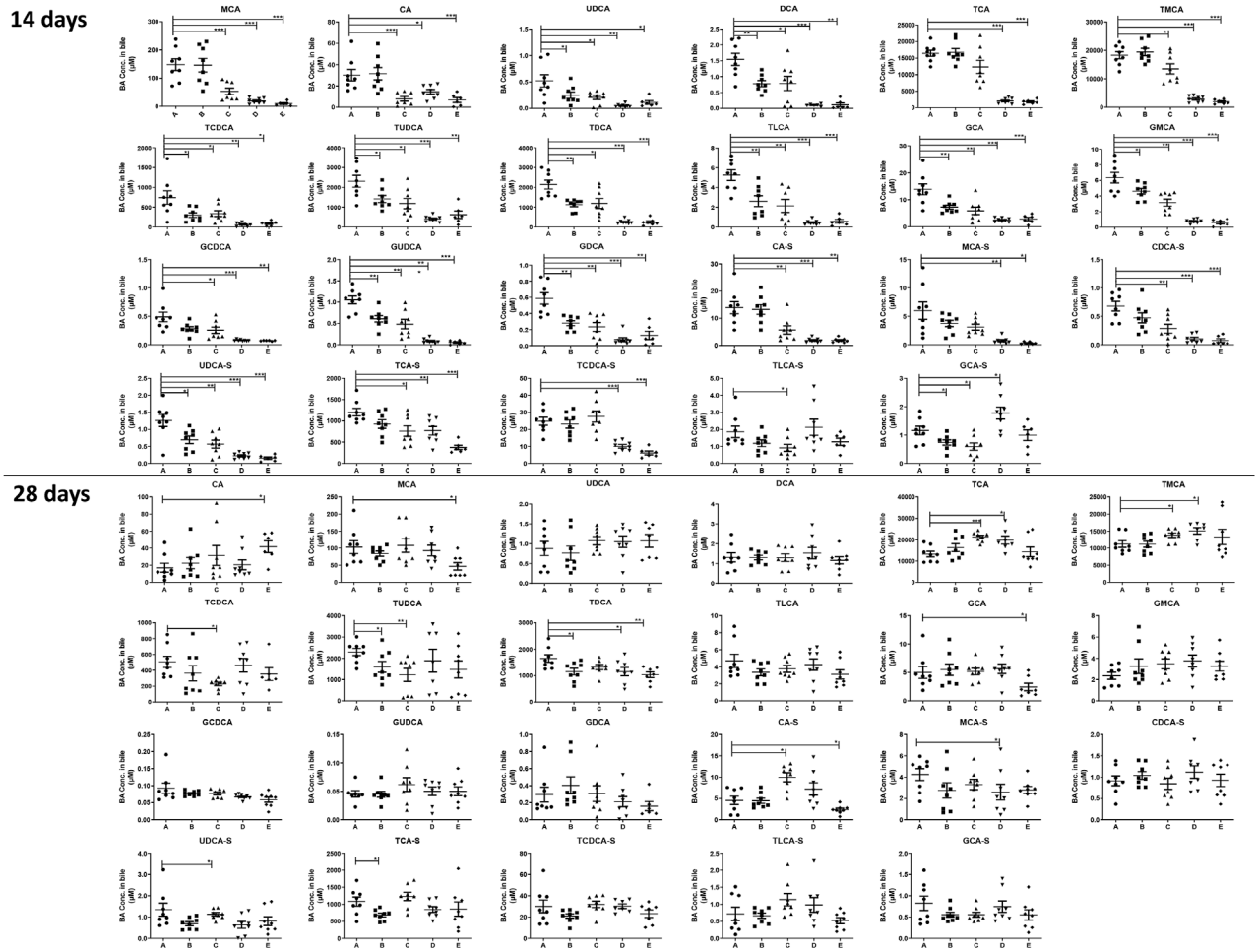

FIGURE 3 | Concentration of the individual BAs in the mouse bile after the anthraquinones or PMR consumption for 14 or 28 days (A: control, B: emodin, C: chrysophanol, D: physcion, E: PMR). The data are expressed as the mean ± SD (n = 6–8). $^{*}p < 0.05$, $^{**}p < 0.01$, $^{***}p < 0.001$ compared with control group.

3.5 Alteration of the Gene and Protein Levels of BA Transporters

To explore the potential mechanisms of the influence of PMR on the homeostasis of BAs, the gene and protein expression of the key BA efflux transporters including Bsep and Mrp2 was investigated in our current study. As shown in **Figure 7**, after orally administering the mice with PMR extract or the anthraquinones for 14 days, the gene and protein expression of Mrp2 was significantly inhibited. In addition, the expression of Bsep was also significantly inhibited by the physcion and PMR extract. After treating the mice for 28 days, the gene and protein expression of Bsep was significantly increased in the physcion and PMR extract groups. Moreover, the expression of Mrp2 also significantly increased in the emodin- and chrysophanol-treated groups.

4 DISCUSSION

BA homeostasis is strictly maintained by a series of uptake and efflux transporters as well as synthesis and metabolism enzymes (Rodrigues et al., 2014). Experimental toxicology studies have identified the disturbed metabolism of BAs as a common and early event of drug-induced liver injury by diverse hepatotoxins (Yamazaki et al., 2013). As indicated by the previous studies, PMR induced liver injury was closely associated with BA homeostasis disruption. In the current work, we explored the hepatotoxic effect of three major PMR-derived anthraquinones including emodin, chrysophanol, and physcion as well as the PMR ethanol extract based on BA disposition and complemented with serum biochemical indicators and histopathological examination in the mice. All these three anthraquinones and the PMR extract were found to induce liver injury as evidenced by the histopathological examination and the hepatotoxic biomarker levels in the serum. Additionally, it was found that all the anthraquinones of interest and PMR extract could alter the BA homeostasis.

To uncover any potential toxicity of the PMR extract or the anthraquinones, the doses were set at high levels and the dose of PMR was around 25-fold the highest recommended human dose obtained from the 2015 edition of the Chinese Pharmacopoeia

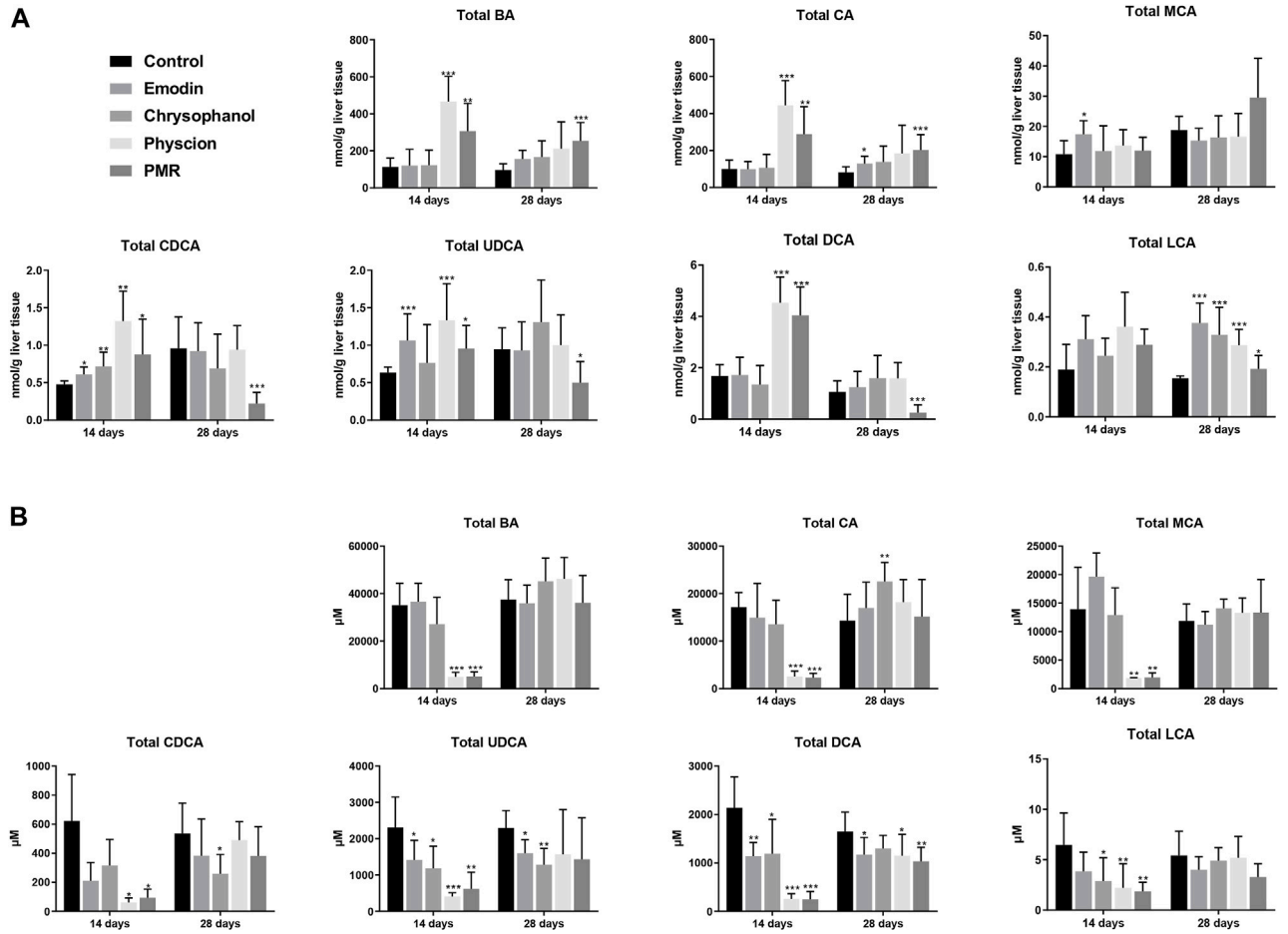

FIGURE 4 | Comparison of the total BA, total CA, total MCA, total CDCA, total UDCA, total DCA, and total LCA in the mouse liver **(A)** and bile **(B)** between different groups of mice following 14- or 28-day treatment with anthraquinones or PMR extract. The data are expressed as the mean ± SD (n = 6–8). $^{*}p < 0.05$, $^{**}p < 0.01$, $^{***}p < 0.001$ compared with control group.

(the dose of human was converted to mice based on the body surface area conversion (US Food and Drug Administration, 2005). According to the previous reports, there is an interaction between the co-occurring components in PMR. Xing et al. (2019) have evidenced that the C_{max} of emodin in the rat plasma could be increased by 3–7 times in the presence of TSG. In our current study, the dose of PMR was selected as 30 g/kg, which was equivalent to 14.1 mg/kg emodin. To mimic the maximum exposure of emodin after administration with PMR extract, the dose of emodin was selected as 100 mg/kg (14.1 mg/kg × 7 = 98.7 mg/kg). In order to compare the impact of these anthraquinones parallelly, the dose of other two anthraquinones, chrysophanol and physcion, was also selected as 100 mg/kg.

Currently, the serum biochemical parameters such as ALT, AST, and ALP are used as conventional biomarkers for the clinical diagnosis (Park et al., 2001; Jung et al., 2011; Dong et al., 2014). In our study, the AST levels were significantly increased after treating for 28 days with the PMR extract or the pure anthraquinones, which correlated well with the histopathological findings. However, neither anthraquinones nor the PMR extract altered the biomarkers tested in our current study including ALT, AST, TG, and γ-GGT after 14-day treatment, while the distinct results were observed that physcion and PMR caused liver damage after 14-day treatment evidenced by the liver histopathological changes. Such discrepancy may be resulted from the limited sensitivity and specificity of ALT and AST in the serum for early detection of liver injury (McGill, 2016). Although, ALT was suggested to be a more sensitive biomarker for liver injury in clinical practice (Senior, 2009), the significant elevation of AST rather than ALT was observed in all the treatment groups in our current study and the previous report in which the rats were treated with the PMR extract (equivalence to 20 g/kg crude material) for 21 days (Ma et al., 2015). Such discrepancy could be due to the species difference between the rodents and humans or AST was suggested to be a more sensitive biomarker for PMR-induced liver injury. McGill reviewed the mechanisms and interpretation of the plasma levels of ALT and AST elevation in liver injury and stated that ALT and AST have poor prognostic utility in acute

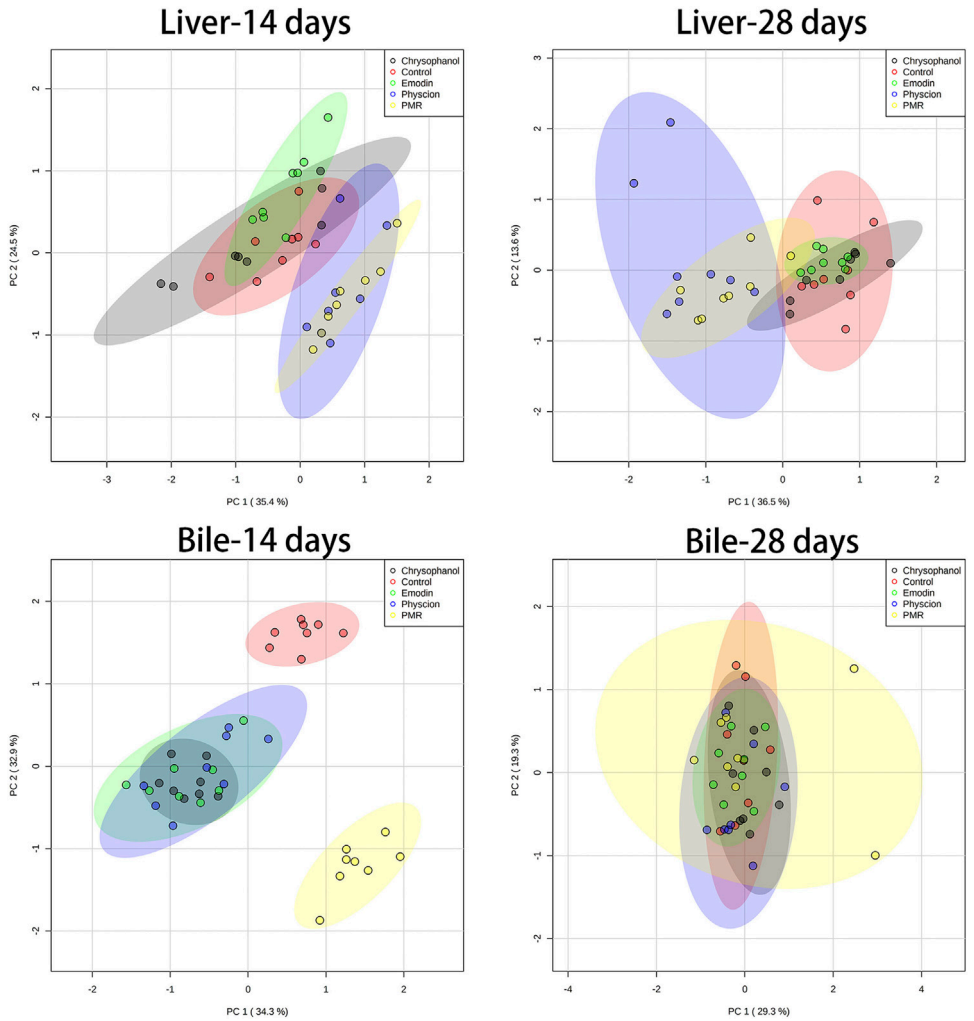

FIGURE 5 | PCA results based on the quantitative analysis of the BAs in the mouse liver and bile from different groups of mice following 14- or 28-day treatment with anthraquinones or PMR extract.

liver injury and liver failure (McGill, 2016). In addition, physcion was reported to be cytotoxic to red blood cells by triggering hemolysis and programmed cell death (Akiel et al., 2021). As a result, unpredictable response to the different degree of hemolysis might also affect the accurate measures of such biochemical testing (Lippi et al., 2006).

In preclinical studies, the change of BAs was also used as an important physiological indicator of liver damage (Casini et al., 1997) and several reports have also recommended the GDCA in the bile, hyodeoxycholic acid (HDCA) in the plasma, or TMCA in the urine as potential biomarkers for PMR induced liver injury in the SD rats (Dong et al., 2015; Zhao et al., 2017). In the current study, the total BAs in the liver were significantly increased accompanied with the significant decrease in the bile after treating with physcion and PMR for 14 days. These results correlated well with the histopathological results that the liver obtained from these two groups showed typical inflammatory cell infiltration. After 28-day treatment, it was noted that the accumulation of the total BAs in the liver was decreased in the physcion treatment group, which may be related to the adaptive protective mechanisms (Zollner et al., 2006). However, such a reduction of total BAs in the liver did not prevent the occurrence of liver damage evidenced by the histopathological findings. A plausible explanation for such hepatic toxicity was that the accumulation of physcion in the liver resulted from long-term treatment leading to hepatocellular damage. It was found that physcion could induce significant cytotoxic effects against the human liver cell line L02, HepG2 cells, rat primary hepatocytes, and sandwich-cultured rat hepatocytes in a dose dependent manner (Xun et al., 2019).

The toxicity of the BAs is related to their structures and the hydrophobic BAs is more toxic than the hydrophilic BAs (LCA ≥ DCA ≥ CDCA >> CA) (Trottier et al., 2006; Schadt et al., 2016). The accumulation of hydrophobic BAs in the liver can result in

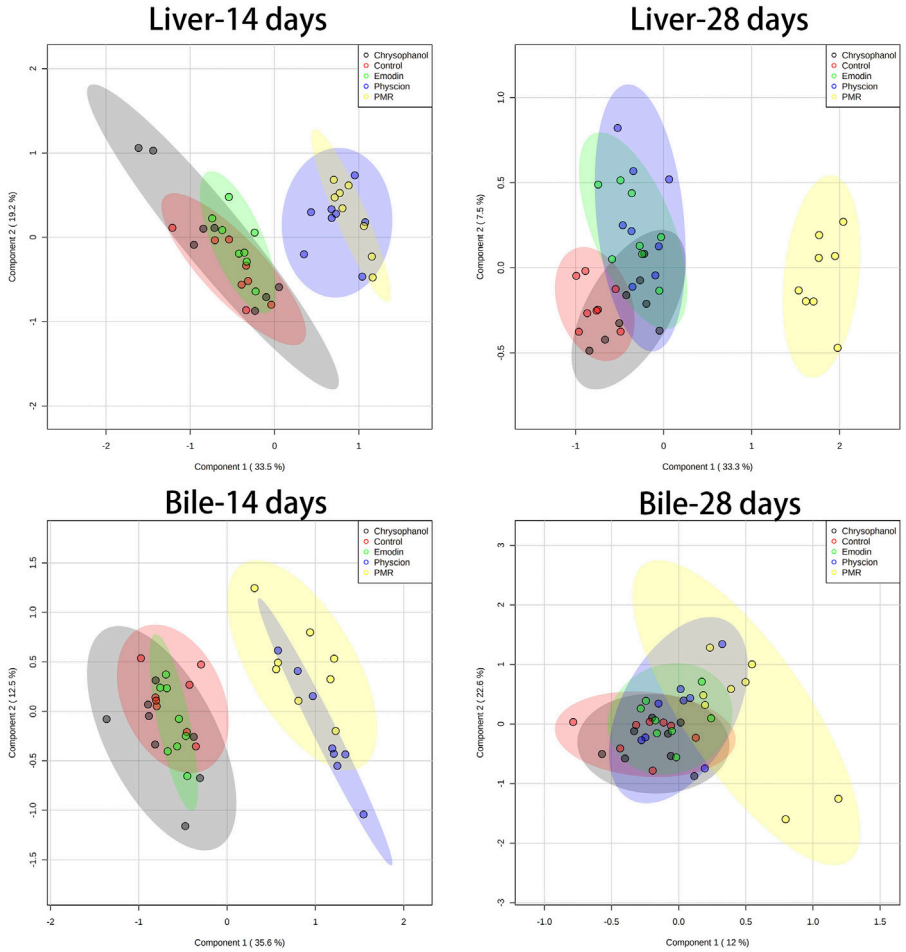

FIGURE 6 | PLS-DA results based on the quantitative analysis of the BAs in the mouse liver and bile from different groups of mice following 14- or 28-day treatment with anthraquinones or PMR extract.

mitochondrial dysfunction by generating reactive oxygen species (ROS), which in turn causes liver injury (Casini et al., 1997; Perez and Briz, 2009). In our study, it was worth noting that after 14-day or 28-day administration with anthraquinones or PMR extract, the hydrophobic BAs (DCA, CDCA, and CA) in the liver were significantly accumulated. Moreover, the significant accumulation of the total LCA was also observed in the liver after treating the mice for 28 days. BA conjugation with glycine or taurine could increase the solubility and decrease the toxicity of the corresponding BAs (Trottier et al., 2006). The significantly decreased proportion of the conjugated BAs in the liver, at least in part, indicated that toxic BA detoxification could be altered by PMR and typical anthraquinones. Taken together, the accumulation of these hydrophobic BAs and inhibition of BA conjugation were considered to contribute to the liver toxicity induced by PMR and anthraquinones of interest. This might also be a possible explanation for the discrepancy between the attenuation of liver total BA accumulation in the physcion treatment group and the liver damage evidenced by histological examination after treating for 28 days.

In human, BAs undergo sulphation to reduce their cytotoxicity (Agellon and Torchia, 2000; Zwicker and Agellon, 2013). Sulfotransferase-2A1(SULT2A1) is the enzyme catalyzing the BAs into BA-sulfates, which are more hydrophilic and readily excreted into feces and urine (Alnouti, 2009). According to previous study, the activity and expression of SULT2A1 could be significantly inhibited by emodin or rhein in the HepG2 cells (Maiti et al., 2014). The inhibition of SULT2A1 might directly contribute to the decrease of liver BA-sulfates level in our current study. Moreover, hepatic transporters also play critical roles in maintaining the BA homeostasis (Agellon and Torchia, 2000). BAs were synthesized from cholesterol in the hepatocytes and secreted across the canalicular membrane in an ATP-dependent fashion *via* BSEP/Bsep and MRP2/Mrp2 (Akita et al., 2001). Since canalicular secretion is considered as the rate-limiting step of the vectorial export of toxic BAs from hepatocytes into bile, impaired BA biliary transport may directly result in hepatic BA accumulation. In addition, basolateral BA efflux transporters, Mrp3 and Mrp4, are also involved in the BA homeostasis and the inhibition of both canalicular and basolateral BA efflux transporters may worsen liver

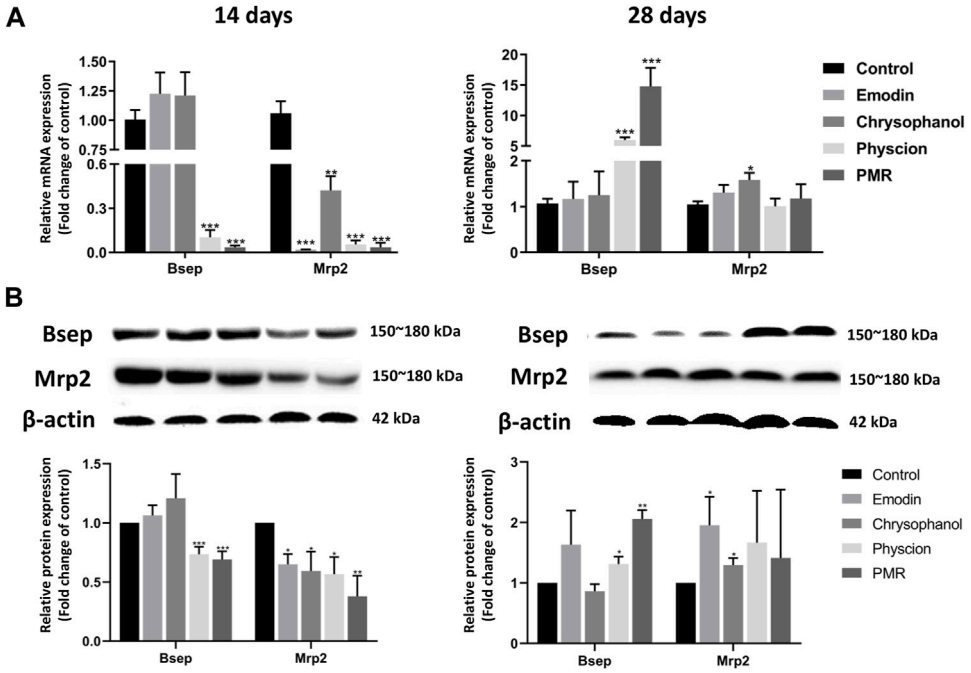

FIGURE 7 | mRNA **(A)** and protein **(B)** expression levels of Bsep and Mrp2 in the mouse livers. Bar plots were represented as the mean ± SD (n = 8 for quantitative real-time PCR, n = 4 for western blotting using each two samples pooled). *$p < 0.05$, **$p < 0.01$, ***$p < 0.001$ compared with control group.

injury (Corsini and Bortolini, 2013; Köck et al., 2014). In our current study, the significant decrease of gene and protein expression of Bsep in the physcion and PMR groups was supposed to be the major factor of the hepatic total BA accumulation after treating for 14 days. After 28 days of treatment, hepatic total BA accumulation was attenuated due to the elevated mRNA and protein expression of Bsep in the physcion group. However, the increased accumulation of hepatic total BAs was contradictory with the significant elevation of Bsep after treatment with PMR extract for 28 days. Such discrepancy could be explained by the concurrent inhibition of the basolateral BA efflux induced by these three anthraquinones in PMR as demonstrated in our previous study (Kang et al., 2017). Unlike Bsep, the inhibition of Mrp2 may not induce the accumulation of hepatic BAs (Iyanagi et al., 1998), which was consistent with our results that the altered protein expression of Mrp2 showed no impact on the hepatic total BA levels in the emodin and chrysophanol treated groups. Furthermore, the inconsistency of the changed expression of Bsep and Mrp2 with the individual hepatic BAs could be due to their distinct affinity to such efflux transporters (Noe et al., 2001). Compared with the control group, the total BAs in the bile were decreased by around 86% and 85%, while the total hepatic BA level was increased by 3.1- and 1.7-fold in the physcion- and PMR-treated groups, respectively. However, in agreement with the previous reports (Wang et al., 2015; Zhao et al., 2017), the expression of BA efflux transporters, Bsep and Mrp2, was increased with the administration prolonging to 28 days, which was in accordance with the disposition of BAs that the percentage of amidated BAs in the liver, the major substrates of Bsep, was significantly decreased. Since the individual BAs such as CDCA, DCA, CA, and LCA are the agonists of Farnesoid X receptor (FXR/Fxr) with CDCA as the most potent one (Stofan and Guo, 2020), the accumulated BAs could activate FXR/Fxr and therefore inhibit the synthesis of BAs and induce the expression of Bsep to attenuate the overload of hepatic BAs (Schaap et al., 2014). Moreover, CA and UDCA were reported to induce the expression Mrp2 with a Fxr-independent manner in the mice (Zollner et al., 2003). Therefore, the regulation of the expression of the two transporters in our current study could be explained as the adaptive response for limiting the hepatic BA overload (Zollner et al., 2006). Additionally, the decrease of part of the BAs in the plasma in our study may result from the decreased reabsorption of BAs due to the inhibition of the excretion of BAs into the bile as well as the inhibition of the bile acid efflux transporters Mrp3 and Mrp4. Also, the plasma BA concentrations could be affected by the hepatocellular uptake from the blood evidenced by the downregulated expression of major hepatic BA uptake transporter, sodium taurocholate cotransporting polypeptide (Ntcp) in our previous study (Kang et al., 2017). In addition, renal elimination, hepatic synthesis and metabolism, and intestinal metabolism and elimination from feces of BAs have also been recognized as another vital factor for the BA levels in the plasma. Therefore, the complex regulation processes might be a plausible reason for the relatively minor alteration of BAs in the plasma.

Taken together, the present study comprehensively elucidated the role of PMR or its major anthraquinones in BA disposition. It was found that PMR or physcion could induce hepatic BA accumulation after treating for 14 days, which were potentially associated with the inhibition of the function and expression of hepatic BA canalicular efflux transporters, Bsep and Mrp2, as well as the basolateral efflux transporters, Mrp3 and Mrp4. Such cholestasis could be attenuated *via* regulating the expression of

BA transporters with a prolonging administration duration up to 28 days. This study, for the first time, investigated the hepatotoxicity of the major anthraquinones from PMR based on BA homeostasis and found that all the tested anthraquinones of interest could change the disposition of the BAs to a different extent in mice. However, in addition to anthraquinones, there are many other components such as stilbene, tannins, dianthrones, and flavonoids in the PMR and the stilbene was reported to increase the systemic exposure of emodin *via* increasing its absorption and inhibiting its metabolism (Li et al., 2020b). That could also be a possible explanation that the hepatoxicity of other traditional Chinese medicine containing anthraquinones was less reported than PMR. It is also worth noting that dianthrones derivatives, such as (*Cis*)-emodin-emodin dianthrones and (*Trans*)-emodin-emodin, have recently been reported to be associated with PMR hepatotoxicity (Yang et al., 2018a; Li et al., 2020). Furthermore, the mutual transformation between the dianthrones derivatives and anthraquinones results in more complicated potential toxic source analysis for PMR induced liver injury (Yang et al., 2018a). Therefore, the influence of the interaction between anthraquinones and other components from PMR on the BA steady-state should be taken into further consideration for the quality control and safe use of PMR in practice. In addition, due to the species difference between the mice and human, the translation of the current results to humans warrants further investigation.

5 CONCLUSION

Both the PMR extract and three anthraquinones of interest could alter the disposition of either the total or individual BAs in the mouse bile, liver, and plasma. Physcion and PMR extract treatment elevated the hepatic total BAs and decreased that in the bile, while it could be attenuated with prolonged administration duration. Hepatic accumulation and biliary excretion of most of the individual BAs were affected by the PMR extract and three anthraquinones. Such alteration was potentially related with the inhibition on the function and expression of dominant BA efflux transporters.

DATA AVAILABILITY STATEMENT

The original contributions presented in the study are included in the article/**Supplementary Material**, Further inquiries can be directed to the corresponding authors.

ETHICS STATEMENT

The animal study was reviewed and approved by the Institution Animal Care and Use Committee, Tongji Medical College, Huazhong University of Science and Technology.

AUTHOR CONTRIBUTIONS

JH and YoZ conceived and supervised the study, designed and coordinated the study, and wrote the manuscript. LK, DL, and XJ designed and coordinated the study, conducted experiments, performed data analyses and visualization, and wrote the manuscript. YaZ, MP, and YH conducted the experiments. LS designed and coordinated the study.

FUNDING

This research was supported by the National Natural Science Foundation of China (81302837, 81773811, 81803834), Hubei Province Natural Science Foundation (2020CFB351), Hubei Province Major Basic Research Development Program (2020BCB045), and Fujian Provincial Key Laboratory of Innovative Drug Target Research (FJ-YW-2020KF01).

SUPPLEMENTARY MATERIAL

The Supplementary Material for this article can be found online at: https://www.frontiersin.org/articles/10.3389/fphar.2022.878817/full#supplementary-material

REFERENCES

Agellon, L. B., and Torchia, E. C. (2000). Intracellular Transport of Bile Acids. *Biochim. Biophys. Acta* 1486 (1), 198–209. doi:10.1016/S1388-1981(00)00057-3

Akiel, M., Alsughayyir, J., Basudan, A. M., Alamri, H. S., Dera, A., Barhoumi, T., et al. (2021). Physcion Induces Hemolysis and Premature Phosphatidylserine Externalization in Human Erythrocytes. *Biol. Pharm. Bull.* 44, 372–378. doi:10.1248/bpb.b20-00744

Akita, H., Suzuki, H., Ito, K., Kinoshita, S., Sato, N., Takikawa, H., et al. (2001). Characterization of Bile Acid Transport Mediated by Multidrug Resistance Associated Protein 2 and Bile Salt export Pump. *Biochim. Biophys. Acta* 1511 (1), 7–16. doi:10.1016/S0005-2736(00)00355-2

Alnouti, Y. (2009). Bile Acid Sulfation: a Pathway of Bile Acid Elimination and Detoxification. *Toxicol. Sci.* 108 (2), 225–246. doi:10.1093/toxsci/kfn268

Bernstein, H., Bernstein, C., Payne, C. M., Dvorakova, K., and Garewal, H. (2005). Bile Acids as Carcinogens in Human Gastrointestinal Cancers. *Mutat. Res.* 589 (1), 47–65. doi:10.1016/j.mrrev.2004.08.001

Berr, F., Pratschke, E., Fischer, S., and Paumgartner, G. (1992). Disorders of Bile Acid Metabolism in Cholesterol Gallstone Disease. *J. Clin. Invest.* 90 (3), 859–868. doi:10.1172/JCI115961

But, P. P., Tomlinson, B., and Lee, K. L. (1996). Hepatitis Related to the Chinese Medicine Shou-Wu-pian Manufactured from Polygonum Multiflorum. *Vet. Hum. Toxicol.* 38 (4), 280–282.

Cárdenas, A., Restrepo, J. C., Sierra, F., and Correa, G. (2006). Acute Hepatitis Due to Shen-Min: a Herbal Product Derived from Polygonum Multiflorum. *J. Clin. Gastroenterol.* 40 (7), 629–632. doi:10.1097/00004836-200608000-00014

Canadian Adverse Reaction Newsletter (2003). Case Presentation: RespirActin. . Available online: http://www.hc-sc.gc.ca/dhp-mps/medeff/bulletin/carn-bcei_v13n1-eng.php (Accessed on 9 September 2021).

Casini, A., Ceni, E., Salzano, R., Biondi, P., Parola, M., Galli, A., et al. (1997). Neutrophil-derived Superoxide Anion Induces Lipid Peroxidation and Stimulates Collagen Synthesis in Human Hepatic Stellate Cells: Role of Nitric Oxide. *Hepatology* 25 (2), 361–367. doi:10.1053/jhep.1997.v25.pm0009021948

China Food and Drug Administration (2014). *CFDA Reminds about the Risk of Liver Injury Induced by Oral assumption of PMR*. Updated 2014. Available online: https://www.nmpa.gov.cn/yaopin/ypjgdt/20140716145801865.html (Accessed on November 01, 2021).

Chinese Pharmacopoeia Commission (2015). *Pharmacopoeia of the People's Republic of China* 1. Beijing, China: China Medical Science Press, 175–177.

Cho, H. C., Min, H. J., Ha, C. Y., Kim, H. J., Kim, T. H., Jung, W. T., et al. (2009). Reactivation of Pulmonary Tuberculosis in a Patient with Polygonum Multiflorum Thunb-Induced Hepatitis. *Gut Liver* 3 (1), 52–56. doi:10.5009/gnl.2009.3.1.52

Complementary Medicines Evaluation Committee (CMEC) (2008). *Warning: Polygonum Multiflorum May Harm the Liver in Some People*. Updated 2008. Available online: http://www.tga.gov.au/archive/labelling-rasml-notices-080414.htm (Accessed on September 9, 2021).

Corsini, A., and Bortolini, M. (2013). Drug-induced Liver Injury: the Role of Drug Metabolism and Transport. *J. Clin. Pharmacol.* 53 (5), 463–474. doi:10.1002/jcph.23

Li, D., Yang, M., and Zuo, Z. (2020a). Overview of Pharmacokinetics and Liver Toxicities of Radix Polygoni Multiflori. *Toxins (Basel)* 12 (11), 729. doi:10.3390/toxins12110729

Dong, H., Slain, D., Cheng, J., Ma, W., and Liang, W. (2014). Eighteen Cases of Liver Injury Following Ingestion of Polygonum Multiflorum. *Complement. Ther. Med.* 22 (1), 70–74. doi:10.1016/j.ctim.2013.12.008

Dong, Q., Li, N., Li, Q., Zhang, C. E., Feng, W. W., Li, G. Q., et al. (2015). Screening for Biomarkers of Liver Injury Induced by Polygonum Multiflorum: a Targeted Metabolomic Study. *Front. Pharmacol.* 6, 217. doi:10.3389/fphar.2015.00217

Dong, X., Fu, J., Yin, X., Cao, S., Li, X., Lin, L., et al. (2016). Emodin: A Review of its Pharmacology, Toxicity and Pharmacokinetics. *Phytother Res.* 30 (8), 1207–1218. doi:10.1002/ptr.5631

García-Cañaveras, J. C., Donato, M. T., Castell, J. V., and Lahoz, A. (2012). Targeted Profiling of Circulating and Hepatic Bile Acids in Human, Mouse, and Rat Using a UPLC-MRM-MS-validated Method. *J. Lipid Res.* 53 (10), 2231–2241. doi:10.1194/jlr.D028803

Li, H. Y., Yang, J. B., Li, W. F., Qiu, C. X., Hu, G., Wang, S. T., et al. (2020b). *In Vivo* hepatotoxicity Screening of Different Extracts, Components, and Constituents of Polygoni Multiflori Thunb. In Zebrafish (*Danio rerio*) Larvae. *Biomed. Pharmacother.* 131, 110524. doi:10.1016/j.biopha.2020.110524

Houten, S. M., Watanabe, M., and Auwerx, J. (2006). Endocrine Functions of Bile Acids. *EMBO J.* 25 (7), 1419–1425. doi:10.1038/sj.emboj.7601049

Huang, J., Bathena, S. P., Csanaky, I. L., and Alnouti, Y. (2011). Simultaneous Characterization of Bile Acids and Their Sulfate Metabolites in Mouse Liver, Plasma, Bile, and Urine Using LC-MS/MS. *J. Pharm. Biomed. Anal.* 55 (5), 1111–1119. doi:10.1016/j.jpba.2011.03.035

Iyanagi, T., Emi, Y., and Ikushiro, S. (1998). Biochemical and Molecular Aspects of Genetic Disorders of Bilirubin Metabolism. *Biochim. Biophys. Acta* 1407 (3), 173–184. doi:10.1016/s0925-4439(98)00044-1

Jiang, L. L., Zhao, D. S., Fan, Y. X., Yu, Q., Lai, Y. S., Li, P., et al. (2018). Transcriptome Analysis to Assess the Cholestatic Hepatotoxicity Induced by Polygoni Multiflori Radix: Up-Regulation of Key Enzymes of Cholesterol and Bile Acid Biosynthesis. *J. Proteomics* 177, 40–47. doi:10.1016/j.jprot.2018.02.014

Jung, K. A., Min, H. J., Yoo, S. S., Kim, H. J., Choi, S. N., Ha, C. Y., et al. (2011). Drug-induced Liver Injury: Twenty Five Cases of Acute Hepatitis Following Ingestion of Polygonum Multiflorum Thunb. *Gut Liver* 5 (4), 493–499. doi:10.5009/gnl.2011.5.4.493

Kang, L., Si, L., Rao, J., Li, D., Wu, Y., Wu, S., et al. (2017). Polygoni Multiflori Radix Derived Anthraquinones Alter Bile Acid Disposition in sandwich-cultured Rat Hepatocytes. *Toxicol. Vitro* 40, 313–323. doi:10.1016/j.tiv.2017.01.022

Köck, K., Ferslew, B. C., Netterberg, I., Yang, K., Urban, T. J., Swaan, P. W., et al. (2014). Risk Factors for Development of Cholestatic Drug-Induced Liver Injury: Inhibition of Hepatic Basolateral Bile Acid Transporters Multidrug Resistance-Associated Proteins 3 and 4. *Drug Metab. Dispos* 42 (4), 665–674. doi:10.1124/dmd.113.054304

Kuipers, F., Bloks, V. W., and Groen, A. K. (2014). Beyond Intestinal Soap-Bbile Acids in Metabolic Control. *Nat. Rev. Endocrinol.* 10 (8), 488–498. doi:10.1038/nrendo.2014.60

Lai, J. M., Chang, J. T., Wen, C. L., and Hsu, S. L. (2009). Emodin Induces a Reactive Oxygen Species-dependent and ATM-P53-Bax Mediated Cytotoxicity in Lung Cancer Cells. *Eur. J. Pharmacol.* 623 (1-3), 1–9. doi:10.1016/j.ejphar.2009.08.031

Laird, A. R., Ramchandani, N., deGoma, E. M., Avula, B., Khan, I. A., and Gesundheit, N. (2008). Acute Hepatitis Associated with the Use of an Herbal Supplement (Polygonum Multiflorum) Mimicking Iron-Overload Syndrome. *J. Clin. Gastroenterol.* 42 (7), 861–862. doi:10.1097/MCG.0b013e3181492515

Li, D., Lyu, Y., Zhao, J., Ji, X., Zhang, Y., and Zuo, Z. (2021). Accumulation of the Major Components from Polygoni Multiflori Radix in Liver and Kidney after its Long-Term Oral Administrations in Rats. *Planta Med.* doi:10.1055/a-1585-5991

Lin, L., Ni, B., Lin, H., Zhang, M., Li, X., Yin, X., et al. (2015). Traditional Usages, Botany, Phytochemistry, Pharmacology and Toxicology of Polygonum Multiflorum Thunb.: a Review. *J. Ethnopharmacol.* 159, 158–183. doi:10.1016/j.jep.2014.11.009

Lippi, G., Salvagno, G. L., Montagnana, M., Brocco, G., and Guidi, G. C. (2006). Influence of Hemolysis on Routine Clinical Chemistry Testing. *Clin. Chem. Lab. Med.* 44 (3), 311–316. doi:10.1515/CCLM.2006.054

Ma, J., Zheng, L., He, Y. S., and Li, H. J. (2015). Hepatotoxic Assessment of Polygoni Multiflori Radix Extract and Toxicokinetic Study of Stilbene Glucoside and Anthraquinones in Rats. *J. Ethnopharmacol.* 162, 61–68. doi:10.1016/j.jep.2014.12.045

Maiti, S., Dutta, S. M., and Chen, G. (2014). Apoptosis Inducing Anthraquinone Rhein and Emodin Differentially Suppress Human Dehydroepiandrosterone Sulfotransferase (hSULT2A1) and Phenol Sulfotransferases (hSULT1A1) in Hep-G2 and Caco-2 Cells. *Mnm* 7 (3), 145–153. doi:10.3233/mnm-140015

McGill, M. R. (2016). The Past and Present of Serum Aminotransferases and the Future of Liver Injury Biomarkers. *EXCLI J.* 15, 817–828. doi:10.17179/excli2016-800

Medicines and Healthcare products Regulatory Agency (Mhra) (2006). *MHRA Raises Concerns about the Safety of Polygonum Multiflorum*. Updated 2006. Available online: https://www.who.int/medicines/publications/newsletter/pn2006_3.pdf?ua=1 (Accessed on November 9, 2021).

Noe, J., Hagenbuch, B., Meier, P. J., and St-Pierre, M. V. (2001). Characterization of the Mouse Bile Salt export Pump Overexpressed in the Baculovirus System. *Hepatology* 33 (5), 1223–1231. doi:10.1053/jhep.2001.24171

Park, G. J., Mann, S. P., and Ngu, M. C. (2001). Acute Hepatitis Induced by Shou-Wu-Pian, a Herbal Product Derived from Polygonum Multiflorum. *J. Gastroenterol. Hepatol.* 16 (1), 115–117. doi:10.1046/j.1440-1746.2001.02309.x

Perez, M. J., and Briz, O. (2009). Bile-acid-induced Cell Injury and protection. *World J. Gastroenterol.* 15 (14), 1677–1689. doi:10.3748/wjg.15.1677

Qu, K., Shen, N. Y., Xu, X. S., Su, H. B., Wei, J. C., Tai, M. H., et al. (2013). Emodin Induces Human T Cell Apoptosis *In Vitro* by ROS-Mediated Endoplasmic Reticulum Stress and Mitochondrial Dysfunction. *Acta Pharmacol. Sin* 34 (9), 1217–1228. doi:10.1038/aps.2013.58

Rodrigues, A. D., Lai, Y., Cvijic, M. E., Elkin, L. L., Zvyaga, T., and Soars, M. G. (2014). Drug-induced Perturbations of the Bile Acid Pool, Cholestasis, and Hepatotoxicity: Mechanistic Considerations beyond the Direct Inhibition of the Bile Salt export Pump. *Drug Metab. Dispos.* 42 (4), 566–574. doi:10.1124/dmd.114.054205err10.1124/dmd.113.054205

Schaap, F. G., Trauner, M., and Jansen, P. L. (2014). Bile Acid Receptors as Targets for Drug Development. *Nat. Rev. Gastroenterol. Hepatol.* 11 (1), 55–67. doi:10.1038/nrgastro.2013.151

Schadt, H. S., Wolf, A., Pognan, F., Chibout, S. D., Merz, M., and Kullak-Ublick, G. A. (2016). Bile Acids in Drug Induced Liver Injury: Key Players and Surrogate Markers. *Clin. Res. Hepatol. Gastroenterol.* 40 (3), 257–266. doi:10.1016/j.clinre.2015.12.017

Senior, J. R. (2009). Monitoring for Hepatotoxicity: what Is the Predictive Value of Liver "function" Tests? *Clin. Pharmacol. Ther.* 85 (3), 331–334. doi:10.1038/clpt.2008.262

Stanimirov, B., Stankov, K., and Mikov, M. (2015). Bile Acid Signaling through Farnesoid X and TGR5 Receptors in Hepatobiliary and Intestinal Diseases. *Hepatobiliary Pancreat. Dis. Int.* 14 (1), 18–33. doi:10.1016/S1499-3872(14)60307-6

Stofan, M., and Guo, G. L. (2020). Bile Acids and FXR: Novel Targets for Liver Diseases. *Front. Med. (Lausanne)* 7, 544. doi:10.3389/fmed.2020.00544

Trottier, J., Milkiewicz, P., Kaeding, J., Verreault, M., and Barbier, O. (2006). Coordinate Regulation of Hepatic Bile Acid Oxidation and Conjugation by Nuclear Receptors. *Mol. Pharm.* 3 (3), 212–222. doi:10.1021/mp060020t

US Food and Drug Administration (2005). *Guidance for Industry: Estimating the Maximum Safe Starting Dose in Initial Clinical Trials for Therapeutics in Adult Healthy Volunteers*. Rockville, MD: Center for Drug Evaluation and Research.

Verkade, H. J., Vonk, R. J., and Kuipers, F. (1995). New Insights into the Mechanism of Bile Acid-Induced Biliary Lipid Secretion. *Hepatology* 21 (4), 1174–1189. doi:10.1016/0270-9139(95)90271-610.1002/hep.1840210442

Wang, T., Wang, J. Y., Zhou, Z. X., Jiang, Z. Z., Li, Y. Y., Zhang, L., et al. (2015). Study on Hepatotoxicity of Aqueous Extracts of Polygonum Multiflorum in Rats after 28-day Oral Administration: Cholestasis-Related Mechanism. *Zhongguo Zhong Yao Za Zhi* 40 (11), 2163–2167.

Wang, L., Sang, M., Liu, E., Banahene, P. O., Zhang, Y., Wang, T., et al. (2017). Rapid Profiling and Pharmacokinetic Studies of Major Compounds in Crude Extract from Polygonum Multiflorum by UHPLC-Q-TOF-MS and UPLC-MS/MS. *J. Pharm. Biomed. Anal.* 140, 45–61. doi:10.1016/j.jpba.2017.03.016

Wu, J., Hu, W., Gong, Y., Wang, P., Tong, L., Chen, X., et al. (2017). Current Pharmacological Developments in 2,3,4',5-tetrahydroxystilbene 2-O-β-D-Glucoside (TSG). *Eur. J. Pharmacol.* 811, 21–29. doi:10.1016/j.ejphar.2017.05.037

Xia, X. H., Yuan, Y. Y., and Liu, M. (2017). The Assessment of the Chronic Hepatotoxicity Induced by Polygoni Multiflori Radix in Rats: a Pilot Study by Using Untargeted Metabolomics Method. *J. Ethnopharmacol.* 203, 182–190. doi:10.1016/j.jep.2017.03.046

Xing, Y., Wang, L., Wang, C., Zhang, Y., Zhang, Y., Hu, L., et al. (2019). Pharmacokinetic Studies Unveiled the Drug-Drug Interaction between Trans-2,3,5,4'-tetrahydroxystilbene-2-O-β-d-glucopyranoside and Emodin that May Contribute to the Idiosyncratic Hepatotoxicity of Polygoni Multiflori Radix. *J. Pharm. Biomed. Anal.* 164, 672–680. doi:10.1016/j.jpba.2018.11.034

Xun, L., Liu, Y., Chu, S., Yang, S., Peng, Y., Ren, S., et al. (2019). Physcion and Physcion 8-O-β-Glucopyranoside: A Review of Their Pharmacology, Toxicities and Pharmacokinetics. *Chem. Biol. Interact.* 310, 108722. doi:10.1016/j.cbi.2019.06.035

Yamazaki, M., Miyake, M., Sato, H., Masutomi, N., Tsutsui, N., Adam, K. P., et al. (2013). Perturbation of Bile Acid Homeostasis Is an Early Pathogenesis Event of Drug Induced Liver Injury in Rats. *Toxicol. Appl. Pharmacol.* 268 (1), 79–89. doi:10.1016/j.taap.2013.01.018

Yan, Y., Shi, N., Han, X., Li, G., Wen, B., and Gao, J. (2020). UPLC/MS/MS-based Metabolomics Study of the Hepatotoxicity and Nephrotoxicity in Rats Induced by Polygonum Multiflorum Thunb. *ACS omega* 5 (18), 10489–10500. doi:10.1021/acsomega.0c00647

Yang, J. B., Li, L., Dai, Z., Wu, Y., Geng, X. C., Li, B., et al. (2016). Polygonumnolides C1-C4; Minor Dianthrone Glycosides from the Roots of Polygonum Multiflorum Thunb. *J. Asian Nat. Prod. Res.* 18 (9), 813–822. doi:10.1080/10286020.2016.1171758

Yang, J. B., Tian, J. Y., Dai, Z., Ye, F., Ma, S. C., and Wang, A. G. (2017). A-Glucosidase Inhibitors Extracted from the Roots of Polygonum Multiflorum Thunb. *Fitoterapia* 117, 65–70. doi:10.1016/j.fitote.2016.11.009

Yang, J. B., Li, W. F., Liu, Y., Wang, Q., Cheng, X. L., Wei, F., et al. (2018a). Acute Toxicity Screening of Different Extractions, Components and Constituents of Polygonum Multiflorum Thunb. On Zebrafish (*Danio rerio*) Embryos *In Vivo*. *Biomed. Pharmacother.* 99, 205–213. doi:10.1016/j.biopha.2018.01.033

Yang, J. B., Yan, Z., Ren, J., Dai, Z., Ma, S., Wang, A., et al. (2018b). Polygonumnolides A1-B3, Minor Dianthrone Derivatives from the Roots of Polygonum Multiflorum Thunb. *Arch. Pharm. Res.* 41 (6), 617–624. doi:10.1007/s12272-016-0816-7

Yang, J. B., Liu, Y., Wang, Q., Ma, S. C., Wang, A. G., Cheng, X. L., et al. (2019). Characterization and Identification of the Chemical Constituents of Polygonum Multiflorum Thunb. By High-Performance Liquid Chromatography Coupled with Ultraviolet Detection and Linear Ion Trap FT-ICR Hybrid Mass Spectrometry. *J. Pharm. Biomed. Anal.* 172, 149–166. doi:10.1016/j.jpba.2019.03.049

Yang, J. B., Gao, H. Y., Song, Y. F., Liu, Y., Wang, Q., Wang, Y., et al. (2021). Advances in Understanding the Metabolites and Metabolomics of Polygonum Multiflorum Thunb: A Mini-Review. *Curr. Drug Metab.* 22 (3), 165–172. doi:10.2174/1389200221666201201091345

Zhang, L., and Chen, J. (2018). Biological Effects of Tetrahydroxystilbene Glucoside: An Active Component of a Rhizome Extracted from Polygonum Multiflorum. *Oxid Med. Cel Longev* 2018, 3641960. doi:10.1155/2018/3641960

Zhang, Y., Wang, N., Zhang, M., Diao, T., Tang, J., Dai, M., et al. (2015). Metabonomics Study on Polygonum Multiflorum Induced Liver Toxicity in Rats by GC-MS. *Int. J. Clin. Exp. Med.* 8 (7), 10986–10992.

Zhang, L., Liu, X., Tu, C., Li, C., Song, D., Zhu, J., et al. (2020a). Components Synergy between Stilbenes and Emodin Derivatives Contributes to Hepatotoxicity Induced by Polygonum Multiflorum. *Xenobiotica* 50 (5), 515–525. doi:10.1080/00498254.2019.1658138

Zhang, L., Niu, M., Wei, A. W., Tang, J. F., Tu, C., Bai, Z. F., et al. (2020b). Risk Profiling Using Metabolomic Characteristics for Susceptible Individuals of Drug-Induced Liver Injury Caused by Polygonum Multiflorum. *Arch. Toxicol.* 94 (1), 245–256. doi:10.1007/s00204-019-02595-3

Zhao, D. S., Jiang, L. L., Fan, Y. X., Dong, L. C., Ma, J., Dong, X., et al. (2017). Identification of Urine Tauro-β-Muricholic Acid as a Promising Biomarker in Polygoni Multiflori Radix-Induced Hepatotoxicity by Targeted Metabolomics of Bile Acids. *Food Chem. Toxicol.* 108, 532–542. doi:10.1016/j.fct.2017.02.030

Zollner, G., Fickert, P., Fuchsbichler, A., Silbert, D., Wagner, M., Arbeiter, S., et al. (2003). Role of Nuclear Bile Acid Receptor, FXR, in Adaptive ABC Transporter Regulation by Cholic and Ursodeoxycholic Acid in Mouse Liver, Kidney and Intestine. *J. Hepatol.* 39 (4), 480–488. doi:10.1016/s0168-8278(03)00228-9

Zollner, G., Marschall, H. U., Wagner, M., and Trauner, M. (2006). Role of Nuclear Receptors in the Adaptive Response to Bile Acids and Cholestasis: Pathogenetic and Therapeutic Considerations. *Mol. Pharm.* 3 (3), 231–251. doi:10.1021/mp060010s

Zwicker, B. L., and Agellon, L. B. (2013). Transport and Biological Activities of Bile Acids. *Int. J. Biochem. Cel Biol* 45 (7), 1389–1398. doi:10.1016/j.biocel.2013.04.012

Conflict of Interest: The authors declare that the research was conducted in the absence of any commercial or financial relationships that could be construed as a potential conflict of interest.

GLOSSARY

ACN Acetonitrile
ALT Alanine aminotransferase
AST Aspartate aminotransferase
BAs Bile acids
BCA Bicinchoninic acid
Bsep Bile salt export pump
CA cholic acid
CDCA Chenodeoxycholic acid
CA-S Cholic acid-sulfate
CMC-Na Carboxymethylcellulose sodium
d4-GCDCA Deuterium-labeled glycochenodeoxycholic acid
DCA Deoxycholicacid
Fxr Farnesoid X receptor
GCA Glyco-cholic acid
GMCA Glyco-β-muricholic acid
H&E Hematoxylin and eosin
HDCA Hyodeoxycholic acid
LCA Lithocholic acid
LC-MS/MS Liquid chromatography with tandem mass spectrometry
MeOH Methanol
Mrp2 Multidrug resistance-associated protein 2
PLS-DA Partial Least Squares Discriminate Analysis
PMR Polygoni Multiflori Radix
ROS Reactive oxygen species
Ntcp Sodium taurocholate cotransporting polypeptide
SULT2A1 Sulfotransferase-2A1
TCA Tauro-cholic acid
TCA-S Tauro-cholic acid-sulfate
TCDCA Tauro-chenodeoxycholic acid
TCDCA-S Tauro-chenodeoxycholic acid-sulfate
TDCA Tauro-deoxycholic acid
TG Triglyceride
TLCA Tauro-lithocholic acid
TLCA-S Tauro-lithocholic acid-sulfate
TMCA Tauro-β-muricholic acid
TUDCA Tauro-ursodeoxycholic acid
TSG 2,3,4′,5-tetrahydroxystilbene 2-*O*-*β*-D-glucoside
UDCA Ursodeoxycholic acid
UDCA-S Ursodeoxycholic acid-sulfate
MCA β-muricholic acid
MCA-S β-Muricholic acid-sulfate
γ-GGT γ-glutamine transferase

frontiers | Frontiers in Pharmacology

REVIEW
published: 02 June 2022
doi: 10.3389/fphar.2022.922488

The Application of UHPLC-HRMS for Quality Control of Traditional Chinese Medicine

Jieyao Ma[1,2], *Kailin Li*[1], *Silin Shi*[1], *Jian Li*[1], *Sunv Tang*[1] *and LiangHong Liu*[1,2]*

[1]School of Pharmaceutical Sciences, Hunan Province Key Laboratory for Antibody-Based Drug and Intelligent Delivery System, Hunan University of Medicine, Huaihua, China, [2]Hunan Provincial Key Laboratory of Dong Medicine, Hunan University of Medicine, Huaihua, China

UHPLC-HRMS (ultra-high-performance liquid chromatography-high resolution mass spectrometry) is a new technique that unifies the application of UHPLC with HRMS. Because of the high sensitivity and good separation ability of UHPLC and the sensitivity of HRMS, this technique has been widely used for structure identification, quantitative determination, fingerprint analysis, and elucidation of the mechanisms of action of traditional Chinese medicines (TCMs) in recent years. This review mainly outlines the advantages of using UHPLC-HRMS and provides a survey of the research advances on UHPLC-HRMS for the quality control of TCMs.

Keywords: UHPLC-HRMS, traditional Chinese medicine (TCM), structure identification, fingerprint analysis, quality control

OPEN ACCESS

Edited by:
Zhichao Xu,
Northeast Forestry University, China

Reviewed by:
Zhe-Sheng Chen,
St. John's University, United States
Qingfa Tang,
Southern Medical University, China
Changhua Xu,
Shanghai Ocean University, China

***Correspondence:**
LiangHong Liu
llhfe@qq.com

Specialty section:
This article was submitted to Experimental Pharmacology and Drug Discovery, a section of the journal Frontiers in Pharmacology

Received: *18 April 2022*
Accepted: *10 May 2022*
Published: *02 June 2022*

Citation:
Ma J, Li K, Shi S, Li J, Tang S and Liu L (2022) The Application of UHPLC-HRMS for Quality Control of Traditional Chinese Medicine. Front. Pharmacol. 13:922488. doi: 10.3389/fphar.2022.922488

INTRODUCTION

Traditional Chinese medicine has been used in China for over thousands of years and a long history of development in China and has made great contributions to improving the quality of life and physical health of Chinese people and people around the world. The clinical therapeutic effect of TCM has been documented over the last thousands of years. For example, *Artemisia annua* L is one of most common herbs and is used to treat malignant sores, kill lice, retain the warmth of joints, and improve vision acuity, and has been prescribed in traditional Chinese medical practice for over two thousand years (Tu et al., 2016). Artemisinin was extracted and isolated from *Artemisia annua* L by Tu Youyou in 1971 and was used to successfully treat malaria. Accordingly, Tu Youyou received the 2011 Lasker Award in clinical medicine and shared the 2015 Nobel Prize in Physiology or Medicine with William C. Campbell and Satoshi Ōmura (Efferth et al., 2015). The study on TCM has attracted much attention by researchers worldwide. However, performing quality control of TCM is the only way to ensure its safety and effectiveness and promote the international development of TCM. The current basic mode of quality control of TCM was established by referring to foreign quality control methods for herbal medicines and chemical drugs (Leong et al., 2020). Thin layer chromatography

Abbreviations: UHPLC-HRMS, Ultra-high-performance liquid chromatography-high resolution mass spectrometry; TCMs, Traditional Chinese medicines; TLC, Thin layer chromatography; HPTLC, High-performance thin layer chromatography; LC-MS, Liquid chromatography combined with mass spectrometry; HPLC-UV/PDA, High-performance liquid chromatography-ultraviolet-visible detector or photodiode array detector; Q-TOF-MS, Quadrupole time-of-flight mass spectrometry; UHPLC/Q-TOF-MS, Ultr-high performance liquid chromatography coupled to Quadrupole time-of-flight mass spectrometry; Q-Orbitrap-MS, Q-Exactive Orbitrap mass spectrometry; UHPLC-ESI-Q-TOF, Ultra-high performance liquid chromatographic electrospray ionization quadrupole- time of flight mass spectrometry; ChP, Chinese Pharmacopoeia; PCA, Principal component analysis.

(TLC) and high-performance liquid chromatography (HPLC) play crucial roles in quality control of TCM in the Chinese Pharmacopoeia (ChP). However, the limitations of TLC include the poor repeatability and stability of the results and a mobile phase with high toxicity (Deng et al., 2019). The shortcomings of HPLC include high price of solvents and columns, and a lack of long-term reproducibility due to the proprietary nature of column packing (Siddiqui et al., 2017). In the last decade of the 20th century, liquid chromatography combined with mass spectrometry (LC-MS) was the most important techniques used in the pharmaceutical industry (Niessen et al., 1999).

Nevertheless, the analytical techniques mostly applied for quality control of TCM are high-performance liquid chromatography-ultraviolet-visible detector or photodiode array detector (HPLC-UV/PDA)and/or HPLC-MS. The main drawback is that these techniques are time consuming and do not provide adequate information of resolution of the compounds in TCM. The UHPLC-HRMS system can provide changeable collision energy values and allow the generation of mass information with accuracy and precision, which is ultimately conducive to elucidating the structures and identifying the fragmentation patterns of the compounds of TCM (Lippert et al., 1999).

The aim of this review is to introduce the applications of UHPLC-HRMS using examples of some of the most advanced work in the field of quality control of TCM.

ADVANTAGES OF UHPLC-HRMS

UHPLC, as the first producer Waters proclaims, has the advantages of "speed, resolution and sensitivity". Application of this technique may result in a new direction for liquid chromatography that could reform the field. Compared to traditional chromatographic techniques, such as high-performance thin layer chromatography (HPTLC) and TLC, UHPLC uses column packing material less than 2 μm, and the pressure generated during the use also increases exponentially. Thus, UHPLC has the following unique advantages in the field of quality control of TCM (Khan et al., 2015; Siddiqui et al., 2017; Zhang et al., 2017; Li L. et al., 2020; Kresge et al., 2020):

- Increased selectivity, sensitivty and range of LC analysis.
- The smaller peak width allows identification of a greater number of peaks.
- Fast resolution and quantification of complex components of TCM.
- Withstands the high pressures used in experiments.
- Saves time and solvent.
- Fewer samples are required.
- Increased resolution performance.
- Reduced analysis costs.
- It is an optimal entry point for mass spectrometry detectors.

Without the standard compounds, it is difficult for UHPLC to provide accurate information about the structure of the compounds in TCMs. Meanwhile, a considerable amount of time is required to isolate and purify the compounds of TCMs. With the development of modern analytical techniques, a variety of high resolution mass spectrometry (HRMS) techniques, such as the quadrupole time-of-flight mass spectrometry (Q-TOF-MS) and Q-Exactive Orbitrap mass spectrometry (Q-Orbitrap-MS), have been widely used for the detection and identification of compounds in TCMs (Wang L. et al., 2017; Liang et al., 2021; Tan et al., 2021). Mass spectrometers are more suitable for rapid and cost-efficient analysis and tentative identification of TCMs, and the types that have been used HRMS mass spectrometers (Lv et al., 2018; Li et al., 2021). These mass spectrometers have the advantages such as high mass accuracy, excellent resolution, a fast scan rate, superior sensitivity, and multiple-stage mass spectrometry scanning (MS^n), and can provide HRMS and MS^n data for some compounds present in TCM using a simple data acquisition method (Yang JB. et al., 2019).

APPLICATION OF UHPLC-HRMS

Chemical Characterization of TCM

UHPLC-HRMS is an advanced form of an analytical technique used to separate and identify the complex mixture of components found in TCM to better recognize the role of individual compounds. It is important to make generalizations about fragmentation pathways of reference compounds by the HRMS technique to speculate the identity of potential compounds in TCM.

For example, phenolic acids and prenyl flavonoid glycosides are important constituents of *Epimedii Folium*. An efficient method was developed to enrich these compounds and identify them in *Epimedium koreanum* Nakai (EK) using the UHPLC-HRMS method. Fifty-one prenyl flavonoid glycosides, 18 phenolic acids, and 42 icariin analogues were successfully identified or tentatively identified from *Epimedium koreanum* using this method (Wang et al., 2010; Yang et al., 2017b). Meanwhile, more than 100 compounds were also identified or tentatively identified from *Epimedii Folium* based on the MS/MS of standards, and the compounds were compared with reference results by the UHPLC-HRMS method (Wang Y. et al., 2017; Pilepić et al., 2018; Li M. Y. et al., 2020; Li N. et al., 2020). *Polygonum multiflorum* Thunb. and its processed products have been widely used in China for hundreds of years. *Polygonum multiflorum* exerts liver-tonic and hair-blacking effects. At present, liver injuries caused by taking *P. multiflorum* have been widely reported. To specifically elaborate the bioactive and hepatotoxic constituents, more than 200 compounds, consisting of phenolic acids, flavones, stilbenes, anthraquinones, naphthalenes and their derivatives, were identified or tentatively identified using characteristic diagnostic fragment ions and references based on the UHPLC-HRMS method (Lin et al., 2015; Wang GY. et al., 2017; Yang JB. et al., 2019; Han et al., 2019; Rui et al., 2020).

Using online UHPLC-HRMS, a rapid and credible analytical method was also developed, which was used to identify the chemical

conponents of *Polygoni cuspidati* folium and its preparation. Twenty-six chemical constituents, such as derivatives of phenylpropionic acid, tannin, stilbene, flavonoids, torachryson, anthraquinone and their derivatives, were identified or tentatively characterized (Wang X. et al., 2018). *Bupleuri radix* and liquorice are commonly used as medication for protecting liver function. It is well known that the saponins in Bupleuri radix and liquorice can not only promote the metabolism of lipids and sugar, but also exhibit anti-inflammatory function and liver-protective effects. These substances were analyzed by UHPLC-HRMS, and 23 saponins and 9 flavonoid glycosides from liquorice, and 18 saponins from *Bupleuri radix* were tentatively identified based on the characteristic fragment filters and neutral loss filters (Shan et al., 2018). *Schisandra chinensis,* known as WuWeiZi in Chinese, has a good effect in astringing the lung to stoping coughs, arresting sweating, preserving semen and preventing diarrhea. A reliable method was developed for the rapid identification of multiple components in *Schisandra chinensis* by their characteristic fragments and neutral losses using UHPLC-HRMS technology. Accordingly, a total of 30 compounds including 15 lignans, nine triterpenoids, three organic acids and three fatty acids were successfully detected and tentatively identified from *Schisandra chinensis* within 30 min (Yang et al., 2017a). Triterpenoid saponins are the major bioactive constituents of Pulsatilla chinensis. Triterpenoid saponins play important roles in various biological activities such as anti-tumour, cognition-enhancing, anti-biosis, anti-inflammation, hypoglycemia and immunological adjuvant. A systematic strategy based on UHPLC-Q-TOF-MS/MS for the efficient characterisation and identification of triterpenoid saponins in crude extracts from Pulsatilla chinensis has been established (Jin et al., 2018). Bamboo leaves extract (BLE) has a variety of physiological functions such as antitumour, anti-inflammation, antioxidant and hypoglycemic activities and the flavonoids of bamboo leaves are the major active constituents. To profile the flavonoids in the complex BLE, a rapid and sensitive analytical method based on UHPLC-ESI-Q-TOF-MS/MS was developed for the structural identification of the flavonoids in Bambusa chungii leaves extract using accurate mass measurements and characteristic fragmentation patterns (Yuan et al., 2020).

The emergence of UHPLC-HRMS has effectively solved the difficult problems of qualitative analysis of complex medicinal ingredients in TCM. However, the analysis of UHPLC-HRMS also has some deficiencies. Firstly, the volatile components could not identified by UHPLC-HRMS, which was mainly performed by gas chromatography–mass spectrometry (GC-MS). Secondly, qualitative identification of chemical constituents of TCM was detected and identified most combining the MS, MS^2, chromatography retention time, bibliography data by comparing the mass spectrometry database, performing diagnostic ions filter and molecular network mining. However, the identification of unknown compounds was still inadequate.

Determination of TCM Components

The UHPLC-HRMS technique has high sensitivity and has been widely used to determine the trace constituents of TCMs.

The dried bark of *Ilex rotunda,* known as Jiubiying, which contains triterpenoids and phenylpropanoids as major bioactive constituents, has been widely applied for clearing heat and removing toxicity in TCM. A validated UHPLC-HRMS method was developed to simultaneously identify and quantify the phenylpropanoids and triterpenoids in the roots, stem bark, stem xylem, leaves, and fruit of *Ilex rotunda*. Meanwhile, the contents of three phenylpropanoids and twelve triterpenoids in the five plant parts were determined with good repeatability, linearity, stability, precision and recovery (Yang et al., 2018). A rapid and reliable UHPLC-ESI-Q-TOF method was also developed to quantify six representative indole alkaloids (vinblastine, vincristine, ajmalicine, vindoline, serpentine, and catharanthine) in *Catharanthus roseus* (Jeong et al., 2018). The radix of *Angelica sinensis* (AS), one of the most important TCMs, is often used for tonifying blood and treatment of amenorrhea and irregular menstruation in females. An UHPLC-HRMS method was established to analyze and identify ferulic acid and phthalides, which could be used to evaluate the quality of AS (Wei et al., 2015a). *Morus alba* L. has an uninterrupted history going back over 4,000 years in China. The leaves of *Morus alba* L have been widely used for the treatment of diabetes as an herbal medicine for thousands of years. An UHPLC-HRMS method was developed for identification and determination of polyhydroxylated alkaloids, such as 1-deoxynojirimycin, with α-glucosidase inhibitor activity in mulberry leaves to evaluate the quality of *Morus alba* L leaves (Ji et al., 2016). *Radix astragali* is one of the most popular TCMs in China due to its effects of invigorating the spleen-stomach and replenishing qi. A UHPLC-HRMS method was used to determine the content of astragaloside I, II and IV in *Radix astragali*, and this method could be effectively applied to evaluate the quality of *Radix astragali* (Han et al., 2016). Poria cocos (Schw.) Wolf has been widely used as a medicine and food in China. An approach based on UHPLC-Q/TOF-MS was utilized to characterize the temporal and spatial variations in the accumulation of specialized metabolites in Fushen, and the quantitative method was successfully applied to simultaneously determine 13 major triterpenoid acids in the nine growth periods and four parts (Yang M. et al., 2021).

Chemical Fingerprint Analysis

Phellodendri Amurensis Cortex (PAC), commonly called Guanhuangbai in ChP, is derived from the dried bark of *Phellodendron amurense* Rupr. Currently, PAC is widely used to treat rheumatoid arthritis, tumors and other diseases. UHPLC/Q-TOF-MS fingerprinting with chemometric methods was first established to identify the major components of Phellodendri amurensis Cortex (PAC). Ten batches of PAC were used to establish the UHPLC/Q-TOF-MS fingerprint. Sixteen common peaks in the fingerprint were obtained, and ten were tentatively identified. The developed fingerprint assay is a powerful method which could be used to conduct quality control of PAC (Li et al., 2010). Ermiao Wan (EW) is a combination formula of *Rhizoma Atractylodis* and *Cortex Phellodendri Chinensis* that is commonly prescribed for patients with gout and hyperuricemia, as described in the ChP (Liu et al., 2006; Yan et al., 2015; Fu et al., 2021; Shan et al., 2021). UHPLC-HRMS fingerprinting combined with the multivariate data mining method (MMA) could provide a

validated, rapid and high-throughput methodology for identification of the chemical constituents to ensure the quality of Ermiao Wan (Yan et al., 2015). SiJunZiTang (SJZT), which consists of four herbs, *Radix Ginseng*, *Atractylodes macrocephala*, *Poria cocos* and *Glycyrrhiza uralensis*, is widely used for nourishing qi and to invigorate the spleen and has protective effects on the intestine and stomach against injury, such as stomachache, rugitus, nausea, vomiting or diarrhea (Liu et al., 2006). UHPLC-HRMS fingerprinting provided clues to the contributions of *Atractylodes macrocephala* and *Poria cocos* in SJZT decoction and allowed quality control of SiJunZiTang (SJZT) (Wang Y. et al., 2013). *Gastrodia elata* was first recorded in Shen Nong's Herbal Medicine Classic and has the functions of calming the liver, spasmolysis and relieving wind in Chinese medicine (Ojemann et al., 2006). The chemical fingerprint of the ethyl acetate fraction of *Gastrodia elata* (EtAcGE) was investigated using UHPLC/HRMS. A total of 38 chemical constituents of EtAcGE were tentatively characterized or identified by comparing the molecular formula and fragment ions with those of known compounds or information available in literatures. The chemical fingerprint and metabolic profile of EtAcGE could provide a basis for the future research on EtAcGE (Tang et al., 2016). *Corydalis yanhusuo* is a well-known Chinese herbal medicine which is frequently used as an analgesic agent in clinics for thousands of years. The *Corydalis yanhusuo*-derived quaternary ammonium alkaloids are effective against myocardial ischemia. The chemical fingerprints of quaternary ammonium alkaloids extracted from the Corydalis yanhusuo speciemens from 37 different sources were identified using UHPLC-HRMS. The fingerprint-efficacy relationship between the chemical fingerprints and cardioprotective effect of Corydalis yanhusuo was investigated (Li et al., 2017). UHPLC-ESI-Q-TOF-MS/MS analysis was conducted to identify the compounds and establish UHPLC fingerprint, explored the bioactive markers of *Codonopsis Radix* (Gao et al., 2019). Zhishi-Xiebai-Guizhi Decoction, has been used for treatment of coronary heart disease and myocardial infarction for nearly two thousand years. An UHPLC-Q-TOF-MS method was utilized for the identification of its multi-constituents, and a total of 148 compounds were identified. In addition, an optimized UHPLC fingerprint analysis, combined with chemometrics was developed for quality assessment (Sang et al., 2020).

Identification of the Authenticity of TCMs

Donkey-hide gelatin, bovine-hide gelatin, pig-hide gelatin, glue of tortoise shell, equine-hide gelatin and deerhorn glue are widely used as TCMs in China to nourish yin and tonify blood. However, the price varies according to the origins of gelatins. To prevent illegal activities such as manufacturing and marketing counterfeit commodities, a UHPLC-HRMS method combined with a principal component analysis (PCA) was first developed and applied to identify donkey-hide gelatin, bovine-hide gelatin, pig-hide gelatin, tortoise shell glue, equine-hide gelatin and deerhorn glue (Cheng et al., 2012; Jiao et al., 2019). The velvet antler is a non-ossifying hairy young horn derived from the male sika deer (*Cervus nippon* Temminck) or red deer (*Cervus elaphus* Linnaeus) that is used as a medicinal antler in ChP (The State Pharmacopoeia Commission., 2020). Velvet antler has different pharmacological effects on the sexual function and immune system based on its bioactive components and chemical composition (Sui et al., 2014). However, many reindeer antlers are used as medicinal antlers in the market, and the price of reindeer antler is much lower than that of sika deer antler and red deer antler. A UHPLC-HRMS method coupled with principal component analysis (PCA) was successfully developed and used to identify antlers derived from *Cervus elaphus* Linnaeus, *Cervus nippon* Temminck and *Rangifer tarandus* Linnaeus to prevent the sale of counterfeit goods (Guo et al., 2019). *Bletilla striata* has a wide range of applications in pharmacological and cosmetic fields, because of the shortage of resources, there are some substitutes. To distinguish the differences and homologies, a UHPLC fingerprint analysis coupled with chemometric methods were developed for characterization and quality control (Wang et al., 2022). The stems of *Kadsura* interior A. C. Smith has the efficacy of tonifying and invigorating the blood. Its closely related species are morphologically similar, thus likely to exert negative effects on clinical efficacy and clinical medication safety. Combining UHPLC-Q/TOF-MS/MS technique and multivariate data analysis to discover differential metabolites and to comprehensively assesse the chemical constituents, six differential compounds in the stems of K. interior were screened out to distinguish it from K. interior, K. heteroclita, K. longipedunculata, and K. japonica (Xu et al., 2022).

Identification of Illegal Additives in TCMs

In recent years, the use of TCMs has increased because they are regarded as healthier and safter than chemical drugs and have few side effects (Yuan et al., 2000; Wang J. et al., 2018). Motivated by interest, some unscrupulous manufacturers added chemical ingredients illegally into TCMs, and such behavior could lead to potentially serious public health consequences (Vaclavik et al., 2014). Therefore, it is very important for researchers to develop methods to detect illegal additives to control the quality of TCM.

A UHPLC-HRMS method with an information-dependent acquisition (IDA) mode was developed to screen, identify and quantify the illegal, adulterated, aphrodisiac chemical ingredients in TCMs, and four chemical drugs, including sildenafil, tadalafil, aildenafil and sulfoaildenafil, were detected in some TCMs (Wang XB. et al., 2018). The UHPLC-HRMS method was also applied to identify the illegal additives in TCMs used to relieve cough and asthma or reduce blood glucose. Nine types of chemical medicines including oxytetracycline, sulfamethoxazole, chlorphenamine, diphenhydramine, pentoxyverine, benproperine, prednisone acetate and diazepam were detected in Chinese traditional patent medicines (Chen et al., 2015; Peng et al., 2015). Three types of chemical medicines including phenformin hydrochloride, glibenclamide and pioglitazone hydrochloride were also qualitatively and quantitatively detected in traditional Chinese medicinal preparations (Zhu et al., 2014; Shen et al., 2016). Unauthorized drugs were also found in health foods and herbal products of gout and anti-osteoporosis TCMs. Dexamethasone was detected and confirmed by comparing the MS/MS fragment ion patterns of a reference

standard.(Kim et al., 2020). An UHPLC-Q-TOF method was validated for screening, confirmation and quantitation of 31 anti-impotence compounds potentially illegally added to herbal-based dietary supplements. Among 200 batches of herbal-based dietary supplements, sildenafil and/or tadalafil were found to be added illegally in two samples, and low concentration of icariin was detected in one sample (Shi et al., 2020). In general, the UHPLC-HRMS method has been shown to be a powerful tool for routine screening and quantitation of illegal ingredients in TCMs.

Exploring the Quality-Marker (Q-Marker)

It is well known that TCMs contain various components, and the synergistic effects of these components are conducive to their effectiveness in clinical applications. Meanwhile, one or several chemical markers were previously selected to control the quality of TCM. However, a bottleneck in TCM research has been the low discovery rate of the effective components and the correlation of their effects (Li et al., 2011; Ren et al., 2020). Therefore, Liu *et al.* introduced a new concept of a quality marker (Q-marker) that was used to control the quality of TCMs in 2016 (Liu et al., 2016).

Some TCMs, such as *Lonicera japonica flos* (LJF) and *Lonicera flos* (LF), are easily confused species. It is very difficult to quickly evaluate their potency using conventional methods. UHPLC-HRMS with partial least squares-discriminant analysis (PLS-DA) was used to screen chemical markers for identification of their herbal origin; then, a bioactivity-guided evaluation method was performed to detect the Q-markers. It was found that four NF-kB inhibitors were presented as the representative Q-markers including the following anti-inflammatory compounds: 3, 5-*O*-dicaffeoylquinic acid (3, 5-diCQA), 3-*O*-caffeoylquinic acid (CA), vogeloside and iamarin (Ding et al., 2017). However, some TCMs need to be processed to reduce toxicity and increase efficiency. The underlying mechanism of processing is still not clear, and a Q-marker database for processed TCMs has not been effectively established. For instance, *Radix Wikstroemia indica* (RWI,"Liao Ge Wang" in Chinese) is a type of Chinese herbal medicine (CHM) frequently used in the Miao nationality of South China. RWI is processed by the "sweat soaking method" which effectively decreases its toxicity and preserves its therapeutic effect (Wei et al., 2015b; Chang et al., 2017). Twenty compounds were identified from the ethanol extract of the raw and processed products of RWI based on UHPLC-HRMS, including daphnoretin, emodin, triumbelletin, dibutyl phthalate, and methyl paraben. Three diterpenoids are regarded as the potential Q-markers for quality and safety assessment of the processed RWI by the "sweat soaking method" (Feng et al., 2018). UHPLC-HRMS combined with orthogonal signal correction-partial least squares regression (OSC-PLSR) and the HPLC fingerprint method was applied to search for the Q-markers of Shenzhiling oral liquid, which is used to treat mild to moderate Alzheimer's disease (AD) (Nie et al., 2016). Sixty-one efficacy-related components were successfully determined by mapping the targets of the disease, and the 3 potential Q-markers of Shenzhiling oral liquid were liquiritin apioside, albiflorin and azelaic acid, which were preliminarily obtained by the above methods (Liu et al., 2019a).

Identification of Metabolites

Drug metabolism refers to a series of organic reactions after the drugs enter the body, which is also known as biotransformation. For complete knowledge of the therapeutic effectiveness of a TCM, it is essential to identify its metabolites.

For instance, *Scutellaria baicalensis* is one of the most common TCMs and can be used for heat-clearing, dehumidifying and lowering blood sugar (Zhao et al., 2019a; Liao et al., 2021). However, with regard to its main bioactive flavonoids, including baicalein, baicalin, wogonin and wogonoside, the *in vivo* metabolism needs further research (Li et al., 2004). A UHPLC-HRMS technique was used in combination with Metabo-lynx™ software to determine the metabolites and excretion profiles of flavonoids in *S. baicalensis* extract in the feces, urine and bile samples of rats after oral administration of the extract. Nearly 20 metabolites were identified *in vivo*. including glucuronide and sulfate conjugates, and acetylated methylated, deoxygenated and hydroxylated products (Du L.-y. et al., 2015; Du LY. et al., 2015). *Bletilla striata* (Thunb.) Reichb. f (Orchidaceae), also known as Bai-ji, is a type of TCM that is commonly used for the treatment of hematemesis, hemoptysis, traumatic bleeding and other similar disorders (He et al., 2017). A UHPLC-HRMS technique combined with the MS^E method was used to identify the metabolic profile of the non-polysaccharide fraction in Sprague-Dawley rats and intestinal bacteria models from *Bletilla striata*. Eight components including 3 metabolites and five prototypes were successfully identified in rat biofluids after oral administration of the non-polysaccharide fraction. The potential metabolic processes, including hydrolysis, deglycosylation, glycosylation, and sulfate conjugation, and pharmacological components could be elaborated using the UHPLC-HRMS method (Yang C. et al., 2019). Tao-Hong-Si-Wu decoction (THSWD) is composed of 6 different TCMs and is widely used for the treatment of blood stasis and gynecologic diseases, such as amenorrhea and dysmenorrhea (Li et al., 2015; Xia et al., 2021). The effect of THSWD on acute blood stasis in rats was systematically studied based on a UHPLC-HRMS metabolomics and a network approach. Fifteen metabolites were screened, and found to be involved ten pathways and five hub metabolites, including L-phenylalanine, L-glutamate, N-acylsphingosine, phosphatidate and arachidonic acid (Ma et al., 2018). Semen Euphorbiae (SE) has significant pharmacological activity. Its toxicity limits its clinical application, and less toxic Semen Euphorbiae Pulveratum (SEP) is often used clinically. a comprehensive metabolomics analysis of serum and urine samples from rats treated with SE and SEP performed by UHPLC/Q-TOF-MS were used to distinguish the differential metabolites of SE and SEP to reveal the metabolic pathways and their significance (Yang Z. et al., 2021).

Elucidation of the Mechanism of Action of TCMs

TCMs have been used to treat various diseases for thousands of years in Asia and have attracted attention by a growing number of scientists in recent years. However, the mechanisms of action

of TCMs are rarely known due to a lack of study by modern scientific methods. The therapeutic efficacy of TCM is usually attributed to the synergistic properties and competitive actions of the TCM formula and its constituents (Zhang et al., 2013).

For example, Taohong Siwu Decoction (TSD), which originated from the "Golden Mirror of Medicine," can be used to remove blood stasis, promote blood circulation, inhibit inflammatory cytokines and enhance immunity (Duan et al., 2020; Nie et al., 2020). UHPLC-HRMS with PCA and OPLS-DA methods was used to explore changes in the endogenous metabolites, investigate the global alteration of metabolites and evaluate the preventive effect of TSD in rats. The potential metabolic biomarkers of TSD were evaluated using OPLS-DA and a *t*-test, and the mechanisms of action of TSD on acute blood stasis were revealed based on the UHPLC-HRMS platform (Zhang et al., 2018). Sijunzi decoction (SJZD), a classic TCM, has been shown to have therapeutic effects on spleen deficiency syndrome. However, there are few reports on the mechanisms of SJZD in disease treatment. UHPLC-HRMS and PLS-DA methods were also developed to analyze the difference in the global metabolite profile within all groups (untreated rats, normal control rats and SJZD group rats), and variable importance projection (VIP >1) and Student's t-test ($p < 0.05$) were applied for biomarker selection. Twenty metabolites showed significant differences in the untreated group, and 6 potentially perturbed metabolic pathways were found, which could be conducive to elucidating the mechanism of action of SJZD (Yan et al., 2017). Meanwhile, an online UHPLC-HRMS identification method was employed to examine the synergistic effect of Platycodonis Radix (PG) in the TCM prescription Shengxian Decoction (SXT) (Zhang et al., 2014). In Asia, it is well known that compatibility with TCM can minimize adverse reactions and improve therapeutic efficacy. For instance, UHPLC-HRMS with PCA and OPLS-DA methods could be developed to analyze the attenuation of the toxic effects of an *Aconiti lateralis* radix preparation (named Fuzi in China) and its compatibility with *Glycyrrhizae* radix et rhizome (named Gancao in China). Twelve biomarkers related to Fuzi toxicity and 6 metabolic pathways were identified. With the above methods, the mechanism of compatibility and toxicity attenuation could be evaluated from the perspective of metabolites and could provide a reference for clinical safety (Liu et al., 2019b; Yang B. et al., 2019). *Cantharidin* is the major bioactive component of the blister beetle, which has strong antitumor activity. Clinical application of *cantharidin* is limited because of its toxic effect. An UHPLC-Q-TOF/MS based metabolomics approach in combination with histopathological examination, cell apoptosis assay, and blood biochemical analysis were used to investigate the mechanisms of action of cantharidin-induced hepatotoxicity (Zhu et al., 2019).

Evaluation of the Quality of TCMs From Different Habitats

Genuine medicinal materials of TCMs refer to those grown in a specific area with high quality and effectiveness. Due to the influence of growing conditions, climate and other factors, analysis of the characteristic constituents of TCM has shown differences in TCMs from different habitats.

For example, *Atractylodis Macrocephalae Rhizoma* (AMR) was widely used to reinforce the spleen, nourish Qi and remove dampness in Chinese medicine and is mainly distributed in Anhui, Jiangxi, Henan, Hebei, Hubei, Zhejiang and other areas. To evaluate the quality of AMR from genuine producing areas (Zhejiang) and other regions, a UHPLC-HRMS technique combined with multivariate statistical analysis was developed to investigate the common and different components of AMR from different regions. Sixteen major differential compounds, such as tyrosine, methylated atractylenolide I, atractylenolide I, II and III, and atractylone were selected from samples of 7 different regions. Because AMR from Zhejiang shows better results than samples from other regions, tyrosine, and dehydroaromadendrene could be used as the index ingredients for evaluation of the genuineness of AMP based on the above methods (Huang et al., 2017). *Moutan Cortex*, the root cortex of *Paeonia suffruticosa* Andr., is an important TCM that is used as an analgesic, antispasmodic and anti-inflammatory agent (Zhang et al., 2020). Based on its origin, it can be classified as a genuine medicinal material, Fengdanpi (Tonglin, Anhui), or general herb (other areas). The UHPLC-HRMS technique combined with the PCA, PLS-DA, and OPLS-DA methods was used to identify and analyze the common and different components of *Moutan Cortex*. The medicinal materials from different origins were clustered into different groups by PCA. Five biomarkers were successfully obtained by the UHPLC-HRMS, PLS-DA and OPLS-DA methods. These could provide a theoretical basis for understanding the chemical material composition and quality evaluation of *Moutan Cortex* (Hu et al., 2016). *Ophiopogonis radix*, the tuberous root of Ophiopogon japonicas (Thunb.) Ker-Gawl (Liliaceae), known as Maidong in Chinese, is a common TCM that is used to alleviate symptoms of diabetes and cardiovascular diseases (Wang et al., 2019). Multiple bioactive constituents analysis based on the UHPLC-HRMS technique combined with multivariate statistical analysis was used to evaluate the effects of two types of *Ophiopogonis radix* that originated form Hangzhou and Sichuang. The results showed that the quality of *Ophiopogonis radix* from genuine producing areas (Sichuan) was better than that from other areas (Zhejiang) (Tan et al., 2019). *Sophora tonkinensis* is widely used as TCM for treating the swelling of the gums, tongue and mouth sores due to flaring up of stomach fire. Alkaloids are the major bioactive components. UHPLC-Q-TOF-MS/MS was applied in identifying and characterizing alkaloids in *S. tonkinensis* root of two different habitats. The Radix *Sophora Tonkinensis* for Guozhou, Sichuan province have difference by comparative analysis of alkaloids for two different habitats (Zong et al., 2022). UHPLC-Q-TOF/MS was also used to compare the differences of *Paeonia lactiflora* from different habitats, Sichuan, Hebei, Henan, Shanxi and Anhui. (Zhao et al., 2019b).

Others

Cordyceps sinensis (Berk.) Sacc. is a well-known TCM and has many active ingredients, such as polysaccharides, nucleosides,

cordycepic acid, and sterols (Wang Z. et al., 2013; Xia et al., 2022; Yuan et al., 2022). *C. sinensis* (Berk.) Sacc. has been commonly used for the treatment of night sweats, hyperlipidemia, hyperglycemia, respiratory disease, renal dysfunction and failure, arrhythmias, other heart disease, and liver disease. To examine the correlation between the quality and chemical constituents of different parts of *C. sinensis* (Berk.) Sacc., UHPLC-HRMS with the PCA and PLS-DA methods was used to analyze the chemical constituents of three parts of Cordyceps including the seats, heads and insect worms. Eleven differentiated compounds were identified from Cordyceps seats, heads and insect worms and mainly consisted of fatty acids and their derivatives (Qin et al., 2018). The established method could provide a scientific reference for clarifying the pharmacodynamics and the mechanism of quality assessment of *C. sinensis* (Berk.) Sacc. and provide a foundation for its rapid identification, quality control and utilization of *C. sinensis* (Berk.) Sacc. Meanwhile, the UHPLC-HRMS technique could be applied to pharmacokinetic studies in rats or humans. For example, this method could be used to determine the content of tumulosis acid and dehydro-tumulosic acid in rat plasma after oral administration of Poria triterpenoid extract powder and soft capsules because different dosage forms could affect the bioavailability of these compounds (Wen et al., 2017).

CONCLUSION

The UHPLC-HRMS technique is widely used for applications in chromatography-mass spectrometric analysis. This technique provides not only rapid and improved chromatographic separation and short chromatographic run time, but also high sensitivity and selectivity, accurate measurement, and reliable chemical fragmentation, that are ultimately helpful for elucidating the structure of various compounds. This technique could be applied to obtain better results than conventional TLC, HPLC-UV and HPLC-MS techniques. In this review, we go over the advantages and applications of UHPLC-HRMS in the analysis of TCM constituents, and examples are provided that focus on the difficult points mentioned above. Attention should be paid to the accuracy of qualitative analysis when applying this method for the quality control of TCM. The mass spectrometry-based natural product database should be a feasible way to identify chemicalls easily, effectively and accurately. The utilization of artificial intelligence in data mining and interpretation will be an effective method.

In summary, UHPLC-HRMS is a very useful tool for the determination of components or metabolites of TCMs that might link to various diseases. UHPLC-HRMS is a simple and rapid method for the quality control of TCMs. It is important to build a mass spectrum database and utilize the artificial intelligence to identify the complex substances of TCMs accurately and establish a reasonable quality appraising standard for TCMs.

AUTHOR CONTRIBUTIONS

LL, JM conceived the study; LL, JM, KL collected and analyzed the relevant literatures; LL and JM wrote the manuscript; SS, JL, ST revised the manuscript.

FUNDING

This project was financially supported by Hunan Province Social Science Innovation Research Base (Ethnic medicine and ethnic culture research base).

REFERENCES

Chang, H., Wang, Y., Gao, X., Song, Z., Awale, S., Han, N., et al. (2017). Lignans from the Root of Wikstroemia Indica and Their Cytotoxic Activity Against PANC-1 Human Pancreatic Cancer Cells. *Fitoterapia* 121, 31–37. doi:10.1016/j.fitote.2017.06.012

Chen, X. H., Qin, J., Su, J., Ren, X. Y., Zeng, L. G., and Kuang, G. (2015). Determination of 8 Kinds of Chemical Medicines Illegally Added in Traditional Chinese Medicines for Relieving Cough and Asthma by UPLC-Q-TOF. *Chin. J. Exp. Traditional Med. Formulae* 21 (04), 64–67. doi:10.13422/j.cnki.syfjx.2015040064

Cheng, X. L., Wei, F., Xiao, X. Y., Zhao, Y. Y., Shi, Y., Liu, W., et al. (2012). Identification of Five Gelatins by Ultra Performance Liquid Chromatography/Time-Of-Flight Mass Spectrometry (UPLC/Q-TOF-MS) Using Principal Component Analysis. *J. Pharm. Biomed. Anal.* 62, 191–195. doi:10.1016/j.jpba.2011.12.024

Deng, Z., Jing, W. G., and Liu, A. (2019). Discussion about Application of Thin Layer Chromatography in Current Quality Standard Control. *Chin. J. Exp. Traditional Med. Formulae* 25, 201–206. doi:10.13422/j.cnki.syfjx.20190202

Ding, G., Wang, Y., Liu, A., Hou, Y., Zhang, T., Bai, G., et al. (2017). From Chemical Markers to Quality Markers: An Integrated Approach of UPLC/Q-TOF, NIRS, and Chemometrics for the Quality Assessment of Honeysuckle Buds. *RSC Adv.* 7 (36), 22034–22044. doi:10.1039/C6RA28152D

Du, L.-y., Qian, D.-w., Shang, E.-x., Jiang, S., Liu, P., Guo, J.-m., et al. 2015a). UPLC-MS Based Metabolite Profiles of Two Major Bioactive Components in Herb Pair Scutellaria-Coptis Metabolized by Intestinal Bacteria Derived from Healthy Rats and Rats with Type 2 Diabetes. *Anal. Methods*. 7(13), 5574–5582. doi:10.1039/C5AY00931F

Du, L. Y., Qian, D. W., Shang, E. X., Liu, P., Jiang, S., Guo, J. M., et al. (2015b). UPLC-Q-TOF/MS-Based Screening and Identification of the Main Flavonoids and Their Metabolites in Rat Bile, Urine and Feces After Oral Administration of Scutellaria Baicalensis Extract. *J. Ethnopharmacol.* 169, 156–162. doi:10.1016/j.jep.2015.04.039

Duan, X., Pan, L., Peng, D., Bao, Q., Xiao, L., Zhou, A., et al. (2020). Analysis of the Active Components and Metabolites of Taohong Siwu Decoction by Using Ultra High Performance Liquid Chromatography Quadrupole Time-of-Flight Mass Spectrometry. *J. Sep. Sci.* 43, 4131–4147. doi:10.1002/jssc.202000498

Efferth, T., Zacchino, S., Georgiev, M. I., Liu, L., Wagner, H., and Panossian, A. (2015). Nobel Prize for Artemisinin Brings Phytotherapy into the Spotlight. *Phytomedicine* 22 (13), A1–A3. doi:10.1016/j.phymed.2015.10.003

Feng, G., Chen, Y.-l., Li, W., Li, L.-l., Wu, Z.-g., Wu, Z.-j., et al. (2018). Exploring the Q-Marker of "sweat Soaking Method" Processed Radix Wikstroemia Indica: Based on the "Effect-Toxicity-Chemicals" Study. *Phytomedicine* 45, 49–58. doi:10.1016/j.phymed.2018.03.063

Fu, X. L., Zhou, J., Tang, W. W., Liu, Y., Li, Z. L., Li, P., et al. (2021). Study on the Compatibility Effect and Active Constituents of Atractylodis Rhizoma in Ermiao Wan Against Acute Gouty Arthritis. *J. Ethnopharmacol.* 279, 114353. doi:10.1016/j.jep.2021.114353

Gao, S., Liu, J., Wang, M., Liu, Y., Meng, X., Zhang, T., et al. (2019). Exploring on the Bioactive Markers of Codonopsis Radix by Correlation Analysis Between Chemical Constituents and Pharmacological Effects. *J. Ethnopharmacol.* 236, 31–41. doi:10.1016/j.jep.2019.02.032

Guo, X. H., Cheng, X. L., Liu, W. X., Li, M. H., Wei, F., and Ma, S. C. (2019). Identification of Velvet Antler and its Mixed Varieties by UPLC-QTOF-MS Combined with Principal Component Analysis. *J. Pharm. Biomed. Anal.* 165, 18–23. doi:10.1016/j.jpba.2018.10.009

Han, L., Wang, P., Wang, Y., Zhao, Q., Zheng, F., Dou, Z., et al. (2019). Rapid Discovery of the Potential Toxic Compounds in Polygonum Multiflorum by UHPLC/Q-Orbitrap-MS-Based Metabolomics and Correlation Analysis. *Front. Pharmacol.* 10, 329. doi:10.3389/fphar.2019.00329

Han, X. Y., Peng, B., Wang, H., Zhang, C., and Zeng, Z. P. (2016). UPLC/Q-TOF-MS-Based Chemical Profiling Approach in Studying the Effects of Amic Solution Hydrolysis on Extraction of Radix Astragali. *World Chin. Med.* 11 (03), 523–528+532. doi:10.3969/j.issn.1673-7202.2016.03.040

He, X., Wang, X., Fang, J., Zhao, Z., Huang, L., Guo, H., et al. (2017). Bletilla Striata: Medicinal Uses, Phytochemistry and Pharmacological Activities. *J. Ethnopharmacol.* 195, 20–38. doi:10.1016/j.jep.2016.11.026

Hu, Y. F., Pei, Y. M., Wu, H., Xu, Q., Xu, G. B., Jiang, L., et al. (2016). Difference Analysis of Chemical Compositions in Moutan Cortex from Different Origins by UPLC-Q-TOF-MS. *Chin. Traditional Herb. Drugs* 47, 2984–2992. doi:10.7501/j.issn.0253-2670.2016.17.005

Huang, X. F., OuYang, H., Li, J. M., Lu, Y. J., Li, W., and Gong, Q. F. (2017). Identification of Characteristic Constituents in Atractylodis Macrocephalae Rhizoma from Different Regions by UPLC-Q-TOF-MS/MS. *Chin. J. Exp. Traditional Med. Formulae* 23, 27–33. doi:10.13422/j.cnki.syfjx.201720027

Jeong, W. T., and Lim, H. B. (2018). A UPLC-ESI-Q-TOF Method for Rapid and Reliable Identification and Quantification of Major Indole Alkaloids in Catharanthus Roseus. *J. Chromatogr. B Anal. Technol. Biomed. Life Sci.* 1080, 27–36. doi:10.1016/j.jchromb.2018.02.018

Jiao, Y., Wang, B., Zhou, Q. Q., Hang, B. J., and Lin, Y. Q. (2019). Petection of Equine-Hide Gelatin in Ejiao by UPLC-MS. *Chin. J. Pharm. Anal.* 39 (5), 864–869. doi:10.16155/j.0254-1793.2019.05.14

Jin, M. M., Zhang, W. D., Jiang, H. H., Du, Y. F., Guo, W., Cao, L., et al. (2018). UPLC-Q-TOF-MS/MS-Guided Dereplication of Pulsatilla Chinensis to Identify Triterpenoid Saponins. *Phytochem. Anal.* 29 (5), 516–527. doi:10.1002/pca.2762

Khan, H., and Ali, J. (2015). UHPLC/Q-ToF-MS Technique: Introduction and Applications. *Loc* 12 (6), 371–378. doi:10.2174/1570178612666150331204147

Kim, N. S., Kim, J., Lim, N. Y., Lee, J. H., Park, S., and Kang, H. (2020). Simultaneous Determination of Illegal Drug Substances in Dietary Supplements for Gout and Osteoporosis Using Ultra-Performance Liquid Chromatography and Liquid Chromatography-Quadrupole-Time-Of-Flight Mass Spectrometry. *J. Pharm. Biomed. Anal.* 179, 113003. doi:10.1016/j.jpba.2019.113003

Kresge, G. A., Grosse, S., Zimmer, A., Grinias, K. M., De Pra, M., Wong, J. T., et al. 2020). Strategies in Developing High-Throughput Liquid Chromatography Protocols for Method Qualification of Pharmacopeial Monographs. *J. Sep. Sci.* 43(15), 2964–2970. doi:10.1002/jssc.202000403

Leong, F., Hua, X., Wang, M., Chen, T., Song, Y., Tu, P., et al. (2020). Quality Standard of Traditional Chinese Medicines: Comparison between European Pharmacopoeia and Chinese Pharmacopoeia and Recent Advances. *Chin. Med.* 15(1), 76–20. doi:10.1186/s13020-020-00357-3

Li, H. B., Jiang, Y., and Chen, F. (2004). Separation Methods Used for Scutellaria Baicalensis Active Components. *J. Chromatogr. B Anal. Technol. Biomed. Life Sci.* 812, 277–290. doi:10.1016/j.jchromb.2004.06.045

Li, L., Wang, Y., and Liu, S. (2020c). Application of Pseudotargeted Method Combined with Multivariate Statistical Analysis for the Quality Assessment of Traditional Chinese Medicine Preparation, Sanhuang Tablet as a Case. *Anal. Bioanal. Chem.* 412(23), 5863–5872.doi:10.1007/s00216-020-02813-3

Li, L., Yang, N., Nin, L., Zhao, Z., Chen, L., Yu, J., et al. (2015). Chinese Herbal Medicine Formula Tao Hong Si Wu Decoction Protects Against Cerebral Ischemia-Reperfusion Injury via PI3K/Akt and the Nrf2 Signaling Pathway. *J. Nat. Med.* 69 (1), 76–85. doi:10.1007/s11418-014-0865-5

Li, M. Y., Sun, E., Xu, F. J., Xu, J. D., and Jia, X. B. (2020a). Analysis Changes of Epimedii Folium's Flavonoids Before and After Processing Based on UPLC-Q/TOF-MS. *Chin. Traditional Herb. Drugs* 51 (11), 2900–2907. doi:10.7501/j.issn.0253-2670.2020.11.007

Li, N., Xie, L., Yang, N., Sun, G., Liu, H., Bi, C., et al. (2020b). Rapid Classification and Identification of Chemical Constituents in Epimedium Koreanum Nakai by UPLC-Q-TOF-MS Combined with Data Post-Processing Techniques. *Phytochem. Anal.* 32 (4), 575–591. doi:10.1002/pca.3007

Li, Q., Guan, H., Wang, X., He, Y., Sun, H., Tan, W., et al. (2017). Fingerprint-Efficacy Study of the Quaternary Alkaloids in Corydalis Yanhusuo. *J. Ethnopharmacol.* 207, 108–117. doi:10.1016/j.jep.2017.06.036

Li, R., Wei, M., Guo, G., Li, Y., Pan, X., Song, X., et al. (2021). Analysis of Main Components in Jujube and Mulberry Extracts by High-Sensitive HPLC-ESI-Q-TOF-MS/MS. *J. Chromatogr. Sci.* 59 (9), 806–812. doi:10.1093/chromsci/bmaa133

Li, S. P., Zhao, J., and Yang, B. (2011). Strategies for Quality Control of Chinese Medicines. *J. Pharm. Biomed. Anal.* 55 (4), 802–809. doi:10.1016/j.jpba.2010.12.011

Li, Y., Zhang, T., Zhang, X., Xu, H., and Liu, C. (2010). Chemical Fingerprint Analysis of Phellodendri Amurensis Cortex by Ultra Performance LC/Q-TOF-MS Methods Combined with Chemometrics. *J. Sep. Sci.* 33 (21), 3347–3353. doi:10.1002/jssc.201000426

Liang, G., Yang, J., Liu, T., Wang, S., Wen, Y., Han, C., et al. (2021). A Multi-Strategy Platform for Quality Control and Q-Markers Screen of Chaiqin Chengqi Decoction. *Phytomedicine* 85, 153525. doi:10.1016/j.phymed.2021.153525

Liao, H., Ye, J., Gao, L., and Liu, Y. (2021). The Main Bioactive Compounds of Scutellaria Baicalensis Georgi. For Alleviation of Inflammatory Cytokines: A Comprehensive Review. *Biomed. Pharmacother.* 133, 110917. doi:10.1016/j.biopha.2020.110917

Lin, L. F., Ni, B., Lin, H., Zhang, M., Yan, L., Qu, C., et al. (2015). Simultaneous Determination of 14 Constituents of Radix Polygoni Multiflori from Different Geographical Areas by Liquid Chromatography-Tandem Mass Spectrometry. *Biomed. Chromatogr.* 29, 1048–1055. doi:10.11669/cpj.2015.12.01310.1002/bmc.3391

Lippert, J. A., Xin, B., Wu, N., and Lee, M. L. (1999). Fast Ultrahigh-Pressure Liquid Chromatography: On-Column UV and Time-Of-Flight Mass Spectrometric Detection. *J. Micro. Sep.* 11 (9), 631–643. doi:10.1002/(SICI)1520-667X(199911)11:93.0.CO;2-I10.1002/(sici)1520-667x(199911)11:9<631:aid-mcs1>3.0.co;2-i

Liu, Y., Wei, M., Yue, K., Wang, R., Ma, Y., Men, L., et al. (2019b). Non-Target Metabonomic Method Provided New Insights on the Therapeutical Mechanism of Gancao Fuzi Decoction on Rheumatoid Arthritis Rats. *J. Chromatogr. B Anal. Technol. Biomed. Life Sci.* 1105, 93–103. doi:10.1016/j.jchromb.2018.11.015

Liu, Y., Yang, J., and Cai, Z. (2006). Chemical Investigation on Sijunzi Decoction and its Two Major Herbs Panax Ginseng and Glycyrrhiza Uralensis by LC/MS/MS. *J. Pharm. Biomed. Anal.* 41 (5), 1642–1647. doi:10.1016/j.jpba.2006.02.033

Liu, C. X., Chen, S. L., Xiao, X. H., Zhang, T. J., Hou, W. B., and Liao, M. L. (2016). A New Concept on Quality Marker of Chinese Materia Medica: Quality Control for Chinese Medicinal Products. *Chin. Traditional Herb. Drugs*, 1443–1457. doi:10.7501/j.issn.0253-2670.2016.09.001

Liu, X. Y., Jiang, W. W., Jiang, H. Q., Su, M., Sun, Y., Zang, H. C., et al. (2019a). Preliminary Discovery of Quality Marker (Q-Marker) of Shenzhiling Oral Liquid Based on "Fingerprint-Efficacy-Pharmacokinetics" Correlation. *Chin. Traditional Herb. Drugs* 50, 4603–4612. doi:10.7501/j.issn.0253-2670.2019.19.012

Lv, X. J., Sun, Z., Wang, P. L., Yang, J., Xu, T. Y., Jia, Q. Q., et al. (2018). Chemical Profiling and Quantification of Dan-Deng-Tong-Nao-Capsule Using Ultra High Performance Liquid Chromatography Coupled with High Resolution Hybrid Quadruple-Orbitrap Mass Spectrometry. *J. Pharm. Biomed. Anal.* 148, 189–204. doi:10.1016/j.jpba.2017.09.034

Ma, Q., Li, P. L., Hua, Y. L., Ji, P., Yao, W. L., Zhang, X. S., et al. (2018). Effects of Tao-Hong-Si-Wu Decoction on Acute Blood Stasis in Rats Based on a LC-Q/TOF-MS Metabolomics and Network Approach. *Biomed. Chromatogr.* 32 (4), e4144. doi:10.1002/bmc.4144

Nie, H. L., Zhang, D. L., Nie, L., Zang, H. C., and Zeng, Y. Z. (2016). HPLC Fingerprint Study and Quality Evaluation of Shenzhiling Oral Solution. *J. Pharmaceutical Res.* 35 (07), 386–389. doi:10.13506/j.cnki.jpr.2016.07.005

Nie, X., Cheng, Y. F., Wang, L., Fu, C. M., He, Y., and Zhang, J. M. (2020). Review of Chemical Constituents, Pharmacological Effects and Clinical Applications of Taohong Siwutang and Predictive Analysis of its Quality Marke. *Chin. J. Exp. Traditional Med. Formula* 26 (04), 226–234. doi:10.13422/j.cnki.syfjx.20191953

Niessen, W. M. (1999). State-of-the-Art in Liquid Chromatography-Mass Spectrometry. *J. Chromatogr. A* 856 (1-2), 179–197. doi:10.1016/S0021-9673(99)00480-X

Ojemann, L. M., Nelson, W. L., Shin, D. S., Rowe, A. O., and Buchanan, R. A. (2006). Tian Ma, an Ancient Chinese Herb, Offers New Options for the Treatment of Epilepsy and Other Conditions. *Epilepsy Behav.* 8 (2), 376–383. doi:10.1016/j.yebeh.2005.12.009

Peng, Y. W., Shen, L. H., Wang, L., Jin, J., and Yang, M. Z. (2015). Detection of Oxytetracycline, Chlorpheniramine Maleate and Prednisone Acetate in Two Chinese Traditional Patent Medicines by UPLC/Q-TOF-MS. *Chin. Tradit. Pat. Med.* 37 (09), 1959–1964. doi:10.3969/j.issn.1001-1528.2015.09.019

Pilepić, K. H., Yang, Z., Chen, J., Chen, X., Wang, Y., Zhao, J., et al. (2018). Flavonoids in Natural and Tissue Cultured Materials of Epimedium Alpinum Identified by Using UHPLC-Q-TOF-MS/MS. *Int. J. Mass Spectrom.* 434, 222–232.

Qin, W. H., Hua, L., Guo, Y. L., Wang, Y. H., Ran, J. C., and Yang, Y. (2018). Differentiation of Different Parts of Cordyceps Sinensis Based on UPLC- Q-TOF- MS Combined with Metabolomics Methods. *Chin. J. Exp. Traditional Med. Formulae* 24 (21), 69–76. doi:10.13422/j.cnki.syfjx.20181910

Ren, J. L., Zhang, A. H., Kong, L., Han, Y., Yan, G. L., Sun, H., et al. (2020). Analytical Strategies for the Discovery and Validation of Quality-Markers of Traditional Chinese Medicine. *Phytomedicine* 67, 153165. doi:10.1016/j.phymed.2019.153165

Rui, W., Xia, W., Zhao, W., Li, B., Li, J., Feng, Y., et al. (2020). Differential Constituents in Roots, Stems and Leaves of Polygonum Multiflorum Thunb. Screened by UPLC/ESI-Q-TOF-MS and Multivariate Statistical Analysis. *J. Chromatogr. Sci.* 58 (2), 136–143. doi:10.1093/chromsci/bmz086

Sang, Q., Jia, Q., Zhang, H., Lin, C., Zhao, X., Zhang, M., et al. (2020). Chemical Profiling and Quality Evaluation of Zhishi-Xiebai-Guizhi Decoction by UPLC-Q-TOF-MS and UPLC Fingerprint. *J. Pharm. Biomed. Anal.* 194, 113771. doi:10.1016/j.jpba.2020.113771

Shan, B., Chen, T., Huang, B., Liu, Y., and Chen, J. (2021). Untargeted Metabolomics Reveal the Therapeutic Effects of Ermiao Wan Categorized Formulas on Rats with Hyperuricemia. *J. Ethnopharmacol.* 281, 114545. doi:10.1016/j.jep.2021.114545

Shan, L., Yang, N., Zhao, Y., Sheng, X., Yang, S., and Li, Y. (2018). A Rapid Classification and Identification Method Applied to the Analysis of Glycosides in Bupleuri Radix and Liquorice by Ultra High Performance Liquid Chromatography Coupled with Quadrupole Time-Of-Flight Mass Spectrometry. *J. Sep. Sci.* 41 (19), 3791–3805. doi:10.1002/jssc.201800619

Shen, L. H., Peng, Y. W., and Chen, G. Q. (2016). Rapid Detection of Phenformin Hydrochloride, Glibenclamide and Pioglitazone Hydrochloride Illegally Mixed in Traditional Chinese Medicinal Preparation for Antidiabetics by UPLC-Q-TOF-MS. *Chin. J. Mod. Appl. Pharm.* 33 (09), 1160–1165. doi:10.13748/j.cnki.issn1007-7693.2016.09.016

Shi, S., Wu, Y., Zhou, M., and Cheng, Q. (2020). Simultaneous Analysis of 31 Anti-impotence Compounds Potentially Illegally Added to Herbal-Based Dietary Supplements by Ultra-High-Performance Liquid Chromatography Coupled with Quadrupole Time-Of-Flight Mass Spectrometry. *J. Chromatogr. B Anal. Technol. Biomed. Life Sci.* 1144, 122077. doi:10.1016/j.jchromb.2020.122077

Siddiqui, M. R., AlOthman, Z. A., and Rahman, N. (2017). Analytical Techniques in Pharmaceutical Analysis: A Review. *Arabian J. Chem.* 10, S1409–S1421. doi:10.1016/j.arabjc.2013.04.016

Sui, Z., Zhang, L., Huo, Y., and Zhang, Y. (2014). Bioactive Components of Velvet Antlers and Their Pharmacological Properties. *J. Pharm. Biomed. Anal.* 87, 229–240. doi:10.1016/j.jpba.2013.07.044

Tan, M., Chen, J., Wang, C., Zou, L., Chen, S., Shi, J., et al. (2019). Quality Evaluation of Ophiopogonis Radix from Two Different Producing Areas. *Molecules* 24 (18), 3220. doi:10.3390/molecules24183220

Tan, X. M., Li, Q., Wang, Y. D., Wang, T. L., Yang, J., Sun, B. D., et al. (2021). UPLC-Q-TOF-MS/MS Analysis of the Guaiane Sesquiterpenoids Oxytropiols A-J and Detection of Undescribed Analogues from the Locoweed Endophytic Fungus Alternaria Oxytropis (Pleosporaceae). *Phytochem. Anal.* 33, 344–354. doi:10.1002/pca.3092

Tang, C., Wang, L., Liu, X., Cheng, M., and Xiao, H. (2016). Chemical Fingerprint and Metabolic Profile Analysis of Ethyl Acetate Fraction of Gastrodia Elata by Ultra Performance Liquid Chromatography/quadrupole-Time of Flight Mass Spectrometry. *J. Chromatogr. B Anal. Technol. Biomed. Life Sci.* 1011, 233–239. doi:10.1016/j.jchromb.2015.09.043

The State Pharmacopoeia Commission (2020). *The People's Republic of China Pharmacopoeia*. Beijing: Chinese Medicine Science and Technology Press, 336–337.

Tu, Y. (2016). Artemisinin-a Gift from Traditional Chinese Medicine to the World (Nobel Lecture). *Angew. Chem. Int. Ed. Engl.* 55 (35), 10210–10226. doi:10.1002/anie.201601967

Vaclavik, L., Krynitsky, A. J., and Rader, J. I. (2014). Targeted Analysis of Multiple Pharmaceuticals, Plant Toxins and Other Secondary Metabolites in Herbal Dietary Supplements by Ultra-High Performance Liquid Chromatography-Quadrupole-Orbital Ion Trap Mass Spectrometry. *Anal. Chim. Acta* 810, 45–60. doi:10.1016/j.aca.2013.12.006

Wang, G. Y., Shang, J., Wu, Y., Ding, G., and Xiao, W. (2017b). Rapid Characterization of the Major Chemical Constituents from Polygoni Multiflori Caulis by Liquid Chromatography Tandem Mass Spectrometry and Comparative Analysis with Polygoni Multiflori Radix. *J. Sep. Sci.* 40 (10), 2107–2116. doi:10.1002/jssc.201601255

Wang, H. Y., Wang, C., Guo, S. C., Chen, Z. C., Peng, Z. T., Duan, R., et al. (2019). Polysaccharide Deriving from Ophiopogonis Radix Promotes Metabolism of Ginsenosides in the Present of Human Gut Microbiota Based on UPLC-MS/MS Assay. *J. Pharm. Biomed. Anal.* 175, 112779. doi:10.1016/j.jpba.2019.112779

Wang, J., Wong, Y. K., and Liao, F. (2018b). What Has Traditional Chinese Medicine Delivered for Modern Medicine? *Expert Rev. Mol. Med.* 20, e4. doi:10.1017/erm.2018.3

Wang, L., Sang, M., Liu, E., Banahene, P. O., Zhang, Y., Wang, T., et al. (2017a). Rapid Profiling and Pharmacokinetic Studies of Major Compounds in Crude Extract from Polygonum Multiflorum by UHPLC-Q-TOF-MS and UPLC-MS/MS. *J. Pharm. Biomed. Anal.* 140, 45–61. doi:10.1016/j.jpba.2017.03.016

Wang, R., Qin, Y., Zhou, J., Wang, J., Shu, H., Zhou, S., et al. (2022). Comprehensive Evaluation of Bletilla Striata and its Substitutes by Combining Phenotypic Characteristic, Chemical Composition, and Anti-Melanogenic Activity. *Phytochemistry* 195, 113059. doi:10.1016/j.phytochem.2021.113059

Wang, X., Qin, Y., Li, G. Q., Chen, S., Ma, J. Q., Guo, Y. L., et al. (2018a). Study on Chemical Constituents in Polygoni Cuspidati Folium and its Preparation by UPLC-ESI-Q-TOF-MS/MS. *J. Chromatogr. Sci.* 56 (5), 425–435. doi:10.1093/chromsci/bmy017

Wang, X. B., Zheng, J., Li, J. J., Yu, H. Y., Li, Q. Y., Xu, L. H., et al. (2018c). Simultaneous Analysis of 23 Illegal Adulterated Aphrodisiac Chemical Ingredients in Health Foods and Chinese Traditional Patent Medicines by Ultrahigh Performance Liquid Chromatography Coupled with Quadrupole Time-Of-Flight Mass Spectrometry. *J. Food Drug Anal.* 26 (3), 1138–1153. doi:10.1016/j.jfda.2018.02.003

Wang, Y., Guo, Z., Jin, Y., Zhang, X., Wang, L., Xue, X., et al. (2010). Identification of Prenyl Flavonoid Glycosides and Phenolic Acids in Epimedium Koreanum Nakai by Q-TOF-MS Combined with Selective Enrichment on "click Oligo (Ethylene Glycol)" Column. *J. Pharm. Biomed. Anal.* 51 (3), 606–616. doi:10.1016/j.jpba.2009.09.033

Wang, Y., He, S., Cheng, X., Lu, Y., Zou, Y., and Zhang, Q. (2013a). UPLC-Q-TOF-MS/MS Fingerprinting of Traditional Chinese Formula SiJunZiTang. *J. Pharm. Biomed. Anal.* 80, 24–33. doi:10.1016/j.jpba.2013.02.021

Wang, Y., Yuan, L., Li, Y. B., and Zhang, Y. J. (2017c). Analysis on Chemical Constituents of Epimedii Folium by UPLC-Q-TOF-MS. *Chin. Traditional Herb. Drugs*, 2625–2631. doi:10.7501/j.issn.0253-2670.2017.13.007

Wang, Z., Li, N., Wang, M., Wang, Y., Du, L., Ji, X., et al. (2013b). Simultaneous Determination of Nucleosides and Their Bases in Cordyceps Sinensis and its Substitutes by Matrix Solid-Phase Dispersion Extraction and HPLC. *J. Sep. Sci.* 36 (14), 2348–2357. doi:10.1002/jssc.201300204

Wei, L., Wang, X., Mu, S., Sun, L., and Yu, Z. (2015b). Ultra High Performance Liquid Chromatography with Electrospray Ionization Tandem Mass Spectrometry Coupled with Hierarchical Cluster Analysis to Evaluate Wikstroemia Indica (L.) C. A. Mey. From Different Geographical Regions. *J. Sep. Sci.* 38 (12), 2093–2100. doi:10.1002/jssc.201401398

Wei, W. L., and Huang, L. F. (2015a). Simultaneous Determination of Ferulic Acid and Phthalides of Angelica Sinensis Based on UPLC-Q-TOF/MS. *Molecules* 20 (3), 4681–4694. doi:10.3390/molecules20034681

Wen, B. Y., Yan, Y., Wang, W. B., and Wang, Z. R. (2017). Pharmacokinetics of Effective Components after Oral Administration of Poria Triterpenoids Extract with Different Forms in Rats. *Chin. J. Exp. Traditional Med. Formula* 23, 97–101. doi:10.13422/j.cnki.syfjx.2017070097

Xia, M.-C., Cai, L., Xu, F., Zhan, Q., Feng, J., Guo, C., et al. (2022). Whole-Body Chemical Imaging of Cordyceps Sinensis by TOF-SIMS to Visualize Spatial Differentiation of Ergosterol and Other Active Components. *Microchem. J.* 177, 107303. doi:10.1016/j.microc.2022.107303

Xia, W., Hu, S., Wang, M., Xu, F., Han, L., and Peng, D. (2021). Exploration of the Potential Mechanism of the Tao Hong Si Wu Decoction for the Treatment of Postpartum Blood Stasis Based on Network Pharmacology and *In Vivo* Experimental Verification. *J. Ethnopharmacol.* 268, 113641. doi:10.1016/j.jep.2020.113641

Xu, J., Liu, J., Li, B., Wei, X., Qi, Y., Zhang, B., et al. (2022). Comparison of Blood Tonic Efficacy and Chemical Constituents of Kadsura Interior A.C. Smith and its Closely Related Species. *Chin. Med.* 17 (1), 14. doi:10.1186/s13020-021-00544-w

Yan, G., Zou, D., Zhang, A., Tan, Y., Sun, H., and Wang, X. (2015). UPLC-Q-TOF-MS/MS Fingerprinting for Rapid Identification of the Chemical Constituents of Ermiao Wan. *Anal. Methods* 7 (3), 846–862. doi:10.1039/C4AY01215A

Yan, Q., Mao, H., and Wei, Y. (2017). Elucidation of Mechanism of Si-Jun-Zi Decoction-Induced Reversal of Spleen Deficiency Syndrome in Rats by LC-QTOF/MS Metabolomics. *Trop. J. Pharm. Res.* 16 (3), 525–533. doi:10.4314/tjpr.v16i3.5

Yang, B., Li, H., Ruan, Q. F., Xue, Y. Y., Cao, D., Zhou, X. H., et al. (2018). A Facile and Selective Approach to the Qualitative and Quantitative Analysis of Triterpenoids and Phenylpropanoids by UPLC/Q-TOF-MS/MS for the Quality Control of Ilex Rotunda. *J. Pharm. Biomed. Anal.* 157, 44–58. doi:10.1016/j.jpba.2018.05.002

Yang, B., Dong, H., Sun, H., Han, Y., Zhang, A. H., Yan, G. L., et al. (2019c). Urine Metabolomics Analysis of Toxicity Attenuation Effects of Fuzi Compatibility with Gancao. *Mod. Chin. Med.* 21 (07), 895–902. doi:10.13313/j.issn.1673-4890.20190702005

Yang, C., Xia, T., Wang, C., Sun, H., Li, Y., Gong, Z., et al. (2019b). Using the UPLC-ESI-Q-TOF-MSE Method and Intestinal Bacteria for Metabolite Identification in the Nonpolysaccharide Fraction from Bletilla Striata. *Biomed. Chromatogr.* 33 (11), e4637. doi:10.1002/bmc.4637

Yang, J. B., Liu, Y., Wang, Q., Ma, S. C., Wang, A. G., Cheng, X. L., et al. (2019a). Characterization and Identification of the Chemical Constituents of Polygonum Multiflorum Thunb. By High-Performance Liquid Chromatography Coupled with Ultraviolet Detection and Linear Ion Trap FT-ICR Hybrid Mass Spectrometry. *J. Pharm. Biomed. Anal.* 172, 149–166. doi:10.1016/j.jpba.2019.03.049

Yang, M., Zhao, Y., Qin, Y., Xu, R., Yang, Z., and Peng, H. (2021b). Untargeted Metabolomics and Targeted Quantitative Analysis of Temporal and Spatial Variations in Specialized Metabolites Accumulation in Poria Cocos (Schw.) Wolf (Fushen). *Front. Plant Sci.* 12, 713490. doi:10.3389/fpls.2021.713490

Yang, S., Shan, L., Luo, H., Sheng, X., Du, J., and Li, Y. (2017a). Rapid Classification and Identification of Chemical Components of Schisandra Chinensis by Uplc-Q-Tof/ms Combined with Data Post-Processing. *Molecules* 22 (10), 1778–1796. doi:10.3390/molecules22101778

Yang, Z., Jiang, M., Yue, Z., Wang, P., Wang, H., Zhang, G., et al. (2021a). Metabonomics Analysis of Semen Euphorbiae and Semen Euphorbiae Pulveratum Using UPLC-Q-Tof/MS. *Biomed. Chromatogr.* 36, e5279. doi:10.1002/bmc.5279

Yang, Z. L., and Zhao, J. (2017b). Qualitative and Quantitative Analysis of Icariin Analogues in Epimedium Koreanum by UPLC-Q-TOF MS. *J. Chin. Mass Spectrom. Soc.* 38 (1), 19–29. doi:10.7538/zpxb.2017.38.01.0019

Yuan, Q., Xie, F., Tan, J., Yuan, Y., Mei, H., Zheng, Y., et al. (2022). Extraction, Structure and Pharmacological Effects of the Polysaccharides from Cordyceps Sinensis: A Review. *J. Funct. Foods* 89, 104909. doi:10.1016/j.jff.2021.104909

Yuan, R., and Lin, Y. (2000). Traditional Chinese Medicine: An Approach to Scientific Proof and Clinical Validation. *Pharmacol. Ther.* 86 (2), 191–198. doi:10.1016/S0163-7258(00)00039-5

Yuan, T., Guo, X.-F., Shao, S.-Y., An, R.-M., Wang, J., and Sun, J. 2021). Characterization and Identification of Flavonoids from Bambusa Chungii Leaves Extract by UPLC-ESI-Q-TOF-MS/MS. *Acta Chromatogr.* 33(3), 281–294. doi:10.1556/1326.2020.00777

Zhang, A., Sun, H., Qiu, S., and Wang, X. (2013). Advancing Drug Discovery and Development from Active Constituents of Yinchenhao Tang, a Famous Traditional Chinese Medicine Formula. *Evid. Based Complement. Altern. Med.* 2013, 257909. doi:10.1155/2013/257909

Zhang, B., Yu, D., Luo, N., Yang, C., and Zhu, Y. (2020). Four Active Monomers from Moutan Cortex Exert Inhibitory Effects against Oxidative Stress by Activating Nrf2/Keap1 Signaling Pathway. *Korean J. Physiol. Pharmacol.* 24 (5), 373–384. doi:10.4196/kjpp.2020.24.5.373

Zhang, F., Zhan, Q., Gao, S., Dong, X., Jiang, B., Sun, L., et al. (2014). Chemical Profile- and Pharmacokinetics-Based Investigation of the Synergistic Property of Platycodonis Radix in Traditional Chinese Medicine Formula Shengxian Decoction. *J. Ethnopharmacol.* 152 (3), 497–507. doi:10.1016/j.jep.2014.01.033

Zhang, X., Li, P., Hua, Y., Ji, P., Yao, W., Ma, Q., et al. (2018). Urinary Metabolomics Study the Mechanism of Taohong Siwu Decoction Intervention in Acute Blood Stasis Model Rats Based on Liquid Chromatography Coupled to Quadrupole Time-Of-Flight Mass Spectrometry. *J. Chromatogr. B Anal. Technol. Biomed. Life Sci.* 1074-1075, 51–60. doi:10.1016/j.jchromb.2017.12.035

Zhang, Y., Feng, B. M., and Lv, X. (2017). Research Progress on Application of UPLC/Q-TOF-MS in Pharmaceutical Analysis. *Nat. Prod. Res. Dev.* 29 (11), 1992–1996. doi:10.16333/j.1001-6880.2017.11.028

Zhao, Q. L., Bian, X. K., Qian, D. W., Zhang, T., Zhu, Z. H., Guo, S., et al. (2019b). Comparative Study on Differences of Paeonia Lactiflora from Different Habitats Based on Fingerprint and Chemometrics. *Zhongguo Zhong Yao Za Zhi* 44 (15), 3316–3322. doi:10.19540/j.cnki.cjcmm.20190424.202

Zhao, T., Tang, H., Xie, L., Zheng, Y., Ma, Z., Sun, Q., et al. (2019a2019). Scutellaria Baicalensis Georgi. (Lamiaceae): a Review of its Traditional Uses, Botany, Phytochemistry, Pharmacology and Toxicology. *J. Pharm. Pharmacol.* 71, 1353–1369. doi:10.1111/jphp.13129

Zhu, F., Ruan, L., Ma, Y., Ji, W., and Liu, H. (2014). Simultaneous Determination of 20 Illegally Added Anti-Diabetic Chemical Components in Hypoglycemic and Weight-Reducing Health Foods by Ultra-high Performance Liquid Chromatography-Tandem Mass Spectrometry]. *Se Pu* 32 (1), 13–20. doi:10.3724/sp.j.1123.2013.08035

Zhu, S. S., Long, R., Song, T., Zhang, L., Dai, Y. L., Liu, S. W., et al. (2019). UPLC-Q-TOF/MS Based Metabolomics Approach to Study the Hepatotoxicity of Cantharidin on Mice. *Chem. Res. Toxicol.* 32 (11), 2204–2213. doi:10.1021/acs.chemrestox.9b00233

Zong, X. X., Wang, Y., Xiong, J. L., Ping, Y. H., and Liang, Q. L. (2022). Characterization of Alkaloids in Radix Sophora Tonkinensis by UPLC-Q-TOF-MS/MS and its Application in the Comparison of Two Different Habitats. *Nat. Prod. Res.* 36 (1), 429–431. doi:10.1080/14786419.2020.1771712

Conflict of Interest: The authors declare that the research was conducted in the absence of any commercial or financial relationships that could be construed as a potential conflict of interest.

frontiers | Frontiers in Pharmacology

ORIGINAL RESEARCH
published: 16 June 2022
doi: 10.3389/fphar.2022.934710

Changes of Physicochemical Properties and Immunomodulatory Activity of Polysaccharides During Processing of *Polygonum multiflorum* Thunb

*Donglin Gu[1,2], Ying Wang[1†], Hongyu Jin[1], Shuai Kang[1], Yue Liu[3], Ke Zan[1], Jing Fan[1], Feng Wei[1] and Shuangcheng Ma[1]**

[1]Institute for Control of Chinese Traditional Medicine and Ethnic Medicine, National Institutes for Food and Drug Control, Beijing, China, [2]School of Traditional Chinese Pharmacy, China Pharmaceutical University, Nanjing, China, [3]School of Traditional Chinese Medicine, Beijing University of Chinese Medicine, Beijing, China

OPEN ACCESS

Edited by:
Wei Cai,
Hunan University of Medicine, China

Reviewed by:
Liqin Ding,
Tianjin University of Traditional Chinese Medicine, China
Tingting Zhou,
Second Military Medical University, China

***Correspondence:**
Shuangcheng Ma
masc@nifdc.org.cn

†These authors have contributed equally to this work and share first authorship

Specialty section:
This article was submitted to Experimental Pharmacology and Drug Discovery, a section of the journal Frontiers in Pharmacology

Received: 03 May 2022
Accepted: 30 May 2022
Published: 16 June 2022

Citation:
Gu D, Wang Y, Jin H, Kang S, Liu Y, Zan K, Fan J, Wei F and Ma S (2022) Changes of Physicochemical Properties and Immunomodulatory Activity of Polysaccharides During Processing of Polygonum multiflorum Thunb. Front. Pharmacol. 13:934710. doi: 10.3389/fphar.2022.934710

The roots of *Polygonum multiflorum* Thunb (PM) have a long history of usage in traditional Chinese medicine and are still widely utilized today. PM in raw or processed form has different biological activities and is commonly used to treat different diseases. Polysaccharides are the main component of PM, and it is unclear whether their physicochemical properties and activities change after processing. In this study, the polysaccharides from thirty-one raw PM (RPMPs) and nine processed PM (PPMPs) were extracted, and the physicochemical properties and immunomodulatory activity *in vitro* of polysaccharide samples were evaluated. Results showed that RPMPs and PPMPs had significant differences in physicochemical properties. RPMPs and PPMPs were both composed of mannose, rhamnose, glucuronic acid, galacturonic acid, glucose, galactose, and arabinose. However, RPMPs and PPMPs had significant differences in their yields, molecular weight (*M*w), and the molar ratio of Glc/GalA ($p < 0.05$), which can be used to distinguish raw and processed PM. The fingerprint of monosaccharide composition was analyzed by chemometrics, and it was further demonstrated that Glc and GalA could be used as differential markers. The immunomodulatory activity assays indicated that RPMPs and PPMPs could significantly enhance phagocytosis and mRNA expression of cytokines in RAW 264.7 cells. In addition, the immunomodulatory activity of PPMPs with lower *M*w was significantly better than that of RPMPs. This study furthers the understanding of the polysaccharides from raw and processed PM and provides a reference for improving the quality standard of PM.

Keywords: ***Polygonum multiflorum*** **Thunb, polysaccharides, processing, fingerprint, immunomodulatory activity**

1 INTRODUCTION

The roots of *Polygonum multiflorum* Thunb (PM) have a long history of use in traditional Chinese medicine (TCM) and are commonly used in raw or processed form to treat different diseases (Chen et al., 2021). Studies have shown that PM mainly contains anthraquinones, stilbene glycosides, polysaccharides, phospholipids, and so on (Liu et al., 2018). According to TCM theory, raw PM has

detoxifying, anti-swelling, anti-malarial, and laxative properties, while processed PM is effective in tonifying the liver and kidney, strengthening tendons and bones, and darkening hair (Yang et al., 2019). Raw and processed PM are widely used as medicines and health products in China, Japan, and Southeast Asia. In China, the processing methods of PM have been practiced since the Tang dynasty. Currently, there are three processing methods for PM in the 2020 edition of "Chinese pharmacopeia", i.e., stew with black bean juice, steam with black bean juice, and steam with water.

It is widely accepted that there are many differences in chemical composition and efficacy between raw and processed PM (Liang et al., 2010). Since the 1990s, the hepatotoxicity and clinical safety of PM have especially come under scrutiny as reports of adverse liver reactions caused by PM and PM-containing preparations have increased (Park et al., 2001; Mazzanti et al., 2004; Panis et al., 2005; Shaw, 2010; Dong et al., 2015). It has been shown that the hepatotoxicity of PM can be reduced after processing (Yu et al., 2011; Lin et al., 2015). According to the TCM theory, proper pharmaceutical processing methods may reduce toxicity, increase effectiveness, and change the pharmacological effects (Li et al., 2017). Some previous studies have suggested that the changes in stilbene glycosides and anthraquinones during the processing of PM may be related to liver injury.

Polysaccharide is an important component of PM, which has immunomodulatory, anti-tumor, antioxidant, and other activities (Chen et al., 2012; Zhu et al., 2017; Qing Zhang et al., 2018; Luo et al.). In recent years, the structure and activity of polysaccharides from PM have been studied in some reports. For example, the alkali-extractable polysaccharide from raw PM activated splenocytes and peritoneal macrophages, causing significant immunomodulation activity (Qing Zhang et al., 2018). Luo et al. (2011) revealed that polysaccharides from raw PM possessed excellent antioxidant capacity against free radicals, lipid oxidation, and protein glycation. Xu et al. (2014, 2) purified the polysaccharide from raw PM, finding it was composed of rhamnose, arabinose, xylose, and glucose. Qing Zhang et al. (2018) obtained two purified polysaccharides from raw PM and found that acidic polysaccharide WPMP-2 had better immunomodulatory activity than neutral polysaccharide WPMP-1. In addition, they also pointed out that WPMP-2 had a more complex branching structure than WPMP-1 and speculated on the partial structure of WPMP-1 and WPMP-2. However, most of these studies focused on structural characterization and activity determination. Currently, there are no reports on whether polysaccharides change during processing and how this affects the activity, which may advance the study of its liver injury mechanism.

In this study, we collected samples of raw and processed PM from different regions and markets, after which we determined the physicochemical properties (neutral sugar content, uronic acid content, molecular weight, and monosaccharide composition) and immunomodulatory activity *in vitro*. Furthermore, the chemometrics methods were utilized to analyze the data from fingerprints and to effectively assess the differences in polysaccharides from raw and processed PM. These findings could serve as a benchmark for enhancing the quality control of PM and promote the research on the immunomodulatory mechanism of polysaccharides.

2 MATERIALS AND METHODS

2.1 Materials and Reagents

Forty batches of raw PM (1–31) and processed PM (32–40) were collected from different locations and markets in China (**Table 1**). Associate Professor Shuai Kang (National Institute for Food and Drug Control, China) authenticated the samples of PM. Sample 31 was a raw product collected from Henan Province, while sample 39 was a processed product of sample 31 according to the 2020 edition of "Chinese pharmacopeia". Sample 39 was processed as follows: the raw PM was mixed with black bean juice and steamed until it was brown inside and outside, then sliced and dried.

Standards included mannose (Man), rhamnose (Rha), glucuronic acid (GlcA), galacturonic acid (GalA), glucose (Glc), galactose (Gal), and arabinose (Ara), all purchased from the National Institute for Food and Drug Control (China). 1-Phenyl-3-methyl-5-pyrazolone was purchased from Sigma (United States). Trifluoroacetic acid (TFA) was purchased from Oka (China). A Millipore Milli-Q Plus system was used to make deionized water (United States). All the other reagents and chemicals were of analytical grade.

2.2 Preparation of RPMPs and PPMPs

Each sample (5.0 g) was immersed in 100.0 mL of 80% ethanol solution for 1 h at 85°C. After filtration, the dry residues were extracted with water (1:20, m/v) in the bath for 2 h at 100°C. After centrifugation (5,000 rpm for 10 min), the supernatant was evaporated to 10.0 ml on a water bath, following which ethanol (95%, w/v) was added to the final concentration of 80% (v/v) for precipitation and kept overnight (>12 h) under 4°C. The precipitate was then collected by centrifugation and washed with ethanol. The precipitate was freeze-dried to obtain the crude polysaccharides (RPMPs and PPMPs). The yields were calculated according to the weight ratio of the freeze-dried polysaccharide to the dried powder.

2.3 Chemical Composition Determination

The polysaccharides from thirty-one raw PM and nine processed PM were obtained. The neutral sugar content was analyzed by the phenol-sulfuric acid method using Glc as the standard (DuBois et al., 1956). The uronic acid content was determined by a modified carbazole sulfate using GalA as the standard (McCready and McComb, 1953). The protein content was determined by Coomassie Brilliant Blue method using bovine serum albumin (BSA) as the standard (Bradford, 1976).

2.4 Determination of Molecular Weight and Polydispersity Index

The molecular weight (*M*w) and the polydispersity index (*PDI*) of polysaccharide samples were determined by high-performance size exclusion chromatography coupled with multi-angle laser

TABLE 1 | Essential information of the 40 polysaccharide samples.

Codes	Origins	Yields (%)	Neutral sugar content (%)	Uronic acid content (%)	Protein content (%)	*Mw* (kDa)	*Mw*/*Mn*	Peak 2/Peak 1
1	Wenshan, Yunnan	3.46	52.68	6.64	19.67	1,126.10	3.12	3.63
2	Qujin, Yunnan	2.86	51.24	8.96	20.32	1,546.30	3.28	3.88
3	Qujin, Yunnan	2.05	40.39	10.26	13.20	1,011.70	3.49	3.55
4	Qujin, Yunnan	3.98	43.98	7.37	21.92	1,464.70	3.25	3.02
5	Qujin, Yunnan	2.81	43.47	6.29	20.93	1,522.30	3.13	3.02
6	Bozhou, Anhui	4.03	42.63	9.92	25.43	966.70	3.55	4.68
7	Bozhou, Anhui	4.47	43.98	10.38	27.54	646.20	4.10	4.95
8	Bozhou, Anhui	3.86	50.08	9.18	15.56	3,028.30	2.84	2.17
9	Bozhou, Anhui	4.32	48.90	6.53	19.08	1,383.30	3.52	3.48
10	Bozhou, Anhui	4.02	43.76	7.47	20.84	1,273.70	3.10	3.57
11	Bozhou, Anhui	4.16	50.28	7.38	21.52	744.50	3.75	4.10
12	Bozhou, Anhui	4.90	59.34	8.29	18.48	792.00	3.59	4.15
13	Bozhou, Anhui	3.59	43.59	6.02	23.94	986.30	2.93	2.72
14	Bozhou, Anhui	5.58	64.91	6.59	22.54	1,409.40	2.97	2.58
15	Bozhou, Anhui	4.89	51.37	7.22	21.85	1,035.80	3.31	3.17
16	Fuyang, Anhui	5.01	42.89	9.19	22.89	1,096.40	3.46	3.07
17	Fuyang, Anhui	3.65	45.41	15.75	21.29	881.40	3.88	3.72
18	Fuyang, Anhui	3.95	50.04	8.94	14.64	810.00	3.38	4.03
19	Fuyang, Anhui	4.48	42.53	9.43	22.78	890.30	2.96	4.37
20	Gaozhou, Guangdong	3.01	41.75	5.29	17.98	1,045.60	2.81	2.34
21	Gaozhou, Guangdong	3.07	42.56	5.92	14.86	780.40	2.56	2.39
22	Gaozhou, Guangdong	3.97	41.35	6.04	15.83	1,119.30	2.95	2.14
23	Deqin, Guangdong	3.09	40.82	11.88	21.77	601.30	4.00	4.05
24	Deqin, Guangdong	4.22	49.94	9.17	20.88	714.60	3.60	3.29
25	Deqin, Guangdong	4.79	44.69	8.07	22.37	1,047.70	2.77	2.18
26	Dazhou, Sichuan	4.44	41.28	9.70	24.69	985.20	3.04	4.59
27	Dazhou, Sichuan	2.76	44.84	6.37	24.46	1,181.60	3.17	4.10
28	Dazhou, Sichuan	3.19	56.85	10.01	13.29	853.40	3.61	3.70
29	Yibin, Sichuan	3.24	49.03	6.36	13.53	2,115.30	2.59	2.25
30	Yibin, Sichuan	2.30	50.36	8.05	18.44	1,473.90	3.07	2.80
31	Nanyang, Henan	3.66	48.57	7.42	19.02	1,161.70	2.10	3.65
Mean ± SD		3.80 ± 0.83	47.21 ± 5.81	8.26 ± 2.15	20.05 ± 3.76	1,151.46 ± 474.69	3.22 ± 0.44	3.40 ± 0.80
32	Bozhou, Anhui	11.20	65.89	5.64	21.08	736.30	1.91	7.62
33	Bozhou, Anhui	12.84	67.84	6.49	17.84	727.70	1.77	6.25
34	Bozhou, Anhui	11.86	61.96	5.79	21.98	663.90	1.94	6.87
35	Bozhou, Anhui	13.14	63.81	5.48	19.87	802.20	1.84	5.33
36	Bozhou, Anhui	12.02	64.75	6.59	20.14	715.80	1.96	5.90
37	Yulin, Guangxi	11.46	68.75	5.45	18.43	446.80	1.94	12.16
38	Anguo, Hebei	14.08	67.02	6.92	17.88	692.00	1.91	6.09
39	Nanyang, Henan	12.56	69.49	4.29	16.96	341.60	1.89	9.00
40	Yuzhou, Henan	20.73	71.05	5.35	13.05	404.70	1.98	9.53
Mean ± SD		13.32 ± 2.75[a]	66.73 ± 2.74[a]	5.78 ± 0.75[a]	18.58 ± 2.50	614.56 ± 169.89[a]	1.903 ± 0.06[a]	7.64 ± 2.21[a]

[a]$p < 0.05$ *denotes a statistically significant difference compared with RPMPs.*

light scattering and refractive index detector (HPSEC-MALLS-RID). The chromatographic signals were collected by Multi-angle Light Scattering Detectors (MALLS, DAWN HELEOS, Wyatt Technology Co., Santa Barbara, CA, United States) and RI detector (Shimadzu Company, Japan) in series. Each sample (10 mg) was dissolved in the mobile phase (1 ml) and then filtered through a 0.45 μm membrane. Two size exclusion columns Shodex SB-806 (300 mm × 7.8 mm, i. d.), and Shodex SB-804 (300 mm × 7.5 mm, i. d.) were used. The mobile phase included a 0.1 mol/L NaCl aqueous solution applied at a flow rate of 0.5 ml/min. An injection volume of 100 μL was used. Each sample was run for 50 min, and the temperature of the column was maintained at 40°C.

2.5 Monosaccharide Composition Analysis

The monosaccharide compositions of polysaccharide samples were determined by the precolumn derivation UPLC (PCD-UPLC) method. Each sample (1 mg/ml) was hydrolyzed with trifluoroacetic acid (TFA, 4 mol/L) at 120°C for 2 h. Then, TFA was removed by washing with methanol three times. Subsequently, the acid hydrolysates were derivatized with 1-Phenyl-3-methyl-5-pyrazolone (0.5 mol/L) at 70°C for 90 min. The injection volume was 2 μL and the samples were analyzed using a ZORBAX Eclipse XDB-C18 column (100 mm × 2.1 mm, 1.8 μm, Agilent, United States) with UV detection at 250 nm. The mobile phase consisting of acetonitrile and 0.125 mol/L KH_2PO_4 (v/v = 16:84, pH 6.9) was used at a flow rate of 0.3 ml/min.

2.6 *In vitro* Experiments

2.6.1 Cell Culture

The Korean Cell Line Bank provided RAW 264.7 murine macrophage cells (Seoul, Republic of Korea). Cells were suspended in Dulbecco's modified Eagle's medium (DMEM; Gibco Inc, New York, United States) supplemented with 10% heat-inactivated fetal bovine serum (FBS) in an atmosphere of 5% CO_2 at 37°C.

2.6.2 Determination of Viability of RAW 264.7 Cells

The proliferation effects of RPMPs and PPMPs on RAW 264.7 cells were identified by using the MTT assay as previously described (Sun et al., 2019, 7). RAW 264.7 cells were seeded at 1×10^4 cells/well in 96-well flat-bottom plates with medium, after which they (5,000 cells/well) were treated with various concentrations of RPMPs and PPMPs (25 μg/ml, 50 μg/ml, 100 μg/ml, 200 μg/ml, 400 μg/ml and 600 μg/ml) or lipopolysaccharides (LPS) (1 μg/ml) for 24 h. The absorbance (A) of each well was read at 490 nm using a microplate reader (Biochrom NanoVue Plus, United States), after which macrophage cell viability was calculated using the following equation: Macrophage cell viability (%) = $[(A_t\text{-}A_0)/(A_t\text{-}A_c)] \times 100$, where A_t is the absorbance of the sample, A_c is the absorbance of the control group, and A_0 is the absorbance of the blank group.

2.6.3 Quantitative Real-Time Polymerase Chain Reaction Assay

The mRNA expression levels of inducible nitric oxide synthase (iNOS), interleukin 6 (IL-6), TNF-α (tumor necrosis factor-alpha), and total RNA were measured by Quantitative real-time polymerase chain reaction (qRT-PCR). Total RNA was isolated using TRIzol reagent, and RNA was transcribed to the cDNA using the RevertAid First Strand cDNA Synthesis Kit according to the manufacturer's protocol. The qRT-PCR was performed using a multicolor detection system (Applied Biosystems, United States). The following sequences for PCR primers from 5′ to 3′ end were used: *IL-6*: forward, 5′-CCATGC CATGGAAGATTCCA AAGATGTAG-3′, *IL-6*: reverse, 5′-CTC GCTCGAGCTACATTTGCCGAAGAGCC C-3'; TNF-α: forward, 5′-CATGATCCGGGACGTGGAG-3′, TNF-α: reverse, 5′-CG ATCACTCCAAAGTGCAGC-3'; *iNOS*: forward, 5′-CAC CTACCCACCCCTACAAA -3′, *iNOS*: reverse, 5′-CAGCCA ACGTGGAGACTACC-3'; Glyceraldehyde-3- phosphate dehydrogenase (*GAPDH*) was used as the internal reference gene. The expression levels concerning the control were estimated by calculating ΔΔCt and subsequently analyzed using the $2^{-\Delta\Delta Ct}$ method.

2.7 Statistical Analysis

The results were expressed as mean ± standard deviation (SD). Statistical differences between groups were assessed by Student's t-test. The PCD-UPLC fingerprints were generated by ChemPattern software (Chemmind Technologies Co, Ltd, Beijing) and analyzed by similarity analysis (SA), principal component analysis (PCA), and partial least squares regression discriminant analysis (PLS-DA).

3 RESULTS AND DISCUSSION

3.1 The Components and Yields of RPMPs and PPMPs

The crude water-soluble polysaccharides were extracted from raw PM (1–31) and processed PM (32–40). The yields, neutral sugar, uronic acid, and protein contents of 40 polysaccharide samples are shown in **Table 1**. The range of RPMPs yields was 2.05–5.58%, and the range of PPMPs yields was 11.20–20.73%. The contents of neutral sugar, uronic acid, and protein of RPMPs were 40.39–64.91%, 5.29–15.75%, and 13.20–25.43%, respectively. The contents of neutral sugar, uronic acid, and protein of PPMPs were 61.96–71.05%, 4.29–6.59%, and 13.05–21.98%, respectively. The results showed there were significant differences between RPMPs and PPMPs in terms of yields, neutral sugar content, and uronic acid content ($p < 0.05$), which could be due to various reasons. It could be that the high temperature steaming during the processing enhances the permeability of the cells and promotes the leaching of polysaccharides. Moreover, the polysaccharides in the black bean juice might remain on the PM during the processing, as they are extracted together with the PPMPs. In addition, it was also found that the PM steaming process was involved in the Maillard reaction, which may explain the significant difference in the yields of RPMPs and PPMPs (Liu et al., 2009).

3.2 HPSEC-MALLS-RID Analysis

Polysaccharides are a kind of macromolecular polymers, and the molecular chain of polysaccharides could be reflected by *M*w and *PDI*. It has also been found that the structure and physiological activities of polysaccharides are closely related to their *M*w (Hou et al., 2012). HPSEC-MALLS-RID is an effective and powerful method for analyzing the *M*w and *PDI* of polysaccharides from TCM. It is also considered to be beneficial for the discrimination and quality control of polysaccharides from TCM. Therefore, to further analyze the differences between RPMPs and PPMPs, the HPSEC chromatograms and the *M*w of 40 polysaccharide samples were compared. **Table 1** summarized the *M*w and *PDI* of RPMPs and PPMPs from different regions and markets. Generally, the *PDI* is a measure of the distribution of *M*w in a given polymer sample, which is often denoted as *PDI* = *M*w/*M*n. Results showed that the *M*w of RPMPs and PPMPs were not similar, ranging from 646.20 to 3,028.30 kDa (RPMPs) and 341.60 to 802.20 kDa (PPMPs), respectively. The average *M*w of thirty-one RPMPs was 1,151.46 kDa, while the average *M*w of nine PPMPs was 606.98 kDa. The difference was also found in the *PDI* of RPMPs and PPMPs, while the *PDI* of thirty-one batches of RPMPs ranged from 2.10 to 4.10, as well as the *PDI* of nine batches ranged from 1.77 to 1.98, thus suggesting that the *M*w distribution of PPMPs was narrower and more concentrated than that of RPMPs (**Figure 1**).

Subsequently, the retention time corresponding to the dextran standard with *M*w 820 kDa (t_R = 28.01 min) was used to divide the main peak into two parts (peak 1, peak 2). As shown in **Figure 2C** and **Table 1**, peak 2 of RPMPs accounted for a lower proportion of the main peak than peak 1. The results revealed that the low *M*w part

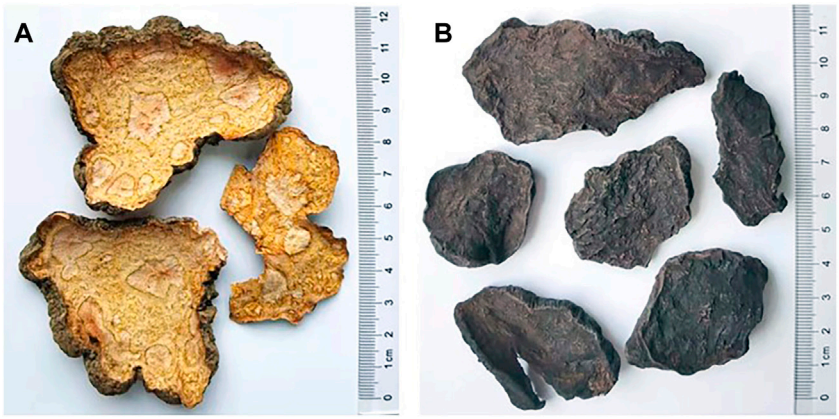

FIGURE 1 | The roots of *Polygonum multiflorum* Thunb **(A)** raw product, and **(B)** processed product.

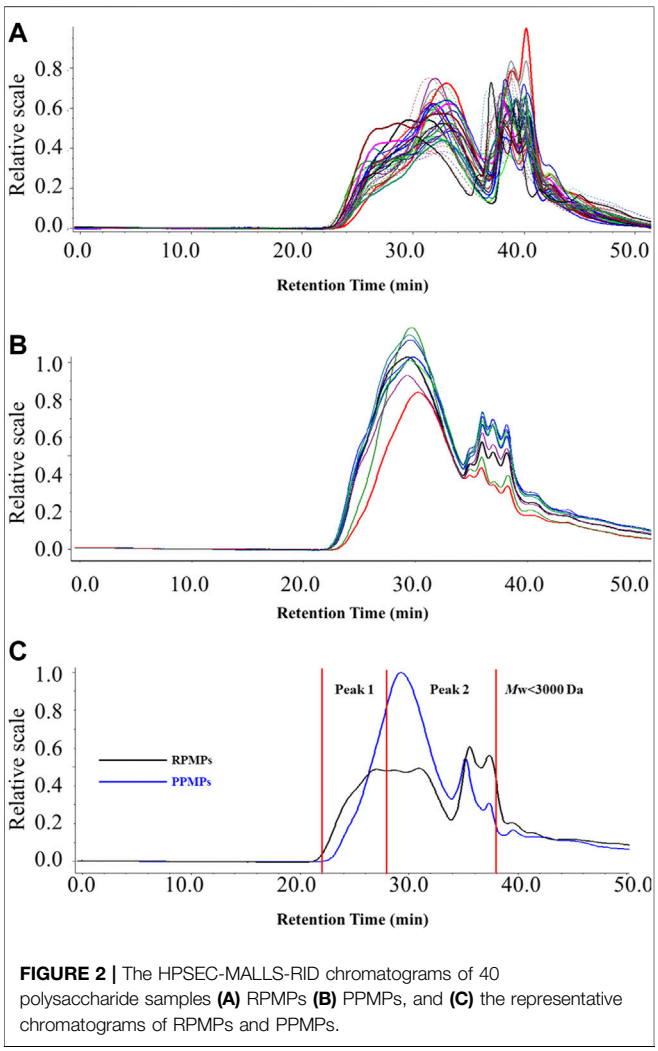

FIGURE 2 | The HPSEC-MALLS-RID chromatograms of 40 polysaccharide samples **(A)** RPMPs **(B)** PPMPs, and **(C)** the representative chromatograms of RPMPs and PPMPs.

(peak 2) of PPMPs was more than that of RPMPs, that is, the content of polysaccharides with low *M*w increased after processing. It is speculated that the polysaccharides from raw PM might be degraded into polysaccharides with lower *M*w due to the extended period of high temperature during the processing, which was similar to the results reported by Sun et al. (2020). They compared the physicochemical properties of water-soluble polysaccharides from raw and wine-processed *Polygonatum sibiricum*, and concluded that most macromolecule polysaccharides were degraded to small molecular polysaccharides during the processing.

3.3 Monosaccharide Composition Analysis of RPMPs and PPMPs

The monosaccharide composition of polysaccharides is an essential parameter for evaluating the structural features of the samples. The monosaccharide compositions of RPMPs and PPMPs were analyzed based on PCD-UPLC following acid hydrolysis. The PCD-UPLC chromatograms from 40 polysaccharide samples are shown in **Figure 3A**. The results showed that RPMPs and PPMPs samples from different regions and markets all consisted of seven types of monosaccharides. The first to the seventh peaks represented Man, Rha, GlcA, GalA, Glc, Gal, and Ara, respectively, and Glc was the main monosaccharide in RPMPs and PPMPs samples.

Although the monosaccharide composition of RPMPs and PPMPs was the same, the molar ratios of monosaccharides between RPMPs and PPMPs were significantly different, especially in the molar ratio of Glc ($p < 0.05$). We found that the molar ratio of Glc/GalA of PPMPs (16.42 ± 3.94) was significantly higher than that of RPMPs (6.50 ± 2.08), as shown in **Table 2**. The results showed that the molar ratio of Glc/GalA could be used as an important marker to distinguish RPMPs and PPMPs.

3.4 PCD-UPLC Fingerprints and Chemometric Analysis

3.4.1 SA of the PCD-UPLC Fingerprints

The PCD-UPLC fingerprints of the 40 polysaccharide samples are displayed in **Figure 3A**. The correlation coefficients method and cosine (cos θ) method were used to evaluate the similarity of the

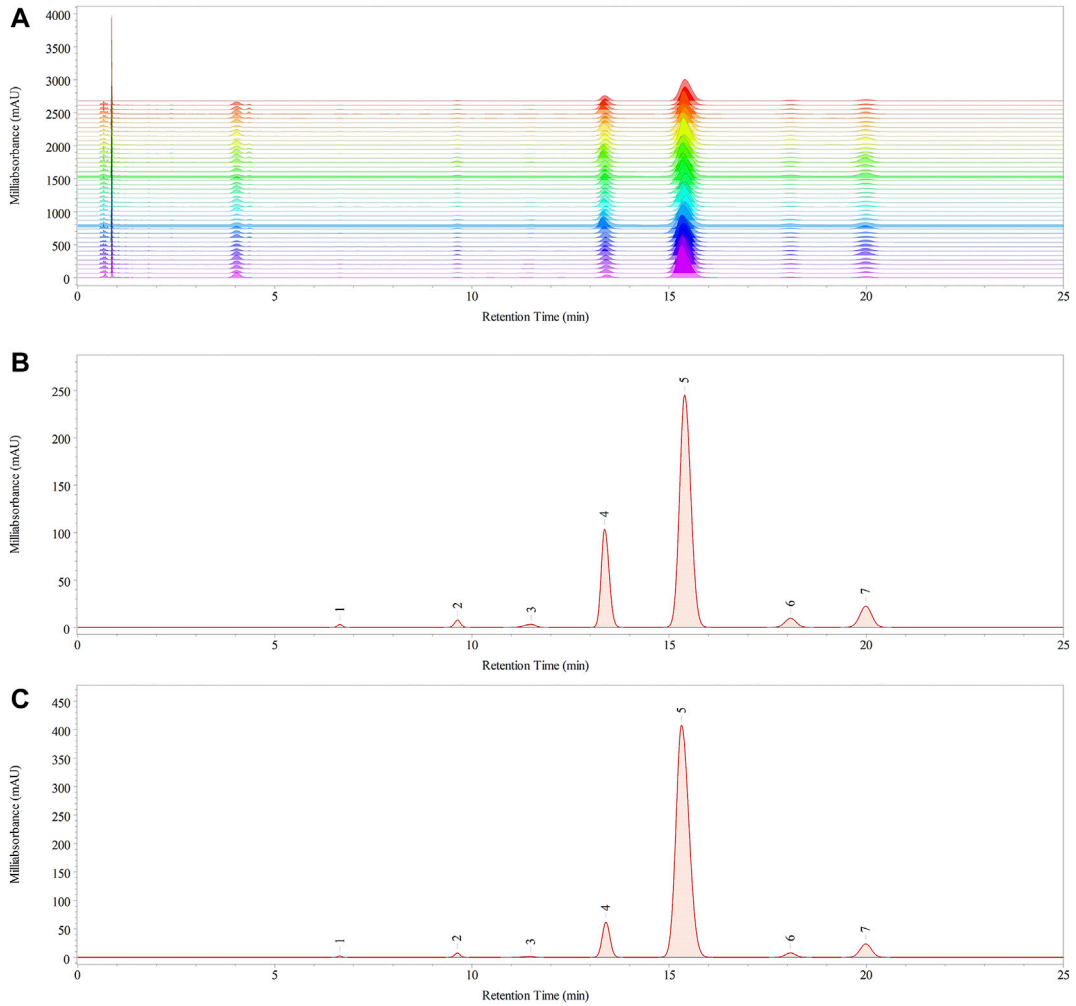

FIGURE 3 | The chromatograms of 40 polysaccharide samples **(A)** PCD-UPLC fingerprints, and the PCD-UPLC standard referential fingerprint of RPMPs **(B)** and PPMPs **(C)**.

monosaccharide composition of 40 polysaccharide samples. The similarity values were calculated based on the common pattern, which was generated by Chempattern software based on the PCD-UPLC chromatograms of PPMPs. The value of cos θ ranged from 0.9762 to 0.9996, and the value of correlation coefficients ranged from 0.9737 to 0.9996. Results showed that the similarity value of all 40 samples was >0.95, which indicated that all samples were highly similar, and there were no obvious differences among RPMPs and PPMPs from different locations ($p > 0.05$). In addition, the standard fingerprint of RPMPs and PPMPs were also established, as shown in **Figures 3B,C**.

3.4.2 PCA of the PCD-UPLC Fingerprints

PCA is the most common method for data analysis in multivariate statistical analysis. PCD-UPLC fingerprints were analyzed by PCA to find out the index of distinguishing RPMPs and PPMPs. The data matrix of relative peak areas of the seven characteristic monosaccharide peaks was worked by ChemPattern software. The score plot and the loading of PCA are shown in **Figure 4**. Results showed that the first three PCs explained 73.92, 18.23, and 3.97% of the variance, respectively, accounting for 96.12% of the total variance, which could reflect the vast majority of the original chromatographic information of the samples. Three main factors could be calculated by the equations as follows:

$$PC1 = 0.02*X - 0.02*X2 + 0.02*X3 - 0.28*X4 + 0.96*X5 + 0.02*X6 - 0.02*X7$$

$$PC2 = 0.03*X1 - 0.23*X2 - 0.10*X3 - 0.59*X4 - 0.18*X5 - 0.34*X6 - 0.66*X7$$

$$PC3 = 0.01*X1 + 0.29*X2 - 0.08*X3 - 0.75*X4 - 0.21*X5 + 0.12*X6 + 0.55*X7$$

In the equations, X1 to X7 were Man, Rha, GlcA, GalA, Glc, Gal, and Ara, respectively. PCA could classify RPMPs and

TABLE 2 | The monosaccharide composition of 40 polysaccharide samples.

Codes	Man	Rha	GlcA	GalA	Glc	Gal	Ara
1	0.02	0.06	0.04	1.00	8.34	0.16	0.34
2	0.01	0.07	0.03	1.00	7.57	0.16	0.38
3	0.01	0.08	0.03	1.00	3.72	0.14	0.35
4	0.02	0.06	0.04	1.00	7.59	0.19	0.34
5	0.02	0.07	0.06	1.00	9.74	0.18	0.32
6	0.02	0.06	0.04	1.00	4.26	0.14	0.29
7	0.01	0.06	0.04	1.00	4.52	0.14	0.34
8	0.01	0.04	0.02	1.00	4.65	0.07	0.18
9	0.01	0.07	0.04	1.00	7.26	0.11	0.34
10	0.01	0.06	0.04	1.00	5.87	0.12	0.29
11	0.01	0.06	0.03	1.00	7.00	0.14	0.31
12	0.01	0.06	0.04	1.00	9.14	0.15	0.33
13	0.01	0.06	0.03	1.00	8.08	0.13	0.32
14	0.01	0.08	0.03	1.00	6.67	0.14	0.38
15	0.01	0.07	0.03	1.00	5.85	0.14	0.34
16	0.01	0.05	0.04	1.00	5.84	0.11	0.27
17	0.01	0.06	0.03	1.00	2.80	0.12	0.34
18	0.01	0.05	0.05	1.00	6.10	0.13	0.26
19	0.03	0.08	0.04	1.00	3.70	0.20	0.40
20	0.01	0.06	0.10	1.00	8.83	0.12	0.30
21	0.01	0.06	0.11	1.00	8.95	0.14	0.36
22	0.01	0.06	0.08	1.00	6.25	0.12	0.39
23	0.01	0.09	0.04	1.00	2.62	0.21	0.41
24	0.01	0.08	0.03	1.00	4.75	0.17	0.45
25	0.01	0.08	0.06	1.00	4.80	0.15	0.48
26	0.07	0.08	0.07	1.00	7.57	0.52	0.35
27	0.02	0.06	0.06	1.00	6.97	0.66	0.30
28	0.01	0.07	0.03	1.00	6.23	0.16	0.34
29	0.01	0.11	0.06	1.00	11.69	0.34	0.50
30	0.01	0.07	0.04	1.00	5.80	0.13	0.32
31	0.01	0.09	0.05	1.00	8.23	0.21	0.50
Mean ± SD	0.01 ± 0.01	0.07 ± 0.01	0.05 ± 0.02	—	6.50 ± 2.08	0.18 ± 0.12	0.35 ± 0.07
32	0.02	0.12	0.09	1.00	21.87	0.21	0.56
33	0.01	0.11	0.06	1.00	17.40	0.25	0.72
34	0.02	0.12	0.05	1.00	13.73	0.25	0.77
35	0.02	0.12	0.05	1.00	12.17	0.23	0.73
36	0.02	0.13	0.04	1.00	13.72	0.24	0.81
37	0.04	0.14	0.06	1.00	16.23	0.33	0.50
38	0.02	0.12	0.06	1.00	14.46	0.24	0.74
39	0.03	0.12	0.10	1.00	23.73	0.21	0.53
40	0.02	0.12	0.06	1.00	14.46	0.24	0.74
Mean ± SD	0..02 ± 0.01	0.12 ± 0.01[a]	0.06 ± 0.01	—	16.42 ± 3.94[a]	0.24 ± 0.04	0.68 ± 0.11[a]

[a]$p < 0.05$ *denotes a statistically significant difference compared with RPMPs.*

PPMPs into two categories. As shown in **Figure 4**, the loading of each variable shows that peak four and peak five had a great influence on the identification of RPMPs and PPMPs, which indicates that Glc and GalA could be chosen as the markers to distinguish raw and processed PM.

3.4.3 PLS-DA of the PCD-UPLC Fingerprints

PLS-DA is an analytical method with supervised pattern recognition, which combines the advantages of multivariate linear regression and PCA. The 40 chromatograms were pretreated, and PLS-DA were analyzed by their pattern. As shown in **Figure 5**, results showed that PLS-DA could effectively separate RPMPs and PPMPs. As with PCA, peak 4 and peak 5 contribute significantly to the differentiation of RPMPs and PPMPs. The contents of these two monosaccharides in analyzed samples were higher, which verified the results of PCA and PLS-DA. This also suggested that the Glc and GalA in polysaccharides from PM might have changed after processing.

3.5 Immunomodulatory Activities of RPMPs and PPMPs

The RPMPs and PPMPs (sample 31 and sample 39) used in this experiment were derived from the same batch of PM. Also, its physicochemical properties were in accordance with the characteristics of common polysaccharides from raw and processed PM.

3.5.1 Effect of RPMPs and PPMPs on Cell Viability of RAW 264.7 Cells

Macrophages are vital immune cells that serve multiple functions. To resist invading pathogens, macrophages can phagocytize and kill

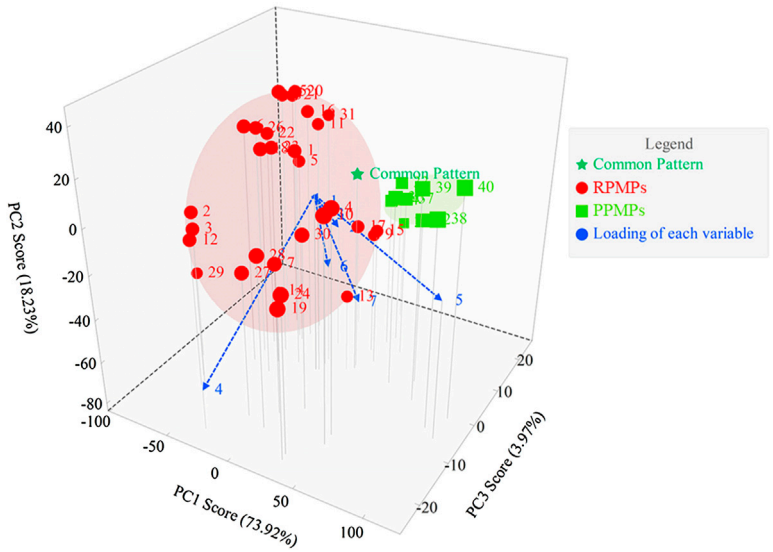

FIGURE 4 | The score plot and loading plot of PCA from PCD-UPLC fingerprints.

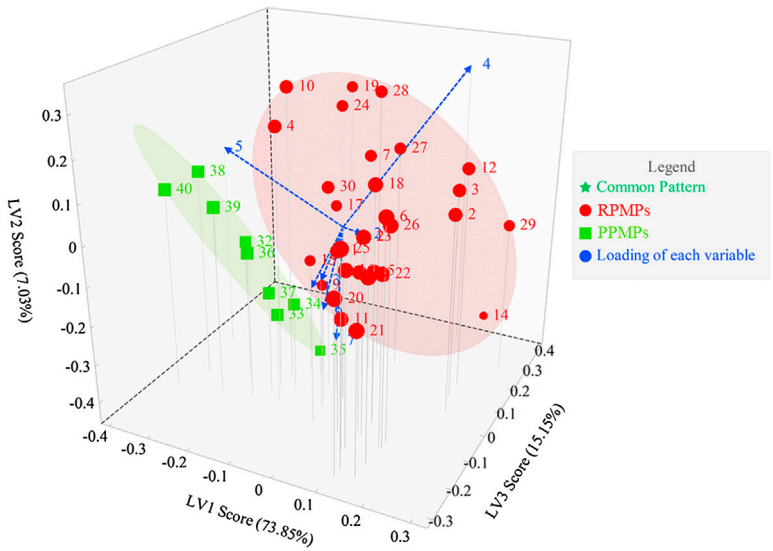

FIGURE 5 | The score plot and loading plot of PLS-DA from PCD-UPLC fingerprints.

harmful bacteria, as well as produce and emit chemokines and cytokines (Mingzhu Zhang et al., 2018; Yang et al., 2020). RAW 264.7 cells are commonly used cell models to evaluate the immune activity of polysaccharides *in vitro*. The viability of RAW 264.7 cells treated by RPMPs and PPMPs was investigated through the MTT assay. RPMPs and PPMPs with a concentration of 25–600 μg/ml were not toxic to RAW 264.7 macrophages. Therefore, the concentration of RPMPs and PPMPs used in this study was lower than 600 μg/mL. As shown in **Figure 6**, treatment with different doses of RPMPs and PPMPs significantly enhanced RAW 264.7 cells ($p < 0.05$). The proliferation of RAW 264.7 cells was similarly aided by this therapy in a dose-dependent manner. When the concentration of RPMPs and PPMPs was 200 μg/ml, the cell viability reached the maximum value of 152.6 and 147.7%, respectively, which was close to that of the LPS treatment group (156.1%). In addition, there was no significant difference between RPMPs and PPMPs at the level of 200 μg/ml ($p > 0.05$).

3.5.2 Effect of RPMPs and PPMPs on Cell Viability of RAW 264.7 Cells

Activated macrophages do induce not only the expression but also enhance the level of cytokines (such as TNF-α and IL-6)

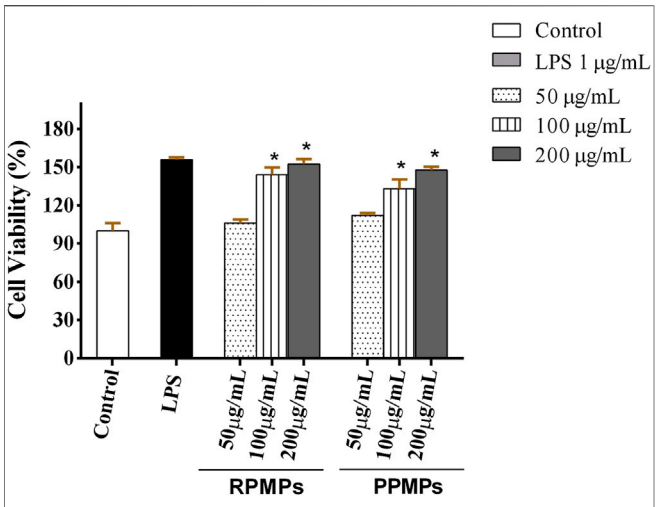

FIGURE 6 | Effects of RPMPs and PPMPs on the viability of RAW 264.7 cells. Results are represented as mean ± SD, $n = 6$. *$p < 0.05$ denotes a statistically significant difference between the treated and control groups.

(Zhan et al., 2020). NO, TNF-α and IL-6 are important bioactive molecules in the human body. NO can activate macrophages and kill pathogenic microorganisms and tumor cells (Ren et al., 2017). IL-6 plays a role in the pathophysiology of inflammatory and immunological disorders as a key regulator of the host's defensive response (Wang et al., 2015). TNF-α may activate macrophages, increase different functional responses, and induce the expression of antitumor and immunomodulatory mediators (He et al., 2012).

Meanwhile, the level of TNF-α, which is related to the production of NO, can induce the up-regulation of iNOS, resulting in the release of NO. Several previous studies investigated the immune modulation effect of polysaccharides by using RAW264.7 macrophages as a cell model *in vitro*. To further evaluate the immunostimulatory effect of RPMPs and PPMPs, the effects of RPMPs and PPMPs on NO, IL-6 and TNF-α at the molecular level, the expression of iNOS, IL-6, and TNF-α were determined by qRT-PCR. As shown in **Figure 7**, RPMPs and PPMPs promoted the mRNA expression of IL-6, TNF-α, and iNOS in a dose-dependent manner compared with the control group. The high-dose experimental group (200 μg/ml) of RPMPs and PPMPs increased 2~3 fold the mRNA expression levels of iNOS, IL-6, and TNF-α ($p < 0.05$) compared with the control group. These results suggested that RPMPs and PPMPs could promote the secretion of NO, IL-6, and TNF-α in RAW 264.7 cells, where the effect of the PPMPs was greater than that of the RPMPs ($p < 0.05$).

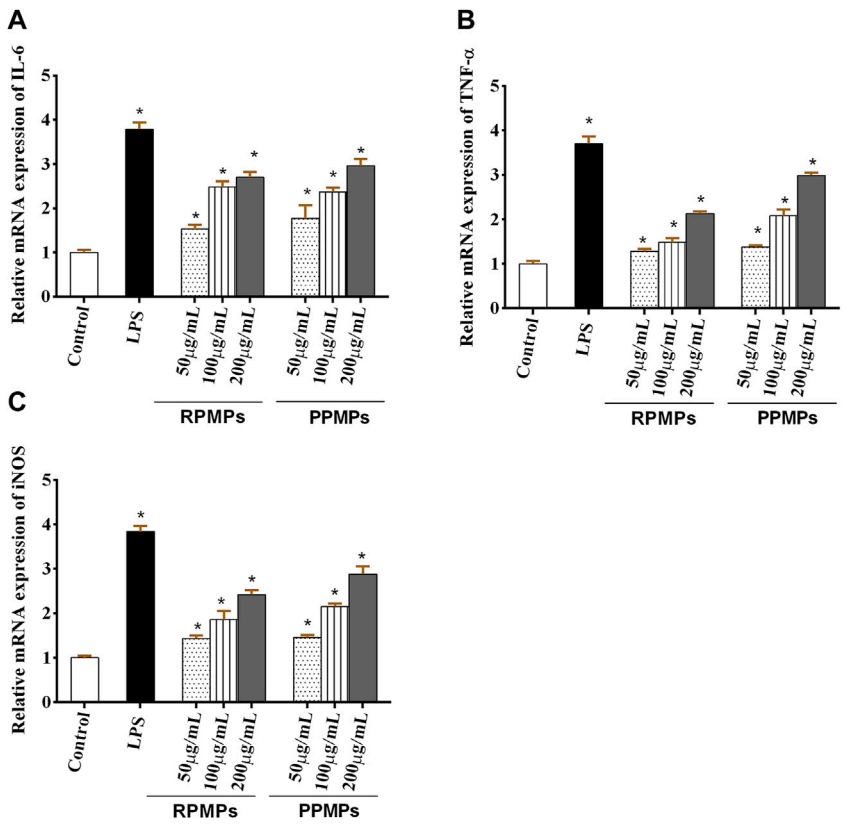

FIGURE 7 | Effects of RPMPs and PPMPs on the mRNA expression of IL-6 **(A)**, TNF-α **(B)**, and iNOS **(C)** in RAW 264.7 cells. *$p < 0.05$ versus the control. The data are presented as mean ± SD ($n = 3$).

3.6 The Change of Physicochemical Properties and Immune Activity of polysaccharides After Processing

PM is a well-known traditional Chinese medicine with a long medicinal history. Polysaccharides are an important component of raw and processed PM. In this study, there were significant differences between RPMPs and PPMPs in yields, neutral sugar contents, uronic acid contents, *M*w, and the molar ratio of Glc/GalA ($p < 0.05$). These results indicated that polysaccharides in PM changed after processing. This change may be due to the permeability of the cell wall increased when water or black bean juice was immersed into PM at high temperature, and black bean juice also flowed into PM during processing. In addition, the high temperature during processing may lead to the degradation of the most macromolecular polysaccharides into small ones, which has also been previously reported (Sun et al., 2020). The darker color and lower *M*w of PPMPs might be related to the Maillard reaction during the processing.

It was proposed that the monosaccharide composition, uronic acid content, configuration, as well as *M*w, were crucial for the immune activity. Recent studies have shown that polysaccharides with different *M*w have different biological activities (Xu et al., 2015). For example, Li et al. (2020) obtained three polysaccharide fractions APS-Ⅰ (>2000 kDa), APS-Ⅱ (about 10 kDa), and APS-Ⅲ (about 300 Da), and evaluated their immune activity, revealing that APS-Ⅱ (about 10 kDa) with moderate *M*w had better immune activity. Hou et al. (2012) pointed out that with the decrease in *M*w of polysaccharides, their water solubility increased and viscosity decreased, which promoted the movement of polysaccharides *in vivo* and increased the biological activity. Qi and Kim (2018) suggested that the *M*w had an important impact on the immunomodulatory effects of polysaccharides from the green alga *Chlorella ellipsoidea*. All the above studies showed that polysaccharide with low *M*w was an important component contributing to immunomodulatory. In our study, both RPMPs and PPMPs had regulatory effects on RAW 264.7 cells, and PPMPs with lower *M*w had significantly better immune activity than RPMPs. It is presumed that the immunomodulatory activity of polysaccharides from PM is related to *M*w. However, homogeneous polysaccharides with different molecular weights need to be prepared to further verify the above inference.

4 CONCLUSION

In this study, the physicochemical properties and immunomodulatory activities of polysaccharides from raw and processed PM were determined and compared. Results showed that there were significant differences in the yields, *M*w, and the molar ratio of Glc/GalA between RPMPs and PPMPs, revealing that the polysaccharides from PM changed after processing. Also, these indexes could be used to distinguish raw and processed PM. In addition, both RPMPs and PPMPs had immunomodulatory activity, and the activity of PPMPs was superior to that of RPMPs, which was consistent with the ancient processing theory that processed PM has a tonic effect. This study provides a reference for improving the quality control standard of PM and the study of its immunomodulatory activity.

DATA AVAILABILITY STATEMENT

The original contributions presented in the study are included in the article/Supplementary Material, further inquiries can be directed to the corresponding author.

AUTHOR CONTRIBUTIONS

DG and YW designed the study, performed the research, analyzed data, and wrote the manuscript; HJ, FW, and SM helped perform the analysis with constructive discussions; SK, KZ, and YL provided some ideas for the experiments and helped analyze data; and JF edited the manuscript. All authors approved the manuscript.

FUNDING

This work was supported by the National Natural Science Foundation of China (Grant No.81973476 and 81903807).

ACKNOWLEDGMENTS

The authors would like to thank all the participants.

REFERENCES

Bradford, M. M. (1976). A Rapid and Sensitive Method for the Quantitation of Microgram Quantities of Protein Utilizing the Principle of Protein-Dye Binding. *Anal. Biochem.* 72, 248–254. doi:10.1006/abio.1976.9999

Chen, Q., Zhang, S.-z., Ying, H.-z., Dai, X.-y., Li, X.-x., Yu, C.-h., et al. (2012). Chemical Characterization and Immunostimulatory Effects of a Polysaccharide from Polygoni Multiflori Radix Praeparata in Cyclophosphamide-Induced Anemic Mice. *Carbohydr. Polym.* 88, 1476–1482. doi:10.1016/j.carbpol.2012.02.055

Chen, W., Wang, P., Chen, H., Xing, Y., Liu, C., Pan, G., et al. (2021). The Composition Differences between Small Black Beans and Big Black Beans from Different Habitats and its Effects on the Processing of *Polygonum Multiflorum*. *Phytochem. Anal.* 32, 767–779. doi:10.1002/pca.3022

Dong, Q., Li, N., Li, Q., Zhang, C. E., Feng, W. W., Li, G. Q., et al. (2015). Screening for Biomarkers of Liver Injury Induced by *Polygonum Multiflorum*: a Targeted Metabolomic Study. *Front. Pharmacol.* 6, 217. doi:10.3389/fphar.2015.00217

DuBois, M., Gilles, K. A., Hamilton, J. K., Rebers, P. A., and Smith, F. (1956). Colorimetric Method for Determination of Sugars and Related Substances. *Anal. Chem.* 28, 350–356. doi:10.1021/ac60111a017

He, X., Shu, J., Xu, L., Lu, C., and Lu, A. (2012). Inhibitory Effect of Astragalus Polysaccharides on Lipopolysaccharide-Induced TNF-A and IL-1β Production in THP-1 Cells. *Molecules* 17, 3155–3164. doi:10.3390/molecules17033155

Hou, Y., Wang, J., Jin, W., Zhang, H., and Zhang, Q. (2012). Degradation of Laminaria Japonica Fucoidan by Hydrogen Peroxide and Antioxidant Activities

of the Degradation Products of Different Molecular Weights. *Carbohydr. Polym.* 87, 153–159. doi:10.1016/j.carbpol.2011.07.031

Li, H., Wang, X., Liu, Y., Pan, D., Wang, Y., Yang, N., et al. (2017). Hepatoprotection and Hepatotoxicity of Heshouwu, a Chinese Medicinal Herb: Context of the Paradoxical Effect. *Food Chem. Toxicol.* 108, 407–418. doi:10.1016/j.fct.2016.07.035

Li, K., Cao, Y.-x., Jiao, S.-m., Du, G.-h., Du, Y.-g., and Qin, X.-m. (2020). Structural Characterization and Immune Activity Screening of Polysaccharides with Different Molecular Weights from Astragali Radix. *Front. Pharmacol.* 11, 582091. doi:10.3389/fphar.2020.582091

Liang, Z., Chen, H., Yu, Z., and Zhao, Z. (2010). Comparison of Raw and Processed Radix Polygoni Multiflori (Heshouwu) by High Performance Liquid Chromatography and Mass Spectrometry. *Chin. Med.* 5, 29. doi:10.1186/1749-8546-5-29

Lin, L., Ni, B., Lin, H., Zhang, M., Li, X., Yin, X., et al. (2015). Traditional Usages, Botany, Phytochemistry, Pharmacology and Toxicology of *Polygonum Multiflorum* Thunb.: A Review. *J. Ethnopharmacol.* 159, 158–183. doi:10.1016/j.jep.2014.11.009

Liu, Z., Chao, Z., Liu, Y., Song, Z., and Lu, A. (2009). Maillard Reaction Involved in the Steaming Process of the Root of *Polygonum Multiflorum*. *Planta Med.* 75, 84–88. doi:10.1055/s-0028-1088349

Liu, Y., Wang, Q., Yang, J., Guo, X., Liu, W., Ma, S., et al. (2018). *Polygonum Multiflorum* Thunb.: A Review on Chemical Analysis, Processing Mechanism, Quality Evaluation, and Hepatotoxicity. *Front. Pharmacol.* 9, 364. doi:10.3389/fphar.2018.00364

Luo, A., Fan, Y., and Luo, A. (2011). *In Vitro* free Radicals Scavenging Activities of Polysaccharide from *Polygonum Multiflorum* Thunb. *J. Med. Plants Res.* 5 (6), 966–972. doi:10.2147/DDDT.S19759

Mazzanti, G., Battinelli, L., Daniele, C., Mastroianni, C. M., Lichtner, M., Coletta, S., et al. (2004). New Case of Acute Hepatitis Following the Consumption of Shou Wu Pian, a Chinese Herbal Product Derived from *Polygonum Multiflorum*. *Ann. Intern. Med.* 140, W–W30. doi:10.7326/0003-4819-140-7-200404060-00042-w3

McCready, R. M., and McComb, E. A. (1953). Enzymes, Course of Action of Polygalacturonase on Polygalacturonic Acids. *J. Agric. Food Chem.* 1, 1165–1168. doi:10.1021/jf60019a006

Mingzhu Zhang, M., Tian, X., Wang, Y., Wang, D., Li, W., Chen, L., et al. (2018). Immunomodulating Activity of the Polysaccharide TLH-3 from Tricholomalobayense in RAW264.7 Macrophages. *Int. J. Biol. Macromol.* 107, 2679–2685. doi:10.1016/j.ijbiomac.2017.10.165

Panis, B., Wong, D. R., Hooymans, P. M., De Smet, P. A., and Rosias, P. P. (2005). Recurrent Toxic Hepatitis in a Caucasian Girl Related to the Use of Shou-Wu-Pian, a Chinese Herbal Preparation. *J. Pediatr. Gastroenterol. Nutr.* 41, 256–258. doi:10.1097/01.MPG.0000164699.41282.67

Park, G. J., Mann, S. P., and Ngu, M. C. (2001). Acute Hepatitis Induced by Shou-Wu-Pian, a Herbal Product Derived from *Polygonum Multiflorum*. *J. Gastroenterol. Hepatol.* 16, 115–117. doi:10.1046/j.1440-1746.2001.02309.x

Qi, J., and Kim, S. M. (2018). Effects of the Molecular Weight and Protein and Sulfate Content of *Chlorella Ellipsoidea* Polysaccharides on Their Immunomodulatory Activity. *Int. J. Biol. Macromol.* 107, 70–77. doi:10.1016/j.ijbiomac.2017.08.144

Qing Zhang, Q., Xu, Y., Lv, J., Cheng, M., Wu, Y., Cao, K., et al. (2018). Structure Characterization of Two Functional Polysaccharides from *Polygonum Multiflorum* and its Immunomodulatory. *Int. J. Biol. Macromol.* 113, 195–204. doi:10.1016/j.ijbiomac.2018.02.064

Ren, Z., Qin, T., Qiu, F., Song, Y., Lin, D., Ma, Y., et al. (2017). Immunomodulatory Effects of Hydroxyethylated Hericium erinaceus Polysaccharide on Macrophages RAW264.7. *Int. J. Biol. Macromol.* 105, 879–885. doi:10.1016/j.ijbiomac.2017.07.104

Shaw, D. (2010). Toxicological Risks of Chinese Herbs. *Planta Med.* 76, 2012–2018. doi:10.1055/s-0030-1250533

Sun, S., Li, K., Xiao, L., Lei, Z., and Zhang, Z. (2019). Characterization of Polysaccharide from *Helicteres Angustifolia* L. And its Immunomodulatory Activities on Macrophages RAW264.7. *Biomed. Pharmacother.* 109, 262–270. doi:10.1016/j.biopha.2018.10.039

Sun, T., Zhang, H., Li, Y., Liu, Y., Dai, W., Fang, J., et al. (2020). Physicochemical Properties and Immunological Activities of Polysaccharides from Both Crude and Wine-Processed *Polygonatum Sibiricum*. *Int. J. Biol. Macromol.* 143, 255–264. doi:10.1016/j.ijbiomac.2019.11.166

Wang, Z. J., Xie, J. H., Kan, L. J., Wang, J. Q., Shen, M. Y., Li, W. J., et al. (2015). Sulfated Polysaccharides from Cyclocarya Paliurus Reduce H2O2-Induced Oxidative Stress in RAW264.7 Cells. *Int. J. Biol. Macromol.* 80, 410–417. doi:10.1016/j.ijbiomac.2015.06.031

Xu, Y., Jiang, X., Wang, S., and Liang, S. (2014). Protective Effects of *Polygonum Multiflorum* Polysaccharide against H_2O_2-Induced Apoptosis in PC12 Cells. *Bio Technol. Indian J.* 10, 10191–10196.

Xu, J., Xu, L. L., Zhou, Q. W., Hao, S. X., Zhou, T., and Xie, H. J. (2015). Isolation, Purification, and Antioxidant Activities of Degraded Polysaccharides from *Enteromorpha Prolifera*. *Int. J. Biol. Macromol.* 81, 1026–1030. doi:10.1016/j.ijbiomac.2015.09.055

Yang, D., Lin, F., Huang, Y., Ye, J., and Xiao, M. (2020). Separation, Purification, Structural Analysis and Immune-Enhancing Activity of Sulfated Polysaccharide Isolated from Sea Cucumber Viscera. *Int. J. Biol. Macromol.* 155, 1003–1018. doi:10.1016/j.ijbiomac.2019.11.064

Yang, J. B., Liu, Y., Wang, Q., Ma, S. C., Wang, A. G., Cheng, X. L., et al. (2019). Characterization and Identification of the Chemical Constituents of *Polygonum Multiflorum* Thunb. By High-Performance Liquid Chromatography Coupled with Ultraviolet Detection and Linear Ion Trap FT-ICR Hybrid Mass Spectrometry. *J. Pharm. Biomed. Anal.* 172, 149–166. doi:10.1016/j.jpba.2019.03.049

Yu, J., Xie, J., Mao, X. J., Wang, M. J., Li, N., Wang, J., et al. (2011). Hepatoxicity of Major Constituents and Extractions of Radix Polygoni Multiflori and Radix Polygoni Multiflori Praeparata. *J. Ethnopharmacol.* 137, 1291–1299. doi:10.1016/j.jep.2011.07.055

Zhan, Q., Wang, Q., Lin, R., He, P., Lai, F., Zhang, M., et al. (2020). Structural Characterization and Immunomodulatory Activity of a Novel Acid Polysaccharide Isolated from the Pulp of Rosa Laevigata Michx Fruit. *Int. J. Biol. Macromol.* 145, 1080–1090. doi:10.1016/j.ijbiomac.2019.09.201

Zhu, W., Xue, X., and Zhang, Z. (2017). Structural, Physicochemical, Antioxidant and Antitumor Property of an Acidic Polysaccharide from *Polygonum Multiflorum*. *Int. J. Biol. Macromol.* 96, 494–500. doi:10.1016/j.ijbiomac.2016.12.064

Conflict of Interest: The authors declare that the research was conducted in the absence of any commercial or financial relationships that could be construed as a potential conflict of interest.

Publisher's Note: All claims expressed in this article are solely those of the authors and do not necessarily represent those of their affiliated organizations, or those of the publisher, the editors and the reviewers. Any product that may be evaluated in this article, or claim that may be made by its manufacturer, is not guaranteed or endorsed by the publisher.

frontiers | Frontiers in Pharmacology

TYPE Original Research
PUBLISHED 26 August 2022
DOI 10.3389/fphar.2022.935336

OPEN ACCESS

EDITED BY
Yasmina Mohammed Abd EL-Hakim,
Zagazig University, Egypt

REVIEWED BY
Hui Yan,
Nanjing University of Chinese Medicine, China
Thanh-Tam Ho,
Duy Tan University, Vietnam

*CORRESPONDENCE
Feng Wei,
weifeng@nifdc.org.cn
Shuangcheng Ma,
masc@nifdc.org.cn

†These authors have contributed equally to this work

SPECIALTY SECTION
This article was submitted to Experimental Pharmacology and Drug Discovery, a section of the journal Frontiers in Pharmacology

RECEIVED 03 May 2022
ACCEPTED 13 July 2022
PUBLISHED 26 August 2022

CITATION
Song Y, Yang J, Hu X, Gao H, Wang P, Wang X, Liu Y, Cheng X, Wei F and Ma S (2022), A stepwise strategy integrating metabolomics and pseudotargeted spectrum–effect relationship to elucidate the potential hepatotoxic components in *Polygonum multiflorum*. *Front. Pharmacol.* 13:935336. doi: 10.3389/fphar.2022.935336

A stepwise strategy integrating metabolomics and pseudotargeted spectrum–effect relationship to elucidate the potential hepatotoxic components in *Polygonum multiflorum*

Yunfei Song[1,2†], Jianbo Yang[2†], Xiaowen Hu[2], Huiyu Gao[2], Pengfei Wang[2], Xueting Wang[2], Yue Liu[1], Xianlong Cheng[2], Feng Wei[2]* and Shuangcheng Ma[1,2]*

[1]School of Chinese Materia Medica, Beijing University of Chinese Medicine, Beijing, China, [2]Institute for Control of Chinese Traditional Medicine and Ethnic Medicine, National Institutes for Food and Drug Control, Beijing, China

Polygonum multiflorum (PM) Thunb., a typical Chinese herbal medicine with different therapeutic effect in raw and processed forms, has been used worldwide for thousands of years. However, hepatotoxicity caused by PM has raised considerable concern in recent decades. The exploration of toxic components in PM has been a great challenge for a long time. In this study, we developed a stepwise strategy integrating metabolomics and pseudotargeted spectrum–effect relationship to illuminate the potential hepatotoxic components in PM. First, 112 components were tentatively identified using ultraperformance liquid chromatography-quadrupole-time-of-flight-mass spectrometry (UPLC-Q-TOF-MS). Second, based on the theory of toxicity attenuation after processing, we combined the UPLC-Q-TOF-MS method and plant metabolomics to screen out the reduced differential components in PM between raw and processed PM. Third, the proposed pseudotargeted MS of 16 differential components was established and applied to 50 batches of PM for quantitative analysis. Fourth, the hepatocytotoxicity of 50 batches of PM was investigated on two hepatocytes, LO2 and HepG2. Last, three mathematical models, gray relational analysis, orthogonal partial least squares analysis, and back propagation artificial neural network, were established to further identify the key variables affecting hepatotoxicity in PM by combining quantitative spectral information with toxicity to hepatocytes of 50 batches of PM. The results suggested that 16 components may have different degrees of hepatotoxicity, which may lead to hepatotoxicity through synergistic effects. Three components (emodin dianthrones, emodin-8-*O*-*β*-D-glucopyranoside, PM 14-17) were screened to have significant hepatotoxicity and could be used as toxicity markers in PM as well as for further studies on the mechanism of toxicity. Above all, the study established an effective strategy to explore the

hepatotoxic material basis in PM but also provides reference information for in-depth investigations on the hepatotoxicity of PM.

KEYWORDS

polygonum multiflorum, hepatotoxicity, pseudotargeted spectrum–effect relationship, plant metabolomics, mathematical model

1 Introduction

Polygonum multiflorum (PM) Thunb., known as one of the "Four Great Herbs" in ancient China (PM, Ginseng, Ganoderma lucidum, Cordyceps sinensis), is widely used in many Chinese prescriptions and patent medicines due to its remarkable therapeutic effects. As early as the Song dynasty, the historical Chinese medicine document "Kai Bao Ben Cao" recorded the pharmacological efficacy of PM as "strengthen muscles and bones, benefit the essence, prolong life" (Lei et al., 2015; Teka et al., 2021). With different therapeutic effects, in general, PM can be divided into raw and processed PM in clinical applications. The Chinese pharmacopoeia states that raw PM has the effects of detoxification, eliminating carbuncles, moistening the intestine, and relieving constipation, while the processed product has been used mainly to tonify the liver and kidney, nourish blood, blacken hair, strengthen the body, dissolve turbidity, and lower blood lipid levels (Chinese Pharmacopoeia Commission, 2020). Meanwhile, modern pharmacological research has shown that the main active ingredients of PM are stilbene glycosides, anthraquinones, glycosides, phospholipids, flavonoids and others, which significantly contribute to delaying senescence, preventing cardiovascular diseases, tonifying the kidney and hair, improving intelligence, enhancing immune function, protecting the liver, moistening the intestine, and defecating as well as have antibacterial and antiinflammatory effects (Lin et al., 2015; Liu et al., 2018).

However, since the 1990s, there has been a rapid increase in reports of liver damage caused by PM, which has attracted attention at home and abroad (But et al., 1996; Park et al., 2001; Han et al., 2019). Thereafter, the drug supervision and administration departments of the United Kingdom, Japan, and China successively issued warnings or regulatory measures for the risk of liver damage from PM and its preparations. In fact, the ancient textbook "Ben Cao Hui Yan" recorded "*Polygonum multiflorum*, taste bitter, astringent, flavor mild, slightly toxic." Processed PM can significantly relieve the toxicity and change the efficacy of PM, and a relatively complete processing method for PM was used in the Song dynasty. Modern pharmacological studies have also confirmed that processing can greatly reduce the risk of hepatotoxicity of PM. However, the chemical composition of PM is complex and diverse, and PM mainly includes stilbenes, anthraquinones, anthranone, glycosides, phospholipids, flavonoids, and tannins (Lin et al., 2015; Teka et al., 2021). The issue of which components of PM cause hepatotoxicity remains a major subject that needs to be addressed.

In general, the traditional research approach was to first isolate and identify compounds from PM and then to evaluate the compounds for hepatotoxicity *in vivo* or *in vitro*. This process was time-consuming and laborious but also neglected the synergistic toxic effects of the compounds in PM, so the hepatotoxicity of PM could not be comprehensively evaluated. Therefore, it was imperative to develop an effective scientific strategy to efficiently screen out the toxic components of PM.

In recent years, with the development of high-resolution mass spectrometry (MS) and metabolomics techniques, ultraperformance liquid chromatography-quadrupole-time-of-flight-MS (UPLC-Q-TOF-MS) has made it possible to characterize complex components in PM in a short time, and metabolomics combined with chemometrics has enabled the rapid search for differential markers between raw and processed PM (Liu et al., 2016; Shang et al., 2021). Moreover, spectrum–efficiency relationship research has opened a new window for the evaluation of modern traditional Chinese medicine (TCM), which combines the complex chemical information of TCM with pharmacological efficacy and screens the important features related to the efficacy by means of chemometric statistical methods or machine learning (Zhang et al., 2018; Rao et al., 2022). In particular, great progress has been made in the joint analysis of the spectrum–effect relationship based on fingerprinting and pharmacodynamics for illuminating active ingredient markers in complex TCMs. However, the lack of ultraviolet absorption of many compounds and trace components and the lack of standard reference materials pose serious challenges for absolute quantification. Xu's proposed pseudotargeted metabolomics, establishing a scheduled MRM method for the semiquantification of metabolites, gave us an inspiration of what to do (Luo et al., 2015; Zheng et al., 2020). Compared with previous methods, the established UPLC-coupled scheduled MRM method was a more powerful technique with significant advantages of high sensitivity, wide universality, low matrix effects, and accurate quantification.

In the current study, a stepwise strategy integrating metabolomics and pseudotargeted spectrum–effect relationship was set up to clarify the potential hepatotoxic components in PM (Figure 1). First, the chemical composition of PM was comprehensively characterized

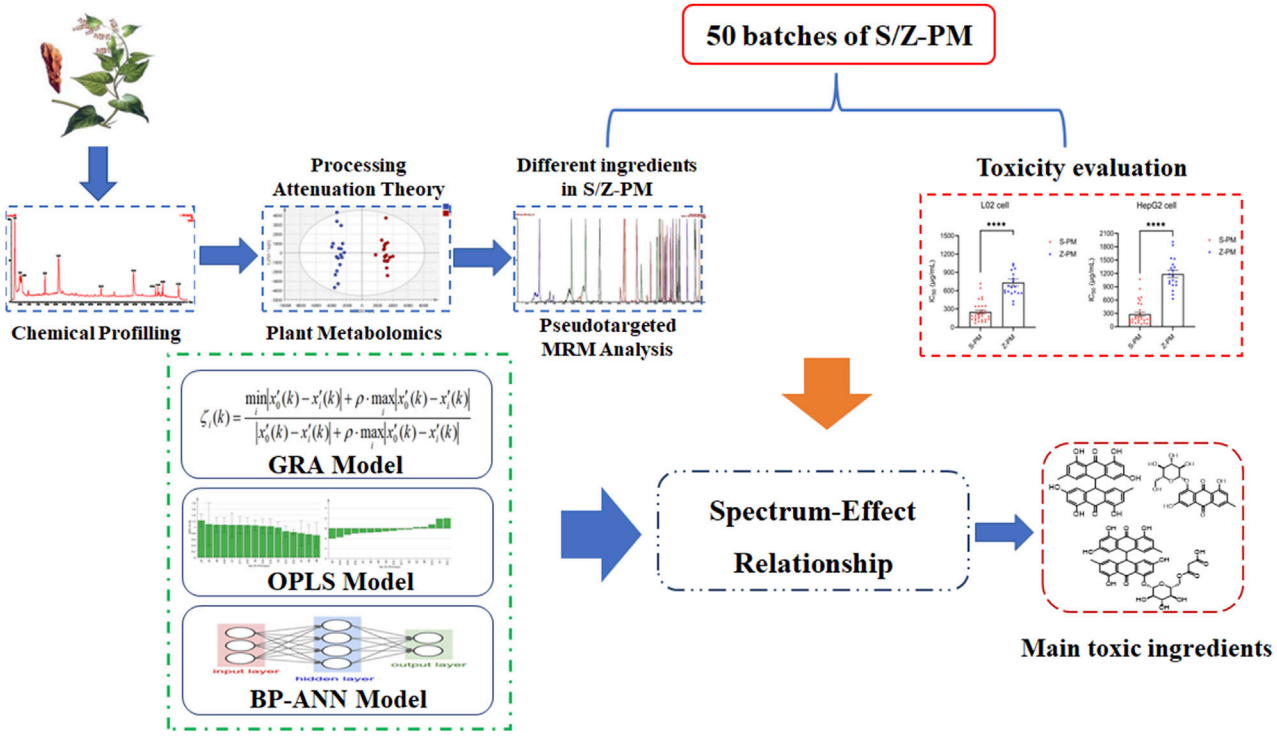

FIGURE 1
Strategy of integrating metabolomics and pseudotargeted spectrum–effect relationship in this study.

using UPLC-Q-TOF-MS. Second, based on the theory of detoxification after PM processing, the distinctive differential components between raw and processed PM were screened out using plant metabolomics. Third, the proposed pseudotargeted MRM semiquantitative profiles of the differential marked components were established in different batches of PM. Fourth, the toxicity of various batches of PM to the hepatocytes L02 and HepG2 was investigated. At last, gray relational analysis (GRA), orthogonal partial least squares (OPLS) analysis, and back propagation artificial neural network (BP-ANN) models were established to correlate the peak areas of pseudotargeted spectra with the IC_{50} values of toxicity to further obtain the hepatotoxic components in PM.

2 Materials and methods

2.1 Materials and reagents

Methanol and acetonitrile of LC/MS grade were obtained from Merck (Darmstadt, Germany). High-performance liquid chromatography–grade ethanol and dimethyl sulfoxide (DMSO) were obtained from Sinopharm Chemical Reagent Co., Ltd (Shanghai, China). Ultra-pure water was prepared using a Milli-Q system (Billerica, MA, United States). Standard products of stilbene glycoside, emodin, etc., were provided by the China National Institute for Food and Drug Control. Physcion-8-*O*-*β*-D-glucopyranoside, physcion-1-*O*-*β*-D-glucopyranoside, and aloe-emodin-3-hydroxymethyl-*β*-D-glucopyranoside were purchased from Standard Technology Co., Ltd (Shanghai, China). The purity of all standards was above 98%. Formic acid was acquired from Tokyo Chemical Industry Co., Ltd. (Tokyo, Japan). A 0.22-μm filter membrane was purchased from Dikema Technology Co., Ltd. (Beijing, China).

The hepatic cell lines HepG2 and L02 were obtained from the cell bank of the Chinese Academy of Sciences (Shanghai, China). Dulbecco's Modified Eagle Medium (DMEM) and Roswell Park Memorial Institute (RPMI) 1640 culture medium (Biological Industries, Israel), fetal bovine serum (FBS; Biosera, France), 1% penicillin-streptomycin (Targetmol, China), and 0.25% trypsin-ethylenediaminetetraacetic acid (Wisent, Canada) were used for cell culture. Staurosporine (STSP) and CCK-8 reagent were obtained from Targetmol (Shanghai, China). A total of 384 cell culture plates were purchased from Jet Bio-Filtration Co., Ltd. (Guangzhou, China). The Victor Nivo multimode plate reader was from PerkinElmer (Shanghai, China).

Sample A: 36 batches of raw and processed PM from different origins or batches. In total, 0.1 g was taken from each batch to make 10 portions of mixed samples as quality control (QC). Sample B: 30 batches of raw PM and 20 batches of processed PM. Samples A and B all met the requirements of the Chinese pharmacopoeia. The samples were stored at the China National Institute for Food and Drug Control (Beijing, China). Detailed sample information can be found in Supplementary Tables S1, S2.

2.2 Sample and standard solution preparation

Sample A (46 samples in total, filtered through a No. 3 sieve): The sample (1.0 g) was weighed precisely and placed in a 50-mL conical flask. Then, 50 mL of 70% ethanol was added, and the mixture was weighed, sonicated for 30 min, cooled, and replenished. The extracted solution was collected for UPLC-Q-TOF-MS analysis.

The standard solution was prepared by weighing 1 mg of standard powder and adding 2 ml of methanol solution to dissolve it for the qualitative test. All standard and sample solutions were filtered through 0.22-μm Millipore filtration before injection.

Sample B (50 samples): 20 g of PM was weighed and extracted with 300 ml of 70% ethanol three times for 30 min each time. Then, the extracted solutions were combined and concentrated under pressure and subsequently freeze-dried to powder. The dry extract powder weighing 40 mg was dissolved in 40 ml of 70% ethanol solution for UPLC-qqq-MS/MS analysis. Of note, 30 mg of dried extract powder was weighed precisely and prepared as a storage solution of 200 mg/ml. Then, a series of concentrations of working solutions (1,000, 400, 160, 64, 25, 10, and 4 μg/ml) was obtained by gradient dilution with culture medium for the *in vitro* cytotoxicity assay.

2.3 Ultraperformance liquid chromatography-quadrupole-time-of-flight-mass spectrometry analysis

2.3.1 Chemical composition characterization

The extract solution of the PM mixed sample in sample A was analyzed using UPLC-Q-TOF-MS. Analysis was performed using an Acquity™ UPLC Class I system equipped with a photodiode array (PDA) detector and Q-TOF SYNAPTG2-Si (Waters, Manchester, United States). Chromatographic conditions: The temperature of the column and autosampler was maintained at 40°C and 6°C. The flow rate was 0.3 ml/min, and the injection volume was 1 μl. The binary mobile phase contained solvent A (0.1% FA in deionized water, v/v) and solvent B (methanol, LC-MS grade). The peptides of the elution gradient were initial 10% B, linear gradient 40% B (22 min), 70% B (33 min), 100% B (44–46 min), 10% B (46.2 min), and holding 10% B to 50 min. The PDA detector used 3D range from 190 to 400 nm. MS conditions: The UPLC-MS system was operated in the negative ion and MS^E data acquisition mode. Experimental parameters were set as follows: capillary voltage at −2.5 kV (ESI^-); source temperature at 115°C; cone voltage at 40 V; ramp trap MS collision energy of 20–50 V; desolvation temperature at 450°C; cone gas flow of 50 L/h; desolvation gas flow of 900 L/h; and scan range of *m/z* 50–1,500 Da. At the same time, an external reference consisting of 1.0 ng/ml solution of leucine enkephalin was used to produce a reference ion at *m/z* 554.2615 Da ($[M-H]^-$) in negative ion mode for real-time mass correction during acquisition. The obtained mass spectrometric data were analyzed using UNIFI software in combination with a self-built database of PM compounds and reference standards as well as fragment ion matching strategies to fully characterize the components of PM.

2.3.2 Plant metabolomics analysis

Processed sample A ($n = 46$) was analyzed using UPLC-Q-TOF-MS under the same chromatographic and mass spectrometric conditions as in Section 2.3.1. The acquired data were further deconvolved into a data matrix (Rt-*m/z*-intensity) by Progenesis QI software (Waters, Milford, MA, United States). After further data preprocessing, chemometric (principal component analysis (PCA), PLS-DA, OPLS-DA) analysis was performed using Simca-P 14.1 software. Combining univariate statistical analysis of *P* and FC values with multivariate statistical analysis of VIP values further screened out the differential ions between raw and processed PM.

2.4 Ultraperformance liquid chromatography-qqq-MS/MS analysis

2.4.1 Scheduled MRM method development

The scheduled MRM ion pairs were established based on the differential ions and secondary fragment ions of PM from the results of Section 2.3.2. Then, combined with the composition identification results of PM, the MRM ion pairs were further confirmed, and the proposed pseudotarget MRM method was constructed. This method was used to perform semiquantitative analysis in sample B, and the peak area data of the marker components were acquired.

The analysis of samples was performed using a Waters Acquity™ UPLC I-Class system equipped with a Xevo TQ-XS mass spectrometer (Waters, Milford, MA, United States). The chromatographic column and chromatographic separation conditions were the same as the conditions of the previous

TABLE 1 Optimized ion pairs and CV and CE parameters of 16 compounds.

No.	Compounds	Ion pair (*m/z*)	CV	CE
X1	Catechin	289.07 > 203.07	30	29
X2	Epicatechin	289.07 > 203.07	30	29
X3	Torachrysone-8-*O*-*β*-D-glucopyranoside	407.13 > 245.08	30	33
X4	7-acetyl-3,8-dihydroxy-6-methyl-1-naphthyl-*β*-D-glucopyranoside	393.12 > 231.06	30	33
X5	Epicatechin-3-*O*-gallate	441.08 > 289.07	30	34
X6	Emodin-8-*O*-*β*-D-glucopyranoside	431.1 > 269.04	30	34
X7	Emodin bianthrones	509.12 > 253.75	30	31
X8	Emodin-physcion bianthrones	523.14 > 253.83	30	30
X9	Physcion bianthrones	537.15 > 254.73	30	41
X10	2,3,5,4′-tetrahydroxystilbene-2-*O*-*β*-D-(2-*O*-monogalloylesters)-glucopyranoside	557.13 > 243.06	30	30
X11	polygonibene E	581.16 > 243.06	30	30
X12	Polygonumnolides C1-C4	671.18 > 416.11	30	26
X13	Polygonumnolides A1-A4	685.19 > 416.11	30	26
X14	PM 14-17	757.17 > 458.12	30	31
X15	PM 22-25	933.24 > 458.12	30	33
X16	PM 5	919.23 > 458.12	30	33

UPLC-Q-TOF-MS method. The optimal MS conditions were as follows: capillary voltage at 2.5 kV under negative mode; source temperature at 150°C; desolvation gas temperature at 500°C; desolvation gas flow at 850 L/h; and cone gas flow at 150 L/h. Ion pairs and CV and CE parameters are detailed in Table 1.

The pseudotargeted MRM method was applied for semiquantitative comparison of PM samples (raw PM: S1-S30, processed PM: Z1-Z20).

2.4.2 Method validation

The developed UPLC-MS/MS method was validated with sample Z-1 as an example in terms of specificity, repeatability, precision, linearity, and stability. Specificity was evaluated by comparing samples with the negative control. Repeatability evaluation was carried out by analyzing six replicate samples independently. Precision was investigated by six consecutive injections of the same sample. Linearity was constructed by fitting the peak area of each compound under the injection of 0.5, 1, 1.5, 2, 2.5, and 3 μl of one sample. The same sample was injected at 0, 6, 12, 24, and 30 h to verify the stability. The relative standard deviation (RSD) of the peak area of the characteristic peaks was used to evaluate the results.

2.5 Hepatotoxicity assay *in vitro*

Two types of hepatocytes, L02 and HepG2, were used to assess the hepatotoxicity of PM extract *in vitro*. L02 and HepG2 cells were inoculated in 384-well cell plates (density: HepG2 1,000 cells/well; L02 800 cells/well) with 40 μl of cell suspension per well and were incubated overnight at 37°C in a 5% CO_2 incubator. HepG2 cells were cultured in DMEM containing 10% FBS and 100 U/mL penicillin and streptomycin, while L02 cells were cultured in RPMI 1640 medium. On the day of the experiment, 10 μl of compound working solution (sample B, PM extracting solution of 0.064, 0.32, 1.6, 8, 40, 200, and 1,000 μg/ml) was added to each well according to the experimental requirements, and this was cultivated at 37°C for 72 h with 5% CO_2 shielded from light. At the end of the incubation, 5 μl of CCK8 reagent was added to the cell plates, and this were incubated for 4 h with 5% CO_2 at 37°C. The absorbance at 450 nm was measured, and the inhibition rate was calculated according to the following equation:

$$\text{Inhibition ratio (\%)} = (OD_S - OD_{NC})/(OD_{STSP} - OD_{NC}) \times 100\%$$

where OD_S stands for the absorbance of the working solution (cell + medium + compound to be tested); OD_{NC} stands for the absorbance of the negative control (cell + medium + DMSO); and OD_{STSP} stands for the absorbance of the positive control (cell + medium + 10 μM STSP).

According to the inhibition ratios of the compounds, the IC_{50} values (the concentration corresponding to 50% of the maximum inhibition response) were calculated from the dose–response curves using GraphPad Prism 9.0. The experiment was performed three times in parallel, and finally, the mean IC_{50} value was obtained for each sample.

2.6 Spectrum–effect relationship analysis

2.6.1 Gray relational analysis

GRA is a method to determine the degree of association between factors based on the similarity of the geometry of the change curves in each factor. As a simple and effective method, GRA has been widely used in the evaluation of spectrum–effect relationship in TCM (Wang et al., 2018; Ma et al., 2020). In this study, the peak area of each feature was taken as the comparison series, and the $1/IC_{50}$ value of the cytotoxicity assessment index was defined as the reference series (all the original data were dimensionless and processed before analysis). The correlation coefficients between the reference series values and each comparison series were calculated, and the average value of the gray correlation coefficient was obtained, which was the gray correlation degree. The influence degree of each characteristic variable on hepatocyte toxicity was evaluated by comparing the gray correlation degrees.

2.6.2 Orthogonal partial least squares analysis

OPLS, a special type of multiple linear regression model, was used to find the relationship between two matrices X and Y by considering orthogonal signal correction based on partial least squares regression (Liang et al., 2017; Liao et al., 2020). In this study, an OPLS model was constructed to characterize the correlation between the hepatotoxicity index IC_{50} and the chemical peaks. The peak area of each characteristic ion was used as the independent variable X, and the IC_{50} value was used as the dependent variable Y. In SIMCA 14.0.1 (Umetrics AB, Umea, Sweden), the VIP and regression coefficients were used to find the main characteristic components that were significantly correlated with hepatotoxicity.

2.6.3 Back propagation artificial neural network analysis

The BP-ANN algorithm is a nonlinear mathematical model based on the structure of neural synaptic connections in the brain. The BP neural network is a kind of multilayer feedforward neural network trained by the error back propagation algorithm and has been one of the most widely used neural network models (Jiang et al., 2018; Shi et al., 2018). The BP neural network can connect the input and output parameters and can continuously modify the weights and biases of each layer through iterative learning to minimize the overall error of the output layer. To screen representative hepatotoxic components from different perspectives, we used MATLAB R2019b (Mathworks, Natick, NJ, United States) to build the BP-ANN model for the association of chromatographic peaks with hepatotoxicity IC_{50}. The BP neural network was established using the characteristic peak area as the input layer neuron, the IC_{50} value as the output layer neuron, the hidden layer of one layer, and the hidden layer node number optimization as 10. Moreover, two parameters were used to evaluate the importance of the variables in the neural network.

MIV was considered to be one of the best indices for evaluating the correlation of variables in the neural network (Xu et al., 2013). The sign of the MIV value represents the direction of the correlation, and the absolute value reflects the importance of the impact. Sensitivity analysis was another important method for evaluating the connection weights in ANN models (Wang et al., 2017; Qiao et al., 2021). The contribution ratios of the characteristic peaks to the cytotoxicity index IC_{50} were calculated by connection weights. The Garson equation was applied to show the relative influence of the independent variables on the dependent variable. The equation was as follows:

$$P_{ac} = \frac{\sum_{b=1}^{N}\left(\frac{|w_{ab}|}{\sum_{d=1}^{M}|w_{dj}|}|e_{bv}|\right)}{\sum_{a=1}^{M}\left(\sum_{b=1}^{N}\left(\frac{|w_{ab}|}{\sum_{d=1}^{M}|w_{dj}|}|e_{bv}|\right)\right)}$$

where P stands for the percentage influence of input neurons, w indicates the weight between input and hidden neurons, e indicates the weight between hidden and output neurons, M indicates the number of input neurons, N indicates the number of hidden neurons, and v indicates the number of output neurons.

3 Results

3.1 Characterization of chemical components in *Polygonum multiflorum*

Based on the literature summary and self-built compound library, the main components of PM are stilbenes and anthraquinones. In addition, PM includes flavonoids, lignans, dianthrones, phospholipids, and polysaccharides. Comparing the negative ion response with the positive ion response, the negative ion mode had more peaks and a much stronger response, so negative ion scan was selected for detection (Supplementary Figure S1). Moreover, the peak profiles of PM between raw and processed PM were basically consistent (Supplementary Figure S2), indicating that processing does not change the types of compounds in PM but the relative content of compounds. Considering the differences in the chemical composition of PM from different batches and origins, a mixed sample was chosen for qualitative analysis. The chromatographic column, mobile phase, elution conditions, and MS conditions were further optimized. A total of 112 components were detected and preliminarily identified through self-built database matching, comparison with standard products and the literature, and fragment ion deduction (Table 2). These tentative compounds could be classified into four types according to the structural

TABLE 2 Ultraperformance liquid chromatography-quadrupole-time-of-flight-mass spectrometry identification results of chemical constituents of *Polygonum multiflorum*.

No	Observed RT (min)	Molecular formula	Component name	Observed *m/z*	Expected *m/z*	Mass error (ppm)	Fragment
1d	1.03	$C_4H_6O_4$	Butanedioic acid	117.0190	117.0193	−3.22	71.0138; 59.0137; 55.0187
2d	1.05	$C_6H_8O_4$	2,3-di-hydro-3,5-dihydroxy-6-methyl-4(*H*)-pyran-4-one	143.0350	143.0349	0.12	129.0187; 96.9687; 114.0557; 78.9591
3d	1.20	$C_7H_6O_5$	Gallic acid	169.0147	169.0142	2.44	125.0246; 96.9687; 110.0254
4d	1.41	$C_{13}H_{16}O_{10}$	Gallic acid-*O*-glucoside	331.0654	331.0665	−3.32	169.0107; 125.0221
5d	1.53	$C_6H_{13}NO_2$	Leucine	130.0871	130.0868	2.31	88.0363; 85.0303
6d	2.25	$C_6H_8O_7$	Citric acid	191.0201	191.0197	2.05	128.0355; 111.0086; 87.0088; 85.0294
7d	2.45	$C_{15}H_{14}O_7$	Gallocatechin	305.0673	305.0666	2.09	213.1246; 241.0027; 125.0245; 96.9604
8d	3.16	$C_{13}H_{16}O_9$	Protocatechuic acid-*O*-glucoside	315.0697	315.0716	−6.03	153.0177; 195.0297; 111.0094
9d	3.82	$C_{11}H_9NO_2$	2-vinyl-1*H*-indole-3-carboxylic acid	186.0545	186.0555	−5.37	142.0658
10c	4.07	$C_{30}H_{26}O_{12}$	Procyanidin B	577.1358	577.1351	1.10	289.0716; 559.1279; 451.1047; 407.0772; 125.0243
11c	4.22	$C_{15}H_{10}O_7$	Quercetin	301.0355	301.0354	0.56	257.0455; 125.0243; 285.0397; 179.0243
12c	4.88	$C_{15}H_{14}O_6$	Catechin	289.0721	289.0717	1.02	271.0553; 245.0812; 137.0244; 123.0450
13d	5.24	$C_8H_8O_4$	Vanillic acid	167.0351	167.0344	4.19	137.0259; 123.0426
14d	5.83	$C_7H_6O_2$	*P*-hydroxybenzaldehyde	121.0296	121.0295	0.99	93.0341
15b	6.54	$C_{21}H_{22}O_{11}$	Rumejaposide D	449.1088	449.1089	−0.15	259.0612; 255.0660; 125.0242; 407.0769; 368.0900
16d	7.31	$C_{11}H_{10}O_3$	Altechromone A	189.0560	189.0557	1.51	147.0448; 124.0157
17c	7.92	$C_{15}H_{14}O_6$	Epicatechin	289.0718	289.0717	0.28	243.0660; 125.0244
18c	8.03	$C_{37}H_{30}O_{16}$	3-*O*-galloyl-procyanidin B2	729.1465	729.1461	0.54	499.1267; 589.1452; 247.0619; 243.0660; 125.0244
19b	8.58	$C_{14}H_{18}O_{10}$	2,3,4,6-tetrahy-droxyacetophenone-3-*O*-*β*-D-glucoside	345.0832	345.0827	1.44	182.0225; 242.0577; 287.0560; 125.0246; 96.9606
20c	8.67	$C_{30}H_{26}O_{12}$	Isomer-Procyanidin B	577.1351	577.1351	-0.12	439.1056; 289.0715; 345.0818; 182.0225
21b	9.12	$C_{26}H_{32}O_{14}$	Isomer-2,3,5,4′-tetrahydroxystilbene-2,3-di-*O*-*β*-D-glucopyranoside	567.1719	567.1719	0.01	405.1186; 387.1069; 241.0503; 281.0445
22d	9.61	$C_{17}H_{20}O_9$	7-hydroxy-3,4-dimethylcoumarin-5-*O*-*β*-D-glucopyranoside	367.1029	367.1034	−1.45	243.0665; 225.0554; 109.0293
23b	9.61	$C_{20}H_{22}O_9$	*Cis*-2,3,5,4′-tetrahydroxystilbene-2-*O*-*β*-D-glucoyranoside	405.1193	405.1191	0.52	243.0665; 189.0560; 137.0245; 93.0344
24c	10.01	$C_{35}H_{34}O_{15}$	Polygonflavanol A	693.1821	693.1825	-0.61	549.1604; 287.0560; 259.0612; 125.0244; 241.0504
25a	10.91	$C_{15}H_{12}O_4$	Emodin anthrone	255.0660	255.0662	−1.29	137.0241; 109.0288; 93.0345
26a	10.92	$C_{22}H_{26}O_8$	1,3-dihydroxy-6,7-dimethylxanthone-1-*O*-*β*-D-glucopyranoside	417.1184	417.1555	−1.75	259.0609; 255.0659; 109.0288; 137.0242
27a	11.08	$C_{20}H_{22}O_{10}$	6-methoxyl-2-acetyl-3-methyl-1,4-naphthoquinone-8-*O*-*β*-D-glucopyranoside	421.1137	421.1140	−0.73	407.0767; 259.0610; 255.0660; 213.0555

(Continued on following page)

TABLE 2 (*Continued*) Ultraperformance liquid chromatography-quadrupole-time-of-flight-mass spectrometry identification results of chemical constituents of *Polygonum multiflorum*.

No	Observed RT (min)	Molecular formula	Component name	Observed *m/z*	Expected *m/z*	Mass error (ppm)	Fragment
28c	11.11	$C_{44}H_{34}O_{20}$	3,3′-di-*O*-galloyl-procyanidin B2	881.1582	881.1571	1.24	729.1451; 513.1201; 407.0767; 273.0391
29a	11.18	$C_{16}H_{10}O_7$	Carboxyl emodin	313.0344	313.0348	−1.28	269.0433; 243.0634; 169.0107
30c	11.65	$C_{22}H_{18}O_{10}$	Epicatechin-3-*O*-gallate	441.0828	441.0827	0.16	289.0714; 169.0145; 125.0245
31c	11.75	$C_{15}H_{10}O_6$	Kaempferol	285.0402	285.0404	−1.08	193.0142; 125.0245
32d	11.89	$C_{28}H_{38}O_{13}$	(+)-lyoniresinol-3-*O*-*β*-D-glucopyranoside	581.2239	581.2240	−0.15	549.1606; 521.1300; 387.1072; 253.0081
33b	12.22	$C_{22}H_{24}O_{10}$	2,3,5,4′-tetrahydroxystilbene-2-*O*-(6-*O*-acetyl)-*β*-D-glucopyranoside	447.1288	447.1296	-1.88	259.0608; 227.0713; 185.0608
34b	12.70	$C_{26}H_{32}O_{14}$	2,3,5,4′-tetrahydroxystilbene-2,3-di-*O*-*β*-D-glucopyranoside	567.1724	567.1719	0.84	405.1179; 269.0455; 243.0664; 225.0553
35a	13.16	$C_{16}H_{12}O_6$	Fallacinol	299.0558	299.0561	−1.15	286.0480; 253.0495; 161.0243; 179.0354
36b	13.21	$C_{26}H_{34}O_{11}$	*β*-D-glucoside,4-[2,3-dihydro-3-(hydroxymethyl)-5-(3-hydroxypropyl)-7-methoxy-2-yl]-2-methoxypheny	521.2054	521.2023	5.95	359.1455; 313.1039; 243.0634
37a	13.26	$C_{21}H_{22}O_{11}$	Isomer-rumejaposide D	449.1090	449.1089	0.19	379.0815; 169.0145; 165.0558; 286.0480
38b	13.51	$C_{60}H_{66}O_{27}$	Multiflorumiside L/K	1,217.3710	1,217.3718	−0.68	811.2458; 646.1675; 243.0665; 405.1189
39b	13.52	$C_{20}H_{22}O_9$	*Trans*-2,3,5,4′-tetrahydroxystilbene-2-*O*-*β*-D-glucopyranoside	405.1191	405.1191	-0.08	243.0665; 225.0554; 109.0293; 215.0713
40a	14.08	$C_{47}H_{46}O_{22}$	PM 12-13	961.2381	961.2408	−2.79	693.1812; 503.1164; 555.1137; 393.0609; 839.2375
41b	14.47	$C_{19}H_{20}O_8$	2,3,5,4′-tetrahydroxystilbene-2-*O*-*β*-D-xyloside	375.1080	375.1085	−1.54	243.0665; 225.0553; 109.0291
42b	14.61	$C_{27}H_{26}O_{13}$	2,3,5,4′-tetrahydroxystilbene-2-*O*-*β*-D-(2-*O*-monogalloyl esters)-glucopyranoside	557.1310	557.1301	1.70	243.0666; 241.0504; 313.0567; 405.1189; 125.0243
43c	15.54	$C_{21}H_{20}O_{12}$	Quercetin 3-*β*-D-glucopyranoside	463.0860	463.0882	−4.81	405.1171; 303.0514; 379.0815; 269.0456
44c	15.60	$C_{15}H_{12}O_7$	Dihydroquercetin	303.0477	303.0505	−9.24	153.0177; 125.0221
45d	15.84	$C_{17}H_{17}NO_4$	*Trans*-*N*-caffeoyltyramine	298.1084	298.1084	−0.28	169.0836; 227.0710; 135.0450
46b	16.45	$C_{27}H_{26}O_{13}$	2,3,5,4′-tetrahydroxystilbene-2-*O*-*β*-D-(3-*O*-monogalloyl esters)-glucopyranoside	557.1310	557.1301	1.77	243.0664; 313.0567; 405.1180; 467.1097; 125.0244
47b	16.59	$C_{27}H_{26}O_{12}$	2,3,5,4′-tetrahydroxystilbene-2-*O*-*β*-D-(2″-*O*-galloyl)-glucopyranoside	541.1355	541.1352	0.65	243.0664; 313.0567; 169.0145; 405.1180; 467.1097
48b	16.82	$C_{14}H_{12}O_3$	Resveratrol	227.0716	227.0713	1.04	181.0648; 143.0502; 135.0446; 117.0344
49b	17.53	$C_{27}H_{26}O_{12}$	*β*-Glucopyranoside, 3-hydroxy-5-[(1*E*)-2-(4-hydroxyphenyl)ethenyl]phenyl, 2-(3,4,5-trihydroxybenzoate)	541.1351	541.1352	−0.05	485.1242; 313.0564; 169.0145
50d	18.00	$C_{19}H_{22}O_9$	7-acetyl-3,8-dihydroxy-6-methyl-1-naphthyl-*β*-D-glucopyranoside	393.1190	393.1191	−0.24	273.0767; 231.0665; 295.0583; 161.0245
51b	18.47	$C_{22}H_{24}O_{10}$	Polygonibene D	447.1292	447.1296	−1.06	255.0660; 243.0664; 241.0502
52c	19.63	$C_{23}H_{24}O_{12}$	Tricin 7-*O*-*β*-D-glucoside	491.1191	491.1195	−0.74	

(Continued on following page)

TABLE 2 (*Continued*) Ultraperformance liquid chromatography-quadrupole-time-of-flight-mass spectrometry identification results of chemical constituents of *Polygonum multiflorum*.

No	Observed RT (min)	Molecular formula	Component name	Observed *m/z*	Expected *m/z*	Mass error (ppm)	Fragment
							269.0451; 313.0553; 148.0526; 355.0447; 439.0652
53d	19.75	$C_{18}H_{19}NO_4$	*N-trans*-feruloyltyramine	312.1240	312.1241	−0.29	274.0120; 269.0451; 178.0516; 148.0526; 123.0452
54a	19.94	$C_{22}H_{26}O_{10}$	Torachrysone-8-*O*-(6′-*O*-acetyl)-*β*-D-glucopyranoside	449.1447	449.1453	−1.39	393.0615; 274.0120; 245.0815; 230.0584; 349.0699
55b	20.13	$C_{29}H_{28}O_{12}$	Tetrahydroxystilbene-*O*-(caffeoyl)-glucopyranoside	567.1498	567.1503	−0.88	243.0634; 405.1207
56b	20.40	$C_{20}H_{22}O_8$	Polydatin	389.1237	389.1242	−1.19	283.0608; 227.0711
57d	20.50	$C_{19}H_{21}NO_5$	*N*-trans-feruloyl-3-methyldopamine	342.1341	342.1347	−1.61	313.0546; 227.0711; 255.0656; 148.0524
58b	20.75	$C_{21}H_{24}O_8$	Desoxyrhaponticin	403.1392	403.1398	−1.62	349.0708; 269.0453; 225.0552; 151.0037
59b	21.65	$C_{30}H_{30}O_{12}$	Polygonibene G	581.1662	581.1665	−0.39	419.1125; 295.0600; 389.1015; 125.0244
60a	21.85	$C_{21}H_{20}O_{10}$	Aloe-emodin-3-(hydroxymethyl)-*O*-*β*-D-glucopyranoside	431.0987	431.0983	0.70	240.0428; 325.0707; 268.0372; 299.0561
61a	22.11	$C_{23}H_{22}O_{11}$	Emodin-8-*O*-(6′-*O*-acetyl)-*β*-D-glucopyranoside	473.1093	473.1089	0.88	269.0459; 225.0558
62b	22.60	$C_{29}H_{28}O_{11}$	2,3,5,4′-tetrahydroxystilbene-2-*O*-*β*-D-(2″-O-coumaroyl)-glucoside	551.1545	551.1553	−1.45	389.1003; 241.9957; 405.1207
63b	22.90	$C_{30}H_{30}O_{12}$	Polygonibene E	581.1669	581.1665	0.83	405.1184; 243.0663; 256.0375
64a	22.95	$C_{25}H_{32}O_{13}$	Polygonimitin E	539.1765	539.1770	−0.91	405.1184; 243.0663; 256.0375; 489.1212; 175.0400
65d	23.09	$C_{36}H_{36}N_2O_8$	Cannabisin D	623.2389	623.2399	−1.66	389.1026; 245.0814; 225.0555
66a	23.73	$C_{20}H_{24}O_9$	Torachrysone-8-*O*-*β*-D-glucopyranoside	407.1346	407.1347	−0.39	245.0820; 230.0587; 215.0352
67a	24.05	$C_{16}H_{12}O_6$	Citreorosein-8-methyl ether	299.0556	299.0561	−1.80	255.0656; 243.0660; 213.0552; 160.0162
68a	24.74	$C_{16}H_{12}O_5$	Emodin-8-methyl ether	283.0611	283.0612	−0.51	240.0426; 175.0400; 145.0296
69c	24.96	$C_{21}H_{20}O_{11}$	Quercetin-3-*O*-rhamnoside	447.0931	447.0933	−0.45	285.0399; 313.0546; 337.0788; 361.0725; 245.0810
70a	25.40	$C_{15}H_{10}O_5$	Isomer-emodin	269.0458	269.0455	0.26	93.03439; 185.0607
71a	25.62	$C_{21}H_{20}O_{10}$	Emodin-8-*O*-*β*-D-glucopyranoside	431.0985	431.0983	0.34	269.0459; 225.0559
72a	26.09	$C_{45}H_{44}O_{21}$	PM 5	919.2315	919.2302	1.35	875.2393; 713.1859; 458.1210; 416.1108
73a	27.03	$C_{45}H_{44}O_{21}$	Isomer-PM 5	919.2303	919.2302	0.07	875.2387; 713.1860; 458.1215
74d	27.22	$C_{36}H_{36}N_2O_8$	(+)-Grossamide	623.2395	623.2399	−0.57	269.0458; 243.0660; 416.1106
75c	27.32	$C_{17}H_{14}O_7$	Tricin	329.0660	329.0666	−2.13	243.0660; 313.0484; 161.0246; 254.0583
76a	27.72	$C_{22}H_{22}O_{10}$	Physcion-1-*O*-*β*-D-glucopyranoside	445.1135	445.1140	−1.15	283.0611; 240.0426; 145.0295; 387.0501
77a	28.11	$C_{15}H_{10}O_6$	Citreorosein	285.0410	285.0404	1.78	

(Continued on following page)

TABLE 2 (*Continued*) Ultraperformance liquid chromatography-quadrupole-time-of-flight-mass spectrometry identification results of chemical constituents of *Polygonum multiflorum*.

No	Observed RT (min)	Molecular formula	Component name	Observed *m/z*	Expected *m/z*	Mass error (ppm)	Fragment
							257.0455; 241.0503; 224.0477; 195.0452; 183.0452
78a	28.46	$C_{17}H_{14}O_5$	1,6-dimethyl ether-emodin	297.0765	297.0768	−1.06	283.0612; 269.0458; 240.0428
79a	28.51	$C_{22}H_{22}O_{10}$	Physcion-8-*O*-*β*-D-glucopyranoside	445.1138	445.1140	−0.40	283.0612; 240.0428; 225.0552; 148.0529
80a	28.80	$C_{22}H_{26}O_{10}$	Isomer-torachrysone-8-*O*-(6′-*O*-acetyl)-*β*-D-glucopyranoside	449.1450	449.1453	−0.66	255.0658; 245.0815; 230.0584; 359.0909; 159.0445
81a	29.00	$C_{21}H_{20}O_{11}$	Citreorosein-*O*-glucoside	447.0931	447.0933	-0.50	243.0659; 211.1340; 329.2333; 125.0245
82a	30.92	$C_{16}H_{12}O_5$	Isomer-physcion	283.0611	283.0612	−0.39	269.0454; 239.0326
83a	31.52	$C_{45}H_{46}O_{19}$	PM 26-27	889.2553	889.2561	−0.80	847.2462; 701.1841; 458.1212; 416.1108; 254.0580
84a	33.16	$C_{17}H_{12}O_6$	2-Acetyl-emodin	311.0562	311.0561	0.15	283.0606; 269.0457; 240.0429
85a	33.40	$C_{37}H_{34}O_{13}$	Polygonumnolide E	685.1922	685.1927	−0.73	671.1752; 416.1109; 309.1735; 254.0586
86a	34.64	$C_{15}H_{10}O_4$	Chrysophanol	253.0498	253.05	−1.19	225.0545
87a	34.74	$C_{15}H_{10}O_5$	Emodin	269.0459	269.0455	1.32	225.0560; 241.0505; 197.0608
88a	36.87	$C_{30}H_{22}O_8$	*Trans*/*cis*-emodin dianthrones	509.1245	509.1242	0.58	254.0582; 225.0545
89a	37.13	$C_{15}H_{10}O_6$	Lunatin	285.0404	285.0404	−0.26	269.0457; 241.0501; 199.1704
90a	37.17	$C_{16}H_{12}O_5$	Physcion	283.0609	283.0612	−0.96	269.0456; 256.0362; 240.0422
91a	38.69	$C_{31}H_{24}O_8$	*Trans*/*cis*-emodin-physcion dianthrones	523.1395	523.1398	−0.68	254.0583
92a	40.37	$C_{32}H_{26}O_8$	*Trans*/*cis*-physcion dianthrones	537.1541	537.1555	−2.60	243.0661; 437.3076; 339.1998
93d	41.55	$C_{16}H_{32}O_2$	Tetradecanoic acid ethyl ester	255.2333	255.2329	1.31	205.1602; 96.9602
94d	42.22	$C_{17}H_{34}O_2$	Hexadecanoic acid methyl ester	269.2485	269.2486	−0.47	177.9736; 129.9760; 221.0857
95d	42.92	$C_{18}H_{36}O_2$	Hexadecanoic acid ethyl ester	283.2645	283.2642	0.75	183.0122; 99.0194; 163.1127
96d	43.13	$C_{20}H_{38}O_2$	Ethyl oleate	309.2796	309.2799	−1.11	163.1127; 177.1283; 223.0358; 227.2015
97d	43.47	$C_{19}H_{38}O2$	Octadecanoic acid methyl ester	297.2796	297.2799	−0.89	241.0502; 119.9469
98d	44.01	$C_{20}H_{40}O_2$	Octadecanoic acid ethyl ester	311.2956	311.2955	0.15	229.1596; 163.1130; 130.9451
99b	12.37; 13.19	$C_{41}H_{46}O_{19}$	(unknown) Dimer of stilbene glycoside	841.2562	841.2561	0.12	647.1770; 485.1239; 259.0608; 227.0713; 125.0243
100b	15.12; 16.18; 17.64; 18.56	$C_{40}H_{42}O_{18}$	(Isomer) Multiflorumiside A1/B1	809.2308	809.2298	1.15	647.1773; 719.1815; 485.1239; 467.1109; 267.0651
101b	19.90; 20.67	$C_{27}H_{24}O_{13}$	Polygonumoside A/B	555.1154	555.1144	1.86	393.0615; 274.0120; 245.0815; 230.0584; 349.0699
102b	21.48; 22.52	$C_{40}H_{42}O_{18}$	Polygonibene A/B/C	809.2295	809.2298	−0.44	647.1766; 485.1236; 255.0657; 405.1174; 125.0244

(Continued on following page)

TABLE 2 (*Continued*) Ultraperformance liquid chromatography-quadrupole-time-of-flight-mass spectrometry identification results of chemical constituents of *Polygonum multiflorum*.

No	Observed RT (min)	Molecular formula	Component name	Observed *m/z*	Expected *m/z*	Mass error (ppm)	Fragment
103a	24.52; 29.27	$C_{23}H_{22}O_{11}$	Isomer-emodin-8-*O*-(6′-*O*-acetyl)-*β*-D-glucopyranoside	473.1091	473.1089	0.26	269.0454; 225.0552; 167.0349
104a	25.27; 26.92; 27.67; 28.47	$C_{46}H_{46}O_{21}$	PM 22-25	933.2457	933.2459	−0.15	889.2548; 809.2265; 703.1669; 458.1210; 283.0611
105a	27.37; 30.01	$C_{42}H_{42}O_{18}$	PM 1-4	833.2306	833.2298	0.90	671.1764; 431.0980; 416.1110; 175.0398; 254.0583
106a	28.64; 29.77; 30.41	$C_{39}H_{34}O_{16}$	PM 14-17	757.1769	757.1774	−0.68	713.1868; 458.1210; 269.0458; 225.0552
107a	29.52; 30.89; 31.57	$C_{43}H_{44}O_{18}$	Polygonumnolides B1-B3	847.2463	847.2455	0.99	707.1738; 685.1909; 416.1108; 283.0607; 240.0428
108a	30.86; 31.06; 31.24; 31.49	$C_{40}H_{36}O_{16}$	PM 30-33	771.1927	771.1931	−0.51	458.1212; 398.0987; 416.1109; 285.0400; 254.0580
109a	32.04; 32.27; 33.51; 33.99	$C_{36}H_{32}O_{13}$	Polygonumnolides C1-C4	671.1775	671.1770	0.76	265.1480; 458.1207; 553.1048; 416.1111; 254.0586
110a	33.41; 33.72; 34.76; 34.92	$C_{37}H_{34}O_{13}$	Polygonumnolides A1-A4	685.1931	685.1927	0.66	671.1752; 416.1109; 309.1735; 254.0586
111b	4.58; 5.69; 6.57; 8.04	$C_{40}H_{44}O_{19}$	(Isomer) Polygonumoside C/D	827.2403	827.2404	−0.07	665.1867; 467.1116; 269.0455; 225.0542; 131.0827
112b	5.91; 10.32; 10.38; 12.75; 13.50	$C_{40}H_{44}O_{18}$	Multiflorumiside A-I	811.2442	811.2455	−1.64	649.1914; 487.1372; 405.1182; 243.0662; 225.0553

a: Anthraquinones and derivatives. b: Stilbenes and derivatives. c: Flavonoids and derivatives. d: Others. The names of PM 1-4, PM 5, PM 14-17, PM 22-25, and PM 26-27 were from Yang, J. B. (2019). Journal of pharmaceutical and biomedical analysis, 172, 149-166.

characteristics, including 43 anthraquinones, 28 stilbene glycosides, 15 flavonoids, and 26 others.

3.2 Metabolomics analysis of raw and processed *Polygonum multiflorum*

The clinical use of PM usually includes both raw and processed PM. Previous studies have shown that the chemical composition of processed PM may change compared with that of raw PM, which may lead to a change in the pharmacological effects. For a fact, various studies have also shown that the toxicity of PM was significantly reduced after processing, which may be due to the significant reduction of toxic ingredients. To date, few studies have been performed to fully clarify the compositional changes in PM after treatment. Here, UPLC-Q-TOF-MS analysis combined with multivariate statistical analysis was used to distinguish between raw and processed PM. The PCA graph shows that the QC samples were closely clustered, indicating that the LC-MS analysis system was credibly reproducible and stable during the testing period. As seen from the PCA plots (Supplementary Figure S3), the raw PM and manufactured PM samples were able to be obviously separated and gathered separately. To further screen out the latent variables for distinguishing between raw and processed PM, OPLS-DA analysis was performed. The R2Y and Q2 of the OPLS-DA model were 0.98 and 0.92, respectively, which indicated excellent fitness and reliability. From the results (Figure 2), it was evident that the raw and processed PM were significantly differentiated under the supervised model. There was no overfitting in the OPLS-DA model by 200-times permutation tests, as shown in Figure 2. Furthermore, with VIP > 1.5, univariate statistical analysis $p < 0.5$, and fold change < 0.5, 126 differential characteristic ions were screened for significant reduction after preparing PM. Combined with the results of the abovementioned component analysis, 13 potential compounds were identified after excluding the interfering fragments and confirming the molecular ions. The results are shown in Table 3.

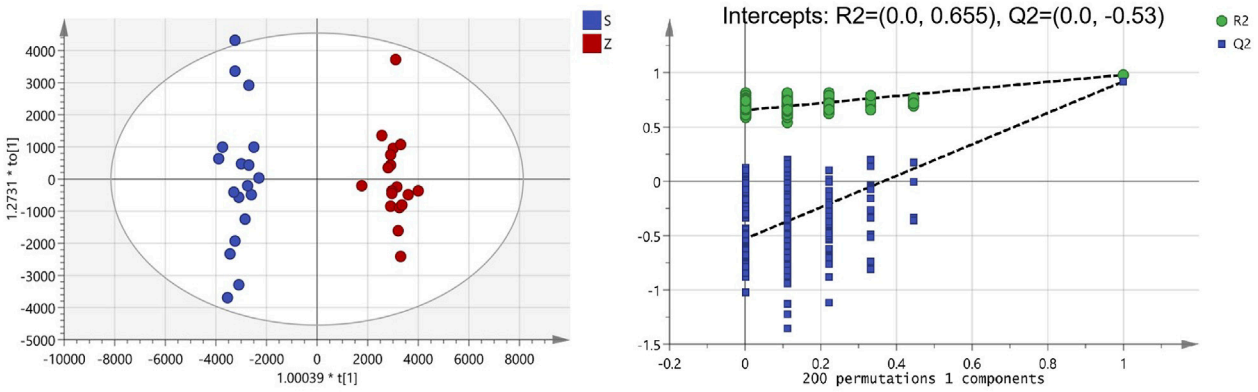

FIGURE 2
Orthogonal partial least squares analysis-DA score chart and permutation test analysis of *Polygonum multiflorum* (PM) samples (S: raw PM; Z: processed PM).

TABLE 3 Detailed information of 13 different compounds between raw and processed *Polygonum multiflorum* .

Compounds	Rt-*m/z* (Da)	VIP	*p*-value	FC-value
Catechin	4.88_289.0716	11.03	$1.50E^{-6}$	0.286
Epicatechin	7.89_290.0786n	4.08	$4.60E^{-4}$	0.397
Torachrysone-8-*O*-*β*-D-glucopyranoside	23.71_408.1413n	9.99	$1.00E^{-9}$	0.225
7-acetyl-3,8-dihydroxy-6-methyl-1-naphthyl-*β*-D-glucopyranoside	17.97_393.1173	3.48	$2.42E^{-10}$	0.137
Epicatechin-3-*O*-gallate	11.59_442.0917n	7.44	$9.32E^{-5}$	0.328
Emodin-8-*O*-*β*-D-glucopyranoside	25.61_431.2031	2.47	$1.75E^{-8}$	0.441
2,3,5,4′-tetrahydroxystilbene-2-*O*-*β*-D-(2-*O*-monogalloylesters)-glucopyranoside	14.58_558.1371n	13.36	$5.97E^{-5}$	0.359
polygonibene E	22.91_582.1726n	5.56	$2.50E^{-7}$	0.366
Polygonumnolides C1-C4	32.40_671.1733	1.83	$5.55E^{-3}$	0.380
Polygonumnolides A1-A4	34.95_685.1887	2.06	$3.15E^{-3}$	0.366
PM 14-17	30.37_758.1799n	1.59	$2.04E^{-3}$	0.157
PM 22-25	27.64_933.2410	1.86	$7.60E^{-5}$	0.186
PM 5	27.10_920.2342n	1.77	$1.23E^{-4}$	0.180

3.3 Pseudotargeted spectrum construction of discriminant metabolites

In MRM-based absolute quantification, calibration curves were often drawn for real compounds based on the conversion of the corresponding peak area into the content. However, absolute quantification usually cannot be achieved owing to the limitations of the standards, and the relative content between different groups can be compared by peak area. In consideration of the potential toxic dianthrone components identified in our previous studies and dianthrone aglycon hydrolyzed in acidic gastric juice *in vivo*, three nuclear parents of dianthrones were summarized (Li et al., 2020; Wang et al., 2021; Yang et al., 2021). Combined with the 13 differential metabolites obtained from the metabonomics analysis, UPLC-qqq-MS/MS semiquantitative profiles were further established. By optimizing the MRM ion pair and CV and CE values, semiquantitative mass spectra of the 16 compounds were constructed. The results are listed below. This method was successfully applied to 30 batches of raw PM and 20 batches of processed PM, and the standardized peak area heatmap is shown in Figure 3.

At last, a methodological investigation on the established scheduled MRM method, including specificity, linearity, precision, repeatability, and stability, was conducted. The

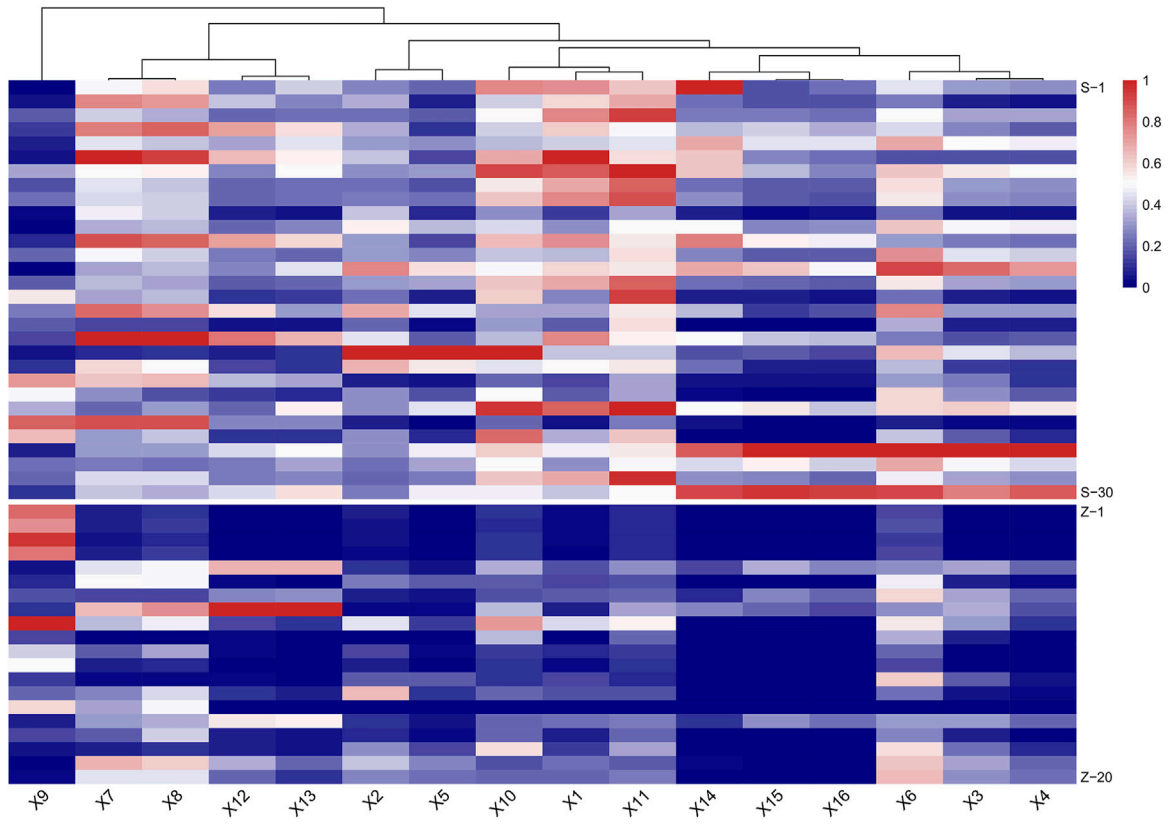

FIGURE 3
Heat map of semiquantitative analysis of 16 target compounds between raw and processed *Polygonum multiflorum* (PM) (S: raw PM; Z: processed PM).

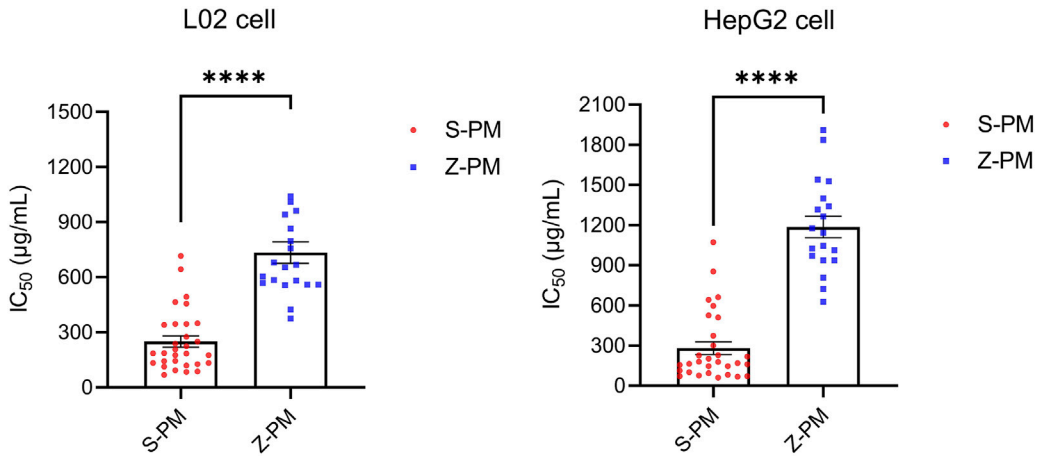

FIGURE 4
Statistical analysis of IC_{50} values of 50 batches of raw and processed *Polygonum multiflorum* on two kinds of hepatocytes ($p < 0.0001$, ****).

TABLE 4 Correlation degree between peak areas of 16 targeted compounds and hepatotoxicity.

Compound	GRA (correlation)		OPLS (R value)	
	L02	HepG2	L02	HepG2
X1	0.763	0.754	0.873	0.478
X2	0.818	0.778	−0.285	0.061
X3	0.806	0.813	0.193	−0.055
X4	0.804	0.816	−0.062	−0.150
X5	0.825	0.814	−0.515	−0.510
X6	0.826	0.776	−0.387	−0.210
X7	0.755	0.718	−0.443	−0.222
X8	0.750	0.707	0.160	0.070
X9	0.718	0.681	−0.101	−0.190
X10	0.800	0.776	−0.266	−0.318
X11	0.786	0.769	−0.191	−0.062
X12	0.733	0.715	0.504	0.506
X13	0.744	0.755	0.239	0.198
X14	0.772	0.779	−0.597	−0.440
X15	0.750	0.774	0.048	−0.121
X16	0.755	0.775	−0.272	−0.252

16 target compounds showed great specificity (Supplementary Figure S4). Among the 16 target analytes, linearity was good in the range of 0.5–3 μl injection with R > 0.98. Precision and repeatability results showed that the RSD values of all 16 compounds were less than 15%. For stability within 30 h, the RSD values ranged between 1.53% and 14.7% for all components.

3.4 Hepatotoxicity evaluation of *Polygonum multiflorum*

It is necessary to evaluate hepatotoxicity *in vitro*, but sometimes a cellular model does not provide an accurate and comprehensive assessment of the hepatotoxicity of TCM. In this study, two commonly used hepatocyte models were chosen, L02 and HepG2, to comprehensively estimate the hepatotoxicity of raw and processed PM extracts. The IC_{50} values for the raw and processed PM are shown in Supplementary Table S3. From Figure 4, the mean IC_{50} values of PM in both types of hepatocytes increased significantly after processing ($p < 0.0001$, ****), indicating the basic theories of processing detoxification. In specific, 30 batches of raw PM had an average IC_{50} value of 250 μg/mL in L02 cells and 281 μg/mL in HepG2 cells. However, 20 batches of processed PM had an average IC_{50} value of 735 μg/ml in L02 cells and 1,185 μg/ml in HepG2 cells.

3.5 Results of spectrum–effect relationship

3.5.1 Gray relational analysis results

The relationship between chromatographic peaks and hepatotoxicity effect was established by the GRA model. The degree of correlation between each chromatographic peak and hepatocyte toxicity is detailed in Table 4. The results showed that the gray relational degree between all 16 chromatographic peaks and the $1/IC_{50}$ of L02 cells was between 0.718 and 0.826. The correlation between the 16 peaks and the $1/IC_{50}$ of HepG2 cells was between 0.618 and 0.816. These results indicated that the 16 chromatographic peaks were closely correlated with hepatocyte toxicity. In total, dianthrone components X7, X8, X9, X12, X13, X14, X15, and X16; anthraquinone glycoside components X3, X4, and X6; stilbene glycosides X10 and X11; and flavanol compounds X1, X2, and X5 were all associated with hepatotoxicity in hepatocytes, which may synergistically contribute to the hepatotoxicity of PM.

3.5.2 Orthogonal partial least squares analysis results

OPLS analysis was conducted using an orthogonalized multiple linear regression model. In this study, an OPLS model was built to analyze the correlation between the chromatographic peaks of 16 compounds and the IC_{50} of L02 and HepG2 hepatocytes (Figure 5). For L02 hepatocytes, the constructed model parameters R2X, R2Y, and Q2 were 0.94, 0.82, and 0.67, respectively. The permutation test was performed without overfitting. The results showed that the VIP values of all compounds were greater than 0.7. Combined with the correlation coefficient of less than 0.1, compounds X14, X5, X6, X7, X9, X2, X16, X10, and X11 were screened out. For HepG2 hepatocytes, the model parameters of R2X, R2Y, and Q2 were 0.93, 0.83, and 0.68, respectively, and the model had no overfitting. X5, X14, X10, X16, X7, X6, X9, X4, and X15 were highlighted with correlation coefficients less than −0.1 and VIP values greater than 0.7. For further analysis, the common significant components screened by both models were dianthrone components X7, X9, X14, and X16; anthraquinone glycoside X6; stilbene glycoside X10; and flavanol X5. These components may be of more prominent importance in the multicomponent synergistic hepatotoxicity of PM.

3.5.3 Back propagation artificial neural network results

BP-ANN is a multilayer network that uses an error back propagation algorithm for constant adjustment of weights. In this experiment, a simple 3-layer BP-ANN neural network was modeled with an input layer, one hidden layer, and an output

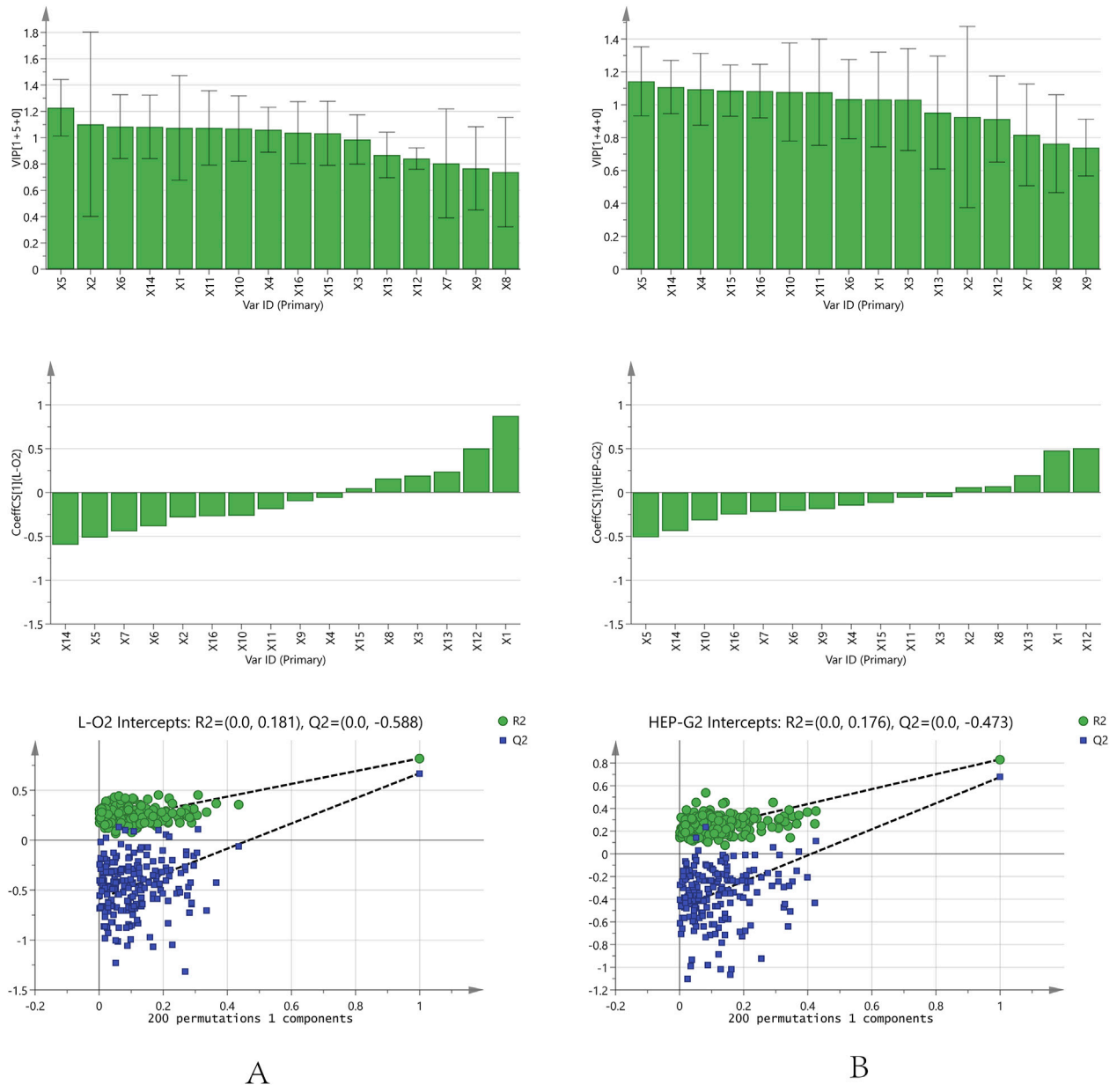

FIGURE 5
Orthogonal partial least squares analysis model correlation analysis and permutation test analysis results [**(A)**: L02 cell; **(B)**: HepG2 cell].

layer. The fitting degree of the model was evaluated using the mean square error (MSE) and regression R value. In the model, 80% of the random sample data were taken as the training set, and 20% of the sample data were used as the validation set. The results (Figure 6) demonstrated that for L02 cells, the established neural network model, where the R of the training and validation datasets reached 0.9380 and 0.9722, the MSE of the training and validation datasets reached 0.006 and 0.0027, respectively. For HepG2 cells, the R and MSE of the training and validation datasets on the model were 0.9555 and 0.9559, 0.0068 and 0.0125, respectively.

As a result of the sensitivity analysis, the 16 compounds all had relatively average contributions (*p* value); the L02 cells ranged from 4.07 to 8.50, and the HepG2 cells ranged from 4.08 to 9.43. The specific data are shown in Table 5, and the 16 compounds had a relatively average influence on hepatocyte toxicity. The hepatotoxicity caused by PM may be due to the synergistic result of multiple components. Furthermore, the

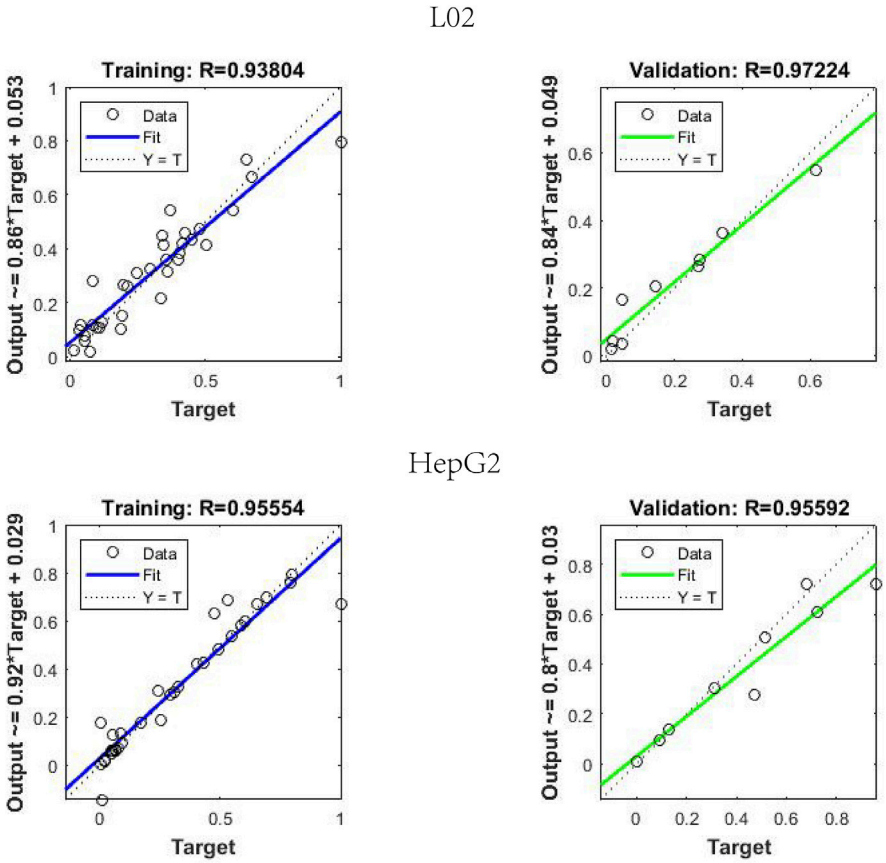

FIGURE 6
Regression R value results in back propagation artificial neural network neural network model.

average influence value (MIV) of the input variables in the network was used to assess the importance of different variables in the BP-ANN model. Variables negatively correlated with the IC_{50} values were sieved out. For L02 cells, the screened components were X7, X6, X10, X4, X15, X9, X2, X14, and X16. For HepG2 cells, X7, X4, X11, X13, X6, and X14 were selected. In summary, the common components screened were dianthrone components X7 and X14 and anthraquinone glycosides X4 and X6. These components may be of great significance as potential hepatotoxic components in PM.

For the key characteristic components screened out using the above three models, the intersection of these components included X6, X7, and X14. It was thought that they may play a more significant role in liver injury caused by PM and could be used as toxicity markers of hepatotoxicity. We acknowledge that PM has complex chemical components and that its hepatotoxicity may be the result of the synergistic action of various components. The 16 components screened above all contained a degree of hepatotoxicity. Moreover, there were many potentially hepatotoxic compounds that we had not discovered and identified that need to be further explored and verified.

4 Discussion

As an invaluable treasure of Chinese civilization, Chinese herbal medicine has the characteristics of multiple components, multiple targets, and multiple pathways. Many previous studies have explored the material basis of PM-induced hepatotoxicity through different methods. The results showed that it was not one type of compound that was responsible for hepatotoxicity in PM, which reflected the complexity and holistic nature of TCM. The hepatotoxicity may be a synergistic effect caused by multiple components acting on multiple targets leading to the toxicity result. In this study, MS fingerprints were combined with pharmacological toxicity to target potential hepatotoxic compounds in PM. Sixteen compounds were found to be potentially associated with hepatotoxicity, including dianthrones X7, X8, X9, X12, X13, X14, X15, and X16; anthraquinone glycosides X3, X4, and X6; stilbene glycosides X10 and X11; and flavanols X1, X2, and X5.

It was noteworthy that the dianthrones were the first compounds found by our team to have hepatotoxicity (Yang et al., 2021). The cis- and trans-structures of X7 were shown to

TABLE 5 Sensitivity analysis and MIV analysis results of 16 compounds in back propagation artificial neural network model.

Compound	*p* Value		MIV	
	L02	HepG2	L02	HepG2
X1	4.07	7.57	0.009	0.015
X2	5.01	9.43	-0.029	0.004
X3	7.29	5.69	0.105	0.029
X4	7.03	6.51	-0.046	-0.131
X5	6.60	4.08	0.002	0.062
X6	7.35	6.05	-0.089	-0.023
X7	6.40	7.40	-0.161	-0.247
X8	8.50	6.19	0.086	0.145
X9	4.99	6.21	-0.038	0.020
X10	7.61	6.63	-0.055	0.033
X11	5.77	6.19	0.022	-0.103
X12	8.12	5.91	0.072	0.178
X13	5.47	6.07	0.002	-0.102
X14	4.88	5.32	-0.015	-0.006
X15	5.70	4.95	-0.040	0.004
X16	5.22	5.79	-0.013	0.032

have IC_{50} values of 10.98 and 15.45 μM, respectively, in the HepaRG cytotoxicity evaluation. The 96-h LD_{50} of (*cis/trans*) X7 in zebrafish embryos was 1.79 and 1.70 μM (Yang J. B. et al., 2018). X7 exhibited hepatotoxicity at a relatively low concentration of 0.5 mg/L in a zebrafish hepatotoxicity model (Li et al., 2020). X12 exhibited weak hepatotoxicity in L02 cells using the CCK-8 assay (Yang et al., 2016). Moreover, the 96-h LD_{50} of X12 (C4) was 3.39 μM in zebrafish embryos, and a delayed appearance of liver yolk sacs in zebrafish occurred at 0.25 mg/L, indicating definite hepatotoxicity (Yang J. B. et al., 2018). X13 manifested moderate cytotoxicity with IC_{50} values of 29.7–31.1 μM against KB tumor cell lines (Yang J. et al., 2018). The hepatotoxicity of other dianthrones still needs further investigation.

Regarding the screened anthraquinone glycoside components, studies have shown that X3 displayed moderate hepatotoxicity with an IC_{50} value of 71.62 μM in HepG2 cells (Hanh et al., 2021). The 96-h LD_{50} of X3 in zebrafish embryos was 1.10 μM (Yang J. B. et al., 2018). In addition, X3 exhibited zebrafish hepatotoxicity at a low concentration of 0.25 mg/L (Li et al., 2020). However, the structure of X4 is similar to that of X3, with the methoxy group changed to the hydroxyl group on the benzene ring. Moreover, X6 was demonstrated to have strong embryotoxicity and hepatotoxicity in zebrafish in the toxicity test (Yang J. B. et al., 2018; Li et al., 2020). In addition, X6 inhibited the mRNA expression of CYP1A2 and CYP2C and moderately inhibited the activity of UDP-glucuronosyl transferase (UGT1A1), which was suspected to contribute to hepatotoxicity (Jiang et al., 2022).

The hepatotoxic components of the stilbene glycosides screened were 2,3,5,4′-tetrahydroxystilbene-2-*O*-*β*-D-(2-*O*-monogalloylesters)-glucopyranoside (X10) and polygonibene E (X11). X10 is a stilbene glycoside, and X11 is a stilbene glycoside dimer. At present, few pharmacological studies have been conducted on the above two stilbene glycoside components. However, some studies have reported that the stilbene glycoside component 2,3,5,4′-tetrahydroxystilbene-2-*O*-*β*-D-glucoyranoside could be a risk factor for hepatotoxicity in PM, which indicates that there may be some potential for hepatotoxicity of stilbene glycosides (Meng et al., 2017).

Regarding the flavanol compounds X1, X2, and X5, oxidation and polymerization have been reported to be the main reasons for the reduction of catechins and flavonoids after processing (Xiang et al., 2021). It has been stated that these polyphenols cause different forms of toxicity, including organ toxicity, genotoxicity, mutagenicity, and cytotoxicity (Islam et al., 2021). For instance, studies have shown that catechin (X1) has antitumor effects and can induce tumor cell apoptosis on account of certain cytotoxicity (Miyamoto et al., 2004). In addition, studies have reported that epicatechin has a concentration-dependent inhibitory effect on tumor cell proliferation and promotes cell death through apoptosis (Varela-Castillo et al., 2018). Epicatechin-3-O-gallate (ECG, X5) induced apoptosis through a TGF-beta superfamily protein, NAG-1 (nonsteroidal antiinflammatory drug-activated gene) (Baek et al., 2004). ECG is a strong inducer of NAG-1, and action on HCT-116 cells leads to an increase in the G (1) phase, leading to cleavage of polyribose polymerase, a phenomenon consistent with apoptosis. In addition, ECG has also been shown to be cytotoxic and hepatotoxic *in vivo* and highly toxic to HSC-2 cancer cells (Babich et al., 2005; Galati et al., 2006).

Other studies have shown that emodin, chrysophanol, and physcion anthraquinones in PM could affect bile acid homeostasis and cause hepatotoxicity (Kang et al., 2022). Some studies also concluded that *cis*-2,3,5,4′-tetrahydroxy-trans-stilbene-2-*O*-*β*-D-glucoside (*cis*-TSG) in PM led to hepatotoxicity through mitochondrial injury (Liu et al., 2022). In addition, cis-TSG was shown to be more closely related to immunological idiosyncratic hepatotoxicity (Meng et al., 2017). Other views also suggested that the synergy between stilbenes and emodin derivatives contributed to hepatotoxicity of PM (Zhang et al., 2020).

In summary, the 16 chemical components all had different degrees of hepatotoxicity and may be responsible for the hepatotoxicity of PM through a synergistic effect. Among these compounds, the three more typical compounds—emodin dianthrones, emodin-8-*O*-*β*-D-glucopyranoside, and PM 14–17—showed strong hepatotoxicity in different models. They may be the key hepatotoxic components in PM. However, there were still many limitations in our experiments, such as the toxicity evaluation involving only *in vitro* cells. In addition, the screened

hepatotoxic compounds lacked standards, and no further toxicity validation was performed.

5 Conclusion

The complexity and diversity of Chinese medicinal components make the discovery of toxic components in Chinese medicine a challenging task. This study integrated a progressive strategy to explore the hepatotoxic components in PM. First, 112 constituents of PM were characterized using UPLC-Q-TOF-MS. Second, plant metabolomics was used to screen for differential components between raw and processed PM. Third, the pseudotargeted mass spectra of the 16 components of 50 batches of PM were established. Then, the hepatotoxicity of 50 batches of PM was evaluated in two hepatocytes. At last, based on three models, GRA, OPLS, and BP-ANN, a spectrum–effect relationship was established to determine the hepatotoxic components in PM. As a result, 16 components with potential hepatotoxicity were found, among which emodin dianthrones, emodin-8-*O*-*β*-D-glucopyranoside, and PM 14-17 were more significantly prominent. These three markers could be used as hepatotoxic markers in PM as well as for in-depth pharmacological and toxicological studies.

Data availability statement

The original contributions presented in the study are included in the article/Supplementary Material; further inquiries can be directed to the corresponding authors.

Author contributions

YS, FW, and SM designed and conceived the experiments; YS, XH, PW, HG, and XW carried out the experiments; YS, JY, XH, and XC did the data analysis; YS, JY, and YL contributed to writing and supervising the manuscript; FW and SM funded the study. All authors reviewed and approved the final manuscript.

Funding

The work was financially supported by the National Natural Science Foundation of China (Grant No. 81973476 and 81773874) and National Major Scientific and Technological Special Project for "Significant New Drugs Development" (2018ZX09735006).

Conflict of interest

The authors declare that the research was conducted in the absence of any commercial or financial relationships that could be construed as a potential conflict of interest.

Publisher's note

Supplementary material

The Supplementary Material for this article can be found online at: https://www.frontiersin.org/articles/10.3389/fphar.2022.935336/full#supplementary-material

References

Babich, H., Krupka, M. E., Nissim, H. A., and Zuckerbraun, H. L. (2005). Differential *in vitro* cytotoxicity of (-)-epicatechin gallate (ECG) to cancer and normal cells from the human oral cavity. *Toxicol. Vitro* 19 (2), 231–242. doi:10.1016/j.tiv.2004.09.001

Baek, S. J., Kim, J. S., Jackson, F. R., Eling, T. E., McEntee, M. F., Lee, S. H., et al. (2004). Epicatechin gallate-induced expression of NAG-1 is associated with growth inhibition and apoptosis in colon cancer cells. *Carcinogenesis* 25 (12), 2425–2432. doi:10.1093/carcin/bgh255

But, P. P., Tomlinson, B., and Lee, K. L. (1996). Hepatitis related to the Chinese medicine Shou-Wu-pian manufactured from Polygonum multiflorum. *Vet. Hum. Toxicol.* 38 (4), 280–282.

Chinese Pharmacopoeia Commission (2020). *Pharmacopoeia of people's Republic of China*. Beijing: China Medical Science Press.

Galati, G., Lin, A., Sultan, A. M., and O'Brien, P. J. (2006). Cellular and *in vivo* hepatotoxicity caused by green tea phenolic acids and catechins. *Free Radic. Biol. Med.* 40 (4), 570–580. doi:10.1016/j.freeradbiomed.2005.09.014

Han, L., Wang, P., Wang, Y., Zhao, Q., Zheng, F., Dou, Z., et al. (2019). Rapid discovery of the potential toxic compounds in Polygonum multiflorum by UHPLC/Q-Orbitrap-MS-Based metabolomics and correlation analysis. *Front. Pharmacol.* 10, 329. doi:10.3389/fphar.2019.00329

Hanh, T. T. H., Anh, L. N., Trung, N. Q., Quang, T. H., Anh, D. H., Cuong, N. X., et al. (2021). Cytotoxic phenolic glycosides from the seeds of Senna tora. *Phytochem. Lett.* 45, 190–194. doi:10.1016/j.phytol.2021.08.020

Islam, B. U., Suhail, M., Khan, M. K., Zughaibi, T. A., Alserihi, R. F., Zaidi, S. K., et al. (2021). Polyphenols as anticancer agents: Toxicological concern to healthy cells. *Phytother. Res.* 35 (11), 6063–6079. doi:10.1002/ptr.7216

Jiang, Y., Zhang, C., Zheng, X., Zhao, Z., and Li, H. J. (2022). Simultaneously screening multiple UGT1A1 inhibitors from Polygonum multiflorum root using ultrafiltration LC-MS. *Biomed. Chromatogr.* 36 (4), e5300. doi:10.1002/bmc.5300

Jiang, Z., Zhao, C., Gong, X., Sun, X., Li, H., Zhao, Y., et al. (2018). Quantification and efficient discovery of quality control markers for Emilia prenanthoidea DC. by Fingerprint-Efficacy Relationship Modelling. *J. Pharm. Biomed. Anal.* 156, 36–44. doi:10.1016/j.jpba.2018.04.020

Kang, L., Li, D., Jiang, X., Zhang, Y., Pan, M., Hu, Y., et al. (2022). Hepatotoxicity of the major anthraquinones derived from polygoni multiflori radix based on bile acid homeostasis. *Front. Pharmacol.* 13, 878817. doi:10.3389/fphar.2022.878817

Lei, X., Chen, J., Ren, J., Li, Y., Zhai, J., Mu, W., et al. (2015). Liver damage associated with Polygonum multiflorum Thunb.: A systematic review of case reports and case series. *Evid. Based. Complement. Altern. Med.* 2015, 459749. doi:10.1155/2015/459749

Li, H. Y., Yang, J. B., Li, W. F., Qiu, C. X., Hu, G., Wang, S. T., et al. (2020). *In vivo* hepatotoxicity screening of different extracts, components, and constituents of Polygoni Multiflori Thunb. in zebrafish (*Danio rerio*) larvae. *Biomed. Pharmacother.* 131, 110524. doi:10.1016/j.biopha.2020.110524

Liang, J., Chen, Y., Ren, G., Dong, W., Shi, M., Xiong, L., et al. (2017). Screening hepatotoxic components in euodia rutaecarpa by UHPLC-QTOF/MS based on the spectrum-toxicity relationship. *Molecules* 22 (8), E1264. doi:10.3390/molecules22081264

Liao, M., Yan, P., Liu, X., Du, Z., Jia, S., Aybek, R., et al. (2020). Spectrum-effect relationship for anti-tumor activity of shikonins and shikonofurans in medicinal Zicao by UHPLC-MS/MS and chemometric approaches. *J. Chromatogr. B Anal. Technol. Biomed. Life Sci.* 1136, 121924. doi:10.1016/j.jchromb.2019.121924

Lin, L., Ni, B., Lin, H., Zhang, M., Li, X., Yin, X., et al. (2015). Traditional usages, botany, phytochemistry, pharmacology and toxicology of Polygonum multiflorum Thunb.: A review. *J. Ethnopharmacol.* 159, 158–183. doi:10.1016/j.jep.2014.11.009

Liu, J., Li, T., Li, R., Wang, J., Li, P., Niu, M., et al. (2022). Hepatic organoid-based high-content imaging boosts evaluation of stereoisomerism-dependent hepatotoxicity of stilbenes in herbal medicines. *Front. Pharmacol.* 13, 862830. doi:10.3389/fphar.2022.862830

Liu, S., Liang, Y. Z., and Liu, H. T. (2016). Chemometrics applied to quality control and metabolomics for traditional Chinese medicines. *J. Chromatogr. B Anal. Technol. Biomed. Life Sci.* 1015-1016, 82–91. doi:10.1016/j.jchromb.2016.02.011

Liu, Y., Wang, Q., Yang, J., Guo, X., Liu, W., Ma, S., et al. (2018). Polygonum multiflorum Thunb.: A review on chemical analysis, processing mechanism, quality evaluation, and hepatotoxicity. *Front. Pharmacol.* 9, 364. doi:10.3389/fphar.2018.00364

Luo, P., Dai, W., Yin, P., Zeng, Z., Kong, H., Zhou, L., et al. (2015). Multiple reaction monitoring-ion pair finder: A systematic approach to transform nontargeted mode to pseudotargeted mode for metabolomics study based on liquid chromatography-mass spectrometry. *Anal. Chem.* 87 (10), 5050–5055. doi:10.1021/acs.analchem.5b00615

Ma, Y., Li, J., Tong, F., Xin, X.-L., and Aisa, H. A. (2020). Optimization of microwave-assisted extraction using response surface methodology and the potential anti-diabetic efficacy of Nigella glandulifera Freyn determined using the spectrum–effect relationship. *Industrial Crops Prod.* 153, 112592. doi:10.1016/j.indcrop.2020.112592

Meng, Y. K., Li, C. Y., Li, R. Y., He, L. Z., Cui, H. R., Yin, P., et al. (2017). Cis-stilbene glucoside in Polygonum multiflorum induces immunological idiosyncratic hepatotoxicity in LPS-treated rats by suppressing PPAR-γ. *Acta Pharmacol. Sin.* 38 (10), 1340–1352. doi:10.1038/aps.2017.32

Miyamoto, Y., Haylor, J. L., and El Nahas, A. M. (2004). Cellular toxicity of catechin analogues containing gallate in opossum kidney proximal tubular (OK) cells. *J. Toxicol. Sci.* 29 (1), 47–52. doi:10.2131/jts.29.47

Park, G. J., Mann, S. P., and Ngu, M. C. (2001). Acute hepatitis induced by Shou-Wu-Pian, a herbal product derived from Polygonum multiflorum. *J. Gastroenterol. Hepatol.* 16 (1), 115–117. doi:10.1046/j.1440-1746.2001.02309.x

Qiao, X., Qu, C., Luo, Q., Wang, Y., Yang, J., Yang, H., et al. (2021). UHPLC-qMS spectrum-effect relationships for Rhizoma Paridis extracts. *J. Pharm. Biomed. Anal.* 194, 113770. doi:10.1016/j.jpba.2020.113770

Rao, S. W., Duan, Y. Y., Pang, H. Q., Xu, S. H., Hu, S. Q., Cheng, K. G., et al. (2022). Spectrum-effect relationship analysis of bioactive compounds in zanthoxylum nitidum (roxb.) DC. By ultra-high performance liquid chromatography mass spectrometry coupled with comprehensive filtering approaches. *Front. Pharmacol.* 13, 794277. doi:10.3389/fphar.2022.794277

Shang, Z., Xu, L., Zhang, Y., Ye, M., and Qiao, X. (2021). An integrated approach to reveal the chemical changes of Ligustri Lucidi Fructus during wine steaming processing. *J. Pharm. Biomed. Anal.* 193, 113667. doi:10.1016/j.jpba.2020.113667

Shi, W., Zhang, C., Zhao, D., Wang, L., Li, P., Li, H., et al. (2018). Discovery of hepatotoxic equivalent combinatorial markers from Dioscorea bulbifera tuber by fingerprint-toxicity relationship modeling. *Sci. Rep.* 8 (1), 462. doi:10.1038/s41598-017-18929-z

Teka, T., Wang, L., Gao, J., Mou, J., Pan, G., Yu, H., et al. (2021). Polygonum multiflorum: Recent updates on newly isolated compounds, potential hepatotoxic compounds and their mechanisms. *J. Ethnopharmacol.* 271, 113864. doi:10.1016/j.jep.2021.113864

Varela-Castillo, O., Cordero, P., Gutiérrez-Iglesias, G., Palma, I., Rubio-Gayosso, I., Meaney, E., et al. (2018). Characterization of the cytotoxic effects of the combination of cisplatin and flavanol (-)-epicatechin on human lung cancer cell line A549. An isobolographic approach. *Exp. Oncol.* 40 (1), 19–23. doi:10.31768/2312-8852.2018.40(1):19-23

Wang, F., Wang, B., Wang, L., Xiong, Z. Y., Gao, W., Li, P., et al. (2017). Discovery of discriminatory quality control markers for Chinese herbal medicines and related processed products by combination of chromatographic analysis and chemometrics methods: Radix Scutellariae as a case study. *J. Pharm. Biomed. Anal.* 138, 70–79. doi:10.1016/j.jpba.2017.02.004

Wang, J., Luo, D., Liang, M., Zhang, T., Yin, X., Zhang, Y., et al. (2018). Spectrum-effect relationships between high-performance liquid chromatography (HPLC) fingerprints and the antioxidant and anti-inflammatory activities of collagen peptides. *Molecules* 23 (12), E3257. doi:10.3390/molecules23123257

Wang, Q., Yan, M., Ma, S., and Wen, H. (2021). Predicting toxic monomer components in Polygonum multiflorum based on quantitative structure-activity relationship. *Chin. J. Pharmacovigil.* 18 (4), 352–360. doi:10.19803/j.1672-8629.2021.04.12

Xiang, X., Su, C., Shi, Q., Wu, J., Zeng, Z., Zhang, L., et al. (2021). Potential hypoglycemic metabolites in dark tea fermented by Eurotium cristatum based on UPLC-QTOF-MS/MS combining global metabolomic and spectrum-effect relationship analyses. *Food Funct.* 12 (16), 7546–7556. doi:10.1039/d1fo00836f

Xu, J. F., Xu, J., Li, S. Z., Jia, T. W., Huang, X. B., Zhang, H. M., et al. (2013). Transmission risks of schistosomiasis japonica: Extraction from back-propagation artificial neural network and logistic regression model. *PLoS Negl. Trop. Dis.* 7 (3), e2123. doi:10.1371/journal.pntd.0002123

Yang, J. B., Li, L., Dai, Z., Wu, Y., Geng, X. C., Li, B., et al. (2016). Polygonumnolides C1-C4; minor dianthrone glycosides from the roots of Polygonum multiflorum Thunb. *J. Asian Nat. Prod. Res.* 18 (9), 813–822. doi:10.1080/10286020.2016.1171758

Yang, J. B., Li, W. F., Liu, Y., Wang, Q., Cheng, X. L., Wei, F., et al. (2018b). Acute toxicity screening of different extractions, components and constituents of Polygonum multiflorum Thunb. on zebrafish (*Danio rerio*) embryos *in vivo*. *Biomed. Pharmacother.* 99, 205–213. doi:10.1016/j.biopha.2018.01.033

Yang, J. B., Song, Y. F., Liu, Y., Gao, H. Y., Wang, Q., Wang, Y., et al. (2021). UHPLC-QQQ-MS/MS assay for the quantification of dianthrones as potential toxic markers of Polygonum multiflorum Thunb: Applications for the standardization of traditional Chinese medicines (TCMs) with endogenous toxicity. *Chin. Med.* 16 (1), 51. doi:10.1186/s13020-021-00463-w

Yang, J., Yan, Z., Ren, J., Dai, Z., Ma, S., Wang, A., et al. (2018a). Polygonumnolides A1-B3, minor dianthrone derivatives from the roots of Polygonum multiflorum Thunb. *Arch. Pharm. Res.* 41 (6), 617–624. doi:10.1007/s12272-016-0816-7

Zhang, C., Zheng, X., Ni, H., Li, P., and Li, H. J. (2018). Discovery of quality control markers from traditional Chinese medicines by fingerprint-efficacy modeling: Current status and future perspectives. *J. Pharm. Biomed. Anal.* 159, 296–304. doi:10.1016/j.jpba.2018.07.006

Zhang, L., Liu, X., Tu, C., Li, C., Song, D., Zhu, J., et al. (2020). Components synergy between stilbenes and emodin derivatives contributes to hepatotoxicity induced by Polygonum multiflorum. *Xenobiotica.* 50 (5), 515–525. doi:10.1080/00498254.2019.1658138

Zheng, F., Zhao, X., Zeng, Z., Wang, L., Lv, W., Wang, Q., et al. (2020). Development of a plasma pseudotargeted metabolomics method based on ultra-high-performance liquid chromatography-mass spectrometry. *Nat. Protoc.* 15 (8), 2519–2537. doi:10.1038/s41596-020-0341-5

frontiers | Frontiers in Pharmacology

TYPE Original Research
PUBLISHED 30 August 2022
DOI 10.3389/fphar.2022.961012

OPEN ACCESS

EDITED BY
Zhichao Xu,
Northeast Forestry University, China

REVIEWED BY
Jinqi Li,
Personalized Drug Therapy Key Laboratory of Sichuan Province, China
Yun Qi,
Chinese Academy of Medical Sciences and Peking Union Medical College, China

*CORRESPONDENCE
Fu Peng,
fujing126@yeah.net
Cheng Peng,
pengchengchengdu@126.com
Jie Xie,
jiexie@sicnu.edu.cn

SPECIALTY SECTION
This article was submitted to Experimental Pharmacology and Drug Discovery,
a section of the journal Frontiers in Pharmacology

RECEIVED 03 June 2022
ACCEPTED 08 August 2022
PUBLISHED 30 August 2022

CITATION
An J, Fan H, Han M, Peng C, Xie J and Peng F (2022), Exploring the mechanisms of neurotoxicity caused by fuzi using network pharmacology and molecular docking.
Front. Pharmacol. 13:961012.
doi: 10.3389/fphar.2022.961012

Exploring the mechanisms of neurotoxicity caused by fuzi using network pharmacology and molecular docking

Junsha An[1], Huali Fan[1], Mingyu Han[1], Cheng Peng[2]*, Jie Xie[3]* and Fu Peng[1]*

[1]Key Laboratory of Drug-Targeting and Drug Delivery System of the Education Ministry and Sichuan Province, Sichuan Engineering Laboratory for Plant-Sourced Drug and Sichuan Research Center for Drug Precision Industrial Technology, West China School of Pharmacy, Sichuan University, Chengdu, China, [2]State Key Laboratory of Southwestern Chinese Medicine Resources, Chengdu University of Traditional Chinese Medicine, Chengdu, China, [3]College of Life Science, Sichuan Normal University, Chengdu, China

Safety has always been an important issue affecting the development of traditional Chinese medicine industry, especially for toxic medicinal materials, the establishment of risk prevention and control measures for toxic herbs is of great significance to improving the use of traditional Chinese medicine in clinical. Fuzi is a kind of traditional Chinese medicine and its toxicity has become the most important obstacle of limit in clinical using. In this paper, network pharmacology and molecular docking technology were used to analyze the main toxic components of Fuzi, the key targets and the mechanism of neurotoxicity. We carried out CCK-8 and WB assays, and detected LDH release and SDH activity. It was verified that aconitine caused neurotoxicity through a variety of pathways, including MAPK signaling pathway, pathways related to Akt protein, destruction of cell membrane integrity, damage of mitochondrial function affecting energy metabolism and apoptosis. What's more, this study confirmed that aconitine could produce neurotoxicity by promoting apoptosis of hippocampus neuron and decreasing its quantity through Nissl Staining and TUNEL assay. This paper found and confirmed multiple targets and various pathways causing neurotoxicity of Fuzi, in order to provide reference for clinical application and related research.

KEYWORDS

fuzi, neurotoxicity, network pharmacology, molecular docking, aconitine

Introduction

Aconiti Lateralis Radix Praeparata (Fuzi in Chinese), known as Chinese aconite, Chinese wolfsbane and monkshood, is the lateral root of *Aconitum Carmichaelii* Debeaux (Zhao et al., 2020). Fuzi is a traditional Chinese medicine in China, which was recorded in the *Shennong herbal Scripture*. In the history of clinical use for thousands of yeas, numerous classical prescriptions such as four inverse soup, zhenwu decoction, and mahuang fuzi xixin decoction have emerged. As for today, modern research have shown that Fuzi has a wide range of pharmacological effects and is extensively used in treatment of cardiovascular diseases, rheumatism arthritis, neuropathic pain and bronchitis (Yang et al., 2018). Although Fuzi has promising therapeutic effects, its toxicities are frequently observed, like cardiac toxicity, neurotoxicity, hepatotoxicity, nephrotoxicity and so on (Chan, 2009). The current research about for cardiac toxicity of Fuzi is relatively wide, but the mechanism of its neurotoxicity still needs further research.

In 2007, the concept of "network pharmacology" was first proposed (Hopkins, 2007), in the same year, Chinese scholars used the biological network to study the traditional Chinese medicine prescriptions. In recent years, the research filed of systems biology has greatly advanced, as a result, the application of network pharmacology in traditional Chinese medicine has been developed and has a series of achievements (Li and Zhang, 2013; Zhang et al., 2019).

In this study, on the basis of related literature reports, we aim to research the mechanism of neurotoxicity of Fuzi, using network pharmacology and molecular docking method, in order to provide reference for clinical application and related research. The workflow of this study is shown in Figure 1.

Materials and methods

Network pharmacology research

Screening the toxic compounds of fuzi and their targets

HERB database (http://herb.ac.cn/) and SymMap database (http://www.symmap.org/) were used to get all active compounds of Fuzi. Then, we retrieved the targets associated with active compounds from CTD database (http://ctdbase.org/), and our filter was set to "Interaction Count >1". We collected all the targets, deleted duplicates and got candidate toxic compounds of Fuzi and potential target genes.

Predicting the targets of neurotoxicity

We searched potential targets of neurotoxicity by using "toxic encephalopathy" and "nerve toxicity" as the key words in GeneCards database (https://www.genecards.org/) and set "Relevance score ≥10" as a filter. Then the results of the two were combined and duplicated targets were removed in order to get potential targets of neurotoxicity.

Prediction of candidate targets and construction of PPI network

We used Venny 2.1.0 database (https://bioinfogp.cnb.csic.es/tools/venny/) to match the candidate targets of toxic compounds and the potential targets of neurotoxicity, and intersection target

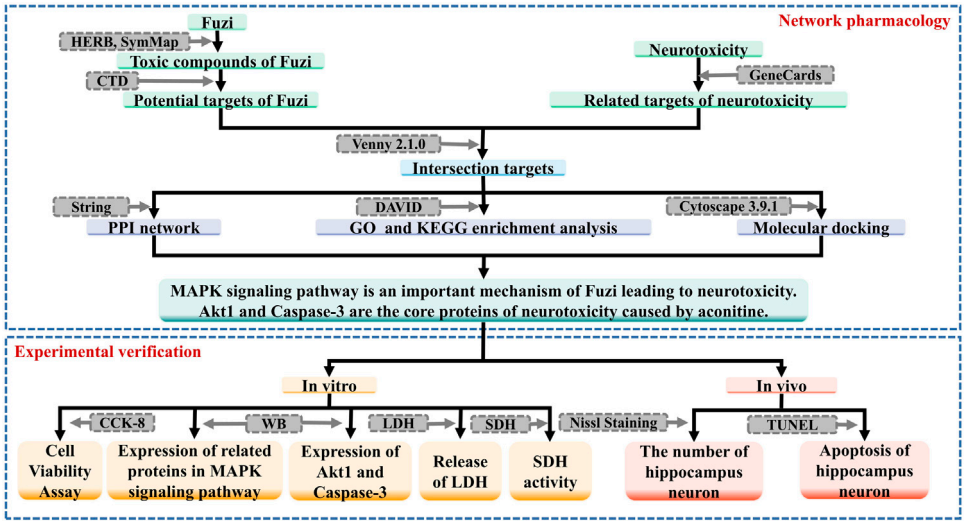

FIGURE 1
The workflow of this study.

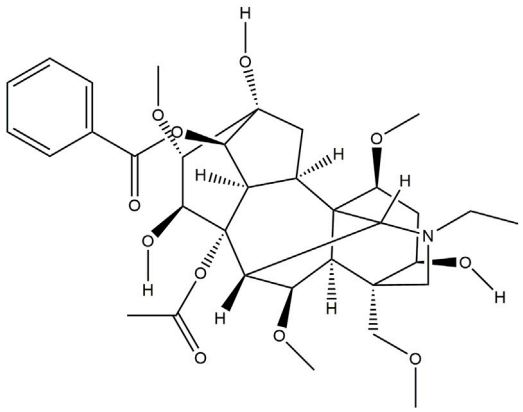

FIGURE 2
Chemical structure of aconitine.

genes were the potential targets in the toxic effect of Fuzi on nerve.

All the targets were uploaded to String database (https://cn.string-db.org/) to build the PPI network interaction. Cytoscape 3.9.1 was used to construct and visualize the PPI network. CytoHubba, a network topology analysis plug-in in Cytoscape, was used for analyzing topology parameters of each target. The value of "Degree" was used as a reference for the importance of the core targets.

After that, we put the candidate toxic compounds of Fuzi and the corresponding 10 core targets into Cytoscape 3.9.1 to construct the relationship network between candidate toxic compounds of Fuzi and the corresponding 10 core targets.

GO biological process and KEGG pathway enrichment analysis

Intersected target genes were uploaded to DAVID database (https://david.ncifcrf.gov/) for performing GO biological process and KEGG pathway enrichment analysis ($p < 0.05$). GO enrichment analysis includes Biological Process (BP), Molecular Function (MF), and Cellular Component (CC) analysis. KEGG is a bioinformatics resource for mining significantly altered metabolic pathways enriched in the gene list. GO and KEGG pathway analysis were visualized using the R programming language.

Molecular docking

PubChem database (https://pubchem.ncbi.nlm.nih.gov/) was used to download the SDF format of key toxic compounds, and OpenBabel software was used to transfer into MOL2 format. The 3D structure of the protein was downloaded in PDB database (http://www.rcsb.org/).

Then, we imported the search results into AutoDock Tool software. The target protein was used as a receptor with the water molecule removed and nonpolar hydrogen added. The key toxic compound was used as a ligand, and the Grid box coordinated and size were set according to the target protein. At last, we selected the binding conformation with the lowest free binding energy by using AutoDock Vina and imported it into PyMol software for visualization.

Experimental validation

Reagents

Aconitine (purity ≥98%), the chemical structure is shown in Figure 2, was obtained from Chengdu Must Bio-Technology Co., Ltd. (Chengdu, China).

Dulbecco's Modified Eagle's Medium (DMEM) was purchased from Hylone (Logan, Utah, United States). 10% Fetal Bovine Serum (FBS) was obtained from GIBCO (NY, United States). The Cell Counting Kit-8 (CCK-8) was bought from Sigma-Aldrich (Nevada, United States). Penicillin-Streptomycin Solution was obtained from Allcare Biomedical Development (Qingdao, China). The primary antibodies against p-MAPK, MAPK1, p53, p-Akt, Akt, Caspase-3 and GAPDH were purchased from Cell Signaling Tech. (MA, United States). Trypsin, Tris-base, glutathione (GSH), acrylamide, SDS, AP, THMED and other reagents were obtained from Amresco (United States). Nissl Staining Solution and LDH Assay Kit were bought from Beyotime (Shanghai, China). SDH Assay Kit was obtained from Nanjing Jiancheng Bioengineering Institute (Nanjing, China). The *In Situ* Cell Death Detection Kit was purchased from Roche (Basel, Switzerland). Alcohol and xylene were obtained from SINOPHARM (Beijing, China). And paraformaldehyde was purchased from Sangon Biotech (Shanghai, China).

Cell culture

SH-SY5Y cells were obtained from cell bank in Shanghai Institutes for Biological Sciences (SIBS, CAS). They were cultured in DMEM medium supplemented with 10% (v/v) FBS and 1% (v/v) penicillin-streptomycin solution, and maintained at 37°C in a humidified chamber with 5% CO_2.

Cell viability assay

Cell viability was measured using CCK-8 assay. SH-SY5Y cells were seeded into 96-well plates in the concentration of 5×10^3 cells per well. After incubating in a cell incubator overnight, SH-SY5Y cells were exposed to aconitine in concentrations of 0, 25, 50, 100, 200, 300, 400 μM for 24 and 48 h. The wells added amount of medium is the blank group. Then, 10 μL of CCK-8 solution was added to each well of the plate. After 1 h of incubating, we measured the optical density (OD) at 450 nm wavelength with a microplate reader. Each experiment was repeated three times. (Cell viability = $[(OD_{Experiment\ group} - OD_{Blank})/(OD_{Control\ group} - OD_{Blank})]\times100\%$)

Western blot assay

SH-SY5Y cells (5×10^5 cells/well) were seeded into 6-well plates and were exposed to aconitine in concentrations of 0, 100, 200, 400 μM for 24 h. Cell proteins were extracted after treatment with RIPA lysis buffer. The BCA method was used to calculate the content of protein. According to the relative molecular mass of target protein, we prepared 10% sodium dodecyl sulfate polyacrylamide gel electrophoresis (SDS-PAGE). An equal amount of the protein (20 μg per sample) was loaded onto SDS-PAGE for separation and transferred onto polyvinylidene difluoride (PVDF) membranes. Then we used 5% BSA for 1 h to block the membranes and used the primary antibodies including anti-p-MAPK, anti-MAPK1, anti-p53, anti-p-Akt, anti-Akt, anti-Caspase-3 and anti-GAPDH overnight at 4°C. After washed with TBST three times and further incubated with HRP-conjugated secondary antibodies for 1 h at room temperature, the protein bands were detected by the CheniDoc MP Imaging System.

Detection of lactate dehydrogenase release

SH-SY5Y cells were incubated in 96-well plates and exposed to aconitine in concentrations of 0, 25, 50, 100, 200, 300, 400 μM for 24 h. Then, 10 μL of Lysis solution was added to each well of the plate to assess maximum LDH release. We collected supernatants after centrifugation at 400 *g* for 5 min and transferred 120 μL of the supernatant from each well to a new assay plate. Finally, we added 60 μL of the detection solution to each well and recorded absorbance at 490 nm after 30min of incubating. Experiments were repeated three times.

Detection of succinate dehydrogenase activity

SH-SY5Y cells were incubated in 6-well plates and exposed to aconitine in concentrations of 0, 100, 200, 400 μM for 24 h. Then we collected supernatants after centrifugation. And the SDH activity was measured using SDH Assay Kit according to the manufacturer's protocol. Experiments were repeated three times.

Animals and treatment

Twenty rats of SPF grade were used in this study. All rats were about six weeks old and divided into two equal groups for different experimental analysis. Each rat in group I (experimental) was given intraperitoneal injection (*i.p.*) of aconitine (1 mg/kg), while each rat in group II, which served as control, received an equal volume of normal saline.

The treatment was last for one week. Then, the rats were sacrificed. We quickly removed the brain tissue. Tissues for examination were fixed and preserved in paraformaldehyde, processed and trimmed, embedded in paraffin, and sectioned to a thickness of 5 μm.

These studies were conducted in compliance with the "Guide for the Care and Use of Laboratory Animals" (National Research Council (US), 2011).

Nissl staining experiment

The brain sections were dewaxed, rehydrated and washed with distilled water three times. Then we used Nissl Staining solution to stain the sections for 5 min and used distilled water to wash them twice. After being stained, the sections were dehydrated with 95% ethanol for 2 min (twice) and xylene for 5 min (twice), and then fixed using neutral gum. The number of hippocampus neuron was visualized with an optical microscope at 40 × and 100 × magnification. Then we used ImageJ software to count normal nerve cells.

TUNEL assay

Apoptosis cells were measured by using *In Situ* Cell Death Detection Kit. After being dewaxed, rehydrated and washed with distilled water three times, the sections were stained according to the manufacturer's instructions and apoptotic cells were stained brown due to the binding of dUTP enzyme to their fragmented DNA. We used an optical microscope at 40× and 100 × magnification to observe apoptosis of hippocampus neuron. Then, we used ImageJ software to calculate the number of apoptotic cells.

Statistical analysis

All statistical analyses were preformed using GraphPad prism 8.0. Differences in multiple groups were analyzed by ANOVA and $p < 0.05$ was considered statistically significant.

Results

Toxic compounds of fuzi and their targets

We used HERB and SymMap database to predict the toxic compounds of Fuzi, and a total of 177 active compounds were retrieved. All the active compounds were input into CTD database for compound retrieval, and 22 candidate toxic compounds of Fuzi were obtained. After we combined the targets of all toxic compounds and deleted the duplicates, a total of 1810 corresponding targets were obtained. Then toxic compounds with corresponding targets greater than 10 were selected as candidate core toxic compounds (Table 1).

Targets of neurotoxicity

In the GeneCards database, 252 potential targets were searched by using "toxic encephalopathy" as the key word, and 290 potential targets were searched by using "nerve toxicity" as the key word. All the collected target genes were merged and duplicated. Then we obtained 474 potential targets of neurotoxicity.

TABLE 1 Basic information of the core toxic components of Fuzi.

Ingredient name	CAS id	Molecule weight	OB score	Targets
Uracil	302-27-2	112.09	42.5256	1602
Palmitic Acid	67701-02-4	256.42	19.2966	216
Aconitine	302-27-2	645.74	7.9514	57
Linoleic Acid	60-33-3	279.40	-	39
Honokiol	35354-74-6	266.33	60.6694	34
14-Deoxy-11,12-Didehydroandrographolide	42895-58-9	332.43	13.6003	16
Juglone	481-39-0	174.15	25.7430	15
Magnolol	528-43-8	266.30	69.1927	11

Prediction of candidate targets and construction of PPI network

Matching the candidate targets of toxic compounds and the potential targets of neurotoxicity, 133 genes were selected as potential targets in the toxic effect of Fuzi on nerve. Then, String database was used to identify the PPI network of the 133 intersection target genes, as shown in Figure 3A.

We uploaded the PPI network in the figure above to Cytoscape 3.9.1 and used the Network Analyzer function in the software to analyze the topology parameters of each target (Table 2).

The top 10 are selected as the core targets according to the ranking of Degree value, followed by ALB, AKT1, TP53, IL6, TNF, INS, CASP3, IL1B, EGFR and BDNF. The visualization results are shown in Figure 3B.

Subsequently, we used Cytoscape3.9.1 to construct the relationship network between candidate toxic compounds of Fuzi and the corresponding 10 core targets in Figure 3C, and selected uracil, palmitic acid and aconitine as the key toxic compounds of Fuzi for subsequent analysis according to Degree value.

GO biological process and KEGG pathway enrichment analysis

To explore the toxic mechanisms, we imported 133 intersection targets into DAVID database for GO and KEGG pathway enrichment analyses. A total of 184 GO functional items were obtained, including 124 biological processes (BP), which mainly involved response to nutrient levels, gliogenesis, neuron death and aging, etc. There were 18 cellular components (CC), mainly including membrane raft, membrane microdomain, organelle outer membrane and vesicle lumen, etc. It also included 42 molecular function (MF), focusing on signaling receptor activator activity and receptor ligand activity. The first 10 items of enrichment results were visualized according to *p*-value, as shown in Figure 4A.

We screened 170 major signaling pathways in KEGG pathway enrichment results. The high ranking enriched pathways involved pathways of neurodegenerative multiple disease, MAPK signaling pathway, HIF-1 signaling pathway, TNF signaling pathway, and various infection and tumor-specific pathways. Other pathways included lipid and atherosclerosis, Hepatitis B and Hepatitis C, endocrine resistance, apoptosis and so on. The most significant enriched 20 pathways in KEGG analysis were shown in Figure 4B.

Among them, MAPK1, TP53, TNF, EGFR, INS, CASP3, IL1B and BDNF in the core targets were all related to MAPK signaling pathway, which is an important mechanism of Fuzi leading to neurotoxicity.

Molecular docking

In order to further verify the molecular mechanism of neurotoxicity of Fuzi, we chose uracil, palmitic acid and aconitine, the key toxic substances of Fuzi, to preliminarily simulate their binding to the core targets (Table 3).

It is generally believed that when the binding energy is less than -5.0 kJ mol^{-1}, this compound has a good binding activity with the core target protein, while when the binding energy is less than -7.0 kJ mol^{-1}, this compound has a strong binding activity with the core target protein (Hsin et al., 2013).

Among the key toxic substances of Fuzi, the binding energy of aconitine with ALB, AKT1 and CASP3 proteins were all less than -7.0 kJ·mol^{-1}, indicating that aconitine was the most stable active ingredient. Figure 5 showed the docking diagram of aconitine with ALB, AKT1 and CASP3 protein molecules.

Aconitine inhibits SH-SY5Y cell viability

Network pharmacology analysis showed that aconitine was the main toxic substance causing neurotoxicity of Fuzi, so we further investigated the toxic effect of aconitine on SH-SY5Y cells. The results of CCK-8 assay showed that aconitine at 300 and 400 μM concentrations could decrease SH-SY5Y cell viability following 24 h treatment and aconitine at all the different concentrations (25, 50, 100, 200, 300 and 400 μM)

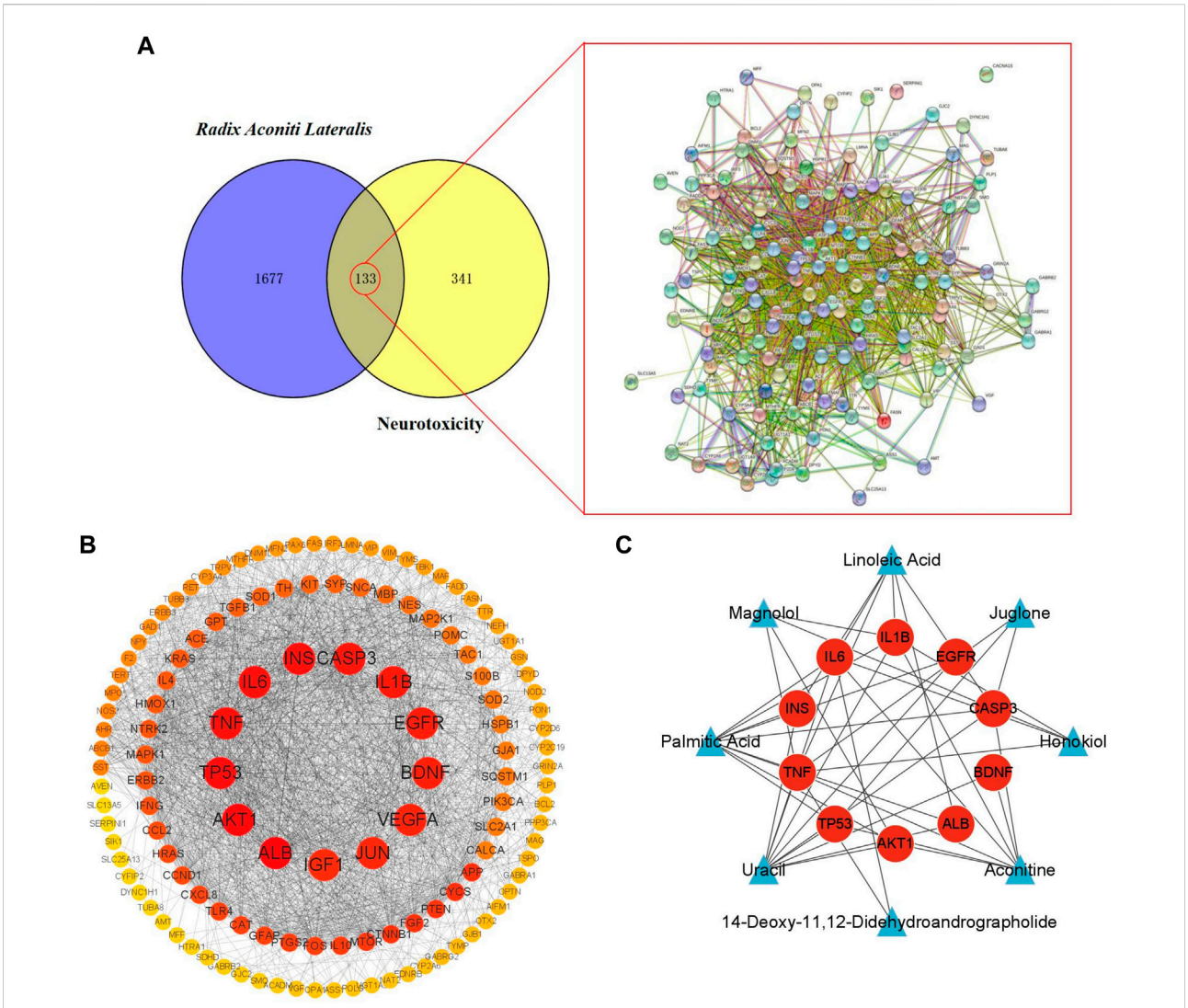

FIGURE 3
Target screening and establishment of PPI network. **(A)** Potential targets of neurotoxicity caused by Fuzi and PPI network. **(B)** PPI network of neurotoxicity targets caused by Fuzi. (The color of the node is marked from red to yellow according to the Degree value in descending order.) **(C)** Relationship network between candidate toxic compounds and core targets of Fuzi. (Blue triangles represent candidate toxic compounds and red circles represent core targets).

significantly decreased SH-SY5Y cell viability after 48 h treatment, and the cell viability rate gradually decreased with the increase of concentration, indicating that aconitine had significant toxic effect on SH-SY5Y cells (Figure 6). Moreover, IC_{50} value of the CCK-8 is 271.4226 μM (48 h).

Aconitine affects MAPK signaling pathway

According to the results of the KEGG enrichment analysis, MAPK signaling pathway was an important mechanism of neurotoxicity caused by Fuzi. Therefore, we further evaluated the expression levels of p53, p-MAPK and MAPK1, which are the core target proteins in MAPK signaling pathway. As shown in Figure 7A, aconitine inhibited the expression of p-MAPK, while the expression of MAPK1 remained basically unchanged. Meanwhile, aconitine also promoted the expression of p53. These results suggested that aconitine can inhibit phosphorylation of MAPK and the toxic effect of aconitine on SH-SY5Y cells was related to MAPK signaling pathways.

Aconitine affects the expression of the core proteins

Molecular docking results showed that Akt1 and Caspase-3 proteins were the core proteins of neurotoxicity caused by

10.3389/fphar.2022.961012

TABLE 2 Topological parameters of candidate targets.

Gene	Degree	Gene	Degree	Gene	Degree	Gene	Degree	Gene	Degree
ALB	174	HRAS	102	PIK3CA	62	MAF	36	EDNRB	18
AKT1	168	CCL2	100	SQSTM1	62	TBK1	36	UGT1A9	16
TP53	160	IFNG	98	CALCA	60	UGT1A1	34	NAT2	16
IL6	156	ERBB2	94	ABCB1	58	FASN	34	VGF	14
TNF	156	MAPK1	94	SST	58	TTR	34	OPA1	14
INS	156	NTRK2	94	AHR	58	FADD	34	ASS1	14
CASP3	146	KRAS	90	MPO	56	NEFH	34	POLG	14
IL1B	144	HMOX1	90	NOS2	56	DPYD	32	ACADM	12
EGFR	136	IL4	90	F2	54	GSN	32	SDHD	10
BDNF	134	GPT	86	TERT	54	PON1	30	SMO	10
VEGFA	130	ACE	86	NPY	52	NOD2	30	GABRB2	10
JUN	126	TGFB1	82	ERBB3	50	CYP2D6	28	GJC2	10
IGF1	124	KIT	80	RET	50	CYP2C19	28	HTRA1	8
CYCS	120	SYP	80	GAD1	50	GRIN2A	26	MFF	8
APP	120	SOD1	80	TUBB3	50	BCL2	24	CYFIP2	6
CTNNB1	118	TH	80	CYP3A4	48	PLP1	24	AMT	6
PTEN	118	SNCA	78	TRPV1	48	TSPO	22	DYNC1H1	6
FGF2	118	MBP	74	MTHFR	46	PPP3CA	22	TUBA8	6
MTOR	116	NES	72	MFN2	42	MAG	22	SLC25A13	4
IL10	110	MAP2K1	68	DNM1L	42	AIFM1	20	SIK1	4
PTGS2	108	POMC	66	FAS	42	GJB1	20	SLC13A5	2
FOS	108	TAC1	64	PAX6	42	OTX2	20	AVEN	2
CAT	106	SOD2	64	LMNA	40	OPTN	20	SERPINI1	2
TLR4	106	S100B	64	VIM	40	GABRA1	20	EDNRB	18
GFAP	106	SLC2A1	62	IRF3	40	GABRG2	20	UGT1A9	16
CXCL8	104	GJA1	62	VIP	40	TYMP	20	NAT2	16
CCND1	102	HSPB1	62	TYMS	36	CYP2A6	18	VGF	14

aconitine. Therefore, we assessed the expression level of p-Akt, Akt and Caspase-3 by western blot. As shown in Figure 7B, treatment of SH-SY5Y cells with aconitine (100, 200, 400 μM) led to apparent repression of phosphorylation level of Akt in a dose-dependent manner, with the expression of Akt remaining unchanged. What's more, aconitine promoted the expression of Caspase-3. The results indicated that the mechanism of neurotoxicity induced by aconitine was associated with inhibition of Akt phosphorylation and promotion of apoptosis.

Aconitine increases the release of LDH

LDH is a stable cytoplasmic enzyme and the release of LDH is a key feature of the plasma membrane damage. Compared with the control group, aconitine at different concentrations (25, 50, 100, 200, 300 and 400 μM) significantly increased the release of LDH in Figure 8A, which suggested that cell membrane damage was an important toxic effect of aconitine and might be a key pathway for other exogenous substances entering the cell.

Aconitine reduces SDH activity

SDH, belonging to cytochrome oxidase, is the only multi-subunit enzyme integrated on the membrane in the TCA cycle. It can provide electrons for the respiratory chain of mitochondrial oxygen demand and productivity, and is a marker enzyme of mitochondrial. As shown in Figure 8B, aconitine at 200 and 400 μM for 24 h significantly decreased SDH activity. Under the action of aconitine, the activity of SDH in nerve cells decreased at high dose, and the dose-effect relationship was obvious.

Aconitine reduces the number of normal hippocampal neurons

The Nissl Staining result is shown in Figure 9, we can observe that the structure of Nissl's body in control group is clear, the basophilic granules distribute evenly and the number is more. However, the number of Nissl's body in experimental group is less than the normal group, and there are a large number of

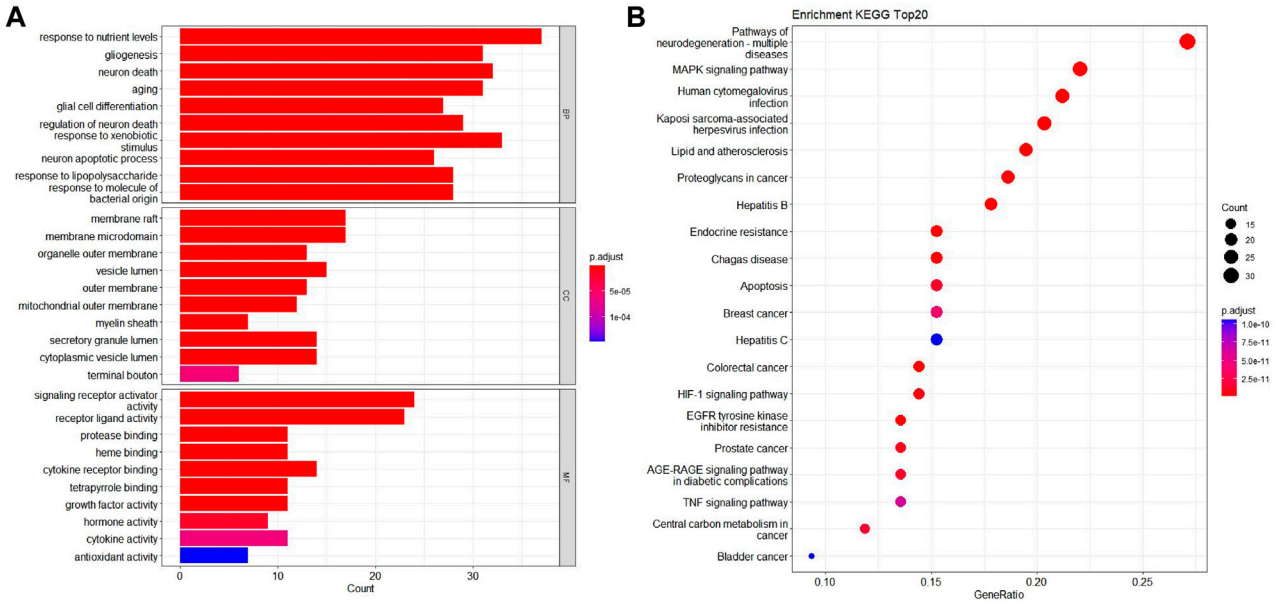

FIGURE 4
GO biological process and KEGG pathway enrichment analysis. **(A)** The bubble diagram of GO enrichment analysis of 133 intersection targets, including the top 10 significant enrichment terms of BP, CC and MF. **(B)** The bar plot diagram of KEGG pathway enrichment analysis of 133 intersection targets (top 20).

TABLE 3 The binding energy between key toxic substances and core targets of Fuzi.

	ALB	AKT1	TP53	IL6	TNF	INS	CASP3	IL1B	EGFR	BDNF
Uracil	−4.6	−5.1	−4.4	−3.7	−3.1	−4.0	−3.8	−2.8	−3.6	−3.9
Palmitic Acid	−5.7	−3.9	−3.8	−3.9	−4.2	−3.6	−4.8	−4.1	−3.5	−3.9
Aconitine	−8.3	−7.4	−6.1	−5.7	−4.9	−4.1	−7.1	−6.3	−5.5	−6.7

basophilic granules gathering which is caused by numerous Nissl's bodies dissolving.

Aconitine induces apoptosis of hippocampus neurons

Compared with the control group, we can see a large number of TUNEL positive cells (brown) in the experimental group obviously. Its expression area is wider and its dyeing is heavier (Figure 10). The result illustrates that aconitine can promote apoptosis of hippocampus neurons.

Discussion

Based on network pharmacology, molecular docking and experimental verification, this study systematically analyzed the potential mechanism of neurotoxicity caused by Fuzi, constructed the relationship network between candidate toxic compounds and neurotoxicity targets, and predicted the main toxic substances, potential targets and signaling pathways.

Network pharmacology analysis showed that uracil, palmitic acid and aconitine might play a crucial role in the neurotoxicity of Fuzi. Uracil is an important component in RNA, and fluorouracil, an antitumor drug with similar structure, has long been reported to have obvious neurotoxicity (Pirzada and AliDafer, 2000). Palmitic acid, as a long-chain saturated fatty acid, is an important component of blood lipids. Studies have shown that palmitic acid induces apoptosis by increasing oxidative stress in nerve cells, thereby producing neurotoxicity (Ng and Say, 2018). In addition, aconitine is considered to be the main toxic substance of Fuzi, Chuanwu and Caowu, and its toxic effects have been widely studied. The above existing

10.3389/fphar.2022.961012

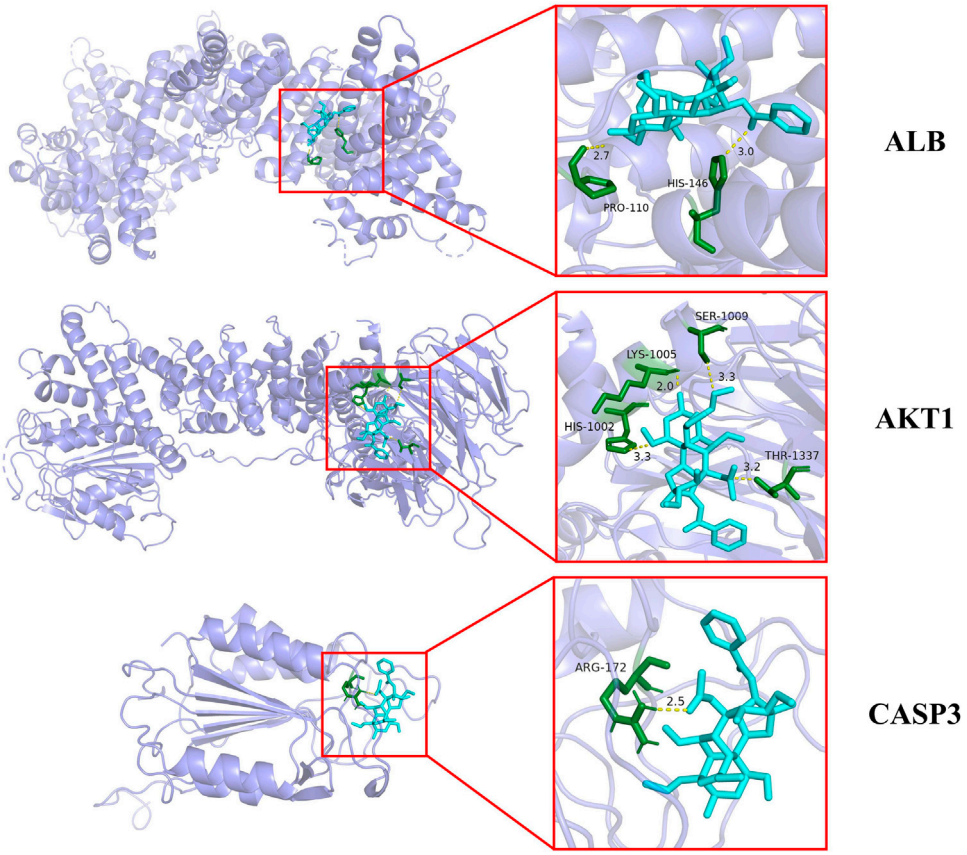

FIGURE 5
Molecular docking patterns of aconitine and core protein molecules. (The yellow lines represent the hydrogen bond interaction force, which is the main force promoting molecule binding with the active site.)

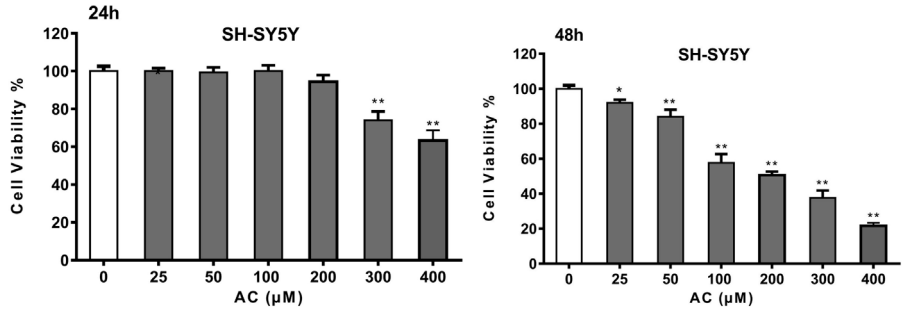

FIGURE 6
Cell Viability of SH-SY5Y cells after 24 and 48 h aconitine treatment. (*$p < 0.05$, **$p < 0.01$ versus control group.)

research results are basically consistent with the prediction results, suggesting that the main toxic substances of Fuzi are closely related to its neurotoxicity.

The result of PPI protein interaction network analysis showed that the potential target genes for neurotoxicity of Aconite were ALB, AKT1, TP53, IL6, TNF, INS, CASP3,

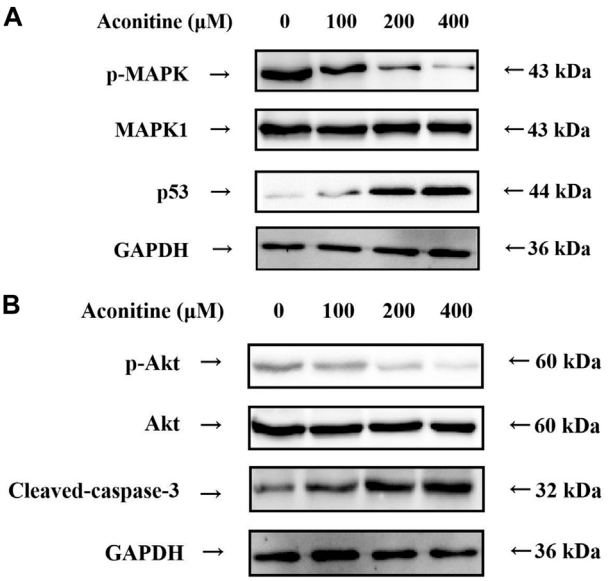

FIGURE 7
Western blot analysis after 48 h aconitine treatment. **(A)** Effects of aconitine on the protein secretion of MAPK pathway in SH-SY5Y cells. **(B)** Effects of aconitine on the secretory levels of p-Akt, Akt and Cleaved-caspase-3 in SH-SY5Y cells.

IL1B, EGFR and BDNF. AKT1 is the core target of PI3K/AKT signaling pathway. MAPK1, TP53, TNF, EGFR, INS, CASP3, IL1B and BDNF are related to MAPK signaling pathway. GO function and KEGG pathway enrichment analysis also confirmed that MAPK signaling pathway played an important role in the neurotoxicity induced by Fuzi.

Molecular docking results displayed that aconitine, the main toxic substance of Fuzi, exhibited good affinity with key targets ALB, AKT1 and CASP3, and the conformation of the binding site was stable. Based on the above results, the main toxic substance aconitine was selected for subsequent experimental verification, and its potential mechanism was discussed in depth.

The results of WB assay confirmed that aconitine affects the transmission of MAPK signaling pathway by inhibiting the MAPK protein phosphorylation and promoting the expression of p53. In KEGG PATHWAY database (https://www.genome.jp/kegg/pathway.html), we found that MAPK and p53 proteins are mainly involved in the classical MAPK pathway, JNK and p38 MAPK pathwayand p53 signaling pathway, and we suspected they are the main signaling pathways of neurotoxicity caused by Fuzi.

At the same time, the WB results showed that aconitine can inhibit the phosphorylation of the key protein Akt and promote the expression of Cleaved-caspase-3. Akt is the core protein of PI3K-Akt signaling pathway, and can control a variety of downstream signaling pathways, therefore, by adjusting the phosphorylation of Akt, Fuzi affects PI3K-Akt signaling pathway and controls various signaling pathways to cause neurotoxicity. And Cleaved-caspase-3, a kind of cysteine protease, is one of the key enzymes in the cell apoptosis pathways. Fuzi can increase its expression, and then promote the apoptosis of nerve cells in the resulting in neurotoxicity.

Aconitine can also increase LDH release and reduce SDH activity. The increase in LDH release suggests that aconitine can destroy the integrity of neuronal cell membrane, and the decrease in SDH activity suggests that aconitine leads to mitochondrial damage, while the damage of cell membrane and mitochondrial dysfunction are the characteristics of irreversible cell damage (Grimm, 2013). Aconitine may affect mitochondrial energy metabolism by inhibiting ATP production and aerobic respiratory function in nerve cells, and destroy the integrity of the cell membrane, leading to the entry of exogenous substances, thereby causing toxicity to nerve cells.

Mitochondrial dysfunction can lead to energy deficiency, which is an important mechanism for neurotoxicity (Liu et al., 2021). Early studies have found that mitochondrial dysfunction is associated with MAPK signaling pathway, leading to neuronal apoptosis and aggravating brain injury (Kleefstra et al., 2011; Gui et al., 2020; Manikanta et al., 2020). The relationship between mitochondrial function and MAPK signaling pathway needs further study. And appropriate targeted regulation of mitochondria may be a new direction to avoid neurotoxicity of Fuzi.

The hippocampus is the most vulnerable areas of the brain and plays an important role in learning function impairment, memory loss and cognitive dysfunction (Knierim, 2015). Apoptosis is the main cause of hippocampus damage. This research verifies that aconitine has toxicity to the nervous system. As shown by the results of Nissl Staining and TUNEL assay, we can find that aconitine produces neurotoxicity by promoting apoptosis of rat hippocampus neurons and reducing the number of neurons.

In fact, the mechanism of these pathways is not a single work, but the interaction influence causes neurotoxicity of Fuzi. However, these signaling pathways also play an important role in treatment in addition to inducing toxicity (Yang et al., 2020; Chen et al., 2022). We are unable to completely block the pathways to avoid the toxicity of Fuzi, and a more effective approach is to remove the toxic components by processing.

Earlier studies have demonstrated that the toxicity of Fuzi mainly derives from diester diterpenne alkaloids including aconitine (Singhuber et al., 2009), which has been confirmed by molecular docking in this article. In the clinic, we can boil Fuzi in water for a long period of time, transforming hypaconitine into monoester-diterpenoid alkaloids and finally into unesterified compounds, which has no toxicity and no influence on its pharmacological activities (Lu et al., 2010; Zhou et al., 2015).

In our study, some drawbacks should be noted. Our research only contains the toxic components that have been confirmed at present and whether there are other toxic compounds in Fuzi

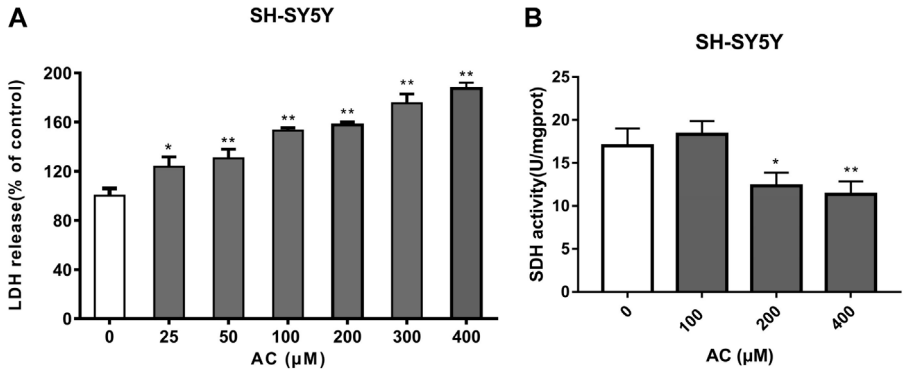

FIGURE 8
Effects of aconitine on mitochondrial function. **(A)** The release of LDH of SH-SY5Y cells after 24 h aconitine treatment. (*$p < 0.05$, **$p < 0.01$ versus control group.) **(B)** The SDH activity of SH-SY5Y cells after 24 h aconitine treatment. (*$p < 0.05$, **$p < 0.01$ versus control group).

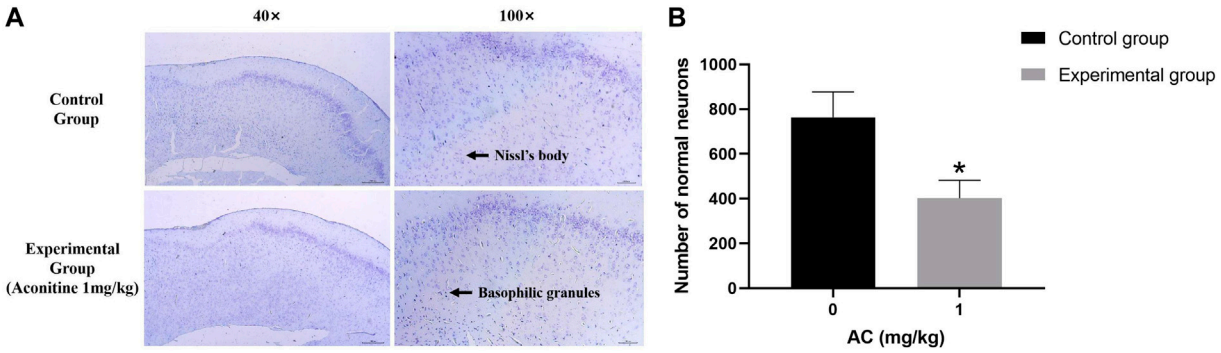

FIGURE 9
Treatment of aconitine for 7 days reduced the activity of hippocampus neurons. **(A)** Representative images magnified 40 and 100 times in hippocampus. **(B)** Quantitatively analyzed the number of Nissl's bodies in control and experimental group (×100). (*$p < 0.05$ versus control group).

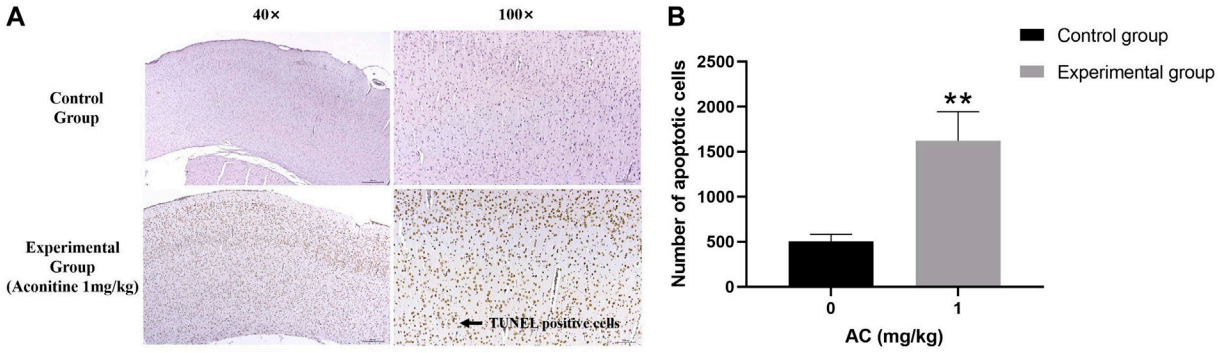

FIGURE 10
Treatment of aconitine for 7 days increased apoptosis of hippocampus neurons. **(A)** Representative images magnified 40 and 100 times in hippocampus. **(B)** Quantitatively analyzed the number of apoptotic cells in control and experimental group (×100). (**$p < 0.01$ versus control group.)

needs to be further studied. In addition, most of the Chinese herbal medicine plays a role in treatment by the form of oral, so its efficacy and toxicity are closely related to metabolites. Unfortunately, our research didn't predict all the bioactive metabolites of Fuzi *in vivo* (Feng et al., 2021).

In recent years, gut microbiota has emerged as a new frontier to understand the development and progress of diseases, especially it can influence the development and diseases of the central nervous system along "microbiota-brain-gut axis" (Quigley, 2017; Strandwitz, 2018). Arachic acid, a composition of Fuzi, is reported to be able to modulate the composition of gut microbiota (Zhuang et al., 2017; Sun et al., 2021). And whether Fuzi can cause neurotoxicity by influencing the gut microbiota still needs to be further discussed.

Conclusion

This research analyzed the potential mechanism of neurotoxicity caused by Fuzi through building the relationship network of "compounds - targets - neurotoxicity" using network pharmacology and molecular docking. The results showed that aconitine, the core toxic compound of Fuzi, caused neurotoxicity through multiple targets and multiple ways, including MAPK signaling pathway, pathways related to Akt protein, destroying cell membrane integrity, damaging mitochondrial function and affecting energy metabolism and cell apoptosis. At the same time, aconitine can promote apoptosis of hippocampus neuron and decrease its quantity, thus producing neurotoxicity. Our research provided reference for clinical application and related research.

Data availability statement

The datasets presented in this study can be found in online repositories. The names of the repository/repositories and accession number(s) can be found in the article/Supplementary material.

Ethics statement

The animal study was reviewed and approved by Animal Care and Use Committee of Chengdu University of Tranditional Chinese Medicine. Written informed consent was obtained from the individual(s) for the publication of any potentially identifiable images or data included in this article.

Author contributions

This manuscript was conceptualized by all the authors. JA conceived ideas, completed the network pharmacology and molecular docking experiments and drafted original draft preparation; HF and MH conducted the experimental verification; JX, FP, and CP administrated funding and revised the manuscript. All authors have read and agreed to the published version of the manuscript.

Funding

The study was supported by National Natural Science Foundation of China (no. 82003879 and U19A2010), the Key Project of Science and Technology Department of Sichuan Province (no. 2020YFS0053 and 2021YFS0044), and Youth Talent Promotion Project of China Association for Science and Technology (CACM-2020-QNRC1-01), Project of State Administration of Traditional Chinese Medicine of China (ZYYCXTD-D-202209) and the Open Research Fund of Chengdu University of Traditional Chinese Medicine Key Laboratory of Systematic Research of Distinctive Chinese Medicine Resources in Southwest China.

Conflict of interest

The authors declare that the research was conducted in the absence of any commercial or financial relationships that could be construed as a potential conflict of interest.

Publisher's note

References

Chan, T. Y. (2009). Aconite poisoning. *Clin. Toxicol.* 47 (4), 279–285. doi:10.1080/15563650902904407

Chen, L., Zhang, C., Cao, J., Bei, G., Wang, X., and Miao, Z. (2022). Yiyi fuzi baijiang decoction alleviates ulcerative colitis partly by regulating TLR4-mediated PI3K/Akt and NF-κB pathways. *Evid. Based. Complement. Altern. Med.* 2022, 8780514. doi:10.1155/2022/8780514

Feng, W., Liu, J., Zhang, D., Tan, Y., Cheng, H., and Peng, C. (2021). Revealing the efficacy-toxicity relationship of Fuzi in treating rheumatoid arthritis by

systems pharmacology. *Sci. Rep.* 11 (1), 23083. Published 2021 Nov 29. doi:10.1038/s41598-021-02167-5

Grimm, S. (2013). Respiratory chain complex II as general sensor for apoptosis. *Biochim. Biophys. Acta* 1827 (5), 565–572. doi:10.1016/j.bbabio.2012.09.009

Gui, C., Ren, Y., Chen, J., Wu, X., Mao, K., Li, H., et al. (2020). p38 MAPK-DRP1 signaling is involved in mitochondrial dysfunction and cell death in mutant A53T α-synuclein model of Parkinson's disease. *Toxicol. Appl. Pharmacol.* 388, 114874. doi:10.1016/j.taap.2019.114874

Hopkins, A. L. (2007). Network pharmacology. *Nat. Biotechnol.* 25 (10), 1110–1111. doi:10.1038/nbt1007-1110

Hsin, K. Y., Ghosh, S., and Kitano, H. (2013). Combining machine learning systems and multiple docking simulation packages to improve docking prediction reliability for network pharmacology. *PLoS One* 8 (12), e83922. doi:10.1371/journal.pone.0083922

Kleefstra, T., Wortmann, S. B., Rodenburg, R. J., Bongers, E. M. H. F., Hadzsiev, K., Noordam, C., et al. (2011). Mitochondrial dysfunction and organic aciduria in five patients carrying mutations in the Ras-MAPK pathway. *Eur. J. Hum. Genet.* 19 (2), 138–144. doi:10.1038/ejhg.2010.171

Knierim, J. J. (2015). The hippocampus. *Curr. Biol.* 25 (23), R1116–R1121. doi:10.1016/j.cub.2015.10.049

Li, S., and Zhang, B. (2013). Traditional Chinese medicine network pharmacology: Theory, methodology and application. *Chin. J. Nat. Med.* 11 (2), 110–120. doi:10.1016/S1875-5364(13)60037-0

Liu, H., Ho, P. W., Leung, C. T., Pang, S. Y. Y., Chang, E. E. S., Choi, Z. Y. K., et al. (2021). Aberrant mitochondrial morphology and function associated with impaired mitophagy and DNM1L-MAPK/ERK signaling are found in aged mutant Parkinsonian LRRK2R1441G mice. *Autophagy* 17 (10), 3196–3220. doi:10.1080/15548627.2020.1850008

Lu, G., Dong, Z., Wang, Q., Qian, G., Huang, W., Jiang, Z., et al. (2010). Toxicity assessment of nine types of decoction pieces from the daughter root of Aconitum carmichaeli (Fuzi) based on the chemical analysis of their diester diterpenoid alkaloids. *Planta Med.* 76 (8), 825–830. doi:10.1055/s-0029-1240688

Manikanta, K., Naveen Kumar, S. K., Hemshekhar, M., Kemparaju, K., and Girish, K. S. (2020). ASK1 inhibition triggers platelet apoptosis *via* p38-MAPK-mediated mitochondrial dysfunction. *Haematologica* 105 (8), e419–e423. doi:10.3324/haematol.2019.233908

National Research Council (Us) (2011). *Committee for the update of the guide for the Care and use of laboratory animals. Guide for the Care and use of laboratory animals*. 8th ed. Washington (DC): National Academies Press US.

Ng, Y. W., and Say, Y. H. (2018). Palmitic acid induces neurotoxicity and gliatoxicity in SH-SY5Y human neuroblastoma and T98G human glioblastoma cells. *PeerJ* 6, e4696. doi:10.7717/peerj.4696

Pirzada, N. A., AliII, and Dafer, R. M. (2000). Fluorouracil-induced neurotoxicity. *Ann. Pharmacother.* 34 (1), 35–38. doi:10.1345/aph.18425

Quigley, E. M. M. (2017). Microbiota-brain-gut Axis and neurodegenerative diseases. *Curr. Neurol. Neurosci. Rep.* 17 (12), 94. doi:10.1007/s11910-017-0802-6

Singhuber, J., Zhu, M., Prinz, S., and Kopp, B. (2009). Aconitum in traditional Chinese medicine: A valuable drug or an unpredictable risk? *J. Ethnopharmacol.* 126 (1), 18–30. doi:10.1016/j.jep.2009.07.031

Strandwitz, P. (2018). Neurotransmitter modulation by the gut microbiota. *Brain Res.* 1693, 128–133. doi:10.1016/j.brainres.2018.03.015

Sun, Y., Wu, D., Zeng, W., Chen, Y., Guo, M., Lu, B., et al. (2021). The role of intestinal dysbacteriosis induced arachidonic acid metabolism disorder in inflammaging in atherosclerosis. *Front. Cell. Infect. Microbiol.* 11, 618265. Published 2021 Mar 18. doi:10.3389/fcimb.2021.618265

Yang, J., Ma, W., Mei, Q., Song, J., Shu, L., Zhang, S., et al. (2020). Protective effect of fuzi lizhong decoction against non-alcoholic fatty liver disease *via* anti-inflammatory response through regulating p53 and PPARG signaling. *Biol. Pharm. Bull.* 43 (11), 1626–1633. doi:10.1248/bpb.b20-00053

Yang, M., Ji, X., and Zuo, Z. (2018). Relationships between the toxicities of Radix aconiti Lateralis preparata (fuzi) and the toxicokinetics of its main diester-diterpenoid alkaloids. *Toxins (Basel)* 10 (10), 391. doi:10.3390/toxins10100391

Zhang, R., Zhu, X., Bai, H., and Ning, K. (2019). Network pharmacology databases for traditional Chinese medicine: Review and assessment. *Front. Pharmacol.* 10, 123. doi:10.3389/fphar.2019.00123

Zhao, L., Sun, Z., Yang, L., Cui, R., Yang, W., and Li, B. (2020). Neuropharmacological effects of aconiti Lateralis Radix Praeparata. *Clin. Exp. Pharmacol. Physiol.* 47 (4), 531–542. doi:10.1111/1440-1681.13228

Zhou, G., Tang, L., Zhou, X., Wang, T., Kou, Z., and Wang, Z. (2015). A review on phytochemistry and pharmacological activities of the processed lateral root of Aconitum carmichaelii Debeaux. *J. Ethnopharmacol.* 160, 173–193. doi:10.1016/j.jep.2014.11.043

Zhuang, P., Shou, Q., Lu, Y., Wang, G., Qiu, J., Wang, J., et al. (2017). Arachidonic acid sex-dependently affects obesity through linking gut microbiota-driven inflammation to hypothalamus-adipose-liver axis. *Biochim. Biophys. Acta. Mol. Basis Dis.* 1863 (11), 2715–2726. doi:10.1016/j.bbadis.2017.07.003

frontiers | Frontiers in Pharmacology

TYPE Review
PUBLISHED 21 October 2022
DOI 10.3389/fphar.2022.947512

OPEN ACCESS

EDITED BY
Zhichao Xu,
Northeast Forestry University, China

REVIEWED BY
Chao Xiong,
Wuhan Polytechnic University, China
Panagiotis Madesis,
University of Thessaly, Greece

*CORRESPONDENCE
Ramalingam Sathishkumar,
rsathish@buc.edu.in
Ashutosh Sharma,
asharma@tec.mx

SPECIALTY SECTION
This article was submitted to Experimental Pharmacology and Drug Discovery, a section of the journal Frontiers in Pharmacology

RECEIVED 18 May 2022
ACCEPTED 10 October 2022
PUBLISHED 21 October 2022

CITATION
Mahima K, Sunil Kumar KN, Rakhesh KV, Rajeswaran PS, Sharma A and Sathishkumar R (2022), Advancements and future prospective of DNA barcodes in the herbal drug industry. *Front. Pharmacol.* 13:947512. doi: 10.3389/fphar.2022.947512

Advancements and future prospective of DNA barcodes in the herbal drug industry

Karthikeyan Mahima[1,2], Koppala Narayana Sunil Kumar[2], Kanakarajan Vijayakumari Rakhesh[3], Parameswaran Sathiya Rajeswaran[1], Ashutosh Sharma[4]* and Ramalingam Sathishkumar[1]*

[1]Plant Genetic Engineering Laboratory, Department of Biotechnology, Bharathiar University, Coimbatore, Tamil Nadu, India, [2]Department of Pharmacognosy, Siddha Central Research Institute, Chennai, Tamil Nadu, India, [3]Department of Chemistry, Captain Srinivasa Murthy Central Ayurveda Research Institute, Chennai, Tamil Nadu, India, [4]Tecnologico de Monterrey, Centre of Bioengineering, Santiago de Queretaro, Queretaro, Mexico

Ethnopharmacological relevance: The past couple of decades have witnessed the global resurgence of medicinal plants in the field of herbal-based health care. Increased consumption of medicinal plants and their derivative products is the major cause of the adulteration issues in herbal industries. As a result, the quality of herbal products is affected by spurious and unauthorized raw materials. Recent development in molecular plant identification using DNA barcodes has become a robust methodology to identify and authenticate the adulterants in herbal samples. Hence, rapid and accurate identification of medicinal plants is the key to success for the herbal industry. Aim of the study: This paper provides a comprehensive review of the application of DNA barcoding and advanced technologies that have emerged over the past 10 years related to medicinal plant identification and authentication and the future prospects of this technology.

Materials and methods: Information on DNA barcodes was compiled from scientific databases (Google Scholar, Web of Science, SciFinder and PubMed). Additional information was obtained from books, Ph.D. thesis and MSc. Dissertations.

Results: Working out an appropriate DNA barcode for plants is challenging; the single locus-based DNA barcodes (*rbcL*, ITS, ITS2, *matK, rpoB, rpoC, trnH-psbA*) to multi-locus DNA barcodes have become the successful species-level identification among herbal plants. Additionally, multi-loci have become efficient in the authentication of herbal products. Emerging advances in DNA barcoding and related technologies such as next-generation sequencing, high-resolution melting curve analysis, meta barcodes and mini barcodes have paved the way for successful herbal plant/samples identification.

Conclusion: DNA barcoding needs to be employed together with other techniques to check and rationally and effectively quality control the herbal drugs. It is suggested that DNA barcoding techniques combined with metabolomics, transcriptomics, and proteomics could authenticate the

herbal products. The invention of simple, cost-effective and improved DNA barcoding techniques to identify herbal drugs and their associated products of medicinal value in a fool-proof manner will be the future thrust of Pharmacopoeial monograph development for herbal drugs.

KEYWORDS

DNA barcoding, herbal products, monographs, quality control, regulatory status

Introduction

Medicinal plants and herbal supplements have contributed to a global resurgence in traditional health systems. Herbal medicines continue to gain international acceptance in modern medical and health care services. In India, traditional medical treatments such as Ayurveda, Naturopathy, Unani, Siddha and Homeopathy benefit humankind in a big way and are employed to treat diverse illnesses. Availability of genuine medicinal plants and its raw materials has increased in the past decade, testifying the worldwide interest in these products (Marichamy et al., 2014; Howard et al., 2020). Globalization of exporting the herbal medicines is expanding in the market leading to mixing of substitute materials or adulterants with genuine raw materials. Medicinal plants with high therapeutic potential are used for novel drug formulations in industries but the lack of standardized operating procedures and analytical methods, complicate the quality control of herbals. Herbal quality regulations vary between countries and authentication of herbal medicines relies on sensory and phytochemical screening techniques to detect species-specific characters and compounds respectively (European Medicine Agency, 2006; World Health Organization, 2004, (Word Health Organisation, 2011; EDQM, 2014). The substitution of unlabelled fillers used in the herbal medicines presents a challenge that risks patient safety and herbal efficacy. Several safety-related issues emerged globally due to the inaccurate or false identification of herbal medicines and their source plants. Therefore, the correct identification of herbal plants and their raw materials is essential for their safe usage.

Several traditional methods were used to authenticate herbal materials, including morphological, microscopic, and chemical identification. In the case of classical taxonomy approach involving the micro and macroscopic characters are not working recently due to the lack of taxonomic expertise available. Still, scientists have different opinions regarding the exact naming of species in the form of synonyms in classical taxonomy. The identification of the taxon is the fundamental activity and one of the primary objectives of plant systematics. It involves expert determination, recognition, comparison and the use of keys. The routine traditional identification decreases due to lack of taxonomist experts and often leads to misidentification among the closely related species.

Additionally, there was a lack of comprehensive morphological keys in different life stages of plants, phenotypic plasticity and genetic variability in the characters, which might significantly contribute to incorrect recognition and false identification of species (Vohra and Khera, 2013). Identification of taxa based on DNA sequence have the advantage that DNA sequence data is present uniformly in all plant parts and is relatively stable. In the last few decades, several genome-based techniques have been developed to identify plant species, but no single universally acceptable tool is known to identify plant species rapidly. Apparently, unique morphological characters and chemical constituents are found to be occasionally tough in distinguishing closely related species. The powdered or processed plant products cannot typically be identified without the help of pharmacognosy experts; however, like all techniques, they also have their own limitations. Pharmacognosy techniques offer herbal products quality and robustness with the involvement of trained experts, which eventually enable to separate the substitute from genuine samples (Li et al., 2011). An array of tools have been established, and each of them has its limitations in finding out the substitutions in the herbal samples (Kumar et al., 2009). The foremost techniques involve AFLP (Amplified Fragment Length Polymorphism) (Gowda et al., 2010), RFLP (Restriction Fragment Length Polymorphism) (Watthanachaiyingcharoen et al., 2010; Lin et al., 2012), CAPS (Cleaved Amplified Polymorphic Sequence), RAPD (Random Amplified Polymorphic DNA) (Hazarika et al., 2014), microsatellite markers or SSR (Simple Sequence Repeats) (Tamhankar et al., 2009), ISSR (Inter Simple Sequence Repeats) (Sharma et al., 2008), and SCOT (Start Codon Targeted Polymorphism) (Wang et al., 2001). By employing these techniques, multiple bands were observed with different sizes in an electrophoretic gel. Based on these qualitative data, different entities were identified and compared. However, the limitations of these techniques lie in the loss of specificity with the primer binding or restriction enzyme binding site. Another major drawback of studies employing the above-mentioned molecular techniques was the hardship of sequencing the multiple bands. In RAPD techniques, this was overcome with SCAR development (Sequence Characterized Amplified Region) markers. SCAR markers were achieved by sequencing a unique band for the species and developing primers from within. Even

though SCAR markers help to identify the taxon at the species level, their function was rather suppressed with the determination of cultivars or varieties among the same species rather than classification among genus or familial level. So, there is a potential need to develop a genome-based approach for the exact identification of plant species (Sucher and Carles, 2008). The concept of "DNA barcoding" offers a comprehensive solution for many problems concerning plant identification. The emergence of DNA barcoding has positively impacted the herbal industry, biodiversity classification, and even the renaissance of taxonomy.

DNA barcoding is a technique used to identify species based on a short-standardized portion of the genome. The three major principles of DNA barcoding are standardization, minimalism, and scalability. DNA barcoding can achieve rapid, time-saving and automated identification of species from all kinds of herbal products. By employing this technique, the extracted DNA from the collected sample using the standard protocol and following the DNA sequence analysis of the target gene harbors high rates of nuclear substitutions to discriminate closely related species while remaining more or less similar for all members of the same species. DNA barcoding was first put forward and universally accepted in animal systems (Hebert et al., 2003). However, in the case of plant species, individual taxons have not yet been discriminated due to the slow mutation rate. However, many studies have investigated universal plant barcodes, but no one has identified and discovered the ideal and universal barcode. Various regions of DNA showing high inter and intra-specific variability have been used as universal and high-resolution DNA barcodes. Two international initiatives were working to develop DNA barcodes in plants, including the Consortium for the Barcode of Life (CBOL) and the International Barcode of Life (iBOL). CBOL is a large group of scientists working intensively to identify DNA barcodes in flora and fauna globally. The iBOL is the largest biodiversity genomics group and their mission is to make DNA barcoding research as a global science. They maintained a cloud-based data storage platform named Barcode of Life Data systems (BOLD) reference library used for global species identification. It has been inferred that an ideal barcode region should have low intra-specific and high inter-specific divergence between the species (Kress and Erickson, 2007). However, there is controversy regarding the effective use of DNA barcodes in plants due to the poor discrimination ability among the species (Hebert et al., 2003; Moritz and Cicero, 2004; Will and Rubinoff, 2004; Ebach and Holdrege, 2005; Will et al., 2005; Newmaster et al., 2009). Several reports have convincingly shown that recognizing hidden diversity, monitoring biological invasions, finding out the different life stages of the seedlings, characterizing the molecular changes during metamorphosis, biodiversity monitoring, identification of fossil seeds, quality trade-in timber industries, monitoring the illegal trading of food products, identification of adulterants in commercial products including herbal supplements and assessment of diversified exotic species was possible with the employment of DNA barcoding techniques (Liu et al., 2011; Muellner et al., 2011; Baker et al., 2012; Gismondi et al., 2012). In CBOL (2009) recommended that single-locus plastid barcode-like *rbcL, matK* and two-locus combined *matK* + *rbcL* are the best plant barcode with high resolution and discriminatory power. The other regions of chloroplast and nuclear genome, such as *trnH-psbA, ycf1, ITS, trnL-F* and ITS2, have been recommended as supplementary DNA barcodes for plant identification (Hollingsworth et al., 2009; Ragupathy et al., 2009; Nithaniyal et al., 2014; Ferri et al., 2015). The application of NGS, whole-plastid genome and metabarcodes has stretched the versatility of DNA barcodes to the next higher level, proving the complete species information can be obtained irrespective of the morphological or life stages. The use of whole-plastid genome, mini-barcodes, and metabarcodes opened up a new way to identify plants (Erickson et al., 2008; Yang et al., 2012; Dormontt et al., 2018; Gao et al., 2019). However, the whole-plastid genome and mini-barcode concept have not been universally accepted due to difficulties obtaining the complete sequence and discrimination ability. However, metabarcoding is an emerging area of research with identifications of taxa from mixed samples by using the high throughput sequencing methods (Taberlet et al., 2012; Cristescu, 2014). DNA barcoding of medicinal plants and herbal products could be relatively challenging in evaluating the data to discriminate the exact species (Verma and Goswami, 2014). Figure 1 annotates the total number of international peer-reviewed manuscripts published from January 2010 to April 2022, denoting the use of DNA barcoding methods in medicinal plant identification. This review was revised to cover approximately 12 years till April 2022 publications of DNA barcoding papers related to medicinal plant and herbal products authentication from different platforms such as Google Scholar, Pubmed, Scopus and Web of Science. The current manuscript institutes the nature and amount of species adulteration reported in the herbal trade market and discusses the newly-developing techniques of DNA barcoding used to identify medicinal plants and, finally, insights into future research directions on DNA barcoding of medicinal plants and herbal medicines.

Current status and role of regulatory authorities in herbal drugs

In recent decades, the demand for traditional medicines and herbal products increased exponentially in all over the globe and it led to the increment of investments in the sector. As the demands grows the quality of raw drug supplied got decremented and to compensate such issues World Health Organization (WHO) came up with various guidelines and regulatory strategies. The guidelines of WHO specifically mentioned the use of incorrect species is a threat to consumer safety (Palhares

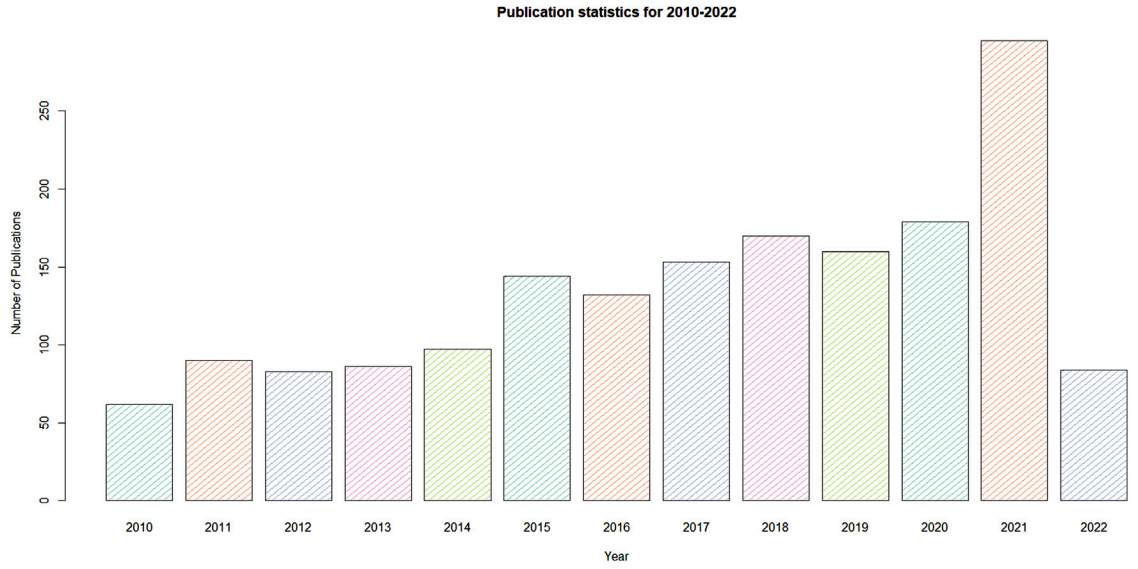

FIGURE 1
Graphical representation of manuscripts published from 2010 to 2022 on identification of medicinal plants using DNA barcoding.

et al., 2015). Authenticating the quality of herbal medicines is one of the major regulatory requirement and countries over the globe came up with various regulatory organizations mitigate the challenge. Each country has its own Pharmacopoeia booklets of standards for drugs, pharmaceuticals, supplements *etc.* These books provide an acceptable quality monograph to maintain standards. The identification and authentication of raw materials using were traditionally carried out using organoleptic, morphological, microscopic characteristics and standard phytochemical assessments. DNA barcode-based authentication is now being applied in all industrial and pharmaceutical sectors to authenticate wide range of herbal raw drugs. In United States of America (USA), Food and Drug Administration (FDA) regulates the current Good Manufacturing Practices (cGMP) for dietary supplements (Palhares et al., 2015). In European Countries, European Medicines Agency (EMA) had guidelines concerning the quality of herbal drugs and products including qualitative and quantitative assays. Additionally, EMA encourage the use of other techniques to offer the assurance of quality in herbal medicines. The Canadian Food Inspection Agency (CFIA) also have the guidelines to authenticate the herbal drugs using the qualitative and quantitative assays (RSC, 1985). DNA barcodes have recently been incorporated into the British Pharmacopoeia for the first time (British Pharmacopoeia Commission, 2017). Recently, United States Pharmacopoeia, British Pharmacopoeia and Indian Pharmacopoeia have in recognition to test herbal drug authentication using ITS barcode candidate or other regions (Prakash et al., 2017). Currently, the Chinese Pharmacopeia have additions of Medicinal Materials DNA Barcode database (MMDBD) along with monographs (Wong et al., 2018). In India, many government organizations are working towards standardization, quality control and elimination of adulteration for herbal medicines. These include the Ministry of AYUSH, Central Council for Research in Ayurvedic Sciences (CCRAS), Central Council for Research in Siddha (CCRS), CSIR-Indian Institute of Integrative Medicine and Indian Pharmacopoeia Commission (IPC). The main objective of IPC is to develop comprehensive monographs about herbal drugs, which is in the form of an official book containing a detailed description of quality standards of herbal medicines, including raw herbs, herbal extracts, processed herbs and powdered ones, along with chemical information, preparation, function and regulation of drugs. However, well-compiled information on Indian herbal drugs with reference to Indian Pharmacopoeia is not yet available. To date total of eight IP editions have been published by the IPC (IPC, 2018). The current eighth edition of IP in 2018 consists of four volumes combining 220 monographs which include Chemical Monographs (170), Herbal Monographs (15), Blood and Blood-related products (10), Vaccines and Immunosera for Human use monographs (02), Radiopharmaceutical monographs (03), Biotechnology-Derived Therapeutic Products (06) and Veterinary monographs (14). The revised monographs are about 366 and seven commissions (IPC, 2018). The Indian Pharmacopoeia Commission has become the first WHO Collaborating Centre for Safety of Medicines and Vaccines in the South-East Asia Region (Basu, 2020). Indian Pharmacopoeia introduced DNA barcoding as a test to validate *Asparagus* species early in 2012, as alternative test when other test

fails in species identification (Rai et al., 2012). This would ensure the wider use of herbal drugs at global level having regional to global markets and consumers across the globe.

Unlabelled malpractices in the herbal industry

Despite various regulatory authorities and strict monitoring, certain malpractices persists on traditional drug trades. Traditional medical system and herbal products were linked with culture, economics, tourism and livelihood of regions, states or countries all around the globe. The industrial demand for medicinal plant resources makes a massive rise, with a matching proportion of adulterated herbal drugs sold out worldwide (Ved and Goraya, 2007). The primary reason for the supplementation of substitutes to authenticate samples is found to be mainly due to deforestation or extinction of many species and incorrect species identification (Mishra et al., 2015). If the demand for a specific herb is more remarkable, then there is an increased risk of adding adulterants and use of poor-quality materials. Another major malpractice in the herbal product industry arises due to the mismanagement of naming system. The traditional system follows vernacular names of plants over scientific names since majority of these system arise before the adaptation of scientific nomenclatures. Herbal formulation and ingredients were mentioned in ancient texts and manuscripts as in regional languages/vernacular names and the lack of experts in the identifying the plants based on these descriptions further escalates the situation. A well-known example was in the case of Brahmi; main ingredient in the production of memory enhanced drugs by Ayurveda and Siddha traditional system of medication. In northern states of India, the plant *Centalla asiatica* were considered as Brahmi while the southern states of India consider *Bacopa monneri* as Brahmi. This happens due to error in deciphering the identification features mentioned in traditional manuscripts and blindly following the vernacular naming of plant mentioned in various location. The plants *C. asiatica* and *B. monneri* comes under different families and have entirely different phytochemical composition and it form different effect in formulations (Santhosh Kumar et al., 2018). Further the traditional species identification is declining due to certain limitations such as lack of high-level taxonomic expertise, morphologically similar cryptic taxa and lack of incomplete morphological keys for particular life changes (de Boer et al., 2015). Another important factor contributing to the increase in malpractices in the herbal industry was the lack of proper regulation in distribution and selling of drugs. Unlike modern medicine traditional drug materials can be directly purchased from outlet without proper prescription from authenticated traditional medical practitioner. Purchasing of an improper drug based on vernacular naming and unwanted substitutions without proper prescription increase the chance of adverse health effect by multiple folds and which was one of the major causes of rejection towards traditional medicines in modern communities.

In addition to the adulteration with a substitute for the genuine biological species in herbal preparations, another problem contributing to falling quality standards of herbal products is related to the accumulation of heavy metals in the herbal-based drugs (Ernst, 2002; Chen et al., 2021). Saper et al., 2004 reported a significant amount of heavy metals in herbal products collected from Indian herbal samples (64% mercury, 41% arsenic and 9% cadmium). The traditional medicines from China, Mexico, Africa and South Asian countries have also been shown to contain heavy metals (Lekouch et al., 2001; Yu et al., 2021). These contaminants can lead to serious harm to patients such as, with problems associated with liver, kidney and respiratory leading to organ failure in the affected persons. There is a need for biological and chemical-based procedures in order to stringently evaluate the quality of herbal products. The quality control parameters for the evaluation of herbal products are summarized in Figure 2. In recent times new techniques have flourished to identify adulterants in the herbal samples, which are collectively termed as 'Omics,' a compilation of three technologies such as genomics, proteomics, and metabolomics (Pandey et al., 2016). Many reports based on wet-lab experiments showed that DNA barcoding technology could be used to find out the adulterants from herbal products and medicinal plants. For example, several reports discussed about the suitability of barcoding in ginseng species, a well-known group of medicinal plants (*Panax*, Araliaceae) and found that core barcodes *matK* and *rbcL* and additional ITS and *trnH-psbA* have been efficient for species identification (Zuo et al., 2011; Wallace et al., 2012). The studies on *Cassia* (Purushothaman et al., 2014), *Ginkgo* (Little, 2014), *Hypericum* (Howard et al., 2019), *Sida* (Vassou et al., 2015) and many other species have shown great utility in using DNA barcodes for the authentication of herbal products and medicinal plants. A few reports have employed modern techniques, such as microscopy, mass spectroscopy and metabolomics for the effective quality control of herbal products (Xiao et al., 2011; Raclariu et al., 2017b; Ichim et al., 2020). Based on the published resources with convincing experimental evidence, we tried our best to tabularize the list of adulterant species present in medicinal plants (Table 1).

DNA barcoding: A genomics-based tool for plant identification

Since its initiation in 2003, DNA barcoding has drawn the attention of the international scientific community, government agencies and the public. Parallel development in the field of biotechnology and plant taxonomy creates a rejuvenated emphasis on the exploration and rapid identification of species. Hebert et al., 2003 proposed a microgenomic

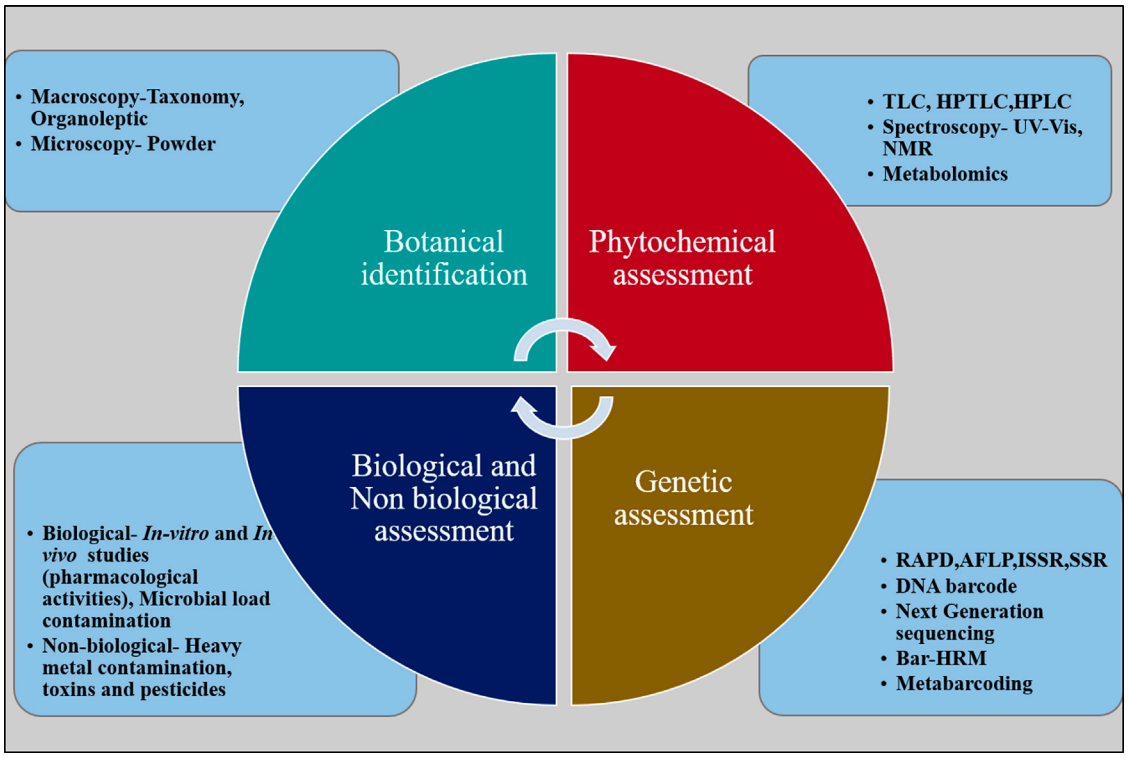

FIGURE 2
Parameters used in quality assessment of herbal products.

identification system or DNA taxonomy, which permits life discrimination by analyzing a small standardized genome segment. This represents one of the promising approaches towards diagnosing biological diversity. It implies that the standard DNA locus is amenable to bidirectional sequencing, which effectively provides high discrimination among the species. These innovations contribute to major advancement in the plant systematics classification and identification of taxa of medicinal importance (Kress et al., 2005). DNA barcoding has become a reality in recent times, and various markers have been used with reference to its universality and high resolution between the species (Chen et al., 2010, 2014). Intended for the discrimination, DNA markers need to be in higher inter and lower intraspecific divergence, called 'DNA barcoding gap.' For several years, CBOL and many studies have searched for emphasized an efficient and universal plant barcode; it was inferred that none of the available loci could work across all species (Chase and Fay, 2009; Chen et al., 2010). The Consortium for Barcode of Life-Plant Working Group (CBOL) recommended the chloroplast (*matK, rbcL*) and combination of *matK* + *rbcL* are to be the ideal barcodes for all the plant species (Kress et al., 2005; Rubinoff et al., 2006; CBOL, 2009; Stoeckle et al., 2011). Recently it has been proposed that by employing the molecular attributes of the whole-plastid genome in plant identification, flawless identification of herbal plants could be achieved. However, this concept and approach have has not yet been accepted universally (Erickson et al., 2008; Sucher and Carles, 2008; Yang et al., 2012; Ahmed, 2022). One of the main reasons is found to be the high sequencing cost and the difficulties in obtaining a complete plastid genome as compared to single-locus barcodes. In many of the taxa, secondary metabolites which are present in the leaves, stems and roots often hamper successful PCR conditions and these shortcomings are known to be overcome by making suitable modifications in the extraction methods. The types of DNA barcode markers and the related techniques have been discussed in the following passages, emphasizing the current trends for overcoming the challenges of DNA barcoding in plants.

Single-locus DNA barcode markers

DNA barcoding studies primarily aim to develop a universal DNA barcode marker in plants to identify taxa. Many reports have recommended developing a universal barcode marker from the plastid and nuclear genome (Newmaster et al., 2006; Kress and Erickson, 2007; Kress, 2017). In 2009, Centre Barcode for Life Plant Working Group compared seven barcode candidates,

TABLE 1 List of known adulterants/substitutes in the herbal drug trade.

S.No	Main drugs	Adulterants	References
1	*Aconitum heterophyllum*	*Cyperus rotundus*	Seethapathy et al. (2014)
2	*Aerva lanata*	*Aerva javanica, Bergenia ligualata*	Sarin, (1996)
3	*Aloe barbadensis*	*Acacia catechu*	Keshari and Pradeep, (2017)
4	*Amomum subulatum*	*Heracleum rigens*	Keshari and Pradeep, (2017)
5	*Andrographis paniculata*	*Swertia chirayta*	Mishra et al. (2015)
6	*Asparagus racemosus*	*Asparagus gonoclados*	Rai et al. (2012)
7	*Atropa belladonna*	*Ailanthus altissima*	Ahmed and Hasan, (2015)
8	*Bacopa monnieri*	*Centella asiatica*	Santhosh Kumar et al. (2018)
9	*Bereberis aristata*	*Coscinium fenestratum*	Santhosh Kumar et al. (2018)
10	*Boerhavia diffusa*	*Boerhavia erecta, Boerhavia repanda, Boerhavia coccinea, Boerhavia verticillata*	Selvaraj et al. (2012)
11	*Cassia fistula*	*Senna auriculata*	Seethapathy et al. (2015)
12	*Cassia angustifolia*	*Cassia obtusifolia*	Sultana et al. (2012)
13	*Cinnamomum obtusifolium*	*Cinnamomum tamala*	Dhanya and Sasikumar, (2010)
14	*Cinnamomum zeylanicum*	*Cinnamomum cassia Cinnamomum malabatrum*	Swetha et al. (2014)
15	*Cinnamomum verum*	*Canella winterana Cinnamomum malabatrum*	Swetha et al. (2014)
16	*Citrullus colocynthis*	*Trichosanthes palmata*	Osathanunkul et al. (2016)
17	*Cuscutare flexa*	*Cuscuta chinensis*	Khan et al. (2010)
18	*Commiphora wightii*	*Boswellia serrata, Hymenodictyon excelsura*	Prakash et al. (2013)
19	*Commiphora mukal*	*Acacia nilatica, Commiphora myrrha*	Ahmed et al. (2011)
20	*Convolvulus microphyllus*	*Evolvulus alsinoides*	Prakash et al. (2013)
21	*Crocus sativus*	*Carthamus tinctorius, Zea mays, Calendula offinalis, Curcuma longa, Nelumbo nucifera*	Jiang et al. (2014)
22	*Emblica ribes*	*Emblica robusta, Embelia tsjeriam-cottam, Maesa indica*	Santhosh Kumar et al. (2018)
23	*Ferula foetida*	*Acacia senegal*	Prakash et al. (2013)
24	*Gloriosa superba*	*Ipomea spp.*	Sagar, (2014)
25	*Glycyrrhiza glabra*	*Glycyrrhiza uralensis; Abrus precatorius*	Khan et al. (2010)
26	*Habenaria edgeworthii*	*Dioscorea bulbifera*	Prakash et al. (2013)
27	*Hemidesmus indicus*	*Decalepis hamiltonii*	(Rai et al., 2012; Kesanakurti et al., 2020)
28	*Holarrhena antidysenterica*	*Wrightia tinctoria, Wrightia tomentosa*	Gahlaut et al. (2013)
29	*Hypericum perforatum*	*Hypericum patulum, Hypericum maculatum*	Raclariu et al. (2017b)
30	*Justicia adhatoda*	*Ailanthus excelsa*	Keshari and Pradeep, (2017)
31	*Mesua ferrea*	*Calophyllum inophyllum*	Keshari and Pradeep, (2017)
32	*Morinda citrifolia*	*Moringa oleifera*	Santhosh Kumar et al. (2018)
33	*Mucuna pruriens*	*Mucuna utilis, Mucuna deeringiana*	Vijayambika et al. (2011)
34	*Myristica fragans*	*Myristica malabarica*	Swetha et al. (2017)
35	*Ocimum tenuiflorum*	*Ocimum basilicum*	Kumar et al. (2020)
36	*Papavar somniferum*	*Amaranthus paniculatus*	Dhanya and Sasikumar, (2010)
37	*Paris polyphylla*	*Acorus calamus*	Arya et al. (2012)
38	*Parmelia perlata*	*Parmelia perforate, Parmelia cirrhata*	Ahmed and Hasan, (2015)
39	*Penthorum sedoides*	*Penthorum chinese*	Duan et al. (2011)
40	*Phyllanthus amarus*	*Phyllanthus debilis, P. urinaria*	Srirama et al. (2010)
41	*Piper kadsura*	*Piper wallichii, piper boehmeriafolium, Piper laetispicum*	Yu et al. (2016)
42	*Piper longum*	*Piper mullesua*	Mishra et al. (2015)
43	*Piper nigrum*	*Capsicum annum, Carica pappaya*	(Parvathy et al., 2014; Mishra et al., 2015)
44	*Plumbago auriculata*	*Plumbago zeylanica*	Keshari and Pradeep, (2017)
45	*Pterocarpus santalinus*	*Capsicum annum*	Keshari and Pradeep, (2017)
46	*Rubia cordifolia* L	*Rubia tinctorum*	Kamani et al. (2021)

(Continued on following page)

TABLE 1 (*Continued*) List of known adulterants/substitutes in the herbal drug trade.

S.No	Main drugs	Adulterants	References
47	*Ruta graveolens*	*Euphorbia dracunculoides*	Al-Qurainy et al. (2011)
48	*Santalum album*	*Erythroxylum monogynum*	Keshari and Pradeep, (2017)
49	*Saraca asoca*	*Polyalthia longifolia, Humboldtia vahliana, Mallotus nudiflorus*	(Beena and Radhakrishnan, 2012; Begum et al., 2014)
50	*Saussurea lappa*	*Saussurea costus*	Sagar, (2014)
51	*Sida cordifolia*	*Sida acuta*	Ran et al. (2010)
52	*Solanum nigrum*	*Solanum melogena*	Prakash et al. (2013)
53	*Swertia chirata*	*Swertia augustifolia*	Osathanunkul et al. (2016)
54	*Terminalia arjuna*	*Terminalia tomentosa, Terminalia bellirica., Terminalia chebula*	Keshari and Pradeep, (2017)
55	*Tinospora cordifolia*	*Tinospora sinensis*	Keshari and Pradeep, (2017)
56	*Tribulus terrestris*	*Tribulus lanuginosus, Tribulus subramanyamii*	Balasubramani et al. (2010)
57	*Ventilago madraspatana*	*Arnebia euchroma*	Ahmed and Hasan, (2015)
58	*Withania somnifera*	*Mucuna pruriens, Trigonella foenum-graceum, Senna auriculata*	Amritha et al. (2020)
59	*Zingiber officinale*	*Zingiber mioga*	Ahmed and Hasan, (2015)

which namely *rbcL, matK, rpoC1, rpoB, trnH-psbA, psbK-psbI* and atpF-atpH) distributed in 550 plant species and suggested that *matK and rbcL* markers could serve as the core barcode candidates for plant species identification and indicated that ITS and *trnH-psbA* could be employed as supplementary markers. In Chen et al. (2010) worked on various medicinal plants and herbal materials from more than 6,600 samples in 753 genera and proposed that ITS2 could serve as a core DNA barcode for medicinal plants and herbal materials. In addition, the chloroplast marker *trnH-psbA* has been proposed as a complementary barcode marker. Both ITS2 and *trnH-psbA* are known to be shorter genes with conserved sequences, which reduces the difficulty of amplification. Chen et al. (2010) in a series of publications, reported that the efficiency of ITS2 and *trnH-psbA* markers aided easy identification of medicinal and herbal materials (Chen et al., 2013, 2014). Since then, many studies have examined several gene regions which helped in the identification of species, including *accD* (He et al., 2014a; Mao et al., 2014), *atpF-atpH* (Ran et al., 2010; Zuo et al., 2011; Thakur et al., 2019, 2021), *rpoB* (Zuo et al., 2011; Singh et al., 2012; Liu et al., 2016), *ndhJ* (He et al., 2014a; 2014b), *ycf1* and *ycf5* (Luo et al., 2010; Dong et al., 2015), *rpoC1* (Luo et al., 2010; Shi et al., 2011; Khan et al., 2012; Singh et al., 2012; Aziz et al., 2015; Naim and Mahboob, 2020).

Multiple-locus DNA barcode markers

It has been shown that single-loci marker cannot always be authenticated for species identification; accordingly, scientists have used a combination of DNA markers. The plant working group CBOL recommended the combined loci of *matK* and *rbcL* as the core barcode for plant species (Fazekas et al., 2008; Newmaster et al., 2008; CBOL, 2009). Additional combinations of markers, including *rbcL* + *trnH-psbA, trnH-psbA* + ITS2, and *matK* + *trnH-psbA*, have also been assessed for their efficiency in discrimination and universality of species identification (Kress et al., 2005; Kress and Erickson, 2007; Li et al., 2012; Tripathi et al., 2013; Mishra et al., 2015; Mahima et al., 2020). Evaluation of the reports related to multiple loci DNA in plant identification revealed that, the combined loci of ITS2 and *trnH-psbA* were found to be the best two-marker combination for the identification of plants and even herbal samples (Zuo et al., 2011; Chen et al., 2014; Vassou et al., 2015; Jamdade et al., 2022). By employing the combined barcode loci a deep phylogenetic tree can be established, which could be applied in the identification of species and also discrimination of closely related species. In addition, the combination of a third locus is also reported for the large datasets but it was observed to have low bias at the species level (Newmaster et al., 2013). The list of successful resolution of DNA barcode for family-level identification are mentioned in Table 2.

High-throughput sequencing technologies

In the last decade, many scientists have employed single or multi-locus of DNA barcode markers in order to identify species distributed across different families, genera and species of medicinal plants. Further, the emergence of Next-generation sequencing made a revolution in the extensive analysis of mitochondrial, chloroplast and nuclear genomes of many organisms. The high-throughput technology platform generates a vast amount of sequence data in a matter of hours or days, with an algorithm to precisely address the needs of each

TABLE 2 List of recommended DNA barcode loci for medicinal plant families.

S.No	Family	Best locus/Loci	References
1	Asteraceae	ITS	Gao et al. (2010)
2	Apiaceae	ITS/ITS2 + *psbA-trnH*, ITS, ITS2	(Liu et al., 2014; Parveen et al., 2019)
3	Apocynaceae	ITS2+*trnH-psbA, matK* + *rbcL*	(Cabelin and Alejandro, 2016; Lv et al., 2020)
4	Araliaceae	ITS2	Liu et al. (2012)
5	Arecaceae	*rbcL*	Naeem et al. (2014)
6	Euphorbiaceae	ITS1, ITS2	Pang et al. (2011)
7	Fabaceae	ITS2	Tahir et al. (2018)
8	Lamiaceae	*matK, rbcL*	Oyebanji et al. (2020)
9	Lauraceae	ITS	Liu et al. (2022)
10	Lemnaceae	*atpF-atpH*	Wang et al. (2010)
11	Meliaceae	ITS	Muellner et al. (2011)
12	Myristicaceae	*matK* + *trnH-psbA*	Newmaster et al. (2008)
13	Orchidaceae	*ndhF, ycf1, matK* + *ycf, ndhF* + *ycf1*	Li et al. (2021)
14	Poaceae	ITS1, ITS2	(Yao et al., 2017; Tahir et al., 2018)
15	Polygonaceae	*trnH-psbA*	Song et al. (2009)
16	Rosaceae	ITS2	Pang et al. (2011)
17	Ranunculaceae	*rbcL* + *matK* + *trnH-psbA*, ITS	Li et al. (2019)
18	Rutaceae	ITS2	Luo et al. (2010)
19	Verbanaceae	*matK, rbcL*	Oyebanji et al. (2020)
20	Zingiberaceae	ITS2, *rbcL, matK*	Vinitha et al. (2014)

application. The technique involves the initial fragmentation of DNA templates followed by the immobilization of the fragments on a solid support. Subsequently, the fragments are amplified and sequenced. Three distinct strategies are being employed in practicing NGS and this technology has been commercialized by Roche's 454 Life Science platform (Indianapolis, IN), Illumina/Solexa Genome Analyzer (San Diego, CA) and Applied Biosystems/SOLiD System (Orange country, CA). Each strategy has its unique enzyme systems, sequencing chemistry, hardware and software systems (Shendure and Ji, 2008; Metzker, 2010). Among all, Roche/454 is found to be more advantageous due to its rapid and longer read length with a hundred thousand to one million reads of 400–500 bp DNA fragments per run (Sarwat and Yamdagni, 2016), even while performing the technique in the identification of plant species. In the routine analysis, the entire genome has been employed for phylogenetics, especially at a deeper level, genome evolution analysis and authenticating medicinal plants for herbal drug preparations (Kircher and Kelso, 2010; Ganie et al., 2015; Sarwat and Yamdagni, 2016). In-plant species, chloroplast genomes are preferred for species identification which contains more information. By July 2021, the chloroplast genome of plants has been published on NCBI. Many plant scientists suggested that the entire plastid genome could be a powerful tool to resolve the phylogenetic relationship between closely related species, identification of the homogeneity of samples and the presence of adulterants in herbal supplements (Li et al., 2015; Zhou et al., 2018). Several reports have been found that Next-generation Sequencing (NGS) technique for the authentication and quality control of herbal medicines (Zhang et al., 2017). Cheng et al. (2014) accomplished a metagenomic analysis of Liuwei Dihuang Wan herbal medicine to find the biological ingredients and contaminations involved. The results showed that quality and stability of different manufacturers are significantly dissimilar. In addition, Speranskaya et al. (2018) performed two sequencing platforms, Illumina and Ion Torrent to identify high-quality qualitative and quantitative results. The whole plastid sequences of 57 *Berberis* species were determined to identify the informative DNA barcodes and understand the phylogeny between species (Kreuzer et al., 2019). In the context of quality control of herbal medicines, Nanopore sequencing has been used for herbal product authentication (Lo and Shaw, 2019).

DNA barcoding technique combined with other technologies

After more than 15 years of development, DNA barcoding has been employed to rapidly identify species using standardized genetic markers (Hebert et al., 2003). This technique has been successfully applied in raw plant herbal extracts and has shown to have a few limitations in herbal products subjected to heating, purification and leaching, which results in DNA degradation and

makes the extraction difficult (Govindaraghavan et al., 2012; Liu et al., 2016; Raclariu et al., 2018). The quality of DNA is known to play an essential role in the authentication of medicinal plants and herbal products. For this purpose, different techniques have been employed to overcome the limitation in performing DNA barcoding, such as DNA mini-barcoding, Bar-HRM technology and Metabarcoding. Additionally, there are a few analytical methods such as, chromatography that has been combined with barcode markers, including TLC (Thin Layer Chromatography), HP-TLC (High Performance-Thin Layer Chromatography), HPLC (High-Performance Liquid Chromatography) and LC-MS (Liquid Chromatography-Mass Spectrometry). These methods have been shown to be highly useful in identifying the active components of medicinal plants and herbal products (Palhares et al., 2015). The first report on Salvia species showed the relationships between the DNA barcoding technique and chemical components (Jianping et al., 2010). The authentication of *Hypericum* from the herbal products using TLC and HPLC combined with Amplicon Metabarcoding (AMB) (Raclariu et al., 2017b). Zhao et al. (2020) demonstrated a systematic method to authenticate *Stephania* species which involved a combination of DNA barcoding, HPLC-QTOF-MS/MS and UHPLC for differentiation, chemical profiles and quality evaluation. NMR (Nuclear Magnetic Resonance) and genome skimming were recently combined to validate *Hemidesmus indicus* from the adulterant species *Decalepis hamiltonii* on both raw materials and finished products. This was the first report on the use of Oxford Nanopore on herbal products enabling genome skimming as a tool for quality assurance perspective for both product and purity (Kesanakurti et al., 2020).

DNA mini-barcoding

DNA mini-barcoding is a complementary technique to DNA barcoding. These mini barcodes were used mainly in discriminating species in a genus. It was a small, highly conserved portion in the usual barcode region, and specialized primers were synthesized to target the area. The main advantage of doing mini barcodes was the ease of sequencing of less than 200 bp and used to make the comparison within the species. Meusnier et al. (2008) demonstrated that DNA-mini barcodes could overcome the difficulties associated with degraded samples of processed herbal products. Recently, ITS2 has been reported as a suitable mini-barcode for identifying medicinal and adulterant species from the family Apiaceae (Parveen et al., 2019). These mini-barcodes are limited by length restrictions and sequences of different lengths are selected as mini-barcodes. The success of mini-barcodes are dependent on specific primers which need to be screened from the available databases such as GenBank, the European Molecular Biology Laboratory or the DNA Data bank from Japan (Hajibabaei et al., 2007; Gao et al., 2019).

Bar-HRM technique

The Bar-HRM technique is based on DNA barcoding coupled with high-resolution melting analysis. The melting curve of PCR amplicons is subject to length of DNA sequence, GC content and difference in base complementary without sequencing or hybridization procedures; thus, *rbcL, matK, trnH-psbA, rpoC* and ITS, *etc.* can be employed to facilitate species identification (Jiang et al., 2014; Yu et al., 2021). HRM monitors the melting curve of the nucleic acid in real-time by adding intercalating dyes, including SYBR Green, Green PLUS, Eva Green, SYTO9 and ResoLight. This new approach has the distinct advantage of performing both PCR amplification and HRM analysis in one completely 'closed tube' and results are available at the end of the run. These advantages make it widely used in the herbal medicine industry and market to determine the origin and quality of raw materials and detect the adulterants in herbal processed products (Sun et al., 2016; Mezzasalma et al., 2017). In addition, HRM analysis is used for clinical research and diagnostics, including the analysis of cancer-specific mutations (Li et al., 2016), authentication of food products (Ganopoulos et al., 2011; Madesis et al., 2013; Sakaridis et al., 2013) and detection of harmful microorganisms in meat products (Sakaridis et al., 2014; Ganopoulos et al., 2015). An overview of the Bar-HRM analysis developed in herbal medicine identification is provided in Table 3. In first reported the advantages in applying and utilizing the HRM approach for the rapid discrimination of seven Greek *Sideritis* species, which was carried out based on nuclear ITS2 DNA barcoding sequence. Since then, another research group has approached plastid DNA region *trnH-psbA* coupled with HRM analysis to distinguish Chinese medicine *Panax notoginseng* from adulterant species (Tong et al., 2014), and the same method was used for the identification of saffron (*Crocus sativus*), Mutong (*Akebia quinata*) and Aristolochia (*Aristolochia manshuriensis*) (Jiang et al., 2014; Hu et al., 2015). These few studies revealed that the HRM analysis could distinguish original species from adulterant species. However, the drawback in the Bar-HRM analysis is the failure in the identification of closely related species where genetic variability is limited. To overcome the issue, (Osathanunkul et al., 2015b), developed a specific mini-barcode in the *rbcL* gene to distinguish three medicinal plants in the Acanthaceae (*Acanthus ebracteatus*, *Andrographis paniculata* and *Rhinacanthus nasutus*). Singtonat and Osathanunkul, (2015) reported that *Thunbergia laurifolia* derived herbal products could be identified by employing four DNA mini barcodes: *matK, rbcL, trnL* and *rpoC*. In addition, mini-barcode coupled with HRM analysis was able to detect the toxic herb *Crotalaria spectabilis* adulterants. *Lavandula* species was successfully authenticated using Bar-HRM technology (Soares et al., 2018). The narcotic plant, *Mitragyna speciosa* has morphological disparities with allied *Mitragyna speciosa* and the results showed that the melting profiles of ITS2 amplicons were

TABLE 3 List of recommended barcode locus/loci for the application of Bar-HRM in medicinal plant identification.

S.No	Description	DNA barcode region	References
1	*Sideritis species*	ITS2	Kalivas et al. (2014)
2	*Panax notoginseng*	*trnH-psbA*	Tong et al. (2014)
3	*Aristolochia manshuriensis*	*trnH-psbA*	Hu et al. (2015)
4	*Acanthus ebracteatus*, *Andrographis paniculata*, and *Rhinacanthus nasutus*	*rbcL*	Osathanunkul et al. (2015a)
5	*Hypericum perforatum* and *Hypericum androsaemum*	ITS1 and *matK*	Costa et al. (2016)
6	*Phyllanthus amarus*	*trnL* and *rbcL*	Buddhachat et al. (2015)
7	Croton species	ITS1, *matK, rbcL, rpoC* and *trnL*	Osathanunkul et al. (2015b)

distinct from allied species (Tungphatthong et al., 2021). Zhao et al. (2021) demonstrated that DNA barcoding coupled with a high-resolution melting curve could be used as a routine test to guarantee the quality of *Ardisia gigantifolia* and to discriminate the genuine species from its common adulterants.

Metabarcoding

Another approach merged from DNA barcoding which has been advocated for identifying taxa from a complex mixture, called 'metabarcoding.' It combines both DNA barcoding and high-throughput sequencing. In the recent times, significant methodological advancements have taken place in high-throughput sequencing along with the employment of bioinformatics tools in order to obtain amplified sequences to identify species diversity from the environment, sediment, and ancient or processed samples (Taberlet et al., 2012; Omelchenko et al., 2019). It is inferred that microbial flora determination was the target for metabarcoding. Additionally, metabarcoding can be implemented to identify multiple plant species as well as processed herbal products using the universal primers (Cheng et al., 2014; Ivanova et al., 2016; Raclariu et al., 2017a, 2017b). For example, Coghlan et al. (2012) demonstrated metabarcoding studies on 15 complex traditional Chinese medicine samples and identified 68 families, including possible toxic species. In Ivanova et al. (2016) tested 15 herbal supplements from the market and found non-listed non-filler plant DNA. Out of 78 *Hypericum perforatum* samples in the herbal market revealed that 68% of samples are authenticated and the rest are adulterants (Raclariu et al., 2017b).

Raclariu et al. (2017a) investigated *Veronica officinalis* and found out that adulterant species *Veronica chamaedrys* could be detected in 62% of the products. Additionally, the same group found adulterant species in 53 *Echinacea* herbal products (Raclariu et al., 2018a; 2018b). Assessment of 79 Ayurvedic herbal products on the European market using DNA metabarcoding analysis revealed that two out of 12 single-ingredient products contained only one species as labeled and from the 27 multiple ingredient products, only eight species could be authenticated and none of the species are not listed on the label. The study highlights that DNA metabarcoding is an appropriate analytical approach for authenticating complex multi-ingredient herbal products (Seethapathy et al., 2019). Recently, Urumarudappa et al. (2020) identified 39 Thai herbal products on the Thai National List of Essential Medicines (NLEM) which revealed that the nuclear region, ITS2, could identify herbal ingredients at the genus and family level as 55% and 63%, respectively. The chloroplast gene, rbcL, is known to enable genus and family level identification in 58% and 73% of cases. The study recommended that advanced chemical techniques combined with DNA metabarcoding could be valid for multi-ingredient herbal products. Moreover, a specific mini-barcode is coupled with DNA metabarcoding technique used for the qualitative and quantitative identification of *Senna* processed herbal products (Yu et al., 2020). All these studies showed varying degree of authentication success since the complex herbal mixtures is known to be influenced by several factors, which also includes the quality and type of material as well as several analytical parameters and variables that are employed in the process of optimization of experimental results (Staats et al., 2016).

There are also a few other limitations of DNA metabarcoding especially if the DNA has been degraded or lost during the manufacturing process of herbal products (de Boer et al., 2015). Generally, with the employment of metabarcoding, one can obtain accurate and reliable high-quality sequences to identify the species through high throughput sequencing within complex multi-ingredient and processed mixtures (Veldman et al., 2014; Jia et al., 2017). Importantly, this technique is useful for qualitative evaluation and not suitable for quantitative assessment, especially in evaluating relative species abundance based on sequence read numbers (Coghlan et al., 2012; Staats et al., 2016). In addition, it can be ascertained that the third-generation sequencing PacBio platform combined with DNA barcoding is bound to make a greater impact on authenticating herbal products in the future (Senapati et al., 2022).

Loop-Mediated Isothermal Amplification (LAMP) and Recombinase Polymerase Amplification (RPA)

Several molecular biology methods are available for the identification of herbal medicines, and the advantages over other methods are rapidity, high sensitivity, and specificity. As an alternative to a Polymerase Chain Reaction (PCR), Loop-Mediated Isothermal Amplification (LAMP) and Recombinase Polymerase Amplification (RPA) were introduced into herbal medicines for safety testing. LAMP can be implemented with impure sample materials as the template and has a short reaction time, and does not require specific equipment. The application of LAMP has exhibited great potential in the field of herbal medicine identification. LAMP amplification is performed with accessible primers to crosscheck their species-specific identification. Species identification is determined by analyzing the turbidity curve along with visual colour changes instead of the agarose gel DNA electrophoresis test. Recent studies proved that the implementation of LAMP analysis is effective in herbal medicine identification. The first report of the LAMP-based method is to discriminate the identity of *Curcuma longa* and *C. aromatica* by targeting the *trnK* gene sequence. The results showed that LAMP analysis is suitable for the identification of herbal medicines (Sasaki and Nagumo, 2007). In the following year, targeting six allele-specific markers (18S ribosomal RNA gene) is used for the detection of *Panax ginseng* from *Panax japonicus* (Sasaki et al., 2008). The identification of traditional Chinese medicine *Cordyceps sinensis* from its adulterant *C. hawresii, C. ramosa, C. militaris*, and *C. barnesi* through the same approach. In the other study, the LAMP method is combined with RAPD to identify *Catharanthus roseus* and the results showed high specificity (Chaudhary et al., 2012). Li et al. (2013) demonstrated the LAMP method targeting internal transcribed spacer (ITS) for the authentication of herbal tea ingredient *Hedyotis diffusa*. Lai et al. (2015) developed a similar approach and evaluated the effectiveness of the ITS2 DNA barcode in differentiating *Taraxacum formosanum* from its adulterants. In 2016, Zhao et al., 2016. Developed a species-specific primer for *Crocus sativus* from its adulterants through LAMP analysis. These studies suggested that the advent of LAMP based specific primers effectively identify medicinal plant species from their non-medicinal adulterants.

Recombinase polymerase amplification (RPA) is a unique isothermal DNA amplification developed by Pipenburg et al. (2006). The DNA barcode-based RPA (BAR-RPA) technique requires recombinase, polymerase, and single-stranded binding protein (SBB) to replace the unwinding chain process of the usual PCR technique. Recombinase polymerase amplification allows rapid amplification (approximately 20 min) of genetic markers under a constant temperature of 35–40°C with or without the use of thermocyclers and coupled with a rapid DNA extraction method (Lobato and O'Sullivan, 2018). The resulting RPA reaction products can be visualized in agarose gel electrophoresis, probe-based fluorescence monitoring, and lateral flow dipstick (LFD). In Tian et al. (2017) reported a reliable protocol of DNA extraction and combine it with RPA-LFD to establish a rapid authentication of *Ficus hirta* from its adulterant, a toxic plant *Gelsemium elegans*. There are few reports that documented the use of the RPA technique for the identification of herbal medicines and their adulterants. This technique can provide an effective detection in the finding of adulteration, forensic medicine, and molecular assays. In addition, such applications of this technology can help to improve the safety of herbal medicines, especially combined with authentication *via* morphological, chemical, or other molecular methods.

Current databases

Establishing a database is essential for identifying and authenticating all flora and fauna, keeping the information updated and organized, and making the sequence data accessible to all scientific communities worldwide. The aim of databases is to collect, manage and analyze the sequence data from the diverse organism and the most popular databases are 1) National Center for Biotechnology Information (NCBI) GenBank, 2) BOLD Systems (Barcode of Life Data Systems) and 3) MMDBD (Medicinal Materials DNA Barcode Database). Currently, MMDBD is the only database having the sequence data of medicinal plants listed in Chinese Pharmacopoeia (Wong et al., 2018).

NCBI GenBank (http:/www.ncbi.nlm.nih.gov/genbank) is an online database that contains the publicly available genetic information of prokaryotes and eukaryotes organisms. This database has a vast sequence of DNA, RNA and proteins. The unknown species could be identified through the BLAST (Basic Local Alignment Search Tool) algorithm. The species with highest similarities are present at the first-come position and an E value ≥ 0. Unlike the BOLD database, NCBI GenBank does not maintain the chromatogram of the sequences submitted to the platform.

The BOLD (http://www.boldsysystem.org) is a virtual platform for all eukaryotes organisms and it is hosted by the University of Guelph in Ontario, Canada. This bioinformatics workbench assists in analyzing, storing, and publishing DNA barcode records and chromatograms. The user can directly submit their data without any significant difficulties and give each species a unique accession ID. BOLD accepts the sequence from more than 150 genetic markers, including *COI*, ITS, *rbcL* and *matK*. These records include sequence data, barcodes, images, taxonomy, maps, and collection coordinates data. The barcode sequence of unknown species can be rapidly and accurately identified using the online database to support their identification/validation. Besides, this online platform helps

collaborate between geographically dispersed research communities with web-based delivery. For example, Vassou et al. (2016) retrieved the 27 medicinal plants *rbcL* sequence from the BOLD public database to create the Ayurvedic Pharmacopoeia of India-Reference DNA Barcode Library (API-RDBL). In addition, the sequence generated for the study were deposited in the BOLD database. Similarly, Gong et al. (2018) constructed the first local reference barcode library for Southern Chinese Medicine using the ITS2 sequence. The partners in the BOLD database are iBOL [[International Barcode of Life (http://www.ibol.org)], CBOL [Consortium for the Barcode of Life (http://www.barcodeoflife.org)] and GBIF [Global Biodiversity Information Facility]. The CBOL is a public online database containing many DNA barcode sequences to identify unknown species. This database originated in 2004 and the founders promote the scientific community to conduct the DNA barcoding conference, meetings, training and classes to reach public support. Currently, its works with 130 organizations in 40 different countries. Their mission is to collect and record all sequence data from eukaryotes worldwide and make it available to public reach. iBOL was established in 2008 and it aims to generate DNA barcode libraries to identify the biodiversity with a standard protocol and bioinformatics tools. iBOL has collaborated with the BIOSCAN program to achieve 2.5 million species with barcodes by 2025.

MMDBD (https://rdccm.cuhk.edu.hk/mherbsdb) is an online platform established in 2010 and that can be used for DNA sequence identification and data retrieval. This platform conta ins the sequence of medicinal plants listed in Chinese Pharmacopoeia and American Herbal Pharmacopoeia. It also offers detailed information on adulterants, medical parts, photographs, biological classification and their status according to endangered species.

Current challenges of DNA barcoding in the herbal industry

Nowadays, the usage of plant-based traditional medicines is increasing and the product demand and utility is projected to be 80% of the world's population who consume the herbal products for wellness and health care. The development of the DNA barcoding technique has been used effectively to identify medicinal plants and herbal products, guaranteeing the safety of consumers. From the careful and comprehensive analysis of literature, it can be ascertained that no one can yet find an efficient barcode for all groups of plants. The limitation of DNA barcoding is to fail the quality of template DNA, the affinity of the primers, the effect of PCR in the herbal products and additives contaminating the DNA samples. In addition, the availability of DNA could be removed or degraded during the manufacturing process, including extensive heat treatment, irradiation, ultraviolet exposure and extractive distillation. DNA is entirely absent in processed products and hence is not suitable for DNA barcoding. Another problem concerning the DNA barcoding technique is that multiple species present in herbal products make PCR biased (Fazekas et al., 2009). The mixtures of herbal drugs can partly overcome PCR bias by doing parallel PCR or cloning specific PCR products into a vector to be able to target the particular species (Newmaster et al., 2013). Another challenge in the field of DNA barcoding is the interference of secondary plant metabolites, including polysaccharides, tannins, alkaloids and polyphenols. These metabolites in plants depend on natural conditions such as seasons, latitude, longitude, and soil fertility, resulting in low-quality DNA and reducing sequencing success. In these cases, metabarcoding and high-throughput sequencing are possible to overcome the issues. In the future, the addition of biological reference material (BRM) and anatomical studies along with sequence data would provide users with high authenticity of medicinal plants and herbal products. Future DNA barcoding perspectives include a novel mini barcode sequence library, BRM library, and anatomical studies for herbal drug authentication.

Future perspectives

In recent times, there has been an increase in the demand for environmentally friendly innovations in all sectors of trade. It also impacted the medicinal and health care fields as the global community leaned more towards alternate medicine. The increase in the demand for herbal medicines is used by approximately 80% of the world population for wellness and healthcare, but it is also accompanied by the loss of quality and safety of the products. At present, the DNA barcoding technique is widely used in medicinal plants and has been proven in the authentication of adulterating herbal medicines. Based on the review of literature, single or multiple loci barcode candidates are used to identify and authenticate the medicinal plants since it has not yet identified a universal barcode candidate for all groups of plants. The limitation of DNA barcoding is the quality of the DNA in the herbal products, and many cases contain degraded DNA in the manufactured products. In such cases, minibarcoding technique is worth solving the problem. Another limitation of DNA barcoding is related to multispecies identification from a mixed herbal product; in these cases, metabarcoding, Bar-HRM, and massive sequencing could overcome the limitations. It is clear that a well-established protocol for analytical methods such as organoleptic, microscopic, physiochemical, biochemical and molecular (DNA barcoding) techniques are needed for authentication and quality control of herbal medicines at the industrial level. For instance, coupling DNA barcoding with next-generation sequencing, metabarcoding, and metabolomics will helps to identify each and every marker in the formulation more accurately than all of the traditional methods.

Conclusion

DNA barcoding-based adulteration detection is still in progress to replace the conventional identification approaches. The chemical analyses are used to detect foreign ingredients and quality control in the herbal drugs, whereas DNA marker-based identification is more beneficial for authenticating the original species. It is essential to add DNA barcoding-based authentication with metabolomics, transcriptomics and proteomics tools to understand adulteration in herbal drugs. This field requires a solid scientific community to add the DNA barcoding protocol in the guidelines to certify the herbal products. Close collaboration between national pharmacopeia agencies and academic or commercial institutes experts in DNA barcoding should be encouraged to pilot DNA barcoding based herbal pharmacovigilance. The routine DNA barcoding authentication could raise the quality and authenticity of the herbal industry along with chemical analytical methods and facilitate pharmacovigilance monitoring and signal detection. In the future, DNA barcoding-based authentication will be allocated in all herbal industries with biomonitoring using available barcodes to detect the adulterants and many DNA barcoding problems will be solved as biological data is progressing rapidly.

Author contributions

KM, KS, KR, PR and AS wrote the manuscript and RS revised it.

Conflict of interest

The authors declare that the research was conducted in the absence of any commercial or financial relationships that could be construed as a potential conflict of interest.

Publisher's note

All claims expressed in this article are solely those of the authors and do not necessarily represent those of their affiliated organizations, or those of the publisher, the editors and the reviewers. Any product that may be evaluated in this article, or claim that may be made by its manufacturer, is not guaranteed or endorsed by the publisher.

References

Ahmed, R., Ali, Z., Wu, Y., Kulkarni, S., Avery, M. A., Choudhary, M. I., et al. (2011). Chemical characterization of a commercial Commiphora wightii resin sample and chemical profiling to assess for authenticity. *Planta Med.* 77, 945–950. doi:10.1055/s-0030-1250674

Ahmed, S. S. (2022). DNA barcoding in plants and animals: A critical review. *Preprints* 2022010310, 1–28. doi:10.20944/preprints202201.0310.v1

Ahmed, S., and Hasan, M. M. (2015). Crude drug adulteration: A concise review. *World J. Pharm. Pharm. Sci.* 4, 274–283.

Al-Qurainy, F., Khan, S., Tarroum, M., Al-Hemaid, F. M., and Ali, M. A. (2011). Molecular authentication of the medicinal herb Ruta graveolens (Rutaceae) and an adulterant using nuclear and chloroplast DNA markers. *Genet. Mol. Res.* 10, 2806–2816. doi:10.4238/2011.November.10.3

Amritha, N., Bhooma, V., and Parani, M. (2020). Authentication of the market samples of Ashwagandha by DNA barcoding reveals that powders are significantly more adulterated than roots. *J. Ethnopharmacol.* 256, 112725. doi:10.1016/j.jep.2020.112725

Arya, D., Joshi, G. C., and Tiwari, L. M. (2012). Status and trade of crude drug in Uttarakhand. *J. Med. Plants Res.* 6, 3434–3444. doi:10.5897/jmpr11.1755

Aziz, N. A. A., Ahmad, M. I., and Naim, D. M. (2015). Molecular DNA identification of medicinal plants used by traditional healers in Malaysia. *Genet. Mol. Res.* 14, 15937–15947. doi:10.4238/2015.December.7.5

Baker, D. A., Stevenson, D. W., and Little, D. P. (2012). DNA barcode identification of black cohosh herbal dietary supplements. *J. AOAC Int.* 95, 1023–1034. doi:10.5740/jaoacint.11-261

Balasubramani, S. P., Murugan, R., Ravikumar, K., and Venkatasubramanian, P. (2010). Development of ITS sequence based molecular marker to distinguish, Tribulus terrestris L. (Zygophyllaceae) from its adulterants. *Fitoterapia* 81, 503–508. doi:10.1016/j.fitote.2010.01.002

Basu, D. (2020). The role played by the Indian pharmacopoeia commission in today's era: A critical study. *Indian Pharmacopoeia Comm. Voice Res.* 9, 34–42.

Beena, C., and Radhakrishnan, V. V. (2012). Quality assessment evaluation of the market samples of important ayurvedic drug asoka bark. *Ann. Phytomedicine* 1, 95–98.

Begum, S. N., Ravikumar, K., and Ved, D. K. (2014). Asoka" - an important medicinal plant, its market scenario and conservation measures in India. *Curr. Sci.* 107, 26–28.

British Pharmacopoeia Commission (2017). *British Pharmacopoeia appendix XI V deoxyribonucleic acid (DNA) based identification techniques for herbal drugs*. London: TSO.

Buddhachat, K., Osathanunkul, M., Madesis, P., Chomdej, S., and Ongchai, S. (2015). Authenticity analyses of Phyllanthus amarus using barcoding coupled with HRM analysis to control its quality for medicinal plant product. *Gene* 573, 84–90. doi:10.1016/j.gene.2015.07.046

Cabelin, V. L. D., and Alejandro, G. J. D. (2016). Efficiency of matK, rbcL, trnH-psbA, and trnL-F (cpDNA) to molecularly authenticate Philippine ethnomedicinal Apocynaceae through DNA barcoding. *Pharmacogn. Mag.* 12, S384–S388. doi:10.4103/0973-1296.185780

Cbol, P. W. G. (2009). A DNA barcode for land plants. *Proc. Natl. Acad. Sci. U. S. A.* 106, 12794–12797. doi:10.1073/pnas.0905845106

Chase, M. W., and Fay, M. F. (2009). Ecology. Barcoding of plants and fungi. *Science* 325, 682–683. doi:10.1126/science.1176906

Chaudhary, A. A., HemantMohsin, M., and Ahmad, A. (2012). Application of loop-mediated isothermal amplification (LAMP)-based technology for authentication of Catharanthus roseus (L.) G. Don. *Protoplasma* 249, 417–422. doi:10.1007/s00709-011-0293-2

Chen, S., Pang, X., Song, J., Shi, L., Yao, H., Han, J., et al. (2014). A renaissance in herbal medicine identification: From morphology to DNA. *Biotechnol. Adv.* 32, 1237–1244. doi:10.1016/j.biotechadv.2014.07.004

Chen, S., Yao, H., Han, J., Liu, C., Song, J., Shi, L., et al. (2010). Validation of the ITS2 region as a novel DNA barcode for identifying medicinal plant species. *PLoS One* 5, e8613–e8618. doi:10.1371/journal.pone.0008613

Chen, X., Liao, B., Song, J., Pang, X., Han, J., and Chen, S. (2013). A fast SNP identification and analysis of intraspecific variation in the medicinal Panax species based on DNA barcoding. *Gene* 530, 39–43. doi:10.1016/j.gene.2013.07.097

Chen, Y., Zou, J., Sun, H., Qin, J., and Yang, J. (2021). Metals in traditional Chinese medicinal materials (tcmm): A systematic review. *Ecotoxicol. Environ. Saf.* 207, 111311. doi:10.1016/j.ecoenv.2020.111311

Cheng, X., Su, X., Chen, X., Zhao, H., Bo, C., Xu, J., et al. (2014). Biological ingredient analysis of traditional Chinese medicine preparation based on high-throughput sequencing: The story for Liuwei Dihuang wan. *Sci. Rep.* 4 (5147), 1–12. doi:10.1038/srep05147

Coghlan, M. L., Haile, J., Houston, J., Murray, D. C., White, N. E., Moolhuijzen, P., et al. (2012). Deep sequencing of plant and animal DNA contained within traditional Chinese medicines reveals legality issues and health safety concerns. *PLoS Genet.* 8, e1002657. doi:10.1371/journal.pgen.1002657

Costa, J., Campos, B., Amaral, J. S., Nunes, M. E., Oliveira, M. B. P. P., and Mafra, I. (2016). HRM analysis targeting ITS1 and matK loci as potential DNA mini-barcodes for the authentication of *Hypericum perforatum* and Hypericum androsaemum in herbal infusions. *Food control.* 61, 105–114. doi:10.1016/j.foodcont.2015.09.035

Cristescu, M. E. (2014). From barcoding single individuals to metabarcoding biological communities: Towards an integrative approach to the study of global biodiversity. *Trends Ecol. Evol.* 29, 566–571. doi:10.1016/j.tree.2014.08.001

de Boer, H. J., Ichim, M. C., and Newmaster, S. G. (2015). DNA barcoding and pharmacovigilance of herbal medicines. *Drug Saf.* 38, 611–620. doi:10.1007/s40264-015-0306-8

Dhanya, K., and Sasikumar, B. (2010). Molecular marker based adulteration detection in traded food and agricultural commodities of plant origin with special reference to spices. *Curr. Trends Biotechnol. Pharm.* 4, 454–489.

Dong, W., Xu, C., Li, C., Sun, J., Zuo, Y., Shi, S., et al. (2015). ycf1, the most promising plastid DNA barcode of land plants. *Sci. Rep.* 5, 8348. doi:10.1038/srep08348

Dormontt, E. E., van Dijk, K. J., Bell, K. L., Biffin, E., Breed, M. F., Byrne, M., et al. (2018). Advancing DNA barcoding and metabarcoding applications for plants requires systematic analysis of herbarium collections-an Australian perspective. *Front. Ecol. Evol.* 6, 1–12. doi:10.3389/fevo.2018.00134

Duan, C., Mei, Z., Gong, S., and Yu, H. (2011). Genetic characterization and authentication of penthorum species using RAPD and SCAR markers. *Res. J. Bot.* 6, 87–94. doi:10.3923/rjb.2011.87.94

Ebach, M. C., and Holdrege, C. (2005). DNA barcoding is no substitute for taxonomy. *Nature* 434, 697. doi:10.1038/434697b

EDQM (2014). *European Pharmacopoeia*. 8th Edition. Strasbourg: Council of Europe.

Erickson, D. L., Spouge, J., Resch, A., Weigt, L. A., and Kress, W. J. (2008). DNA barcoding in land plants: Developing standards to quantify and maximize success. *Taxon* 57, 1304–1316. doi:10.1002/tax.574020

Ernst, E. (2002). Heavy metals in traditional Indian remedies. *Eur. J. Clin. Pharmacol.* 57, 891–896. doi:10.1007/s00228-001-0400-y

European Medicine Agency (EMA) (2006). *Document No*.Guideline on specifications: Test procedures and acceptance criteria for herbal substances, herbal preparations and herbal medicinal products. London, UK: EMA/CPMP/QWP

Fazekas, A. J., Burgess, K. S., Kesanakurti, P. R., Graham, S. W., Newmaster, S. G., Husband, B. C., et al. (2008). Multiple multilocus DNA barcodes from the plastid genome discriminate plant species equally well. *PLoS One* 3, e2802. doi:10.1371/journal.pone.0002802

Fazekas, A. J., Kesanakurti, P. R., Burgess, K. S., Percy, D. M., Graham, S. W., Barrett, S. C. H., et al. (2009). Are plant species inherently harder to discriminate than animal species using DNA barcoding markers? *Mol. Ecol. Resour.* 9, 130–139. doi:10.1111/j.1755-0998.2009.02652.x

Ferri, G., Corradini, B., Ferrari, F., Santunione, A. L., Palazzoli, F., and Alu', M. (2015). Forensic botany II, DNA barcode for land plants: Which markers after the international agreement? *Forensic Sci. Int. Genet.* 15, 131–136. doi:10.1016/j.fsigen.2014.10.005

Gahlaut, A., Gothwal, A., Hooda, V., and Dabur, R. (2013). RAPD patterns of some important medicinal plants and their substitutes used in Ayurveda to identify the genetic variations. *Int. J. Pharm. Pharm. Sci.* 5, 239–241.

Ganie, S. H., Upadhyay, P., Das, S., and Prasad Sharma, M. (2015). Authentication of medicinal plants by DNA markers. *Plant gene.* 4, 83–99. doi:10.1016/j.plgene.2015.10.002

Ganopoulos, I., Argiriou, A., and Tsaftaris, A. (2011). Adulterations in Basmati rice detected quantitatively by combined use of microsatellite and fragrance typing with High Resolution Melting (HRM) analysis. *Food Chem.* 129, 652–659. doi:10.1016/j.foodchem.2011.04.109

Ganopoulos, I., Xanthopoulou, A., Mastrogianni, A., Drouzas, A., Kalivas, A., Bletsos, F., et al. (2015). High resolution melting (HRM) analysis in eggplant (solanum melongena L.): A tool for microsatellite genotyping and molecular characterization of a Greek genebank collection. *Biochem. Syst. Ecol.* 58, 64–71. doi:10.1016/j.bse.2014.11.003

Gao, T., Yao, H., Song, J., Zhu, Y., Liu, C., and Chen, S. (2010). Evaluating the feasibility of using candidate DNA barcodes in discriminating species of the large Asteraceae family. *BMC Evol. Biol.* 10, 324. doi:10.1186/1471-2148-10-324

Gao, Z., Liu, Y., Wang, X., Wei, X., and Han, J. (2019). DNA mini-barcoding: A derived barcoding method for herbal molecular identification. *Front. Plant Sci.* 10, 987. doi:10.3389/fpls.2019.00987

Gismondi, A., Rolfo, M. F., Leonardi, D., Rickards, O., and Canini, A. (2012). Identification of ancient Olea europaea L. and Cornus mas L. seeds by DNA barcoding. *C. R. Biol.* 335, 472–479. doi:10.1016/j.crvi.2012.05.004

Gong, L., Qiu, X. H., Huang, J., Xu, W., Bai, J. Q., Zhang, J., et al. (2018). Constructing a DNA barcode reference library for southern herbs in China: A resource for authentication of southern Chinese medicine. *PLoS One* 13 (7), 1–12. doi:10.1371/journal.pone.0201240

Govindaraghavan, S., Hennell, J. R., and Sucher, N. J. (2012). From classical taxonomy to genome and metabolome: Towards comprehensive quality standards for medicinal herb raw materials and extracts. *Fitoterapia* 83, 979–988. doi:10.1016/j.fitote.2012.05.001

Gowda, B., Chandrika, K., Prasanna, K. T., and Kirana, V. C. (2010). AFLP authentication of Embelia ribes Burm.F and Embelia tsjeriam cottama. DC. *Int. J. Sci. Nat.* 1, 58–60.

Hajibabaei, M., Singer, G. A. C., Hebert, P. D. N., and Hickey, D. A. (2007). DNA barcoding: How it complements taxonomy, molecular phylogenetics and population genetics. *Trends Genet.* 23, 167–172. doi:10.1016/j.tig.2007.02.001

Hazarika, T. K., Hazarika, B. N., and Shukla, A. C. (2014). Genetic variability and phylogenetic relationships studies of genus Citrus L. with the application of molecular markers. *Genet. Resour. Crop Evol.* 61, 1441–1454. doi:10.1007/s10722-014-0188-0

He, Y., Hou, P., Fan, G., Arain, S., and Peng, C. (2014a). Comprehensive analyses of molecular phylogeny and main alkaloids for Coptis (Ranunculaceae) species identification. *Biochem. Syst. Ecol.* 56, 88–94. doi:10.1016/j.bse.2014.05.002

He, Y., Wan, F., Xiong, L., Li, D. M., and Peng, C. (2014b). Identification of two chemotypes of Pogostemon cablin (Blanco) Benth. Through DNA barcodes. *Z. Naturforsch. C J. Biosci.* 69 C, 253–258. doi:10.5560/ZNC.2013-0180

Hebert, P. D. N., Cywinska, A., Ball, S. L., and DeWaard, J. R. (2003). Biological identifications through DNA barcodes. *Proc. Biol. Sci.* 270, 313–321. doi:10.1098/rspb.2002.2218

Hollingsworth, P. M., Forrest, L. L., Spouge, J. L., Hajibabaei, M., Ratnasingham, S., van der Bank, M., et al. (2009). A DNA barcode for land plants. *Proc. Natl. Acad. Sci. U. S. A.* 106, 12794–12797. doi:10.1073/pnas.0905845106

Howard, C., Hill, E., Kreuzer, M., Mali, P., Masiero, E., Slater, A., et al. (2019). DNA authentication of St John's wort (*Hypericum perforatum* L.) commercial products targeting the ITS region. *Genes* 10 (286), 1–20. doi:10.3390/genes10040286

Howard, C., Lockie-Williams, C., and Slater, A. (2020). Applied barcoding: The practicalities of dna testing for herbals. *Plants* 9 (1150), 1–24. doi:10.3390/plants9091150

Hu, J., Zhan, Z. L., Yuan, Y., Huang, L. Q., and Liu, Y. (2015). [HRM identification of Chinese medicinal materials Mutong]. *China J. Chin. Mat. Medica* 40, 2304–2308.

Ichim, M. C., Häser, A., and Nick, P. (2020). Microscopic authentication of commercial herbal products in the globalized market: Potential and limitations. *Front. Pharmacol.* 11, 876. doi:10.3389/fphar.2020.00876

Ichim, M. C. (2019). The DNA-based authentication of commercial herbal products reveals their globally widespread adulteration. *Front. Pharmacol.* 10, 1227–1229. doi:10.3389/fphar.2019.01227

IPC (2018). Pharmacopoeia, I. Gov. India minist. Heal. Fam. Welfare, publ. *Indian Pharmacopoeial Comm. Gov. India Ghaziabad Vol.* III, 1616.

Ivanova, N. V., Kuzmina, M. L., Braukmann, T. W. A., Borisenko, A. V., and Zakharov, E. V. (2016). Authentication of herbal supplements using next-generation sequencing. *PLoS One* 11 (5), 1–24. doi:10.1371/journal.pone.0156426

Jamdade, R., Mosa, K. A., El-Keblawy, A., Al Shaer, K., Al Harthi, E., Al Sallani, M., et al. (2022). DNA barcodes for accurate identification of selected medicinal plants (caryophyllales): Toward barcoding flowering plants of the united Arab emirates. *Diversity* 14, 262. doi:10.3390/d14040262

Jia, J., Xu, Z., Xin, T., Shi, L., and Song, J. (2017). Quality control of the traditional patent medicine yimu wan based on SMRT sequencing and DNA barcoding. *Front. Plant Sci.* 8 (926), 1–11. doi:10.3389/fpls.2017.00926

Jiang, C., Cao, L., Yuan, Y., Chen, M., Jin, Y., and Huang, L. (2014). Barcoding melting curve analysis for rapid, sensitive, and discriminating authentication of saffron (Crocus sativus L.) from its adulterants. *Biomed. Res. Int.* 2014, 1–10. doi:10.1155/2014/809037

Jianping, H., Chang, L., Minhui, L., Lin-chun, S., Jingyuan, S., Hui, Y., et al. (2010). Relationship between DNA barcoding and chemical classification of Salvia medicinal herbs. *Chin. Herb. Med.* 2, 16–29. doi:10.3969/j.issn.1674-6384.2010.01.002

Kalivas, A., Ganopoulos, I., Xanthopoulou, A., Chatzopoulou, P., Tsaftaris, A., and Madesis, P. (2014). DNA barcode ITS2 coupled with high resolution melting (HRM) analysis for taxonomic identification of Sideritis species growing in Greece. *Mol. Biol. Rep.* 41, 5147–5155. doi:10.1007/s11033-014-3381-5

Kamani, G., Sanghani, R., Savalia, V., and Pandya, D. (2021). Detection of adulteration in rubia cordifolia – A chromatographic approach. *Res. J. Pharm. Technol.* 14, 4013–4018. doi:10.52711/0974-360X.2021.00695

Kesanakurti, P., Thirugnanasambandam, A., Ragupathy, S., and Newmaster, S. G. (2020). Genome skimming and NMR chemical fingerprinting provide quality assurance biotechnology to validate Sarsaparilla identity and purity. *Sci. Rep.* 10 (19192), 1–11. doi:10.1038/s41598-020-76073-7

Keshari, P., and Pradeep (2017). Controversy, adulteration and substitution: Burning problems in Ayurveda Practices. *Int. Ayurvedic Med. J.*, 2504–2516.

Khan, S., Al-Qurainy, F., Nadeem, M., and Tarroum, M. (2012). Development of genetic markers for Ochradenus arabicus (Resedaceae), an endemic medicinal plant of Saudi Arabia. *Genet. Mol. Res.* 11, 1300–1308. doi:10.4238/2012.May.14.4

Khan, S., Mirza, K. J., and Abdin, M. Z. (2010). Development of RAPD markers for authentication of medicinal plant Cuscuta reflexa. *Eurasian J. Biosci.* 1, 1–7. doi:10.5053/ejobios.2010.4.0.1

Kircher, M., and Kelso, J. (2010). High-throughput DNA sequencing - concepts and limitations. *BioEssays* 32, 524–536. doi:10.1002/bies.200900181

Kress, W. J., and Erickson, D. L. (2007). A two-locus global DNA barcode for land plants: The coding rbcL gene complements the non-coding trnH-psbA spacer region. *PLoS One* 2, e508. doi:10.1371/journal.pone.0000508

Kress, W. J. (2017). Plant DNA barcodes: Applications today and in the future. *J. Syst. Evol.* 55, 291–307. doi:10.1111/jse.12254

Kress, W. J., Wurdack, K. J., Zimmer, E. A., Weigt, L. A., and Janzen, D. H. (2005). Use of DNA barcodes to identify flowering plants. *Proc. Natl. Acad. Sci. U. S. A.* 102, 8369–8374. doi:10.1073/pnas.0503123102

Kreuzer, M., Howard, C., Adhikari, B., Pendry, C. A., and Hawkins, J. A. (2019). Phylogenomic approaches to DNA barcoding of herbal medicines: Developing clade-specific diagnostic characters for Berberis. *Front. Plant Sci.* 10 (586–616), 1–16. doi:10.3389/fpls.2019.00586

Kumar, A., Rodrigues, V., Baskaran, K., Shukla, A. K., and Sundaresan, V. (2020). DNA barcode based species-specific marker for Ocimum tenuiflorum and its applicability in quantification of adulteration in herbal formulations using qPCR. *J. Herb. Med.* 23, 100376. doi:10.1016/j.hermed.2020.100376

Kumar, P., Gupta, V. K., Misra, a. K., Modi, D. R., and Pandey, B. K. (2009). Potential of molecular markers in plant biotechnology. *Plant omi. J.* 2, 141–162.

Lai, G.-H., Chao, J., Lin, M.-K., Chang, W.-T., Peng, W.-H., Sun, F.-C., et al. (2015). Rapid and sensitive identification of the herbal tea ingredient Taraxacum formosanum using loop-mediated isothermal amplification. *Int. J. Mol. Sci.* 16, 1562–1575. doi:10.3390/ijms16011562

Lekouch, N., Sedki, A., Nejmeddine, A., and Gamon, S. (2001). Lead and traditional Moroccan pharmacopoeia. *Sci. Total Environ.* 280, 39–43. doi:10.1016/S0048-9697(01)00801-4

Li, D. Z., Gao, L. M., Li, H. T., Wang, H., Ge, X. J., Liu, J. Q., et al. (2011). Comparative analysis of a large dataset indicates that internal transcribed spacer (ITS) should be incorporated into the core barcode for seed plants. *Proc. Natl. Acad. Sci. U. S. A.* 108, 19641–19646. doi:10.1073/pnas.1104551108

Li, H. Q., Chen, J. Y., Wang, S., and Xiong, S. Z. (2012). Evaluation of six candidate DNA barcoding loci in Ficus (Moraceae) of China. *Mol. Ecol. Resour.* 12, 783–790. doi:10.1111/j.1755-0998.2012.03147.x

Li, H., Xiao, W., Tong, T., Li, Y., Zhang, M., Lin, X., et al. (2021). The specific DNA barcodes based on chloroplast genes for species identification of Orchidaceae plants. *Sci. Rep.* 11 (1424), 1–15. doi:10.1038/s41598-021-81087-w

Li, J., Song, M., Xiong, C., Zhao, B., and Sun, W. (2016). Application of barcode high-resolution melting for rapid authentication of the medicinal plant Psammosilene tunicoides. *Biotechnol. Biotechnol. Equip.* 30, 790–796. doi:10.1080/13102818.2016.1181988

Li, M., Wonga, Y. L., Jiang, L. L., Wonga, K. L., Wong, Y. T., Lau, C. B. S., et al. (2013). Application of novel loop-mediated isothermal amplification (LAMP) for rapid authentication of the herbal tea ingredient Hedyotis diffusa Willd. *Food Chem.* 141, 2522–2525. doi:10.1016/j.foodchem.2013.05.085

Li, Q. J., Wang, X., Wang, J. R., Su, N., Zhang, L., Ma, Y. P., et al. (2019). Efficient identification of pulsatilla (ranunculaceae) using DNA barcodes and micro-morphological characters. *Front. Plant Sci.* 10, 1196. doi:10.3389/fpls.2019.01196

Li, X., Yang, Y., Henry, R. J., Rossetto, M., Wang, Y., and Chen, S. (2015). Plant DNA barcoding: From gene to genome. *Biol. Rev. Camb. Philos. Soc.* 90, 157–166. doi:10.1111/brv.12104

Lin, T. C., Yeh, M. S., Cheng, Y. M., Lin, L. C., and Sung, J. M. (2012). Using ITS2 PCR-RFLP to generate molecular markers for authentication of Sophora flavescens Ait. *J. Sci. Food Agric.* 92, 892–898. doi:10.1002/jsfa.4667

Little, D. P. (2014). Authentication of Ginkgo biloba herbal dietary supplements using DNA barcoding. *Genome* 57, 513–516. doi:10.1139/gen-2014-0130

Liu, J., Shi, L., Han, J., Li, G., Lu, H., Hou, J., et al. (2014). Identification of species in the angiosperm family Apiaceae using DNA barcodes. *Mol. Ecol. Resour.* 14, 1231–1238. doi:10.1111/1755-0998.12262

Liu, J., Yan, H. F., and Ge, X. J. (2016). The use of DNA barcoding on recently diverged species in the genus Gentiana (Gentianaceae) in China. *PLoS One* 11, e0153008. doi:10.1371/journal.pone.0153008

Liu, Q., Zhuo, L., Liu, L., Zhu, S., Sunnassee, A., Liang, M., et al. (2011). Seven cases of fatal aconite poisoning: Forensic experience in China. *Forensic Sci. Int.* 212, e5–e9. doi:10.1016/j.forsciint.2011.05.009

Liu, Z. F., Ma, H., Zhang, X. Y., Ci, X. Q., Li, L., Hu, J. L., et al. (2022). Do taxon-specific DNA barcodes improve species discrimination relative to universal barcodes in Lauraceae? *Bot. J. Linn. Soc.* 199, 741–753. doi:10.1093/botlinnean/boab089

Liu, Z., Zeng, X., Yang, D., Chu, G., Yuan, Z., and Chen, S. (2012). Applying DNA barcodes for identification of plant species in the family Araliaceae. *Gene* 499, 76–80. doi:10.1016/j.gene.2012.02.016

Lo, Y. T., and Shaw, P. C. (2019). Application of next-generation sequencing for the identification of herbal products. *Biotechnol. Adv.* 37, 107450. doi:10.1016/j.biotechadv.2019.107450

Lobato, I. M., and O'Sullivan, C. K. (2018). Recombinase polymerase amplification: Basics, applications and recent advances. *Trends Anal. Chem.* 98, 19–35. doi:10.1016/j.trac.2017.10.015

Luo, K., Chen, S. L., Chen, K. L., Song, J. Y., Yao, H., Ma, X., et al. (2010). Assessment of candidate plant DNA barcodes using the Rutaceae family. *Sci. China. Life Sci.* 53, 701–708. doi:10.1007/s11427-010-4009-1

Lv, Y. N., Yang, C. Y., Shi, L. C., Zhang, Z. L., Xu, A. S., Zhang, L. X., et al. (2020). Identification of medicinal plants within the Apocynaceae family using ITS2 and psbA-trnH barcodes. *Chin. J. Nat. Med.* 18, 594–605. doi:10.1016/S1875-5364(20)30071-6

Madesis, P., Ganopoulos, I., Sakaridis, I., Argiriou, A., and Tsaftaris, A. (2013). Advances of DNA-based methods for tracing the botanical origin of food products. *Food Res. Int.* 60, 163–172. doi:10.1016/j.foodres.2013.10.042

Mahima, K., Sudhakar, J. V., and Sathishkumar, R. (2020). Molecular phylogeny of the Ficus virens complex (Moraceae). *Genome* 63, 597–606. doi:10.1139/gen-2019-0210

Mao, Y. R., Zhang, Y. H., Nakamura, K., Guan, B. C., and Qiu, Y. X. (2014). Developing DNA barcodes for species identification in Podophylloideae (Berberidaceae). *J. Syst. Evol.* 52, 487–499. doi:10.1111/jse.12076

Marichamy, K., Yasoth Kumar, N., and Ganesan, A. (2014). Sustainable development in exports of herbals and Ayurveda, Siddha, Unani and homoeopathy (ayush) in India. *Sci. Park* 1, 1–6. doi:10.9780/23218045/1202013/49

Metzker, M. L. (2010). Sequencing technologies — The next generation. *Nat. Rev. Genet.* 11, 31–46. doi:10.1038/nrg2626

Meusnier, I., Singer, G. A. C., Landry, J. F., Hickey, D. A., Hebert, P. D. N., and Hajibabaei, M. (2008). A universal DNA mini-barcode for biodiversity analysis. *BMC Genomics* 9, 214–217. doi:10.1186/1471-2164-9-214

Mezzasalma, V., Ganopoulos, I., Galimberti, A., Cornara, L., Ferri, E., and Labra, M. (2017). Poisonous or non-poisonous plants? DNA-based tools and applications for accurate identification. *Int. J. Leg. Med.* 131, 1–19. doi:10.1007/s00414-016-1460-y

Mishra, P., Kumar, A., Nagireddy, A., Mani, D. N., Shukla, A. K., Tiwari, R., et al. (2015). DNA barcoding: An efficient tool to overcome authentication challenges in the herbal market. *Plant Biotechnol. J.* 14, 8–21. doi:10.1111/pbi.12419

Moritz, C., and Cicero, C. (2004). DNA barcoding: Promise and pitfalls. *PLoS Biol.* 2, e354. doi:10.1371/journal.pbio.0020354

Muellner, A. N., Schaefer, H., and Lahaye, R. (2011). Evaluation of candidate DNA barcoding loci for economically important timber species of the mahogany family (Meliaceae). *Mol. Ecol. Resour.* 11, 450–460. doi:10.1111/j.1755-0998.2011.02984.x

Naeem, A., Khan, A. A., Cheema, H. M. N., Khan, I. A., and Buerkert, A. (2014). DNA barcoding for species identification in the Palmae family. *Genet. Mol. Res.* 13, 10341–10348. doi:10.4238/2014.December.4.29

Naim, D. M., and Mahboob, S. (2020). Molecular identification of herbal species belonging to genus Piper within family Piperaceae from northern Peninsular Malaysia. *J. King Saud Univ. - Sci.* 32, 1417–1426. doi:10.1016/j.jksus.2019.11.036

Newmaster, S. G., Fazekas, A. J., and Ragupathy, S. (2006). DNA barcoding in land plants: Evaluation of rbcL in a multigene tiered approach. *Can. J. Bot.* 84, 335–341. doi:10.1139/B06-047

Newmaster, S. G., Fazekas, A. J., Steeves, R. A. D., and Janovec, J. (2008). Testing candidate plant barcode regions in the Myristicaceae. *Mol. Ecol. Resour.* 8, 480–490. doi:10.1111/j.1471-8286.2007.02002.x

Newmaster, S. G., Grguric, M., Shanmughanandhan, D., Ramalingam, S., and Ragupathy, S. (2013). DNA barcoding detects contamination and substitution in North American herbal products. *BMC Med.* 11, 222. doi:10.1186/1741-7015-11-222

Newmaster, S. G., Ragupathy, S., and Janovec, J. (2009). A botanical renaissance: State-of-the-art DNA bar coding facilitates an Automated Identification Technology system for plants. *Int. J. Comput. Appl. Technol.* 35, 50–60. doi:10.1504/IJCAT.2009.024595

Nithaniyal, S., Newmaster, S. G., Ragupathy, S., Krishnamoorthy, D., Vassou, S. L., and Parani, M. (2014). DNA barcode authentication of wood samples of threatened and commercial timber trees within the tropical dry evergreen forest of India. *PLoS One* 9, e107669. doi:10.1371/journal.pone.0107669

Omelchenko, D. O., Speranskaya, A. S., Ayginin, A. A., Khafizov, K., Krinitsina, A. A., Fedotova, A. V., et al. (2019). Improved protocols of ITS1-based metabarcoding and their application in the analysis of plant-containing products. *Genes (Basel)* 10 (122), 1–16. doi:10.3390/genes10020122

Osathanunkul, M., Madesis, P., and De Boer, H. (2015a). Bar-HRM for authentication of plant-based medicines: Evaluation of three medicinal products derived from Acanthaceae species. *PLoS One* 10 (9), 1–14. doi:10.1371/journal.pone.0128476

Osathanunkul, M., Suwannapoom, C., Osathanunkul, K., Madesis, P., and De Boer, H. (2016). Evaluation of DNA barcoding coupled high resolution melting for discrimination of closely related species in phytopharmaceuticals. *Phytomedicine* 23, 156–165. doi:10.1016/j.phymed.2015.11.018

Osathanunkul, M., Suwannapoom, C., Ounjai, S., Rora, J. A., Madesis, P., and De Boer, H. (2015b). Refining DNA barcoding coupled high resolution melting for discrimination of 12 closely related Croton species. *PLoS One* 10 (5), 1–11. doi:10.1371/journal.pone.0138888

Oyebanji, O. O., Chukwuma, E. C., Bolarinwa, K. A., Adejobi, O. I., Adeyemi, S. B., and Ayoola, A. O. (2020). Re-evaluation of the phylogenetic relationships and species delimitation of two closely related families (Lamiaceae and Verbenaceae) using two DNA barcode markers. *J. Biosci.* 45, 96. doi:10.1007/s12038-020-00061-2

Palhares, R. M., Drummond, M. G., Cosenza, G. P., Das Graças Lins Brandão, M., and Oliveira, G. (2015). Medicinal plants recommended by the world health organization: DNA barcode identification associated with chemical analyses guarantees their quality. *PLoS One* 10, 1–29. doi:10.1371/journal.pone.0127866

Pandey, R., Tiwari, R. K., and Shukla, S. S. (2016). Omics: A newer technique in herbal drug standardization and quantification. *J. Young Pharm.* 8, 76–81. doi:10.5530/jyp.2016.2.4

Pang, X., Song, J., Zhu, Y., Xu, H., Huang, L., and Chen, S. (2011). Applying plant DNA barcodes for Rosaceae species identification. *Cladistics.* 27, 165–170. doi:10.1111/j.1096-0031.2010.00328.x

Parvathy, V. A., Swetha, V. P., Sheeja, T. E., Leela, N. K., Chempakam, B., and Sasikumar, B. (2014). DNA barcoding to detect chilli adulteration in traded black pepper powder. *Food Biotechnol.* 28, 25–40. doi:10.1080/08905436.2013.870078

Parveen, I., Techen, N., and Khan, I. A. (2019). Identification of species in the aromatic spice family Apiaceae using DNA mini-barcodes. *Planta Med.* 85, 139–144. doi:10.1055/a-0664-0947

Piepenburg, O., Williams, C. H., Stemple, D. L., and Armes, N. A. (2006). DNA detection using recombination proteins. *PLoS Biol.* 4, e204–e1121. doi:10.1371/journal.pbio.0040204

Prakash, J., Srivastava, S., Ray, R. S., Singh, N., Rajpali, R., and Singh, G. N. (2017). Current status of herbal drug standards in the Indian pharmacopoeia. *Phytother. Res.* 31, 1817–1823. doi:10.1002/ptr.5933

Prakash, O., JyothiKumar, A., and Manna, N. K. (2013). Adulteration and substitution in Indian medicinal plants: An overview. *J. Med. Plants Stud.* 1, 127–132.

Purushothaman, N., Newmaster, S. G., Ragupathy, S., Stalin, N., Suresh, D., Arunraj, D. R., et al. (2014). A tiered barcode authentication tool to differentiate medicinal Cassia species in India. *Genet. Mol. Res.* 13, 2959–2968. doi:10.4238/2014.April.16.4

Raclariu, A. C., Heinrich, M., Ichim, M. C., and de Boer, H. (2018a). Benefits and limitations of DNA barcoding and metabarcoding in herbal product authentication. *Phytochem. Anal.* 29, 123–128. doi:10.1002/pca.2732

Raclariu, A. C., Heinrich, M., Ichim, M. C., and de Boer, H. (2018). Benefits and limitations of DNA barcoding and metabarcoding in herbal product authentication. *Phytochem. Anal.* 29, 123–128. doi:10.1002/pca.2732

Raclariu, A. C., Mocan, A., Popa, M. O., Vlase, L., Ichim, M. C., Crisan, G., et al. (2017a). Veronica officinalis product authentication using DNA metabarcoding and HPLC-MS reveals widespread adulteration with Veronica chamaedrys. *Front. Pharmacol.* 8 (378), 1–13. doi:10.3389/fphar.2017.00378

Raclariu, A. C., Paltinean, R., Vlase, L., Labarre, A., Manzanilla, V., Ichim, M. C., et al. (2017b). Comparative authentication of *Hypericum perforatum* herbal products using DNA metabarcoding, TLC and HPLC-MS. *Sci. Rep.* 7 (1291), 1–12. doi:10.1038/s41598-017-01389-w

Raclariu, A. C., Ţebrencu, C. E., Ichim, M. C., Ciupercă, O. T., Brysting, A. K., and de Boer, H. (2018b). What's in the box? Authentication of Echinacea herbal products using DNA metabarcoding and HPTLC. *Phytomedicine* 44, 32–38. doi:10.1016/j.phymed.2018.03.058

Ragupathy, S., Newmaster, S. G., Murugesan, M., and Balasubramaniam, V. (2009). DNA barcoding discriminates a new cryptic grass species revealed in an ethnobotany study by the hill tribes of the Western Ghats in southern India. *Mol. Ecol. Resour.* 9, 164–171. doi:10.1111/j.1755-0998.2009.02641.x

Rai, P. S., Bellampalli, R., Dobriyal, R. M., Agarwal, A., Satyamoorthy, K., and Anantha Narayana, D. B. (2012). DNA barcoding of authentic and substitute samples of herb of the family Asparagaceae and Asclepiadaceae based on the ITS2 region. *J. Ayurveda Integr. Med.* 3, 136–140. doi:10.4103/0975-9476.100177

Ran, J. H., Wang, P. P., Zhao, H. J., and Wang, X. Q. (2010). A test of seven candidate barcode regions from the plastome in picea (pinaceae). *J. Integr. Plant Biol.* 52, 1109–1126. doi:10.1111/j.1744-7909.2010.00995.x

RSC (1985). *Food and drugs act. C. F-27.*

Rubinoff, D., Cameron, S., and Will, K. (2006). Are plant DNA barcodes a search for the Holy Grail? *Trends Ecol. Evol.* 21, 1–2. doi:10.1016/j.tree.2005.10.019

Sagar, P. K. (2014). Adulteration and substitution in endangered, ASU herbal medicinal plants of India, their legal status, scientific screening of active phytochemical constituents. *Int. J. Pharm. Sci. Res.* 5, 4023–4039. doi:10.13040/IJPSR.0975-8232.5(9).4023-39

Sakaridis, I., Ganopoulos, I., Argiriou, A., and Tsaftaris, A. (2013). A fast and accurate method for controlling the correct labeling of products containing buffalo meat using High Resolution Melting (HRM) analysis. *Meat Sci.* 94, 84–88. doi:10.1016/j.meatsci.2012.12.017

Sakaridis, I., Ganopoulos, I., Soultos, N., Madesis, P., Tsaftaris, A., and Argiriou, A. (2014). Identification of lactic acid bacteria isolated from poultry carcasses by high-resolution melting (HRM) analysis. *Eur. Food Res. Technol.* 238, 691–697. doi:10.1007/s00217-013-2134-3

Santhosh Kumar, J. U., Krishna, V., Seethapathy, G. S., Ganesan, R., Ravikanth, G., and Shaanker, R. U. (2018). Assessment of adulteration in raw herbal trade of important medicinal plants of India using DNA barcoding. *3 Biotech.* 8, 135. 3 Biotech. doi:10.1007/s13205-018-1169-3

Saper, R. B., Kales, S. N., Paquin, J., Burns, M. J., Eisenberg, D. M., Davis, R. B., et al. (2004). Heavy metal content of Ayurvedic herbal medicine products. *J. Am. Med. Assoc.* 292, 2868–2873. doi:10.1001/jama.292.23.2868

Sarin, Y. K. (1996). Illustrated manual of herbal drugs used in Ayurveda. Available at: https://books.google.co.in/books?id=y9SItgAACAAJ.

Sarwat, M., and Yamdagni, M. M. (2016). DNA barcoding, microarrays and next generation sequencing: Recent tools for genetic diversity estimation and authentication of medicinal plants. *Crit. Rev. Biotechnol.* 36, 191–203. doi:10.3109/07388551.2014.947563

Sasaki, Y., Komatsu, K., and Nagumo, S. (2008). Rapid detection of Panax ginseng by loop-mediated isothermal amplification and its application to authentication of ginseng. *Biol. Pharm. Bull.* 31, 1806–1808. doi:10.1248/bpb.31.1806

Sasaki, Y., and Nagumo, S. (2007). Rapid identification of Curcuma longa and C. aromatica by LAMP. *Biol. Pharm. Bull.* 30, 2229–2230. doi:10.1248/bpb.30.2229

Seethapathy, G. S., Balasubramani, S. P., and Venkatasubramanian, P. (2014). nrDNA ITS sequence based SCAR marker to authenticate Aconitum heterophyllum and Cyperus rotundus in Ayurvedic raw drug source and prepared herbal products. *Food Chem.* 145, 1015–1020. doi:10.1016/j.foodchem.2013.09.027

Seethapathy, G. S., Ganesh, D., Santhosh Kumar, J. U., Senthilkumar, U., Newmaster, S. G., Ragupathy, S., et al. (2015). Assessing product adulteration in natural health products for laxative yielding plants, Cassia, Senna, and Chamaecrista, in Southern India using DNA barcoding. *Int. J. Leg. Med.* 129, 693–700. doi:10.1007/s00414-014-1120-z

Seethapathy, G. S., Raclariu-Manolica, A. C., Anmarkrud, J. A., Wangensteen, H., and de Boer, H. J. (2019). DNA metabarcoding authentication of ayurvedic herbal

products on the European market raises concerns of quality and fidelity. *Front. Plant Sci.* 10, 68. doi:10.3389/fpls.2019.00068

Selvaraj, D., Shanmughanandhan, D., Sarma, R. K., Joseph, J. C., Srinivasan, R. V., and Ramalingam, S. (2012). DNA barcode ITS effectively distinguishes the medicinal plant boerhavia diffusa from its adulterants. *Genomics Proteomics Bioinforma.* 10, 364–367. doi:10.1016/j.gpb.2012.03.002

Sen, S., and Chakraborty, R. (2017). Revival, modernization and integration of Indian traditional herbal medicine in clinical practice: Importance, challenges and future. *J. Tradit. Complement. Med.* 7, 234–244. doi:10.1016/j.jtcme.2016.05.006

Senapati, A., Basak, S., and Rangan, L. (2022). A review on application of DNA barcoding technology for rapid molecular diagnostics of adulterants in herbal medicine. *Drug Saf.* 45, 193–213. doi:10.1007/s40264-021-01133-4

Sharma, J., Gairola, S., Sharma, Y. P., and Gaur, R. D. (2014). Ethnomedicinal plants used to treat skin diseases by Tharu community of district Udham Singh Nagar, Uttarakhand, India. *J. Ethnopharmacol.* 158, 140–206. doi:10.1016/j.jep.2014.10.004

Sharma, R. K., Gupta, P., Sharma, V., Sood, A., Mohapatra, T., and Ahuja, P. S. (2008). Evaluation of rice and sugarcane SSR markers for phylogenetic and genetic diversity analyses in bamboo. *Genome* 51, 91–103. doi:10.1139/G07-101

Shendure, J., and Ji, H. (2008). Next-generation DNA sequencing. *Nat. Biotechnol.* 26, 1135–1145. doi:10.1038/nbt1486

Shi, L. C., Zhang, J., Han, J. P., Song, J. Y., Yao, H., Zhu, Y. J., et al. (2011). Testing the potential of proposed DNA barcodes for species identification of Zingiberaceae. *J. Syst. Evol.* 49, 261–266. doi:10.1111/j.1759-6831.2011.00133.x

Singh, H., Parveen, I., Raghuvanshi, S., and Babbar, S. B. (2012). The loci recommended as universal barcodes for plants on the basis of floristic studies may not work with congeneric species as exemplified by DNA barcoding of Dendrobium species. *BMC Res. Notes* 5, 42–11. doi:10.1186/1756-0500-5-42

Singtonat, S., and Osathanunkul, M. (2015). Fast and reliable detection of toxic Crotalaria spectabilis Roth. in Thunbergia laurifolia Lindl. herbal products using DNA barcoding coupled with HRM analysis. *BMC Complement. Altern. Med.* 15, 162–168. doi:10.1186/s12906-015-0692-6

Soares, S., Grazina, L., Costa, J., Amaral, J. S., Oliveira, M. B. P. P., and Mafra, I. (2018). Botanical authentication of lavender (Lavandula spp.) honey by a novel DNA-barcoding approach coupled to high resolution melting analysis. *Food control.* 86, 367–373. doi:10.1016/j.foodcont.2017.11.046

Song, J., Yao, H., Li, Y., Li, X., Lin, Y., Liu, C., et al. (2009). Authentication of the family Polygonaceae in Chinese pharmacopoeia by DNA barcoding technique. *J. Ethnopharmacol.* 124, 434–439. doi:10.1016/j.jep.2009.05.042

Speranskaya, A. S., Khafizov, K., Ayginin, A. A., Krinitsina, A. A., Omelchenko, D. O., Nilova, M. V., et al. (2018). Comparative analysis of Illumina and Ion Torrent high-throughput sequencing platforms for identification of plant components in herbal teas. *Food control.* 93, 315–324. doi:10.1016/j.foodcont.2018.04.040

Srirama, R., Senthilkumar, U., Sreejayan, N., Ravikanth, G., Gurumurthy, B. R., Shivanna, M. B., et al. (2010). Assessing species admixtures in raw drug trade of Phyllanthus, a hepato-protective plant using molecular tools. *J. Ethnopharmacol.* 130, 208–215. doi:10.1016/j.jep.2010.04.042

Staats, M., Arulandhu, A. J., Gravendeel, B., Holst-Jensen, A., Scholtens, I., Peelen, T., et al. (2016). Advances in DNA metabarcoding for food and wildlife forensic species identification. *Anal. Bioanal. Chem.* 408, 4615–4630. doi:10.1007/s00216-016-9595-8

Stoeckle, M. Y., Gamble, C. C., Kirpekar, R., Young, G., Ahmed, S., and Little, D. P. (2011). Commercial teas highlight plant DNA barcode identification successes and obstacles. *Sci. Rep.* 1, 42–47. doi:10.1038/srep00042

Sucher, N. J., and Carles, M. C. (2008). Genome-based approaches to the authentication of medicinal plants. *Planta Med.* 74, 603–623. doi:10.1055/s-2008-1074517

Sultana, S., Ahamad, M., Khan, M. Z. A., and Arshad, Muhammad (2012). Authentication of herbal drug Senna (Cassia angustifolia vahl.): A village pharmacy for indo-pak subcontinent. *Afr. J. Pharm. Pharmacol.* 6, 2299–2308. doi:10.5897/AJPP12.446

Sun, W., Li, J. jian, Xiong, C., Zhao, B., and Chen, S. lin (2016). The potential power of bar-HRM technology in herbal medicine identification. *Front. Plant Sci.* 7 (367), 1–10. doi:10.3389/fpls.2016.00367

Swetha, V. P., Parvathy, V. A., Sheeja, T. E., and Sasikumar, B. (2017). Authentication of Myristica fragrans Houtt. using DNA barcoding. *Food control.* 73, 1010–1015. doi:10.1016/j.foodcont.2016.10.004

Swetha, V. P., Parvathy, V. A., Sheeja, T. E., and Sasikumar, B. (2014). DNA barcoding for discriminating the economically important cinnamomum verum from its adulterants. *Food Biotechnol.* 28, 183–194. doi:10.1080/08905436.2014.931239

Taberlet, P., Coissac, E., Pompanon, F., Brochmann, C., and Willerslec, E. (2012). Towards next-generation biodiversity assessment using DNA metabarcoding. *Mol. Ecol.* 21, 2045–2050. doi:10.1111/j.1365-294X.2012.05470.x

Tahir, A., Hussain, F., Ahmed, N., Ghorbani, A., and Jamil, A. (2018). Assessing universality of DNA barcoding in geographically isolated selected desert medicinal species of Fabaceae and Poaceae. *PeerJ* 6, e4499. doi:10.7717/peerj.4499

Tamhankar, S., Ghate, V., Raut, A., and Rajput, B. (2009). Molecular profiling of "chirayat" complex using inter simple sequence repeat (ISSR) markers. *Planta Med.* 75, 1266–1270. doi:10.1055/s-0029-1185543

Thakur, V. V., Tiwari, S., Tripathi, N., and Tiwari, G. (2019). Molecular identification of medicinal plants with amplicon length polymorphism using universal DNA barcodes of the atpF–atpH, trnL and trnH–psbA regions. *3 Biotech.* 9 (188), 1–10. doi:10.1007/s13205-019-1724-6

Thakur, V. V., Tripathi, N., and Tiwari, S. (2021). DNA barcoding of some medicinally important plant species of Lamiaceae family in India. *Mol. Biol. Rep.* 48, 3097–3106. doi:10.1007/s11033-021-06356-3

Tian, E., Liu, Q., Ye, H., Li, F., and Chao, Z. (2017). A DNA barcode-based RPA assay (BAR-RPA) for rapid identification of the dry root of Ficus hirta (wuzhimaotao). *Molecules* 22 (2261), 1–10. doi:10.3390/molecules22122261

Tong, Y., Jiang, C., Huang, L., Cui, Z., and Yuan, Y. (2014). Molecular identification of Radix Notoginseng powder by DNA melt curve analysis. *Chin. J. Pharm. Anal.* 34, 1384–1390.

Tripathi, A. M., Tyagi, A., Kumar, A., Singh, A., Singh, S., Chaudhary, L. B., et al. (2013). The internal transcribed spacer (ITS) region and trnH-psbA [corrected] are suitable candidate loci for DNA barcoding of tropical tree species of India. *PLoS One* 8, e57934. doi:10.1371/journal.pone.0057934

Tungphatthong, C., Urumarudappa, S. K. J., Awachai, S., Sooksawate, T., and Sukrong, S. (2021). Differentiation of Mitragyna speciosa, a narcotic plant, from allied Mitragyna species using DNA barcoding-high-resolution melting (Bar-HRM) analysis. *Sci. Rep.* 11, 6738. doi:10.1038/s41598-021-86228-9

Urumarudappa, S. K. J., Tungphatthong, C., Prombutara, P., and Sukrong, S. (2020). DNA metabarcoding to unravel plant species composition in selected herbal medicines on the National List of Essential Medicines (NLEM) of Thailand. *Sci. Rep.* 10 (18259), 1–11. doi:10.1038/s41598-020-75305-0

Vassou, S. L., Kusuma, G., and Parani, M. (2015). DNA barcoding for species identification from dried and powdered plant parts: A case study with authentication of the raw drug market samples of Sida cordifolia. *Gene* 559, 86–93. doi:10.1016/j.gene.2015.01.025

Vassou, S. L., Nithaniyal, S., Raju, B., and Parani, M. (2016). Creation of reference DNA barcode library and authentication of medicinal plant raw drugs used in Ayurvedic medicine. *BMC Complement. Altern. Med.* 16, 186. doi:10.1186/s12906-016-1086-0

Ved, D. K., and Goraya, G. S. (2007). *Demand and supply of medicinal plants in India*. New: NMPB. Available at: http://nmpb. nic.in/FRLHT/Contents.pdf.Delhi FRLHT, Bangalore, India, 1–18

Veldman, S., Otieno, J., Gravendeel, B., van Andel, T., and de Boer, H. (2014). Conservation of endangered wild harvested medicinal plants: Use of DNA barcoding. *Nov. Plant Bioresour. Appl. Food Med. Cosmet.*, 81–88. doi:10.1002/9781118460566.ch6

Verma, S. K., and Goswami, G. K. (2014). DNA evidence: Current perspective and future challenges in India. *Forensic Sci. Int.* 241, 183–189. doi:10.1016/j.forsciint.2014.05.016

Vijayambika, C., Jegadeesan, M., and Ganthi, A. S. (2011). Comparative anatomical studies on seeds of Mucuna Adans. and Canavalia Dc. species. *Indian J. Nat. Prod. Resour.* 2, 81–87.

Vinitha, M. R., Kumar, U. S., Aishwarya, K., Sabu, M., and Thomas, G. (2014). Prospects for discriminating Zingiberaceae species in India using DNA barcodes. *J. Integr. Plant Biol.* 56, 760–773. doi:10.1111/jipb.12189

Vohra, P., and Khera, K. (2013). DNA Barcoding: Current advances and future prospects - a review. *Asian J. Biol. Life Sci.* 2, 185–189.

Wallace, L. J., Boilard, S. M. A. L., Eagle, S. H. C., Spall, J. L., Shokralla, S., and Hajibabaei, M. (2012). DNA barcodes for everyday life: Routine authentication of Natural Health Products. *Food Res. Int.* 49, 446–452. doi:10.1016/j.foodres.2012.07.048

Wang, J., Ha, W.-Y., Ngan, F.-N., But, P. P.-H., and Shaw, P.-C. (2001). Application of sequence characterized amplified region (SCAR) analysis to authenticate Panax species and their adulterants. *Planta Med.* 67, 781–783. doi:10.1055/s-2001-18340

Wang, W., Wu, Y., Yan, Y., Ermakova, M., Kerstetter, R., and Messing, J. (2010). DNA barcoding of the Lemnaceae, a family of aquatic monocots. *BMC Plant Biol.* 10, 205. doi:10.1186/1471-2229-10-205

Watthanachaiyingcharoen, R., Komatsu, K., Zhu, S., Vajragupta, O., and Leelamanit, W. (2010). Authentication of Coscinium fenestratum among the other Menispermaceae plants prescribed in Thai folk medicines. *Biol. Pharm. Bull.* 33, 91–94. doi:10.1248/bpb.33.91

Will, K. W., Mishler, B. D., and Wheeler, Q. D. (2005). The perils of DNA barcoding and the need for integrative taxonomy. *Syst. Biol.* 54, 844–851. doi:10.1080/10635150500354878

Will, K. W., and Rubinoff, D. (2004). Myth of the molecule: DNA barcodes for species cannot replace morphology for identification and classification. *Cladistics.* 20, 47–55. doi:10.1111/j.1096-0031.2003.00008.x

Wong, T., But, G. W., Wu, H., Tsang, S. S., Lau, D. T., and Shaw, P. (2018). Medicinal materials DNA barcode database (MMDBD) version 1.5—One-stop solution for storage, BLAST, alignment and primer design. *Database (Oxford).* 2018, 1. doi:10.1093/database/bay112

Word Health Organisation (WHO) (2011). *Quality control methods for herbal materials*.

World Health Organization (WHO) (2004). *WHO guidelines on safety monitoring of herbal medicines in pharmacovigilance systems*. Geneva: World Health Organization, 82. https://apps.who.int/iris/handle/10665/44479.

Xiao, W. L., Motley, T. J., Unachukwu, U. J., Lau, C. B. S., Jiang, B., Hong, F., et al. (2011). Chemical and genetic assessment of variability in commercial Radix Astragali (Astragalus spp.) by ion trap LC-MS and nuclear ribosomal DNA barcoding sequence analyses. *J. Agric. Food Chem.* 59, 1548–1556. doi:10.1021/jf1028174

Yang, H. Q., Dong, Y. R., Gu, Z. J., Liang, N., and Yang, J. B. (2012). A preliminary assessment of matK, rbcL and trnH-psbA as DNA barcodes for Calamus (Arecaceae) species in China with a note on ITS. *Ann. Bot. Fenn.* 49, 319–330. doi:10.5735/085.049.0603

Yao, P. C., Gao, H. Y., Wei, Y. N., Zhang, J. H., Chen, X. Y., and Li, H. Q. (2017). Evaluating sampling strategy for DNA barcoding study of coastal and inland halo-tolerant poaceae and chenopodiaceae: A case study for increased sample size. *PLoS One* 12, e0185311–e0185314. doi:10.1371/journal.pone.0185311

Yu, J., Wu, X., Liu, C., Newmaster, S., Ragupathy, S., and Kress, W. J. (2021). Progress in the use of DNA barcodes in the identification and classification of medicinal plants. *Ecotoxicol. Environ. Saf.* 208, 111691. doi:10.1016/j.ecoenv.2020.111691

Yu, N., Gu, H., Wei, Y., Zhu, N., Wang, Y., Zhang, H., et al. (2016). Suitable DNA barcoding for identification and supervision of piper kadsura in Chinese medicine markets. *Molecules* 21, E1221. doi:10.3390/molecules21091221

Yu, X., Tan, W., Gao, H., Miao, L., and Tian, X. (2020). Development of a specific mini-barcode from plastome and its application for qualitative and quantitative identification of processed herbal products using DNA metabarcoding technique: A case study on Senna. *Front. Pharmacol.* 11, 585687–585689. doi:10.3389/fphar.2020.585687

Zhang, N., Erickson, D. L., Ramachandran, P., Ottesen, A. R., Timme, R. E., Funk, V. A., et al. (2017). An analysis of Echinacea chloroplast genomes: Implications for future botanical identification. *Sci. Rep.* 7, 216. doi:10.1038/s41598-017-00321-6

Zhao, B., Xiong, C., Wu, L., Xiang, L., Shi, Y., Sun, W., et al. (2021). DNA barcoding coupled with high resolution melting for rapid identification of Ardisia gigantifolia and its toxic adulterants. *Biotechnol. Biotechnol. Equip.* 35, 641–649. doi:10.1080/13102818.2021.1885993

Zhao, M., Shi, Y., Wu, L., Guo, L., Liu, W., Xiong, C., et al. (2016). Rapid authentication of the precious herb saffron by loop-mediated isothermal amplification (LAMP) based on internal transcribed spacer 2 (ITS2) sequence. *Sci. Rep.* 6, 25370–25379. doi:10.1038/srep25370

Zhao, W., Liu, M., Shen, C., Liu, H., Zhang, Z., Dai, W., et al. (2020). Differentiation, chemical profiles and quality evaluation of five medicinal Stephania species (Menispermaceae) through integrated DNA barcoding, HPLC-QTOF-MS/MS and UHPLC-DAD. *Fitoterapia* 141, 104453. doi:10.1016/j.fitote.2019.104453

Zhou, J., Cui, Y., Chen, X., Li, Y., Xu, Z., Duan, B., et al. (2018). Complete chloroplast genomes of Papaver rhoeas and Papaver orientale: Molecular structures, comparative analysis, and phylogenetic analysis. *Molecules* 23 (437), 1–15. doi:10.3390/molecules23020437

Zuo, Y., Chen, Z., Kondo, K., Funamoto, T., Wen, J., and Zhou, S. (2011). DNA barcoding of Panax species. *Planta Med.* 77, 182–187. doi:10.1055/s-0030-1250166

Frontiers in Pharmacology

Explores the interactions between chemicals and living beings

The most cited journal in its field, which advances access to pharmacological discoveries to prevent and treat human disease.

Discover the latest Research Topics

See more →

Frontiers

Avenue du Tribunal-Fédéral 34
1005 Lausanne, Switzerland
frontiersin.org

Contact us

+41 (0)21 510 17 00
frontiersin.org/about/contact